Engineering of 3D mesenchymal tissues for bone regeneration and hematopoiesis modeling

Inauguraldissertation

zur

Erlangung der Würde eines Doktors der Philosophie vorgelegt der

Philosophisch-Naturwissenschaftlichen Fakultät

der Universität Basel

von

Thibaut Klein

Aus Frankreich

2022

Genehmigt von der Philosophisch-Naturwissenschaftlichen Fakultät
auf Antrag von:

Prof. Dr. I. Martin
Prof. Dr. med. C. Lengerke

Basel, 17. Dezember 2019

Prof. Dr. Martin Spiess
Dekan der Philosophisch-
Naturwissenschaftlichen Fakultät

Acknowledgements.

La Nature ne se laisse point dévoiler, et il n'est ni levier ni machine qui puisse la contraindre à faire voir à mon esprit ce qu'elle a résolu de lui cacher. *Faust -672- (1806); Johann Wolfgang Goethe*

Mysterious, even in broad daylight, Nature won't let her veil be raised: What your spirit can't bring to sight, Won't by screws and levers be displayed. *Faust -672- (1806); Johann Wolfgang Goethe*

I wish to thank my supervisor, Prof. Dr. Ivan Martin for giving me the inestimable opportunity to work in his laboratory.

I sincerely thank the members of my PhD Committee for their precious inputs, availability and patience:

Prof. Dr. Markus Affolter

Prof. Dr. Claudia Lengerke

Prof. Dr. Nicolas Matt

I am infinitely grateful to every single person who dedicated any second of their precious time to help, support and encourage me as you all allowed me to progress in life and science. I also want to warmly thank the ones who did not do so and this, for the exact same reasons bringing the exact same consequences.

Here I mention all the past and present members of the Tissue Engineering Group, especially the mighty "Circle of trust" (I have a word for each of you but it would be longer than the thesis… Surtout toi, Arny!): Thank you very much!

I then want to acknowledge the members of the collaborating Groups (especially Dr. Morgane Hilpert, Dr. Takafumi Shimizu, Dr. Anna Paczulla and Dr. Martina Konantz) and all the scientists from the DBM Facilities for their outstanding skills and amazing help (Merci Manu!).

To finish, a "special thanks" to my family and friends.

Un immense merci à mes parents pour les principes et l'amour qu'ils m'ont donnés et mon frère (même si on s'est parfois mis dessus, on s'est bien amusés). Merci à mes amis d'être toujours là (ceux du Cercles, PA surtout et vous tous). Merci Marie pour ton soutien dans la dernière ligne droite. Enfin, merci à tous mes Frères :. Merci à tous de m'avoir épaulé durant ces années parfois difficiles mais toujours riches en enseignements.

En reprenant Méléagant *: Au fond, tout cela n'est pas grand-chose. Pourquoi d'ailleurs l'Univers s'en rendrait-il compte ? Nous sommes sur une toute petite poussière expulsée par une explosion, qui dérive et tournoie sur elle-même, en attendant sa fin matérielle. Sur cette miette, de minuscules organismes gesticulent grotesquement et bousculent ce qui est vraiment important sans le Voir. Tout cela pourrait n'avoir aucun sens.*

Malgré tout, nous avons une chance infinie. Perit ut Vivat :.

Table of Content

Chapter 1. Introduction

1.1 The bone organ, anatomy and function

1.1.1 Bone structure and composition

Adult bone is a mineralized connective tissue which exerts important functions in the body, such as locomotion, support and protection of organs, calcium and phosphate homeostasis and harboring of hematopoiesis in the bone marrow (BM). Bone structure is stable in shape lifelong except in certain case like pathologies or pregnancy. The adult human skeleton has a total of 213 bones composed of 80% cortical bone and 20% trabecular bone overall. Cortical bone is dense and solid and surrounds the trabecular bone which is composed of a honeycomb-like structural network forming the BM compartment. Bones are surrounded by the periosteum, a fibrous connective tissue sheet on their outer cortical surface, except at joints where bone is lined by articular cartilage. The endosteum is a membranous structure covering the trabecular bone in contact with BM [1]–[3] (Figure 1).

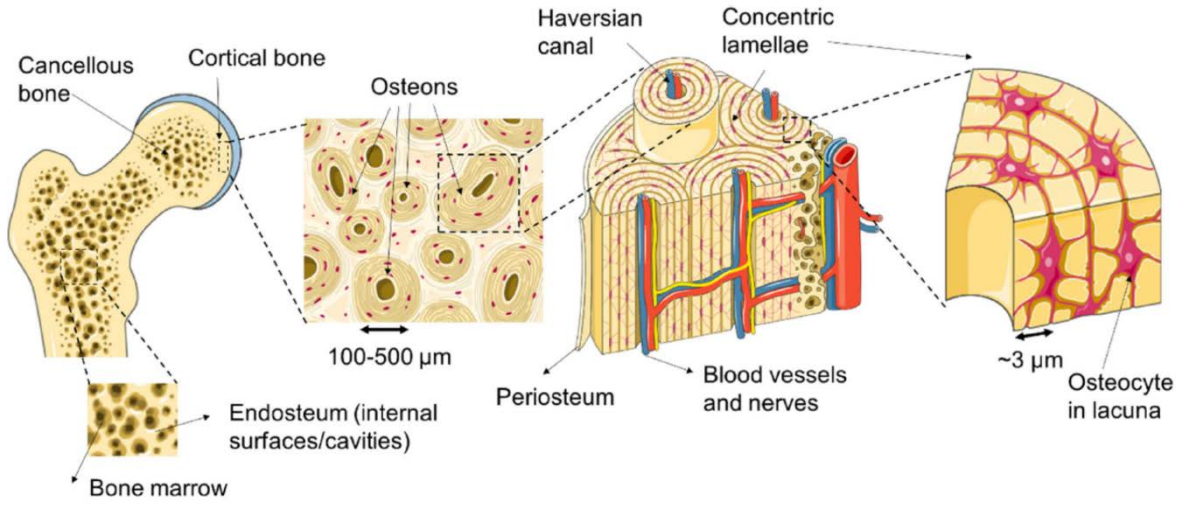

Figure 1. Detail of femur bone anatomy. Cross section through cortical and cancellous bone indicating anatomical and cellular features of the organ. Adapted from [4]

Bone extracellular matrix (ECM) determines the mechanical properties of the skeleton. Similarly to other connective tissues, cells are not its primary constituents. One important role for the ECM is to serve as a scaffold onto which minerals are deposited. It is composed of an inorganic and an organic phase providing load-bearing strength.

The inorganic phase is mostly composed by hydroxyapatite (HA; Ca10(PO4)6(OH)2) with citrate, carbonate and ions such as F−, K+ , Sr2+, Pb2+, Zn2+, Cu2+, and Fe2+. It is the largest source calcium with 99% of it as crystalline hydroxyapatite. Calcium plays a major role in the mechanisms of nerve impulse transmission, muscular contraction and blood coagulation and mediates cell-ECM interactions from fertilization to apoptosis and cell migration [5] as well as in bone homeostasis [6].

The organic phase is mainly composed of Type 1 collagen (Col1) bringing elasticity and flexibility to the bone while being involved in binding of mineral components. In addition to Col1, other ECM proteins represent 30% of the 315 proteins identified via secretome analysis [7], [8]. The most abundant are osteocalcin, osteopontin and bone sialoprotein. Matrix metalloproteinases are the major protease family first described in bone tissue responsible for the cleavage of the matrisome (global components of the ECM proteome) and various proteoglycans have an important role in its maturation [9].

Bone tissue exhibits four main cell types [10]: Osteoblasts (Ob) are largely known as bone-forming cells and deposit Coll1-rich mineralized ECM. Osteocytes are long-lived cells deriving from and 10 times more abundant than Ob after becoming embedded within their secreted ECM and are committed to remove damaged organelles and macromolecules by autophagy. Bone lining cells are quiescent Ob that cover the bone surfaces, where bone resorption or bone formation are not required [6].Those three first cell types differenciate from a common progenitor, namely Mesenchymal Stromal Cells (MSC) Lastly, Osteoclasts (Oc) originating from Hematopoietic Stem Cells (HSC) are responsible for bone resorption [11], [12].

During embryonic development, bone formation occurs by two mechanisms Figure 2.

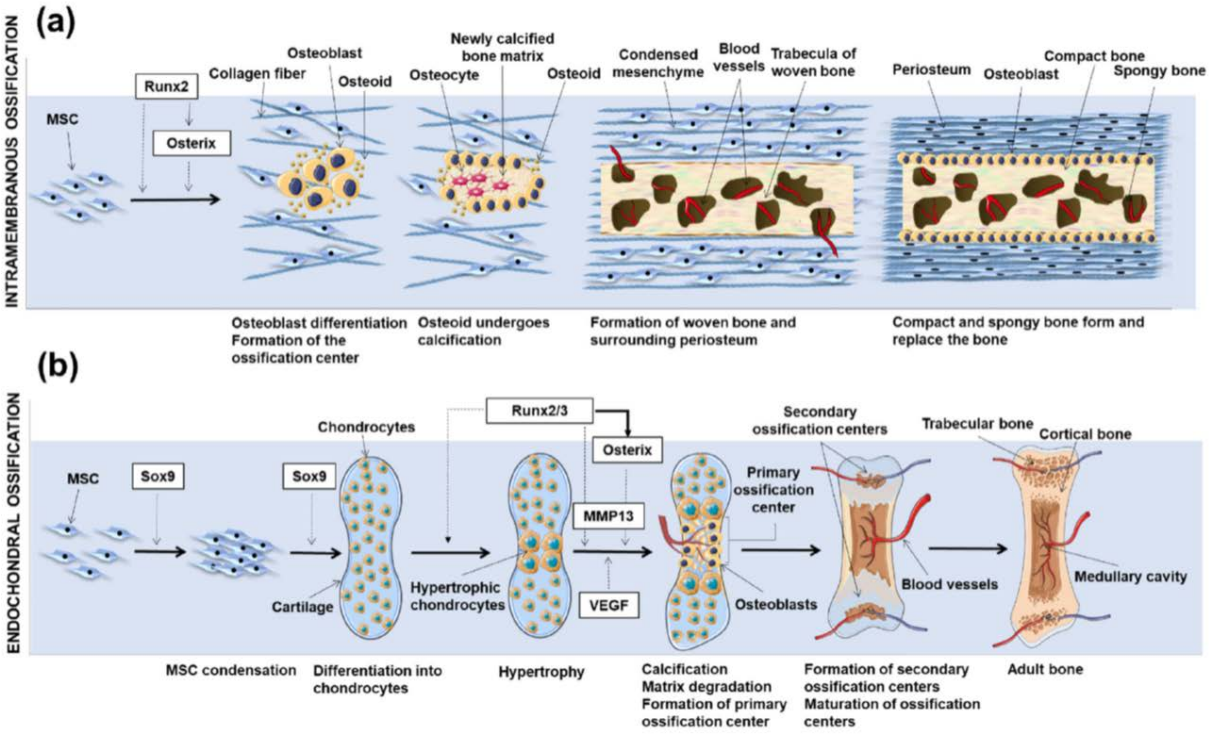

Figure 2. Bone formation from MSCs displaying key cell types and proteic actors. (a) Schematic representation of intramembranous ossification. (b) Schematic representation of endochondral ossification.

• Intramembranous ossification starts when MSC begin to replicate and form a small, dense cluster of cells in which they differentiate into Ob. Runx2 is the master gene inducing osteogenic differentiation directly inducing the expression of Osterix. Successively, Ob mature in Oc while replacing connective tissue membrane sheets with mineralized matrix [13]. The surface of trabeculae is filled with matrix forming the compact bone while spongy bone persists at the inner part. Flat bones of the skull, the mandible, and the clavicles are formed by intramembranous ossification process.

• Endochondral ossification starts in the limb bud with proliferating MSC which condensate and differentiate into the chondrogenic lineage, determining the formation of a cartilaginous template mainly composed of type 2 collagen. Sox9 and Runx2/3 are indispensable transcription factors for the initiation of chondrogenesis and the hypertrophy of chondrocytes, respectively. Successively, chondrogenic MSC become hypertrophic and upregulate type 10 collagen. At this stage, the cartilaginous template is progressively

remodeled while hypertrophic cells differentiate in Ob. Invading blood vessels deliver an influx of HSC and osteoprogenitors that populate the newly formed BM cavity [14].

Main molecular actors have been characterized after genetic studies in human and animal models which suggest that the canonical Wnt pathway, together with BMP signaling and key transcription factor RUNX2, have an important role in skeletal development, osteoblast differentiation and bone formation. There are at least 30 bone morphogenetic proteins (BMPs) that form the largest group of the TGF (transforming growth factor)-β superfamily. BMPs are so named for their osteo-inductive properties, and regulate differentiation of MSC into components of bone, cartilage or adipose tissue[15]–[17]. Establishment of a blood vessel network by vasculogenesis and angiogenesis is essential during bone formation and homeostasis [18][19]. Chondrocytes and bone-forming osteoblasts release vascular endothelial growth factor (VEGF). VEGF stimulates the migration of endothelial cells and the formation of an immature vascular network [20]. The rate of ossification depends on vascularization, and only the cells that are near capillaries contribute to bone formation.

1.1.2 Bone homeostasis and regeneration

Despite its inert appearance, bone is a highly dynamic organ that is continuously remodeled to maintain robust structure and function [21]. Remodeling sites may develop randomly but also in areas that require repair or in reaction to mechanical cues. Old bone is replaced by new bone, in a cycle composed of three phases: Initiation of bone resorption by Oc, Transition from resorption to new bone formation and New bone formation by Ob [22].Imbalance of this tightly coupled process can cause pathological conditions resulting in osteoporosis (bone loss) or osteosclerosis (bone gain) [23]. Thus, Ob and Oc proliferation, differentiation, and function are under tight molecular control; osteoclastogenesis is regulated by the ratio of receptor activator of NF-κB ligand (RANKL) to osteoprotegerin (OPG) expression in Ob-lineage cells. [24]

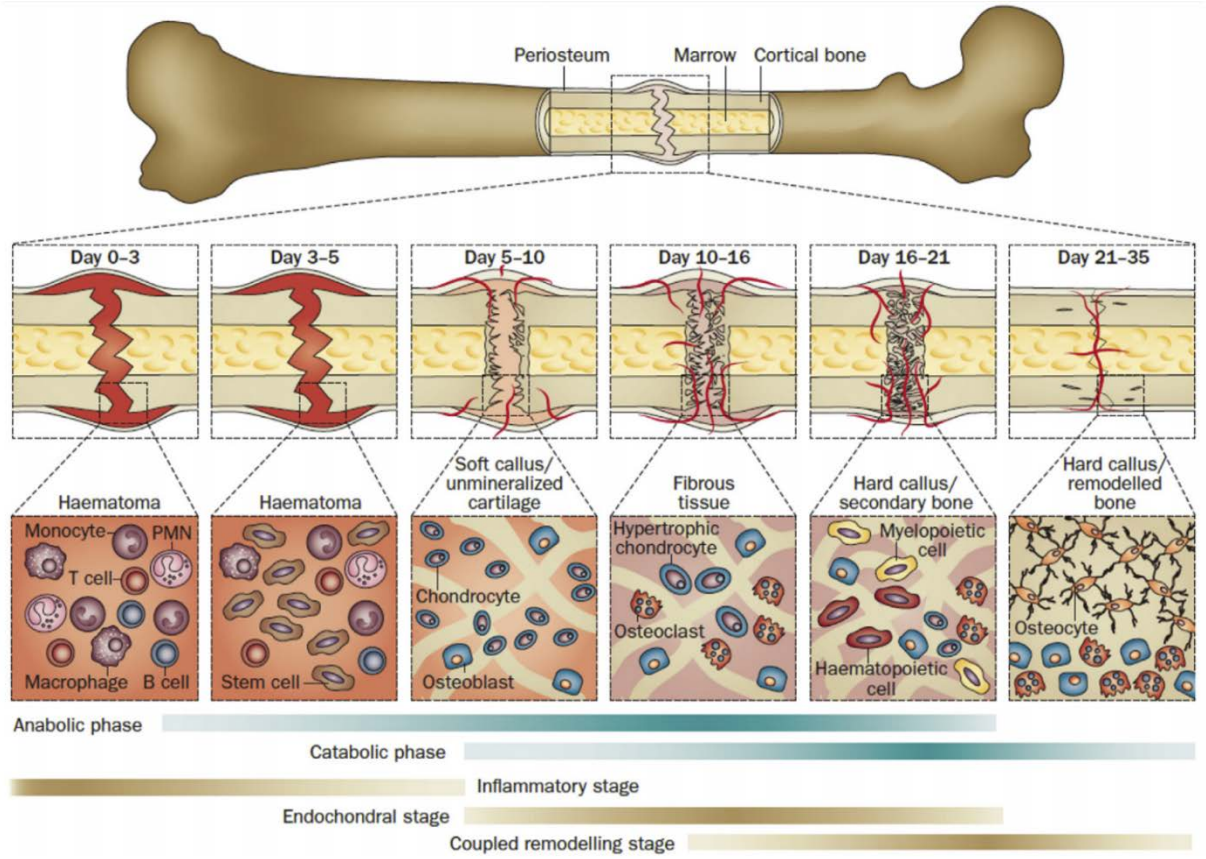

Figure 3. Spatiotemporal sequence of bone healing of the femur (time scale of healing is equivalent to a mouse closed femur fracture fixed with an intramedullary rod). Modified from [25].

When loads are high enough in the skeleton to exceed local critical stress limits and yielding beyond the elastic point, microcracking or fracture may occur. Bone is characterized by an intrinsic regenerative capacity in response to injury [26], [27]. Its repair is also dependent on the blood vessel network. Upon disruption of blood vessels, bone fracture triggers inflammation. Pro-inflammatory signals, tumor necrosis factor-α (TNFα) and interleukin-1β (IL1β), recruit cells for bone formation[20]. This inflammatory stage results in clot formation and is followed by the recapitulation of normal fetal skeletogenesis. Oc degrade necrotic tissue, while Ob cells form new bone. [25], [28].

1.1.3 Bone Damages, clinical procedures and limitations

Worldwide more than 20 million patients are annually affected by a loss of bone tissue caused by trauma, infections, tumors, avascular necrosis or congenital disorders impairing the regeneration process and leading to surgical intervention. With 1 million procedures every

year in the European Union [29], the cost is estimated at about 40 billion Euro and is set to increase by 25% by 2025 [6] especially in regards to the aging of the population [12].

To date the clinical gold standard treatment for bone repair consists in the transplantation of autologous bone grafts with the advantage to be biocompatible and non-immunogenic. They provide osteogenic cells, osteoinductive (sustaining osteoprogenitors) growth factors, and an osteoconductive scaffold, all essential for new bone growth Unfortunately, this strategy is associated with severe donor-site morbidity, high risk of infections and logistic shortcomings. Allografts or xenografts exist as alternative, but have been associated with pathogen transmission and host rejection [30], (Table 1).

Bone graft	Advantages	Disadvantages
Autografts	Optimal osteogenic, osteoinductive, and osteoconductive properties; gold standard for bone grafting; without the risks of immunogenicity and disease transmission	Pain and morbidity in the donor site, limited quantity and availability, need for further surgery, hematoma, infection, the need for general sedation or anesthesia, longer operative time, and blood loss
Allografts	Osteoinductive and osteoconductive properties, without donor site morbidity, possible with local anesthesia, high availability, easy handling	Lack of osteogenic properties, potential antigenic response and disease transmission, variable osteoinductivity, limited supply, loss of biologic and mechanical properties due to its processing, non-availability worldwide due to religious and financial concerns and increased cost
Xenografts	Osteoinductive and osteoconductive properties, low cost, high availability	Lack of osteogenic properties, the risk of immunogenicity and transmission of infectious and zoonotic diseases, poor outcome

Table 1. Some advantages and disadvantages of the most commonly used bone graft types

Other strategies are tested experimentally in patients. Concentrated bone marrow can be combined intraoperatively with a synthetic or natural osteoconducting matrix (bone substitutes) before implantation [31], [32] but still leave bone defect in 20% of the cases. Another consists in the delivery of recombinant growth and differentiation factors such as recombinant BMP-2, capable to induce osteogenesis of resident progenitor cells. However, this approach has been associated with aberrant bone formation, neurotoxicity, cancer development, high costs and short recombinant BMP-2 half-life resulting a difficult tuning of the local application [29], [33], [34].

Long bone segmental critical size defects (4–7 cm length, i.e. after tumor resection) will not heal spontaneously due to cellular insufficiency. Other conditions like non-union (fracture failing to resorb) has been addressed with mitigate success with the use of calcium phosphate bioceramics [35]. Cell therapy solutions providing MSCs intended to enhance osteogenesis. Nevertheless, healing were insufficient to prove enhanced bone [36] an BM and their direct used did not end up in reliable results [37]. Thus, stringent clinical scenario where enhancing

bone regeneration is mandatory requires more than can be achieved only in the operating room.

1.2 Bone tissue engineering

1.2.1 Regenerative medicine and tissue engineering paradigm (TE)

“Regenerative medicine aims at helping the body to form new functional tissue to replace lost or defective ones” [38]. Among regenerative medicine fields, tissue engineering (TE) is composed of multidisciplinary methods at the interface of biology and engineering tackling the difficulties currently encountered in clinical treatments [21]. Skeletal TE started in the early 1970’s as pediatric orthopedic surgeon (W. T. Green), aimed at generating new cartilage using chondrocytes seeded onto spicules of bone and implanted in nude mice [39].

In general, the TE paradigm (Figure 4, a)) consists in incremental steps aiming at the repair of one patient’s organ using its own tissues.

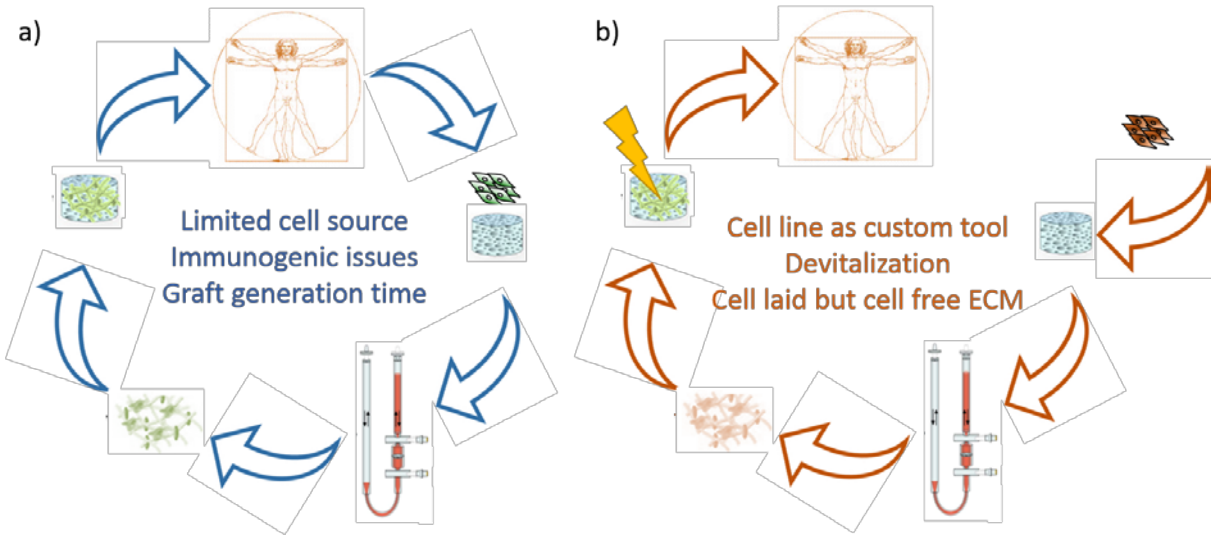

Figure 4: Tissue engineering (TE) paradigms. a) Conventional TE approach based on patient cells. b) Amended TE paradigm based on the use of a cell line and generation of ECM decorated scaffolds for bone TE, devitalized (yellow lightning) prior to implantation.

The paradigm starts with a biopsy-based cell isolation and its proliferation in vitro followed by the seeding of the expanded cells onto a scaffold. Specific culture protocols are applied to stimulate the cells and instruct them to develop a tissue proxy. This step may necessitate specific bioreactor systems optimizing the culture conditions. Ultimately, the in vitro matured tissue now considered as a graft is implanted back to the donor patient.

To address unmet clinical needs in bone regeneration, TE proposed many strategies (Figure 5) relying on the combination of three-dimensional (3D) scaffolds and/or signals and/or autologous progenitor cells [40], [41].

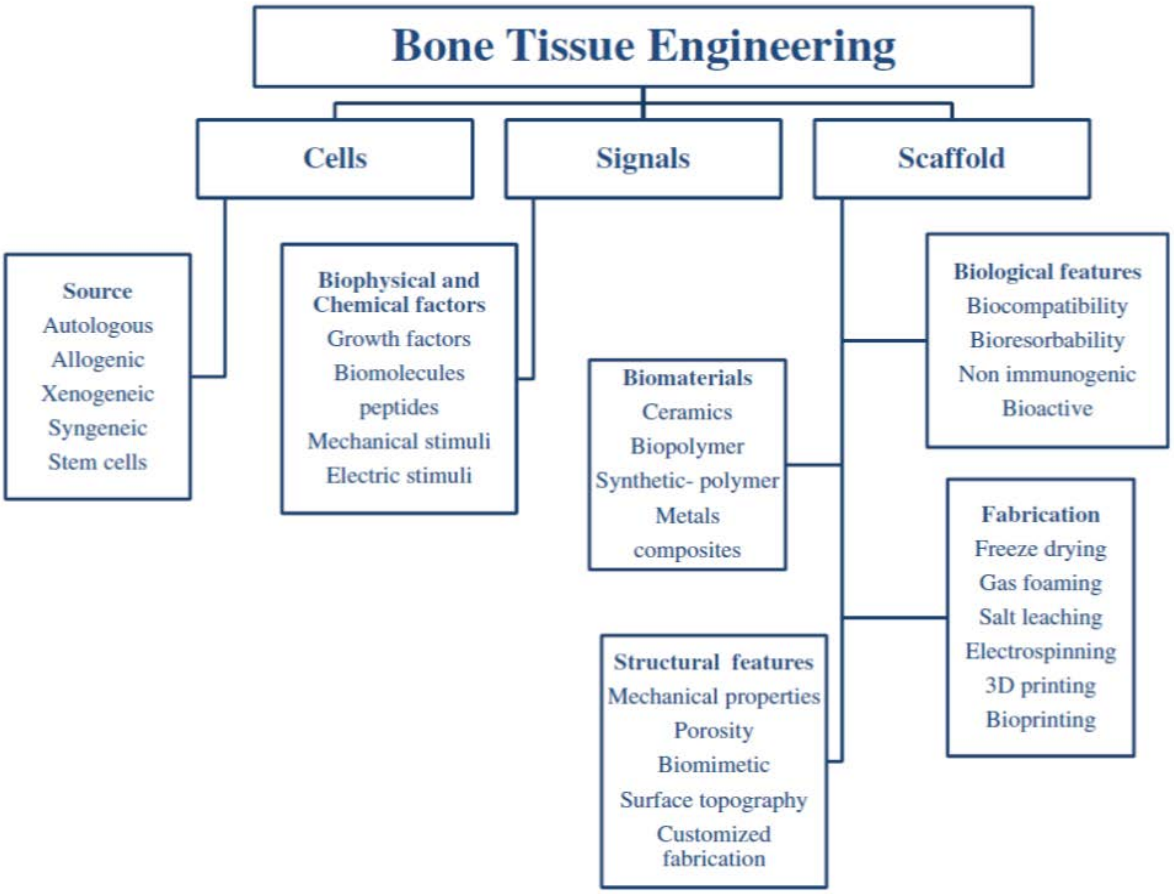

Figure 5. Strategies for bone tissue engineering underlines several key players for cell attachment, growth, and bone tissue formation. From [42].

However, these approaches are still associated with drawbacks and limitations such as the inter-donor variability, limited cell supply [43], [44] and controversy exists about their efficacy and cost-effectiveness. A more attractive strategy (Figure 4, b))consists in the removal of the cellular fraction (devitalization) from the graft prior to its implantation in order to avoid immuno-matching requirements resulting in a graft able to drive tissue repair [45].

1.2.2 Optimal culture conditions

Controlled in vitro culture systems are needed to ensure sterility and simulate the physiologic conditions required for cellular or tissular functions including optimal pH, oxygen concentration, temperature, nutrient transfer, waste removal and promoting cell-cell and cell-matrix interactions [46]. Generation of skeletal tissues based on human MSC usually involves two steps: (1) expansion of MSC to obtain the needed amount of cells for the specific defect/scaffold dimension and (2) their subsequent seeding on scaffolds and differentiation into mature cells.

If 2-dimensional (2D) approaches are the gold standard for classic cell culture and cell expansion, TE requires 3-dimensional (3D) culture systems to recapitulate native tissue architecture. In general, bioreactors and microfluidic systems are designed to perform at least one of the following five functions [47]:

-Achieving uniform cell distribution

-Keeping constant and optimized concentration of gasses and nutrients

-Performing mass transport to the tissue

-Increasing tissue maturation by applying physical stimuli

-Providing information about the formation of 3D tissue by attaching sensors and designing transparent chambers

For the generation of small tissues, passive diffusion is sufficient for a thickness of 100–200. Over this distance, an active fluid circulation is required to overcome the diffusion limit. For this reason, commercially available bioreactors often comprise medium displacement systems, generally used in conjunction with chambers, columns or cartridges to hold the cell-seeded scaffold. Nevertheless, a universal consensus on the optimal bioreactor solution for bone TE is yet to be reached [48], [49]. Among existing bioreactor systems, perfusion-based bioreactors show greater potential towards bone TE applications [50]. Indeed, flow perfusion leads to upregulated expression of osteogenic marker genes including Runx2, ALP, BMP-2, bone sialoprotein, and osteopontin [51] while ECM production is significantly increased by increasing flow velocity and shear stress[52].

1.2.3 Mesenchymal Stromal cells for TE

Mesenchymal stem cells (MSC) were described by Friedenstein et al. in 1970 as fibroblastic cell type producing clonal colonies with the capacity to generate bone in guinea-pig models [53]. Murine models trace MSC back from mesodermal precursors, such as lateral plate mesoderm-derived mesoangioblast-cells from the embryonic dorsal aorta. Other reports suggest they partly descend from a subpopulation of neural crest cells and thus the precise embryonic origin of MSC is still under discussion [54], [55]. In the adult BM, MSCs have been reported to typically localize near the sinusoidal endothelium in close association with the resident HSC. In addition to BM, MSC have also been found in many other tissues, including the synovial membrane, adipose tissue, dental pulp tissue or perinatal tissue, such as umbilical cord blood and umbilical cord tissue. tissues [56].

The International Society for Cellular Therapy (ISCT) defined criteria in 2006 to define human MSC based on their positivity for CD73, CD90 and CD105 markers (>95%) and negativity for CD45, CD34, CD14 or CD11b, CD79α or CD19, and HLA class II (<2%) [57], [58] (Table 2).

Selection type (and comments)	CD No.	Name	Acronym
Negative	**CD11b**	**Integrin subunit alpha M**	**ITGAM**
Negative	**CD14**	**CD14 molecule**	**CD14**
Negative	**CD19**	**CD19 molecule**	**CD19**
Negative (not in all MSC populations)	**CD34**	**CD34 molecule**	**CD34**
Negative	**CD45**	**Protein tyrosine phosphatase, receptor type C**	**PTPRC**
Negative	**CD79a**	**CD79a molecule**	**CD79A**
Negative (unless stimulated with IFN-γ)	—	**Human leukocyte antigen, antigen D Related**	**HLA-DR**
Positive	CD9	CD9 molecule	CD9
Positive	CD10	Membrane metalloendopeptidase	MME
Positive	CD13	Alanyl aminopeptidase, membrane	ANPEP
Positive	CD29	Integrin subunit beta 1	ITGB1
Positive	CD44	CD44 molecule (Indian blood group)	CD44
Positive	CD49f	Integrin subunit alpha 6	ITGA6
Positive	CD54	Intercellular adhesion molecule 1	ICAM1
Positive	CD71	Transferrin receptor	TFRC
Positive	**CD73**	**5′-nucleotidase ecto**	**NT5E**
Positive	**CD90**	**Thy-1 cell surface antigen**	**THY1**
Positive	**CD105**	**Endoglin**	**ENG**

Table 2: Potential surface markers for MSC identification and enrichment. Bolded text indicates the minimal markers recommended by the International Society for Cellular Therapy (ISCT) defining human multipotent mesenchymal stromal cells by positive and negative selection. Adapted from [58]

Despite these specifications, fibroblasts may be named as MSC displaying similar immunophenotypes, differentiation potential, and proliferative capacities [59].

In vitro, MSC are plastic adherent cells that can differentiate into osteoblasts, adipocytes, and chondrocytes after exposure to specific soluble factors [60]. They retain sufficient proliferative and differentiation potential to generate an ECM forming bone-like tissue when differentiated in porous scaffolds under osteoinductive conditions [61] and to repair the skeletal organ upon implantation [62]. They thus have been considered as a versatile and frequently utilized cell source in TE and clinics for bone regeneration [29]. As a result of over five decades of investigation, MSCs exert their healing effects not only through engraftment and

differentiation but also through paracrine signaling and cell-cell contacts communication. They have also been described as modulating immune cells through the actions of a number of molecules, including VEGF, BMP2 and prostaglandin E2 (PGE2) [58], [63].

In addition to growth factors, MSCs also secrete microvesicles (>200 µm) and exosomes (~50–200 µm). Recent evidence suggests that several of the functional components in these cargo could regulate processes of bone formation, inhibit osteoclast activity and promote fracture repair [64]. Nevertheless, the number of MSC within BM aspirate varies among patients (0.001–0.01% of the nucleated cells). Thus, their expansion in culture is needed to reach clinically relevant numbers for therapeutic purposes.

1.2.4 Scaffolding material

Scaffolds characteristics for bone TE need to meet certain requirements for physiological processes described above (Figure 5). Indeed, from immune reaction to wound healing (mainly angiogenesis and bone remodeling…), cell migration is an essential physiological process that requires either specific cellular adaptations to mechanical features of the ECM or, to the contrary, remodeling by the cell striding through [65]. Scaffolding biomaterials composition and porosity should thus allow those cellular movements. Most used biomaterials have been recently reviewed and classified in 3 categories [42], [48]. The first generation of biomaterials has been developed with the aim to “achieve a suitable combination of physical properties to match those of the replaced tissue with a minimal toxic response to the host”. Biologically inert once implanted these materials mainly serves as joint replacements and reinforcements bars. The second generation include osteoconductive biomaterial as synthetic and naturally-derived biodegradable polymers (e.g. collagen, polyesters), calcium phosphates (synthetic or derived from natural materials such as corals, devitalized human or bovine bone), calcium carbonate (natural or synthetic), calcium sulfates, and bioactive glasses. Most commonly used scaffolding biomaterials in clinic and TE applications are calcium-phosphate based such as hydroxyapatite achieving comparable porosity than trabecular bone. The first use of calcium phosphates for bone repair was reported in 1920 by Albee and Morrison in dogs and mainly rabbits, starting research in ceramics [66]. Nevetheless, hydroxyapatite based material are highly stable despite in vivo remodeling remaining potential weak points in the bone [11], [67]. Third generation

biomaterials are designed to incorporate instructive cues into the material rendering them osteoinductive (property of biomaterials to ectopically induce bone formation). Some of these approaches involve insoluble (ECM) and soluble (growth factors, cytokines, hormones and chemicals), factors conjugated or not with external stimuli (mechanical loading, compressive stress, shear stress, cyclic stretch, use of conducting polymers, magnetic actuation) [40], [68]. This latter generation of material paved the way for cell-free but cell laid biomaterials.

1.2.5 Decellularized ECM for bone regeneration

The role of ECM in TE has gained increasing recognition since it can modulate tissue morphology and cellular behavior [65], [69], [70]. Its use has been explored from autologous living MSC “cell sheets” embedded in their excreted ECM [71] to entire decellularized organs (heart, lung kidney liver mainly from porcine or rat origin) [72]. The extension of this concept, the use of cell-free scaffolds (Figure 3) decorated by a cell-laid ECM relies on the capacity of inductive signals, trapped in the secreted ECM, to instruct endogenous cells toward tissue repair [73]–[76]. The collagenous ECM and especially bone devitalized ECM promotes BMP-induced osteogenesis [77] and can be optimized by enrichment in VEGF and/or BMP2 known to enhance both vascularization and bone formation in vivo. Decorated scaffolds have already been used in bone TE in vitro resulting in an enhancement of MSCs differentiation and improved mineralized matrix deposition [45], [78]–[80]. Furthermore, ECM-based scaffolds promote a switch from a predominately M1-like macrophage (pro-inflammatory, cytotoxic) population immediately post-implantation to a population enriched in M2-like macrophages (anti-inflammatory and pro-healing) 1–2 weeks post-implantation thus favoring remodeling and tissue regeneration [81].

The preparation of cell-free ECM-based biomaterials involves devitalization and/or decellularization [61], [82] (Table 3) challenging to keep structure and more sensitive components intact.

Material used for decellularization	Advantages	Disadvantages
Chemical Ex: 1. Acids (per acetic acid, acetic acid) 2. Bases [NaOH, $Ca(OH)_2$, $CaCl_2$, $MgSO_4$]	Solubilize the cytoplasmic components, remove the nucleic acids; it can be used for the preclinical sterilization Removes the dermis	Removes the collagen from the matrix, it disrupts and affects the strength of ECM Eliminate the growth factors and affect the mechanical properties of ECM
Hypotonic solution Ex: Tris–HCl Hypertonic solution Ex: NaCl	Lysis the cell and reduce the time Separates the DNA from protein	Minimal change in ECM Minimal damage of stromal architecture
Detergents Ex: (a) Ionic (SDS) (b) Non-ionic (Triton X-100) (c) Zwitter ion (3-[(3-cholamidopropyl)dimethylammonio]-1- propanesulfonate) (CHAPS)	Solubilize the cell membrane, complete removal of cells It removes cells from thick tissue It has property of both ionic and non-ionic	Highly damage the ECM and loss of GAGs Disrupt and remove the ECM proteins Disrupt the stromal architecture and poor removal of cells
Biological agents (a) Enzymatic: Ex: Trypsin (b) Non-enzymatic Ex: EDTA	Disrupts the protein–protein interaction Separates the cells by separating the metal ions	Disrupts the collagen structure Ineffective cell removal
Physical Ex: (a): Freeze–thawing (b) Hydrostatic pressure	Lysis the cell Increase in the pressure results cell lysis	Disrupt the ECM architecture Expensive

Table 3. Advantages and disadvantages of various methods used for tissue decellularization. Adapted from [82].

In this regard, controlled apoptosis triggering stands as an attractive technique of devitalizing tissue to preserve cell-laid ECM. Notably, the absence of cells allows the storage of decorated scaffolds as off-the-shelf materials and permits to bypass the immuno-matching requirements needed by cell-based strategies. Thus, devitalized ECM are envisioned as biomaterials may become the gold standard[83], [84]. As MSC lose their capacity to proliferate and differentiate in osteoblastic lineage while secreting abundant ECM after a ten passages, a death-inducible human MSC line capable to secrete the ECM and undergo apoptosis after induction has been developed [85]. Using this unlimited and well-characterized cellular tool acellular ECM grafts can be generated in perfusion bioreactor.

1.3 Bone marrow and hematopoiesis

1.3.1 Hematopoiesis

The hematopoietic system supplies our body with more than 4×1011 mature blood cells every day ensuring oxygen transport, immunity, and tissue remodeling [86]. Hematopoietic Stem Cells (HSC) are the key cells with the unique capability to give rise to all blood-cell lineages [87]. The identification of human HSCs was accomplished in 1992 through isolation of a candidate population from the fetal bone marrow [88]. Since then, the cellular and molecular regulation of specific HSC properties such as long-term self-renewal is being elucidated mainly thanks to the study of fish [89] and murine HSCs [90], since experimental access to human bone marrow (BM) remains complicated.

The exact origin and developmental events giving rise to the hematopoietic system in humans are still under investigation. HSCs emerge in the later embryo (intra-embryonic hematopoiesis) in the aorta-gonad mesonephros region, budding from the endothelial floor of the dorsal aorta. The development of this cell population is evolutionarily conserved among many vertebrates and co-expresses endothelial and hematopoietic markers [91], [92]. During later intra utero development, HSCs migrate to the fetal liver, and finally home into the BM, where most hematopoietic progenitors reside throughout adult life [93].

In the adult, HSCs remain in a quiescent state and exit dormancy to restore the homeostasis of the hematopoiesis before returning to a quiescent state. The reversion of HSCs to a quiescent state may minimize replicative stress and DNA damage accumulation, HSC exhaustion, malignant evolution and other possible BM failure [94], [95].

Functional mature blood and immune cells are derived from HSCs [96]. According to the current model, initiation of differentiation is associated with the loss of self-renewal, and several subsequent binary branching decisions lead to a hierarchical tree-like model of hematopoiesis[97], [98] (Figure 1).

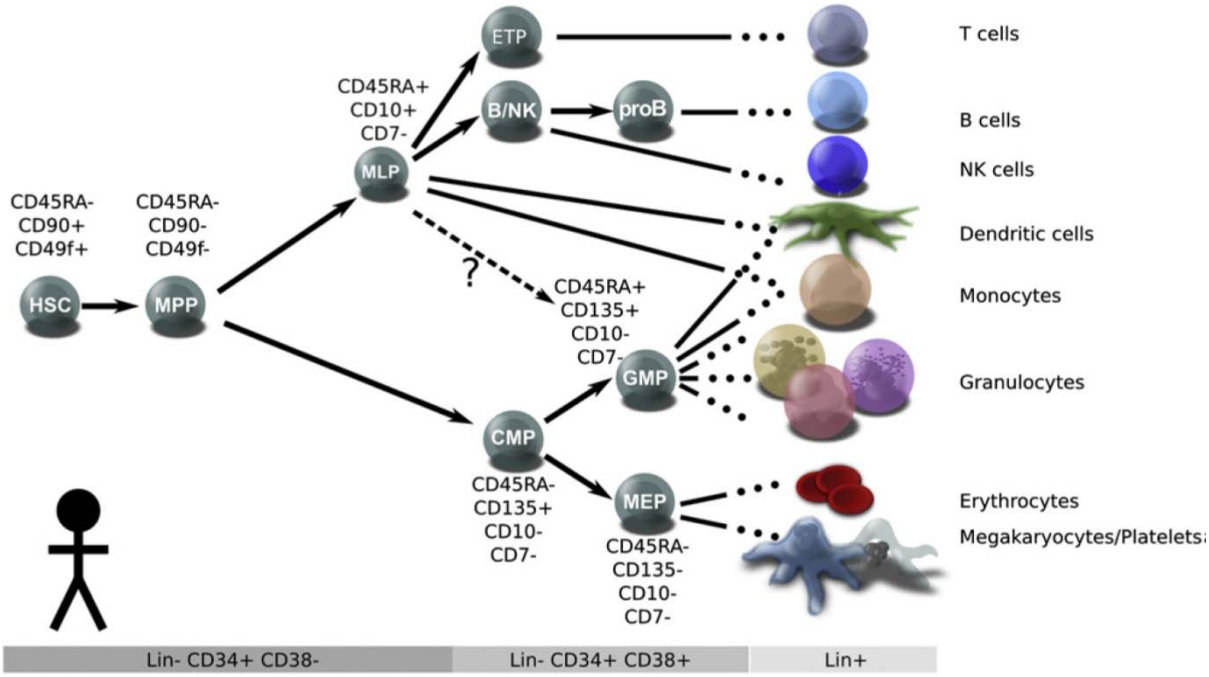

Figure 1. Current model of lineage determination in the adult human hematopoietic hierarchy. The major classes of stem and progenitor cells are defined by cell surface phenotypes listed next to each population and in the gray bars below. Mature blood cells are shown on the right, and inferred lineage relationships are depicted with arrows. Adapted from [87].

This model is mainly based on analyses of FACS-purified cell populations confirmed by in vitro colony formation capacity or long-term in vivo reconstitution of the whole blood tissue in preconditioned murine recipients by transplantation assays. The gold standard functional test consists in xenotransplantation in drastically immunodeficient NSG mouse strains (Non-Obese Diabetic [NOD], Severe Combined ImmunoDeficiency [SCID], IL-2R common ɣ chain deletion (gc-/-)), which lack not only B- and T-, but also functional natural killer (NK)-cells, allowing higher human engraftment rates [99].

Human phenotypic HSCs are defined by their surface markers as CD34+CD38-CD45RA-CD90+ cells. It was recently reported that the adhesion molecule CD49f (integrin α6) also characterizes primitive HSCs. The positivity for this marker has proven to be sufficient for HSC engraftment and blood lineage reconstitution by one single cell after transplantation [100].

The differentiation of phenotypic HSCs toward mature lineages has been extensively reviewed [87]. HSCs exiting quiescence differentiate into multipotent progenitors (MPPs, CD34+CD38-

CD45RA-CD90-) displaying in vitro multi lineage differentiation potential but limited long-term engraftment capacity. MPP will then commit to either lymphoid or myeloid lineages, respectively described as multi lymphoid progenitors (MLPs, CD34+CD38-CD45RA+) and common myeloid progenitors (CMPs, CD34+CD38+CD45RA-). Hematopoietic stem and progenitor cells (HSPCs, CD34+CD38-) define the population commonly used for human transplantation in clinical scenarios, which is composed by HSCs, MPPs and MLPs. MLPs will then only mature and give rise to lymphocytes B, T and NK cells, but both MLPs and CMPs can give rise to granulocyte/macrophages progenitors (GMPs, CD34+CD38-CD45RA+) at the origin of dendritic cells, monocytes and granulocytes (grouping neutrophils, eosinophils, basophils, mast cells). Myelo-erythroid progenitors (MEPs, CD34+CD38-CD45RA-CD135-) will only mature to produce erythroid and megakaryocyte cells later resulting in erythrocytes and platelets. In parallel and grouping some of the previous progenitors, larger groups of CD34+CD38- cells can be considered as committed progenitors and CD34+CD38+ cells as maturing progenitors. It is important to note that CD38 was shown to be unstable in vitro and can be lost in culture without associated phenotype change [101]. These tightly controlled events take place in the adult in a specific microenvironment in the BM, termed the niche, which ensures hematopoietic homeostasis by controlling the proliferation, self-renewal, differentiation of HSCs in health and in response to stress or injury [86].

1.3.2 Hematopoietic Stem Cells Niche

The concept of a stem cell niche for HSCs was first described in 1978 by R. Schoffield [102]. Since then, the adult HSC niche has predominantly been studied with the help of conditional transgenic mouse models to detect and explore in vivo the expression and localization of key niche factors, which has been reviewed extensively [103]. In human, due to difficult accessibility to the adult BM, its exact composition and features remain controversial [25] (Figure 2).

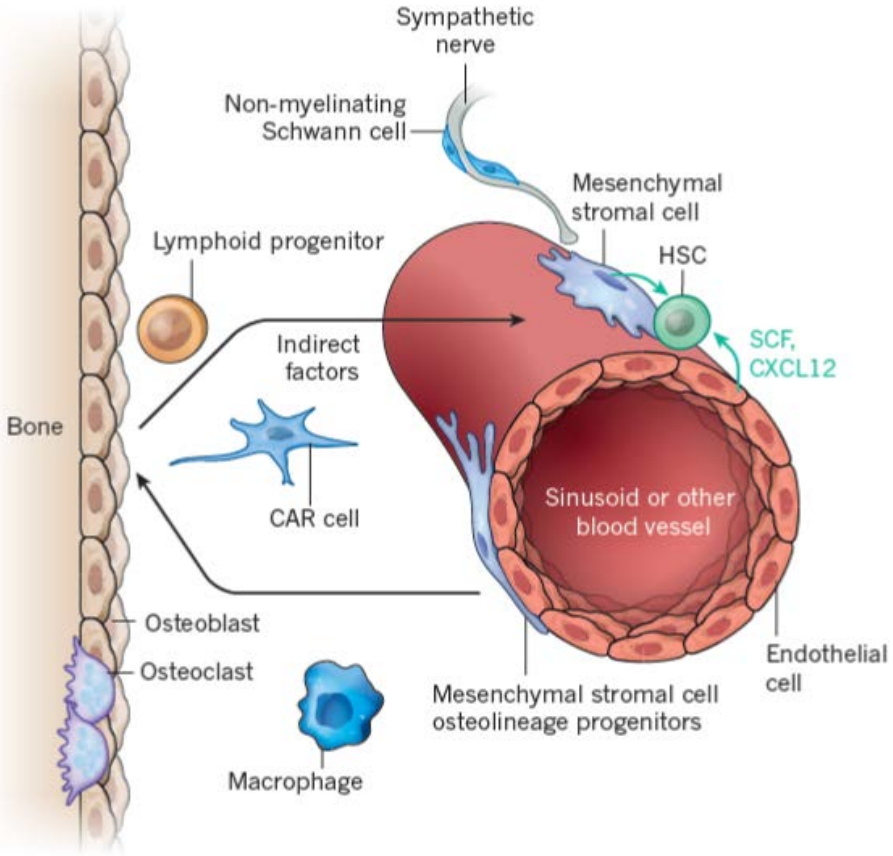

Figure 2. Hematopoietic stem cell (HSC) niche in the bone marrow (here, in rodent model). The HSC niche regroups several cell types (hematopoietic and non-hematopoietic) identified in mice and putative in human, as well as soluble factors (SCF, CXCL12) controlling blood tissue homeostasis in the adult. Adapted from [104].

The human HSC niche is thought to be composed by multiple hematopoietic and non-hematopoietic cell types including mesenchymal stromal cells [105] and more differentiated osteoblasts, osteoclast macrophages, fibroblasts and vascular endothelial cells [104]. Both sympathetic and sensory nerves innervate the bone and BM controlling homing or the release of HSCs and HSPCs from the marrow to peripheral organs [86]. Based on the study of human BM specimens, HSCs reside preferentially in endosteal regions (osteoblastic niche; in the periphery of the BM). Interestingly, a second niche has been described in mice where HSCs are associated to the perivascular microenvironment and more precisely close to sinusoidal vessels (vascular niche; central area of the BM). HSCs from this area also display superior regenerative and self-renewal capacity from those localizing close to the bone surface, the zone preferentially populated by HSPCs [106].

Each “niche cell type” is necessary yet not sufficient. HSC niches are much more complex than the sum of different cell types. Besides the cell-to-cell interactions, multiple factors [107] present in the surrounding extracellular matrix are also synthetized and contribute to HSC niche homeostasis. Two of the best studied cytokines are CXC-chemokine ligand 12 (CXCL12, also known as SDF1α) and stem cell factor (SCF, also known as KIT ligand), which bind to CXC-chemokine receptor 4 (CXCR4) and KIT on HSCs, respectively. Under basal conditions, these cytokines ensure homing to the BM, retention and quiescence of HSCs [108].

A pathological HSC niche results in reduced CXCL12 expression from mesenchymal stromal cells and HSPC mobilization. The HSC niche can also be altered by malignant cells, which disrupts the hemostatic role of multiple stromal cell populations. This might induce increased niche support to malignant cells over normal HSCs [109]–[111].

1.3.3 Blood associated disorders

Common blood disorders include anemia, bleeding disorders, blood clots, and blood cancers. As part of the latter, Myeloproliferative Neoplasms (MPNs) are clonal HSC diseases characterized by increased proliferation of the erythroid, megakaryocytic, or myeloid lineages. MPNs regroups three phenotypic entities: polycythemia vera (PV), essential thrombocythemia (ET) and primary myelofibrosis (PMF) [112], [113] (Figure 3).

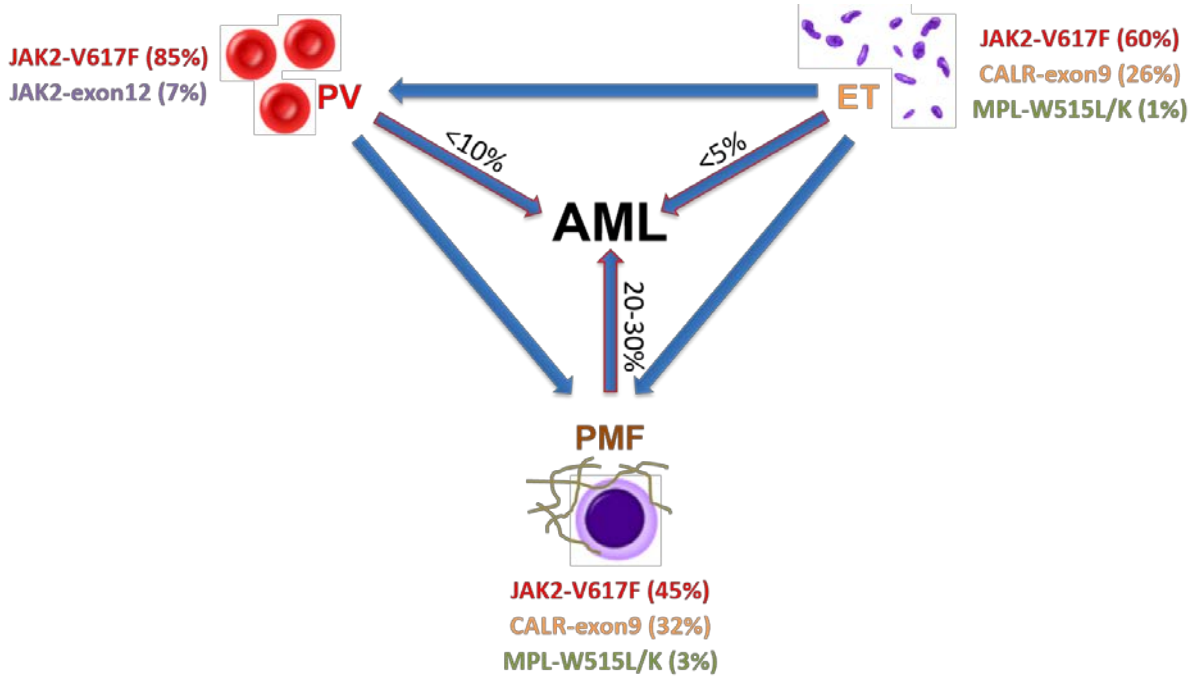

Figure 3. Pathology of myeloproliferative neoplasms (MPN). MPN regroups polycythemia vera (PV), essential thrombocythemia (ET) and primary myelofibrosis (PMF) associated with specific mutated genes (observed frequencies in %). Some of these conditions can derive to another pathology of MPN (blue arrows) and each of them has a probability (blue-red arrows, in %) to evolve towards acute myeloid leukemia (AML). Observed symptoms are splenomegaly, headaches, fatigue, bleeding and thrombotic complications.

The most frequent acquired mutation is JAK2-V617F, is found in >95% of PV patients, and also in about half of the patients with ET or PMF [114]–[117]. This mutation is present in purified phenotypic HSCs, in myeloid lineages of the peripheral blood and in variable proportions of lymphoid cells [118]–[120]. Quantification of the JAK2 mutant allele burden can be used to monitor the size of the mutant clone in the peripheral blood. Each MPN phenotype has an intrinsic risk of evolution into acute myeloid leukemia (AML) depending on numerous different factors (exposure to myelosuppressive therapy, cytogenetic abnormalities and increased number of mutations in cancer associated genes) [121]. AML remains a devastating disease with less than 30% of patients surviving five years after diagnosis. Although the outlook for patients with AML has improved over the past 30 years, still more than half of younger adults and about 90% of elderly patients diagnosed with AML die from the disease [122], [123]. Additionally, leukemic cells surviving chemotherapy in vivo were shown to reside in osteoblastic BM niches [124], which also harbor the most primitive and potent HSCs, as described in 3.2.

Both BM niche disruption due to malignant HSCs and systemic damages (infections, acute blood cells loss, chemotherapy, or irradiation-induced cytotoxicity) alter BM homeostasis. However, the subsequent consequences on HSC biology are still poorly described in humans. MPN transition toward leukemia is associated with poor prognosis and currently the gold clinical standard of care is allogeneic HSC transplants. Transplants have been successfully performed clinically for over 40 years, but their efficacy can be limited due to variable engraftment or donor availability [125]. The development of novel and efficient in vitro systems would contribute to bypass these limitations.

1.3.4 In vitro HSC niche modeling

The capacity of HSCs to survive, self-renew, proliferate and give rise to all blood cell lineages makes them a valuable option for the treatment of blood-associated disorders[87], [126]. However, the scarcity of HSC in adults together with the insufficient number of compatible donors highly restrains the treatment potential [127]. These constraints have led to the development of in vitro systems to expand HSCs for therapeutic purposes [128]. In vitro culture systems initially developed by Dexter and colleagues in 1977 established that BM stromal layers support ex vivo hematopoiesis [129].

Despite substantial improvements, the development of suitable in vitro conditions supporting HSC culture remains a challenge. Typical 2D strategies focus on the maintenance/expansion of CD34 positive hematopoietic progenitor cells on specific materials and/or in co-culture with stromal cell types (murine or human) serving as feeder-layer [130], and supplemented with several growth factors. [131]–[134]. Such strategies result in a mild HSC expansion while maintaining their repopulation capacity [135], [136]. Currently, the use of induced pluripotent stem cells for large-scale production of blood cells is under assessment[127]. This approach could address therapeutic demands on blood cells, but its capacity to mimic and study the human HSC niche biology is rather limited.

2D culture systems cannot reflect the complexity of in vivo microenvironments. 3D approaches explore the use of hydrogels or polymeric scaffold, coated or not with collagen/fibronectin substrates capable of hosting HSC [135], [137]. However, results offered by these models might not be very reliable since the purity of CD34+ seeded cells is variable [138]. A better phenotypic HSC characterization is required to improve this and only few studies assessed the in vitro/in vivo functionality of expanded HSCs. Moreover, these culture systems are based on high concentrations or non-physiologic levels of growth factors. Finally the rare existing 3D macroscale models reviewed [139] require non-commercial devices or animal models for their generation [140], restricting their availability and implementation. The modelling of a HSC niche in disease has partially been explored but mainly based on malignant cells lines [141] known to have limited needs for their survival. An ideal model for blood associated disorders should be able to sustain maintenance and expansion of primary patient hematopoietic progenitors.

Thus, considering the need of a better understanding of healthy and pathological hematopoiesis, as well as the clinical perspectives, the establishment of an improved in vitro protocol sustaining HSC culture while recapitulating human niche biology and mechanisms driving their homeostasis is required. Nevertheless, 3D studies for HSC culture is a promising tool for the engineering of HSC niches [139]. Despite the use of several human cell types, ECM and serum-free soluble compounds, appropriate 3D culture systems remain critical. In this regard, perfusion systems allow homogenous cell seeding, culturing and ECM deposition within scaffolds with superior waste removal and nutrient supply, while introducing the notion of flow as culture parameter [142]. Finally, as the native HSC niche is located in the core of the bone, the use of a porous hydroxyapatite based scaffold is a good template to mimic trabecular BM [143].

1.4 References

[1] P. Driscoll, “Gray’s Anatomy, 39th Edition,” Emerg. Med. J., vol. 23, no. 6, pp. 492–492, Jun. 2006.

[2] B. Clarke, “Normal bone anatomy and physiology.,” Clinical journal of the American Society of Nephrology : CJASN, vol. 3 Suppl 3. 2008.

[3] D. B. Burr and O. Akkus, “Bone Morphology and Organization,” in Basic and Applied Bone Biology, Elsevier Inc., 2013, pp. 3–25.

[4] D. Lopes, C. Martins-Cruz, M. B. Oliveira, and J. F. Mano, “Bone physiology as inspiration for tissue regenerative therapies,” Biomaterials, vol. 185, pp. 240–275, 2018.

[5] S. Gopal, H. A. B. Multhaupt, and J. R. Couchman, “Calcium in Cell-Extracellular Matrix Interactions,” in Advances in Experimental Medicine and Biology, vol. 1131, Springer New York LLC, 2020, pp. 1079–1102.

[6] M. R. Iaquinta et al., “Innovative biomaterials for bone regrowth,” International Journal of Molecular Sciences, vol. 20, no. 3. MDPI AG, 01-Feb-2019.

[7] A. I. Alford, K. M. Kozloff, and K. D. Hankenson, “Extracellular matrix networks in bone remodeling,” International Journal of Biochemistry and Cell Biology, vol. 65. Elsevier Ltd, pp. 20–31, 31-May-2015.

[8] J. Henkel et al., “Bone Regeneration Based on Tissue Engineering Conceptions-A 21st Century Perspective,” Bone Research, vol. 1. Sichuan University, pp. 216–248, 25-Sep-2013.

[9] K. B. S. Paiva and J. M. Granjeiro, “Matrix Metalloproteinases in Bone Resorption, Remodeling, and Repair,” in Progress in Molecular Biology and Translational Science, vol. 148, Elsevier B.V., 2017, pp. 203–303.

[10] E. H. Burger, J. Klein-Nulend, and T. H. Smit, “Strain-derived canalicular fluid flow regulates osteoclast activity in a remodelling osteon - A proposal,” J. Biomech., vol. 36, no. 10, pp. 1453–1459, Oct. 2003.

[11] J. Scheinpflug et al., “Journey into bone models: A review,” Genes, vol. 9, no. 5. MDPI AG, 01-May-2018.

[12] R. Florencio-Silva, G. R. D. S. Sasso, E. Sasso-Cerri, M. J. Simões, and P. S. Cerri, “Biology of Bone Tissue: Structure, Function, and Factors That Influence Bone Cells,” BioMed Research International, vol. 2015. Hindawi Publishing Corporation, 2015.

[13] H. M. Kronenberg, “Developmental regulation of the growth plate,” Nature, vol. 423, no. 6937. pp. 332–336, 15-May-2003.

[14] V. S. Salazar, L. W. Gamer, and V. Rosen, “BMP signalling in skeletal development, disease and repair,” Nature Reviews Endocrinology, vol. 12, no. 4. Nature Publishing Group, pp. 203–221, 01-Apr-2016.

[15] H. K. Datta, W. F. Ng, J. A. Walker, S. P. Tuck, and S. S. Varanasi, “The cell biology of bone metabolism,” Journal of Clinical Pathology, vol. 61, no. 5. pp. 577–587, May-2008.

[16] M. H. Lee, T. G. Kwon, H. S. Park, J. M. Wozney, and H. M. Ryoo, “BMP-2-induced Osterix expression is mediated by Dlx5 but is independent of Runx2,” Biochem. Biophys. Res. Commun., vol. 309, no. 3, pp. 689–694, Sep. 2003.

[17] M. H. Lee et al., “BMP-2-induced Runx2 Expression Is Mediated by Dlx5, and TGF-β1 Opposes the BMP-2-induced Osteoblast Differentiation by Suppression of Dlx5 Expression,” J. Biol. Chem., vol. 278, no. 36, pp. 34387–34394, Sep. 2003.

[18] C. R. M. Black, V. Goriainov, D. Gibbs, J. Kanczler, R. S. Tare, and R. O. C. Oreffo, “Bone Tissue Engineering,” Curr. Mol. Biol. Reports, vol. 1, no. 3, pp. 132–140, Sep. 2015.

[19] S. Stegen, N. van Gastel, and G. Carmeliet, “Bringing new life to damaged bone: The importance of angiogenesis in bone repair and regeneration,” Bone, vol. 70, pp. 19–27, Jan. 2015.

[20] U. H. Langen et al., “Cell-matrix signals specify bone endothelial cells during developmental osteogenesis,” Nat. Cell Biol., vol. 19, no. 3, pp. 189–201, Mar. 2017.

[21] J. J. Li, M. Ebied, J. Xu, and H. Zreiqat, “Current Approaches to Bone Tissue Engineering: The Interface between Biology and Engineering,” Adv. Healthc. Mater., vol. 7, no. 6, Mar. 2018.

[22] E. F. Eriksen, “Cellular mechanisms of bone remodeling,” Reviews in Endocrine and Metabolic Disorders, vol. 11, no. 4. pp. 219–227, Dec-2010.

[23] X. Feng and J. M. McDonald, “Disorders of Bone Remodeling,” Annu. Rev. Pathol. Mech. Dis., vol. 6, no. 1, pp. 121–145, Feb. 2011.

[24] X. Chen, Z. Wang, N. Duan, G. Zhu, E. M. Schwarz, and C. Xie, “Osteoblast–osteoclast interactions,” Connective Tissue Research, vol. 59, no. 2. Taylor and Francis Ltd, pp. 99–107, 04-Mar-2018.

[25] T. A. Einhorn and L. C. Gerstenfeld, “Fracture healing: mechanisms and interventions.”

[26] D. G. Little, M. Ramachandran, and A. Schindeler, “The anabolic and catabolic responses in bone repair,” J. Bone Joint Surg. Br., vol. 89-B, no. 4, pp. 425–433, Apr. 2007.

[27] R. Dimitriou, E. Jones, D. McGonagle, and P. V Giannoudis, “Bone regeneration: current concepts and future directions,” BMC Med., vol. 9, no. 1, p. 66, Dec. 2011.

[28] R. Marsell and T. A. Einhorn, “The biology of fracture healing,” Injury, vol. 42, no. 6, pp. 551–555, 2011.

[29] J. Stanovici et al., “Bone regeneration strategies with bone marrow stromal cells in orthopaedic surgery,” Current Research in Translational Medicine, vol. 64, no. 2. Elsevier Masson SAS, pp. 83–90, 01-Jun-2016.

[30] R. R. Betz, “Limitations of autograft and allograft: new synthetic solutions.,” Orthopedics, vol. 25, no. 5 Suppl, pp. s561-70, May 2002.

[31] P. V. Giannoudis, H. Dinopoulos, and E. Tsiridis, “Bone substitutes: an update.,” Injury, vol. 36 Suppl 3. 2005.

[32] M. Scaglione, L. Fabbri, D. Dell’omo, F. Gambini, and G. Guido, “Long bone nonunions treated with autologous concentrated bone marrow-derived cells combined with dried bone allograft,” Musculoskelet. Surg., vol. 98, no. 2, pp. 101–106, 2014.

[33] A. Nauth, J. Ristiniemi, M. D. McKee, and E. H. Schemitsch, “Bone morphogenetic proteins in open fractures: past, present, and future.,” Injury, vol. 40 Suppl 3. 2009.

[34] I. H. A. Ali and D. P. Brazil, “Bone morphogenetic proteins and their antagonists: Current and emerging clinical uses,” British Journal of Pharmacology, vol. 171, no. 15. John Wiley and Sons Inc., pp. 3620–3632, 2014.

[35] R. Z. Legeros, C. A. Garrido, S. E. Lobo, and F. M. Turíbio, “Biphasic calcium phosphate bioceramics for orthopaedic reconstructions: Clinical outcomes,” Int. J. Biomater., 2011.

[36] E. Gómez-Barrena, P. Rosset, D. Lozano, J. Stanovici, C. Ermthaller, and F. Gerbhard, “Bone fracture healing: Cell therapy in delayed unions and nonunions,” Bone, vol. 70. Elsevier Inc., pp. 93–101, 01-Jan-2015.

[37] P. Hernigou, A. Poignard, F. Beaujean, and H. Rouard, “Percutaneous autologous bone-marrow grafting for nonunions: Influence of the number and concentration of progenitor cells,” J. Bone Jt. Surg. - Ser. A, vol. 87, no. 7, pp. 1430–1437, Jul. 2005.

[38] S. Bajada, I. Mazakova, B. Ashton, J. Richardson, N. Ashammakhi, and S. Bajada, “Stem Cells in Regenerative Medicine Stem cells for regeneration,” 2008.

[39] C. A. Vacanti, “The history of tissue engineering,” J. Cell. Mol. Med., vol. 10, no. 3, pp. 569–576, Jul. 2006.

[40] X. Yu, X. Tang, S. V. Gohil, and C. T. Laurencin, “Biomaterials for Bone Regenerative Engineering,” Advanced Healthcare Materials, vol. 4, no. 9. Wiley-VCH Verlag, pp. 1268–1285, 01-Jun-2015.

[41] A. R. Shrivats, M. C. McDermott, and J. O. Hollinger, “Bone tissue engineering: State of the union,” Drug Discovery Today, vol. 19, no. 6. Elsevier Ltd, pp. 781–786, 2014.

[42] Pearlin, S. Nayak, G. Manivasagam, and D. Sen, “Progress of Regenerative Therapy in Orthopedics,” Current Osteoporosis Reports, vol. 16, no. 2. Current Medicine Group LLC 1, pp. 169–181, 01-Apr-2018.

[43] R. Siddappa, R. Licht, C. van Blitterswijk, and J. de Boer, “Donor variation and loss of multipotency during in vitro expansion of human mesenchymal stem cells for bone tissue engineering,” J. Orthop. Res., vol. 25, no. 8, pp. 1029–1041, Aug. 2007.

[44] A. R. Amini, C. T. Laurencin, and S. P. Nukavarapu, “Bone tissue engineering: Recent advances and challenges,” Crit. Rev. Biomed. Eng., vol. 40, no. 5, pp. 363–408, 2012.

[45] N. Sadr et al., “Enhancing the biological performance of synthetic polymeric materials by decoration with engineered, decellularized extracellular matrix,” Biomaterials, vol. 33, no. 20, pp. 5085–5093, Jul. 2012.

[46] H. C. Chen and Y. C. Hu, “Bioreactors for tissue engineering,” Biotechnology Letters, vol. 28, no. 18. pp. 1415–1423, Sep-2006.

[47] R. F. Canadas, A. P. Marques, R. L. Reis, and J. M. Oliveira, “Bioreactors and microfluidics for osteochondral interface maturation,” in Advances in Experimental Medicine and Biology, vol. 1059, Springer New York LLC, 2018, pp. 395–420.

[48] D. Confalonieri, A. Schwab, H. Walles, and F. Ehlicke, “Advanced Therapy Medicinal Products: A Guide for Bone Marrow-derived MSC Application in Bone and Cartilage Tissue Engineering.,” Tissue Eng. Part B. Rev., vol. 24, no. 2, pp. 155–169, 2018.

[49] C. Kleinhans et al., “A perfusion bioreactor system efficiently generates cell-loaded bone substitute materials for addressing critical size bone defects,” Biotechnol. J., vol. 10, no. 11, pp. 1727–1738, Nov. 2015.

[50] E. J. Arnsdorf, P. Tummala, and C. R. Jacobs, “Non-canonical Wnt signalling and N-cadherin related β-catenin signalling play a role in mechanically induced osteogenic cell fate,” PLoS One, vol. 4, no. 4, Apr. 2009.

[51] B. Birru, K. Mekala, and S. Rao Parcha, “Mechanistic role of perfusion culture on bone regeneration,” J. Biosci., vol. 44, 2038.

[52] W. L. Grayson, P. H. G. Chao, D. Marolt, D. L. Kaplan, and G. Vunjak-Novakovic, “Engineering custom-designed osteochondral tissue grafts,” Trends in Biotechnology, vol. 26, no. 4. pp. 181–189, Apr-2008.

[53] A. J. Friedenstein, R. K. Chailakhjan, and K. S. Lalykina, “THE DEVELOPMENT OF FIBROBLAST COLONIES IN MONOLAYER CULTURES OF GUINEA-PIG BONE MARROW AND SPLEEN CELLS,” Cell Prolif., vol. 3, no. 4, pp. 393–403, 1970.

[54] C. A. Gregory, H. Singh, A. S. Perry, and D. J. Prockop, “The Wnt signaling inhibitor Dickkopf-1 is required for reentry into the cell cycle of human adult stem cells from bone marrow,” J. Biol. Chem., vol. 278, no. 30, pp. 28067–28078, Jul. 2003.

[55] H. Miwa and T. Era, “Tracing the destiny of mesenchymal stem cells from embryo to adult bone marrow and white adipose tissue via pdgfrα expression,” Dev., vol. 145, no. 2, Jan. 2018.

[56] B. Sacchetti et al., “No identical ‘mesenchymal stem cells’ at different times and sites: Human committed progenitors of distinct origin and differentiation potential are incorporated as adventitial cells in microvessels,” Stem Cell Reports, vol. 6, no. 6, pp. 897–913, Jun. 2016.

[57] M. Dominici et al., “Minimal criteria for defining multipotent mesenchymal stromal cells. The International Society for Cellular Therapy position statement,” Cytotherapy, vol. 8, no. 4, pp. 315–317, Aug. 2006.

[58] R. E. B. Fitzsimmons, M. S. Mazurek, A. Soos, and C. A. Simmons, “Mesenchymal stromal/stem cells in regenerative medicine and tissue engineering,” Stem Cells International, vol. 2018. Hindawi Limited, 2018.

[59] M. Soundararajan and S. Kannan, “Fibroblasts and mesenchymal stem cells: Two sides of the same coin?,” J. Cell. Physiol., vol. 233, no. 12, pp. 9099–9109, 2018.

[60] M. Manfrini et al., “Mesenchymal stem cells from patients to assay bone graft substitutes,” J. Cell. Physiol., vol. 228, no. 6, pp. 1229–1237, Jun. 2013.

[61] J. Ng, K. Spiller, J. Bernhard, and G. Vunjak-Novakovic, “Biomimetic Approaches for Bone Tissue Engineering,” Tissue Engineering - Part B: Reviews, vol. 23, no. 5. Mary Ann Liebert Inc., pp. 480–493, 01-Oct-2017.

[62] E. Schipani and H. M. Kronenberg, Adult mesenchymal stem cells. 2008.

[63] N. G. Singer and A. I. Caplan, “Mesenchymal Stem Cells: Mechanisms of Inflammation,” Annu. Rev. Pathol. Mech. Dis, vol. 6, pp. 457–478, 2011.

[64] A. Pethő, Y. Chen, and A. George, “Exosomes in Extracellular Matrix Bone Biology,” Current Osteoporosis Reports, vol. 16, no. 1. Current Medicine Group LLC 1, pp. 58–64, 01-Feb-2018.

[65] K. M. Yamada and M. Sixt, “Mechanisms of 3D cell migration,” Nature Reviews Molecular Cell Biology. Nature Publishing Group, 2019.

[66] F. H. ALBEE and H. F. MORRISON, “STUDIES IN BONE GROWTH,” Ann. Surg., vol. 71, no. 1, p. 32???39, Jan. 1920.

[67] L. Wang and G. H. Nancollas, “Calcium orthophosphates: Crystallization and Dissolution,” Chem. Rev., vol. 108, no. 11, pp. 4628–4669, Nov. 2008.

[68] S. F. Badylak, “The extracellular matrix as a biologic scaffold material,” Biomaterials, vol. 28, no. 25, pp. 3587–3593, Sep. 2007.

[69] Y. Bi et al., “Extracellular matrix proteoglycans control the fate of bone marrow stromal cells,” J. Biol. Chem., vol. 280, no. 34, pp. 30481–30489, Aug. 2005.

[70] T. Rozario and D. W. DeSimone, “The extracellular matrix in development and morphogenesis: A dynamic view,” Developmental Biology, vol. 341, no. 1. Academic Press Inc., pp. 126–140, 2010.

[71] M. Chen et al., “Mesenchymal stem cell sheets: a new cell-based strategy for bone repair and regeneration,” Biotechnology Letters, vol. 41, no. 3. Springer Netherlands, pp. 305–318, 15-Mar-2019.

[72] D. A. Taylor, L. C. Sampaio, Z. Ferdous, A. S. Gobin, and L. J. Taite, “Decellularized matrices in regenerative medicine,” Acta Biomaterialia, vol. 74. Acta Materialia Inc, pp. 74–89, 01-Jul-2018.

[73] P. H. Krebsbach and L. G. Villa-Diaz, “The Role of Integrin α6 (CD49f) in Stem Cells: More than a Conserved Biomarker,” Stem Cells Dev., vol. 26, no. 15, pp. 1090–1099, Aug. 2017.

[74] Q. P. Pham, F. Kurtis Kasper, L. Scott Baggett, R. M. Raphael, J. A. Jansen, and A. G. Mikos, “The influence of an in vitro generated bone-like extracellular matrix on osteoblastic gene expression of marrow stromal cells,” Biomaterials, vol. 29, no. 18, pp. 2729–2739, Jun. 2008.

[75] N. Datta, H. L. Holtorf, V. I. Sikavitsas, J. A. Jansen, and A. G. Mikos, “Effect of bone extracellular matrix synthesized in vitro on the osteoblastic differentiation of marrow stromal cells,” Biomaterials, vol. 26, no. 9, pp. 971–977, Mar. 2005.

[76] N. Datta, Q. P. Pham, U. Sharma, V. I. Sikavitsas, J. A. Jansen, and A. G. Mikos, “In vitro generated extracellular matrix and fluid shear stress synergistically enhance 3D osteoblastic differentiation,” Proc. Natl. Acad. Sci. U. S. A., vol. 103, no. 8, pp. 2488–2493, Feb. 2006.

[77] G. Chen and Y. Lv, “Decellularized bone matrix scaffold for bone regeneration,” in Methods in Molecular Biology, vol. 1577, Humana Press Inc., 2018, pp. 239–254.

[78] Y. Kang, S. Kim, J. Bishop, A. Khademhosseini, and Y. Yang, “The osteogenic differentiation of human bone marrow MSCs on HUVEC-derived ECM and β-TCP scaffold,” Biomaterials, vol. 33, no. 29, pp. 6998–7007, Oct. 2012.

[79] Y. Kang, S. Kim, A. Khademhosseini, and Y. Yang, “Creation of bony microenvironment with CaP and cell-derived ECM to enhance human bone-marrow MSC behavior and delivery of BMP-2,” Biomaterials, vol. 32, no. 26, pp. 6119–6130, Sep. 2011.

[80] R. A. Thibault, L. Scott Baggett, A. G. Mikos, and F. K. Kasper, “Osteogenic differentiation of mesenchymal stem cells on pregenerated extracellular matrix scaffolds in the absence of osteogenic cell culture supplements.,” Tissue Eng. Part A, vol. 16, no. 2, pp. 431–40, Feb. 2010.

[81] B. N. Brown et al., “Macrophage phenotype as a predictor of constructive remodeling following the implantation of biologically derived surgical mesh materials,” 2011.

[82] A. A. Khan, S. K. Vishwakarma, A. Bardia, and J. Venkateshwarulu, “Repopulation of decellularized whole organ scaffold using stem cells: an emerging technology for the development of neo-organ,” J. Artif. Organs, vol. 17, no. 4, pp. 291–300, Dec. 2014.

[83] Q. Yao, Y. W. Zheng, Q. H. Lan, L. Kou, H. L. Xu, and Y. Z. Zhao, “Recent development and biomedical applications of decellularized extracellular matrix biomaterials,” Materials Science and Engineering C, vol. 104. Elsevier Ltd, 01-Nov-2019.

[84] A. Haumer, P. E. Bourgine, P. Occhetta, G. Born, R. Tasso, and I. Martin, “Delivery of cellular factors to regulate bone healing,” Advanced Drug Delivery Reviews, vol. 129. Elsevier B.V., pp. 285–294, 01-Apr-2018.

[85] P. Bourgine, C. Le Magnen, S. Pigeot, J. Geurts, A. Scherberich, and I. Martin, “Combination of immortalization and inducible death strategies to generate a human mesenchymal stromal cell line with controlled survival,” Stem Cell Res., vol. 12, no. 2, pp. 584–598, 2014.

[86] S. Pinho and P. S. Frenette, “Haematopoietic stem cell activity and interactions with the niche,” Nat. Rev. Mol. Cell Biol., vol. 20, no. 5, pp. 303–320, 2019.

[87] S. Doulatov, F. Notta, E. Laurenti, and J. E. Dick, “Hematopoiesis: A human perspective,” Cell Stem Cell, vol. 10, no. 2. pp. 120–136, 03-Feb-2012.

[88] C. M. Baum, I. L. Weissman, A. S. Tsukamoto, A. M. Buckle, and B. Peault, “Isolation of a candidate human hematopoietic stem-cell population,” Proc. Natl. Acad. Sci. U. S. A., vol. 89, no. 7, pp. 2804–2808, 1992.

[89] S. J. Wattrus and L. I. Zon, “Stem cell safe harbor: the hematopoietic stem cell niche in zebrafish.,” Blood Adv., vol. 2, no. 21, pp. 3063–3069, 2018.

[90] A. Rongvaux et al., “Development and function of human innate immune cells in a humanized mouse model,” Nat. Biotechnol., vol. 32, no. 4, pp. 364–372, 2014.

[91] A. Medvinsky and E. Dzierzak, “Definitive hematopoiesis is autonomously initiated by the AGM region,” Cell, vol. 86, no. 6, pp. 897–906, Sep. 1996.

[92] G. Swiers, N. A. Speck, and M. F. T. R. de Bruijn, “Visualizing Blood Cell Emergence from Aortic Endothelium,” Cell Stem Cell, vol. 6, no. 4. pp. 289–290, 02-Apr-2010.

[93] A. Ivanovs, S. Rybtsov, E. S. Ng, E. G. Stanley, A. G. Elefanty, and A. Medvinsky, “Human haematopoietic stem cell development: From the embryo to the dish,” Dev., vol. 144, no. 13, pp. 2323–2337, 2017.

[94] A. Nakamura-Ishizu, H. Takizawa, and T. Suda, “The analysis, roles and regulation of quiescence in hematopoietic stem cells,” Development (Cambridge), vol. 141, no. 24. Company of Biologists Ltd, pp. 4656–4666, 15-Dec-2014.

[95] D. Walter et al., “Exit from dormancy provokes DNA-damage-induced attrition in haematopoietic stem cells,” Nature, vol. 520, no. 7548, pp. 549–552, Apr. 2015.

[96] L. Velten et al., “Continuous Process,” vol. 19, no. 4, pp. 271–281, 2017.

[97] L. Wahlster and G. Q. Daley, “Progress towards generation of human haematopoietic stem cells,” Nat. Cell Biol., vol. 18, no. 11, pp. 1111–1117, 2016.

[98] L. Velten et al., “Human haematopoietic stem cell lineage commitment is a continuous process,” Nat. Cell Biol., vol. 19, no. 4, pp. 271–281, Mar. 2017.

[99] L. D. Shultz et al., “ Human Lymphoid and Myeloid Cell Development in NOD/LtSz- scid IL2R γ null Mice Engrafted with Mobilized Human Hemopoietic Stem Cells ,” J. Immunol., vol. 174, no. 10, pp. 6477–6489, May 2005.

[100] R. Majeti, C. Y. Park, and I. L. Weissman, “Identification of a Hierarchy of Multipotent Hematopoietic Progenitors in Human Cord Blood,” Cell Stem Cell, vol. 1, no. 6, pp. 635–645, Dec. 2007.

[101] D. Von Laer et al., “Loss of CD38 antigen on CD34+ CD38+ cells during short-term culture [5],” Leukemia, vol. 14, no. 5, pp. 947–948, 2000.

[102] R. Schofield, “The relationship between the spleen colony-forming cell and the haemopoietic stem cell. A hypothesis,” Blood Cells, vol. 4, no. 1–2, pp. 7–25, 1978.

[103] K. Szade et al., “Where Hematopoietic Stem Cells Live: The Bone Marrow Niche,” Antioxidants and Redox Signaling, vol. 29, no. 2. Mary Ann Liebert Inc., pp. 191–204, 10-Jul-2018.

[104] S. J. Morrison and D. T. Scadden, “The bone marrow niche for haematopoietic stem cells,” Nature, vol. 505, no. 7483, pp. 327–334, 2014.

[105] A. García-García, C. L. F. de Castillejo, and S. Méndez-Ferrer, “BMSCs and hematopoiesis,” Immunol. Lett., vol. 168, no. 2, pp. 129–135, 2015.

[106] B. Guezguez et al., “Regional localization within the bone marrow influences the functional capacity of human HSCs,” Cell Stem Cell, vol. 13, no. 2, pp. 175–189, Aug. 2013.

[107] C. C. Zhang and H. F. Lodish, “Cytokines regulating hematopoietic stem cell function,” Current Opinion in Hematology, vol. 15, no. 4. pp. 307–311, Jul-2008.

[108] T. Itkin and T. Lapidot, “SDF-1 keeps HSC quiescent at home,” Blood, vol. 117, no. 2. pp. 373–374, 13-Jan-2011.

[109] L. M. Calvi and D. C. Link, “The hematopoietic stem cell niche in homeostasis and disease,” Blood, vol. 126, no. 22, pp. 2443–2451, 2015.

[110] Q. Wei and P. S. Frenette, “Niches for Hematopoietic Stem Cells and Their Progeny,” Immunity, vol. 48, no. 4. Cell Press, pp. 632–648, 17-Apr-2018.

[111] J. Hoggatt, Y. Kfoury, and D. T. Scadden, “Hematopoietic Stem Cell Niche in Health and Disease,” Annu. Rev. Pathol. Mech. Dis., vol. 11, no. 1, pp. 555–581, May 2016.

[112] T. Barbui, J. Thiele, H. Gisslinger, G. Finazzi, A. M. Vannucchi, and A. Tefferi, “The 2016 revision of WHO classification of myeloproliferative neoplasms: Clinical and molecular advances,” Blood Reviews, vol. 30, no. 6. Churchill Livingstone, pp. 453–459, 01-Nov-2016.

[113] T. Barbui et al., “The 2016 WHO classification and diagnostic criteria for myeloproliferative neoplasms: document summary and in-depth discussion,” Blood cancer journal, vol. 8, no. 2. p. 15, 09-Feb-2018.

[114] R. Kralovics et al., “A gain-of-function mutation of JAK2 in myeloproliferative disorders,” N. Engl. J. Med., vol. 352, no. 17, pp. 1779–1790, Apr. 2005.

[115] R. L. Levine et al., “Activating mutation in the tyrosine kinase JAK2 in polycythemia vera, essential thrombocythemia, and myeloid metaplasia with myelofibrosis,” Cancer Cell, vol. 7, no. 4, pp. 387–397, 2005.

[116] C. James et al., “A unique clonal JAK2 mutation leading to constitutive signalling causes polycythaemia vera,” Nature, vol. 434, no. 7037, pp. 1144–1148, Apr. 2005.

[117] E. J. Baxter et al., “Acquired mutation of the tyrosine kinase JAK2 in human myeloproliferative disorders,” Lancet, vol. 365, no. 9464, pp. 1054–1061, Mar. 2005.

[118] C. H. M. Jamieson et al., “The JAK2 V617F mutation occurs in hematopoietic stem cells in polycythemia vera and predisposes toward erythroid differentiation,” Proc. Natl. Acad. Sci. U. S. A., vol. 103, no. 16, pp. 6224–6229, Apr. 2006.

[119] F. Delhommeau et al., “Evidence that the JAK2 G1849T (V617F) mutation occurs in a lymphomyeloid progenitor in polycythemia vera and idiopathic myelofibrosis,” Blood, vol. 109, no. 1, pp. 71–77, Jan. 2007.

[120] S. Li, R. Kralovics, G. De Libero, A. Theocharides, H. Gisslinger, and R. C. Skoda, “Clonal heterogeneity in polycythemia vera patients with JAK2 exon12 and JAK2-Y617F mutations,” Blood, vol. 111, no. 7, pp. 3863–3866, Apr. 2008.

[121] A. Iurlo, D. Cattaneo, and U. Gianelli, “Blast transformation in myeloproliferative neoplasms: Risk factors, biological findings, and targeted therapeutic options,” International Journal of Molecular Sciences, vol. 20, no. 8. MDPI AG, 02-Apr-2019.

[122] G. Marcucci and C. D. Bloomfield, “ASH SAP 6 2016 Acute Myeloid Leukemia,” pp. 1–15, 2015.

[123] F. Ferrara and C. A. Schiffer, “Acute myeloid leukaemia in adults,” in The Lancet, 2013, vol. 381, no. 9865, pp. 484–495.

[124] F. Ishikawa et al., “Chemotherapy-resistant human AML stem cells home to and engraft within the bone-marrow endosteal region,” Nat. Biotechnol., vol. 25, no. 11, pp. 1315–1321, Nov. 2007.

[125] K. Hodby and D. Pamphilon, “Concise review: Expanding roles for hematopoietic cellular therapy and the blood transfusion services,” Stem Cells, vol. 29, no. 9. pp. 1322–1326, Sep-2011.

[126] L. Metheny, P. Caimi, and M. de Lima, “Cord Blood Transplantation: Can We Make it Better?,” Front. Oncol., vol. 3, 2013.

[127] M. Hansen, M. von Lindern, E. van den Akker, and E. Varga, “Human induced pluripotent stem cell-derived blood products: state of the art and future directions,” FEBS Lett., pp. 1–16, 2019.

[128] P. Flores-Guzmán, V. Fernández-Sánchez, and H. Mayani, “Concise Review: Ex Vivo Expansion of Cord Blood-Derived Hematopoietic Stem and Progenitor Cells: Basic Principles, Experimental Approaches, and Impact in Regenerative Medicine,” Stem Cells Transl. Med., vol. 2, no. 11, pp. 830–838, Nov. 2013.

[129] T. M. Dexter, T. D. Allen, and L. G. Lajtha, “Conditions controlling the proliferation of haemopoietic stem cells in vitro,” J. Cell. Physiol., vol. 91, no. 3, pp. 335–344, 1977.

[130] M. C. Prewitz et al., “Tightly anchored tissue-mimetic matrices as instructive stem cell microenvironments,” Nat. Methods, vol. 10, no. 8, pp. 788–794, Aug. 2013.

[131] M. Jiang et al., “Maintenance of human haematopoietic stem and progenitor cells in vitro using a chemical cocktail,” Cell Discov., vol. 4, no. 1, 2018.

[132] A. E. Boitano et al., “Aryl hydrocarbon receptor antagonists promote the expansion of human hematopoietic stem cells,” Science (80-.)., vol. 329, no. 5997, pp. 1345–1348, Sep. 2010.

[133] I. Fares et al., “Pyrimidoindole derivatives are agonists of human hematopoietic stem cell self-renewal,” Science (80-.)., vol. 345, no. 6203, pp. 1509–1512, Sep. 2014.

[134] M. A. Walasek, R. van Os, and G. de Haan, “Hematopoietic stem cell expansion: challenges and opportunities,” Ann. N. Y. Acad. Sci., vol. 1266, no. 1, pp. 138–150, Aug. 2012.

[135] M. S. V. Ferreira et al., “Two-dimensional polymer-based cultures expand cord blood-derived hematopoietic stem cells and support engraftment of NSG mice.,” Tissue Eng. Part C. Methods, vol. 19, no. 1, pp. 25–38, Jan. 2013.

[136] M. S. Ventura Ferreira et al., “Cord blood-hematopoietic stem cell expansion in 3D fibrin scaffolds with stromal support,” Biomaterials, vol. 33, no. 29, pp. 6987–6997, Oct. 2012.

[137] A. Raic, L. Rödling, H. Kalbacher, and C. Lee-Thedieck, “Biomimetic macroporous PEG hydrogels as 3D scaffolds for the multiplication of human hematopoietic stem and progenitor cells,” Biomaterials, vol. 35, no. 3, pp. 929–940, Jan. 2014.

[138] T. Mortera-Blanco, A. Mantalaris, A. Bismarck, N. Aqel, and N. Panoskaltsis, “Long-term cytokine-free expansion of cord blood mononuclear cells in three-dimensional scaffolds,” Biomaterials, vol. 32, no. 35, pp. 9263–9270, Dec. 2011.

[139] S. M. Dellatore, A. S. Garcia, and W. M. Miller, “Mimicking stem cell niches to increase stem cell expansion,” Current Opinion in Biotechnology, vol. 19, no. 5. pp. 534–540, Oct-2008.

[140] Y. S. Torisawa et al., “Bone marrow-on-a-chip replicates hematopoietic niche physiology in vitro,” Nat. Methods, vol. 11, no. 6, pp. 663–669, 2014.

[141] T. M. Blanco, A. Mantalaris, A. Bismarck, and N. Panoskaltsis, “The development of a three-dimensional scaffold for ex vivo biomimicry of human acute myeloid leukaemia,” Biomaterials, vol. 31, no. 8, pp. 2243–2251, 2010.

[142] D. Wendt, A. Marsano, M. Jakob, M. Heberer, and I. Martin, “Oscillating perfusion of cell suspensions through three-dimensional scaffolds enhances cell seeding efficiency and uniformity,” Biotechnol. Bioeng., vol. 84, no. 2, pp. 205–214, Oct. 2003.

[143] J. R. Porter, T. T. Ruckh, and K. C. Popat, “Bone tissue engineering: A review in bone biomimetics and drug delivery strategies,” Biotechnol. Prog., vol. 25, no. 6, pp. 1539–1560, Nov. 2009.

Chapter 2. Aims of the thesis

1.5 General aim of the thesis

The bone organ has two main functions in the adult. a) It provides mechanical support and protects organs, while b) the bone marrow hosts hematopoiesis, a process ensuring lifelong production and renewal of the blood tissue. Therefore, the general aim of my thesis is to engineer mesenchymal tissues able to support bone healing and bone marrow functions. Their recapitulation in vitro by using primary hMSCs (or mesenchymal cell lines) could: (i) help fulfilling a clinical need in bone regenerative medicine by providing engineered off-the-shelf coated extracellular matrix (ECM) with tunable compositions, and (ii) provide an animal-free model to study bone biology and hematology in health and disease. These aims are addressed through a combination of hMSCs and 3D perfusion bioreactor systems.

1.6 Specific aims of the chapters

1.6.1 Chapter 1: Engineering of VEGF-enriched mesenchymal tissues

Article: *Engineered extracellular matrices (ECMs) as biomaterials of tunable composition and function*

This chapter serves as proof of concept that a material coated with the ECM secreted by a standardized, immortalized and death-inducible mesenchymal cell line (MSOD) is able to trigger a process of endogenous bone regeneration upon in vivo implantation. In this first chapter, vascular endothelial growth factor alpha (VEGFa) is used as first instructive signal to engineer VEGF-enriched grafts for bone regeneration. The originality of the present approach here described lies on the opportunity to trigger apoptosis in MSOD cells in order to generate devitalized constructs. The use of this controlled mechanism leads to a clean and efficient cell death while preserving ECM components compared to standard devitalization procedures (e.g. freeze/thaw treatment). The better preservation of ECM components and embedded VEGFa leads to a dense vasculature and enhanced bone formation upon implantation in nude rat's calvarias defects.

1.6.2 Chapter 2: Engineering of BMP2-enriched mesenchymal tissues

Project Report: *3D in vitro engineering of decellularized osteoinductive grafts using a custom-designed hMSC line*

This chapter explores another genetic modification of the MSOD cell line to overexpress Bone Morphogenic Protein 2 (BMP2) as main osteoinductive factor. By exploiting the same concept described in Chapter 1, the goal is to generate and characterize a BMP2-overexpressing MSOD cell line (MSOD-B), and the subsequent cell-free BMP2 enriched ECM grafts, in 3D-perfusion bioreactors. The osteoinductivity of BMP2 engineered grafts in comparison to non-enriched scaffolds or uncoated material is evaluated in vivo, and revealing mature bone formation in the sole condition of devitalized MSOD-B grafts.

1.6.3 Chapter 3: Engineering of mesenchymal tissues supporting healthy hematopoiesis

Article: *In vitro biomimetic engineering of a human hematopoietic niche with functional properties*

As some bone tissue engineering applications are aiming at transplanting osteoinductive material to restore functionality of the full bone organ, these grafts should be also engineered to contain bone marrow (BM) and to sustain hematopoiesis. This chapter pursues the establishment of an in vitro BM niche based on the principles described in the previous chapters, but with hydroxyapatite scaffolds seeded with primary hMSC. This BM analog offers an experimentally accessible and tunable platform to study human hematopoiesis. The resulting 3D engineered niche (eN) recapitulates some of the composition of the BM hematopoietic microenvironment elements. eN can sustain hematopoiesis, as revealed by the maintenance and expansion of CD34+ hematopoietic stem and progenitors cells (HSPCs) from human cord blood. Importantly, eN preserve their functionality both in vitro and in vivo.

1.6.4 Chapter 4: Engineering of mesenchymal tissues supporting malignant hematopoiesis

Project Report: *In vitro engineering of a human bone marrow proxy to model myeloproliferative neoplasms.*

This chapter extends the use of the previously described eN in the malignant context of myeloproliferative neoplasm (MPN). The capacity of eN in maintaining MPN phenotypes and function has been assessed replacing healthy hematopoietic cells by HSPCs from patient's phlebotomies. This chapter also explores the possibility to standardize the eN by using MSOD cells cultured on collagen sponges in 3D perfusion bioreactors. This work validates the possibility to extend the concept of engineered BM proxy to disease modeling and standardization, setting the basis for personalized and custom-designed drug testing platforms.

Chapter 3. Engineering of VEGF-enriched mesenchymal tissues

Article: *Engineered extracellular matrices (ECMs) as biomaterials of tunable composition and function*

FULL PAPER

Engineered Extracellular Matrices as Biomaterials of Tunable Composition and Function

*Paul Emile Bourgine, Emanuele Gaudiello, Benjamin Pippenger, Claude Jaquiery, Thibaut Klein, Sebastien Pigeot, Atanas Todorov Jr., Sandra Feliciano, Andrea Banfi, and Ivan Martin**

Engineered and decellularized extracellular matrices (ECM) are receiving increasing interest in regenerative medicine as materials capable to induce cell growth/differentiation and tissue repair by physiological presentation of embedded cues. However, ECM production/decellularization processes and control over their composition remain primary challenges. This study reports engineering of ECM materials with customized properties, based on genetic manipulation of immortalized and death-inducible human mesenchymal stromal cells (hMSC), cultured within 3D porous scaffolds under perfusion flow. The strategy allows for robust ECM deposition and subsequent decellularization by deliberate cell-apoptosis induction. As compared to standard production and freeze/thaw treatment, this grants superior preservation of ECM, leading to enhanced bone formation upon implantation in calvarial defects. Tunability of ECM composition and function is exemplified by modification of the cell line to overexpress vascular endothelial growth factor alpha (VEGF), which results in selective ECM enrichment and superior vasculature recruitment in an ectopic implantation model. hMSC lines culture under perfusion-flow is pivotal to achieve uniform scaffold decoration with ECM and to streamline the different engineering/decellularization phases in a single environmental chamber. The findings outline the paradigm of combining suitable cell lines and bioreactor systems for generating ECM-based off-the-shelf materials, with custom set of signals designed to activate endogenous regenerative processes.

1. Introduction

The role of the extracellular matrix (ECM) in tissue engineering has gained increasing recognition, not only as supportive structural template[1,2] but also as reservoir of inductive cues capable to instruct regenerative processes.[3,4] If processed as acellular materials, ECMs can be stored off-the-shelf[5] and bypass immuno-matching requirements, thereby offering an engaging alternative to living tissue grafts engineered out of autologous cells.

ECM can be derived from pre-existing tissue (native ECM, nECM) after isolation and subsequent decellularization[6] (e.g., demineralized bone matrix, Matrigel). Their structure/composition can match the target tissue, whereby the inherent biological recognition[7] would potentially result in effectiveness of repair. However, in addition to purification, immunogenicity and pathogen transmission issues,[8] nECM typically suffers from batch-to-batch variability,[8] derived from the source of material. Moreover, the decellularization protocols can significantly impair the nECM integrity[9,10] (structure and composition) and challenge the generation of cell-free material with standardized potency.[11,12]

These limitations have driven the development of synthetic ECM (sECM) alternatives. These include scaffolding materials capable of driving endogenous repair events by relying on the targeted delivery of bioactive substances embedded or presented within ECM molecules.[1] The emergence of technical advances such as matrix–peptide-conjugation,[13,14] proteolytic site integration[15] or advanced micropatterning[16] converged toward enabling recapitulation of the natural protein diversity and distribution found in nECM.[14,17] Predominantly developed in the form of hydrogels, sECM thus currently holds great promise as fully tunable system of increasing complexity. Despite their proof-of-principle effectiveness in specific regenerative contexts, including bone repair[13] and induction of angiogenesis,[18] sECMs carry inherent limits. To date, synthetic strategies only allow for the release of single or a limited combination of growth factors, and their presentation (biochemically, temporally, and spatially) remains artificial.[13]

In the attempt of combining the physiological diversity of multiple interacting molecules found in nECM with the tunability of artificially designed sECM, biomaterials manufactured by decoration of scaffolds with cell-laid ECM (engineered ECM,

Dr. P. E. Bourgine, Dr. E. Gaudiello, B. Pippenger, Prof. C. Jaquiery, T. Klein, S. Pigeot, Dr. A. Todorov Jr., S. Feliciano, Dr. A. Banfi, Prof. I. Martin
Departments of Biomedicine and of Surgery
University Hospital Basel
University of Basel
Hebelstrasse 20, CH-4031 Basel, Switzerland
E-mail: Ivan.martin@usb.ch
Dr. P. E. Bourgine
Department of Biosystems Science and Engineering
Eidgenössische Technische Hochschule (ETH) Zurich
Mattenstrasse 26, CH-4058 Basel, Switzerland

DOI: 10.1002/adfm.201605486

eECM) have been proposed.[19–21] Previous studies reported the feasibility of in vitro engineering tissue inductive ECM, which following decellularization retained some of their instructive functions.[21] However, these were based on the use of human primary cells, inherently limited by donor-related variability and lack of control toward target properties.

In this study, we aimed at exemplifying the paradigm of standardized and customized eECM. In particular, we tested the hypothesis that designed human cell lines can be used to achieve efficient ECM deposition and decellularization, with the possibility of targeted enrichment in the content and delivery of specific molecules. The developed strategy was based on immortalized human mesenchymal stromal cells (hMSC)[22] carrying an inducible suicide function serving as intrinsic decellularization strategy.[23] Cells were cultured in 3D under perfusion flow to achieve efficiency and uniformity of tissue manufacturing. The resulting eECM was demonstrated to function as a customizable biomaterial, with regeneration potency both in ectopic and orthotopic models of bone formation and tissue vascularization.

2. Results

2.1. Engineering of ECM Constructs

Constructs were generated by dynamic seeding and differentiation of the Mesenchymal Sword of Damocles (MSOD) stromal cell line on porous ceramic materials cultured within a perfusion bioreactor (Figure S1, Supporting Information). A two-phase protocol was adopted, consisting in one week of proliferation medium (PM) to increase cell numbers and ensure colonization of the material. This was subsequently followed by three weeks of osteogenic medium (OM) supplementation to promote cell osteogenic differentiation while stimulating ECM production. This resulted in a total culture period of four weeks.

After overnight seeding, cells were shown to be homogenously distributed within the pores of the ceramic by tetrazolium assay (MTT staining, **Figure 1**A). A total of 0.52 million (±0.0077) cells were found on the ceramic scaffolds (day 1, Figure 1B), corresponding to a 70% seeding efficiency. A 3.1-fold cell expansion was reached after one week in PM, followed by an additional 3.8-fold increase in cell number during the subsequent three weeks in OM (Figure 1B). At the end of the 3D culture, ceramic scaffolds were decorated with a layer of cells and collagen-rich ECM, extending from the surface toward the pore voids (scanning electron microscopy (SEM) and Masson's trichrome, Figure 1A and Figure S2A,B, Supporting Information), as compared to the original "naked" material (Figure S3, Supporting Information). This was confirmed by immunofluorescence, revealing MSOD cells largely embedded in a collagen type 1 matrix (Figure 1C). Similar results were obtained using alternative scaffolds, in a variety of compositions and architectures (Figure S4, Supporting Information), indicating the robustness of the method.

During the four weeks culture on the ceramic scaffolds, the MSOD cells differentiated toward the osteogenic lineage. This was shown by detection of osteocalcin (OC) in the cytosol of MSOD cells, also present to a limited extent in the surrounding ECM (Figure 1D). Gene expression analysis of typical osteogenic markers confirmed immunofluorescence observations, with the increased expression of RUNX2, alkalyne-phosphatase (ALP), OC, osterix (OSX), and bone sialoprotein (BSP) of 2.1-, 12.1-, 3.2-, 17.1-, and 6.1-fold, respectively (Figure 1E), as compared to undifferentiated cells (day 0, seeding day). Matrix metallopeptidase 13 (MMP-13) was also strongly upregulated (17-fold, Figure 1E), consistent with the process of collagen matrix remodeling toward mineralization.[24] Cell differentiation was further confirmed at the protein level by intracellular staining and subsequent flow-cytometric quantification of Stro-1, ALP, and OC protein expression, selected as markers of mesenchymal progenitors, early and late-osteoblastic differentiation, respectively. After four weeks of culture in bioreactor, the majority of cells positively expressed OC (82.2%, Figure 1D), ALP was produced by 26.5% (Figure 1F), while solely 3.7% expressed the Stro-1 progenitor marker. In comparison, the starting MSOD population was shown to express 1.6%, 0.6%, and 4.1% of OC, ALP, and Stro-1 (day 0, Figure 1F).

Taken together, these data demonstrate the possibility to engineer ECM-coated scaffolds by proliferation and induction of osteogenic differentiation of the MSOD line on a ceramic substrate under perfusion flow.

2.2. Decellularization of Engineered ECM

The resulting constructs were decellularized (or not, Living) either by means of standard Freeze and Thaw (F&T) technique or induction of apoptosis (Apoptized) by convecting the chemical inducer of apoptosis within the generated tissues thanks to the perfusion culture.

Both decellularization methods resulted in an important cell death, with 92.4% and 97.5% positivity for Annexin-V/PI in the F&T and Apoptized groups, respectively (**Figure 2**A). Living grafts displayed 13.6% of cell death (Figure 2A). These results were confirmed by MTT staining, indicating cellular metabolic activity only in Living grafts (Figure 2B). The use of the perfusion system offered the possibility to dynamically remove cellular/DNA debris postdecellularization, leading to 81.4% and 72.5% of DNA removal in F&T and Apoptized constructs, respectively (Figure S5, Supporting Information).

The impact of the decellularization procedures was subsequently assessed by total collagen quantification, as main structural proteins of the ECM. As compared to the Living grafts, total collagen content was reduced by 74.2% following F&T treatment, whereas it was maintained in the Apoptized group (Figure 2C). In addition to structural proteins, luminex-based analysis was performed to evaluate the content of a panel of representative factors involved in angiogenic (vascular endothelial growth factor alpha (VEGF),[25] Interleukin-8 (IL-8),[26] stromal cell-derived factor 1 alpha (SDF-1α),[27]) inflammation (IL-8,[28] macrophage colony-stimulating factor (M-CSF)[29]), osteoclastogenesis (SDF-1α[30]) processes, and hMSC recruitment (M-CSF,[29] SDF-1α[30]). As compared to F&T, the apoptotic method allowed for superior preservation of ECM-embedded cytokines (Figure 2D), with content of IL-8, M-CSF, and VEGF being, respectively, 4.8-, 1.9-, and 3.5-fold higher. However, none of the decellularization methods entirely preserved the

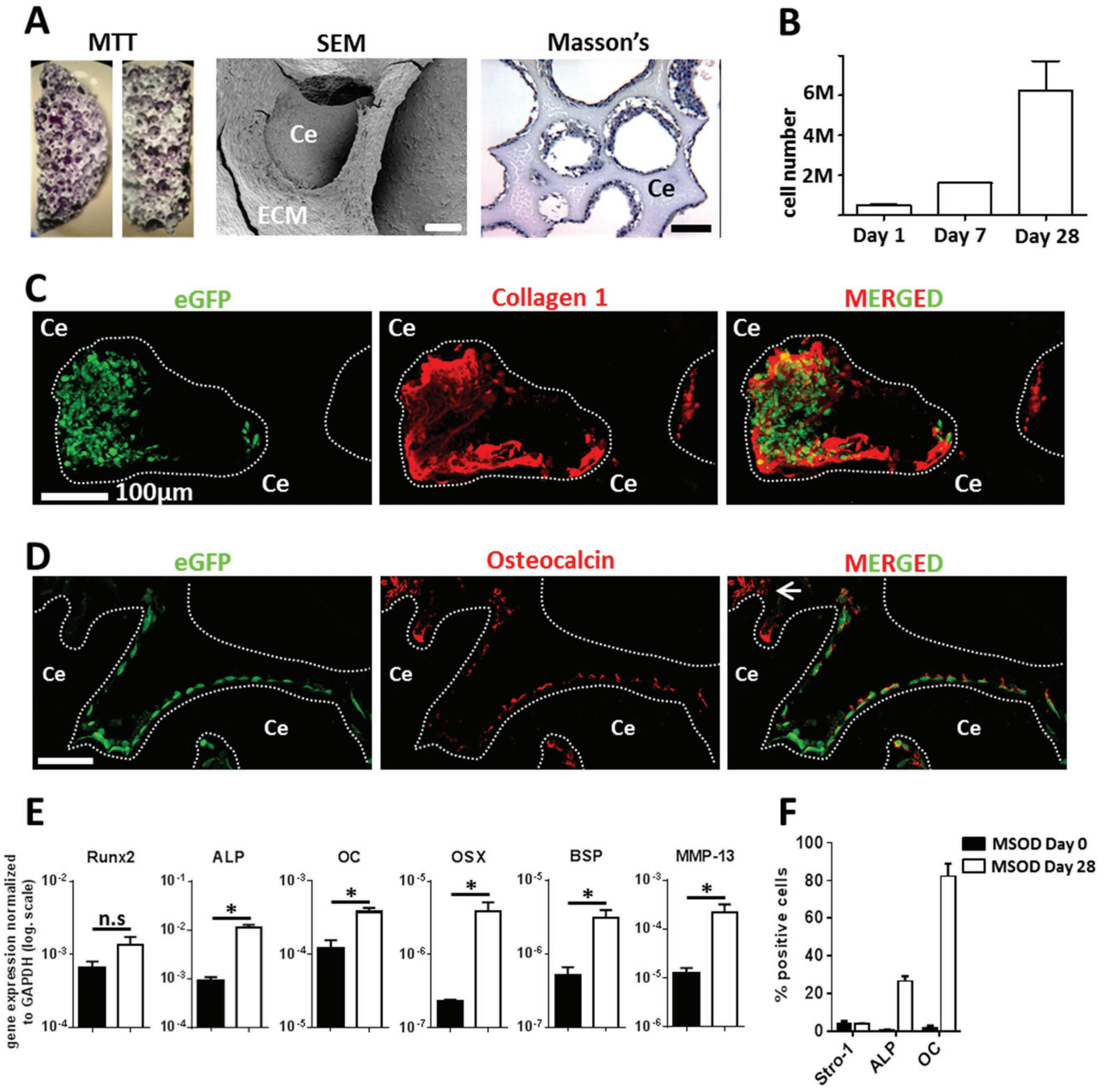

Figure 1. Engineering of ECM-coated scaffold in perfusion bioreactor. A) Representative MTT, scanning electron microscopy, and Masson's trichrome staining of the engineered construct after four weeks in perfusion bioreactor (scale bar = 100 µm). Cells and associated ECM are deposited on the surface of the material. Ce = ceramic, ECM = extracellular matrix. B) Proliferation of MSOD cells during the bioreactor culture phase at day 1, 7, and 28. C) Immunofluorescence analysis of the deposited ECM. MSOD cells (GFP positive, green) are embedded within a collagen type 1 (red) matrix that fills the pore of the material. eGFP = enhanced Green Fluorescent Protein, Scale bar = 100 µm. D) Immunofluorescence analysis of the deposited ECM. Osteocalcin (red) is predominantly detected in the cytosol of the MSOD cells (green). To a limited extent, osteocalcin could also be detected in the ECM (white arrow). Scale bar = 100 µm. E) Gene expression pattern of MSOD prior to (white) and after culture in perfusion bioreactor (black) ($n = 3$, $^*P < 0.05$, n.s = not significant). ALP = alkalyne phosphatase, OC = osteocalcin, OSX = osterix, BSP = bone sialopro F) Percentage of Stro-1, alkalyne phosphatase (ALP), and osteocalcin (OC) positive cells within the MSOD population before (black) and after four weeks of perfusion bioreactor culture (white).

ECM composition, as exemplified by the marked loss in SDF-1α in both F&T (85%) and Apoptized (73%) groups when compared to Living grafts.

Hence, the use of a dedicated cell line with intrinsic decellularization capacity resulted in ECM-coated materials with enhanced preservation of composition.

2.3. Bone Repair Capacity of Engineered Grafts

The bone-forming capacity of generated constructs was assessed by implantation into critically sized cranial defects in nude rats (Figure S6A, Supporting Information). The acellular scaffold (empty) was also implanted as control condition.

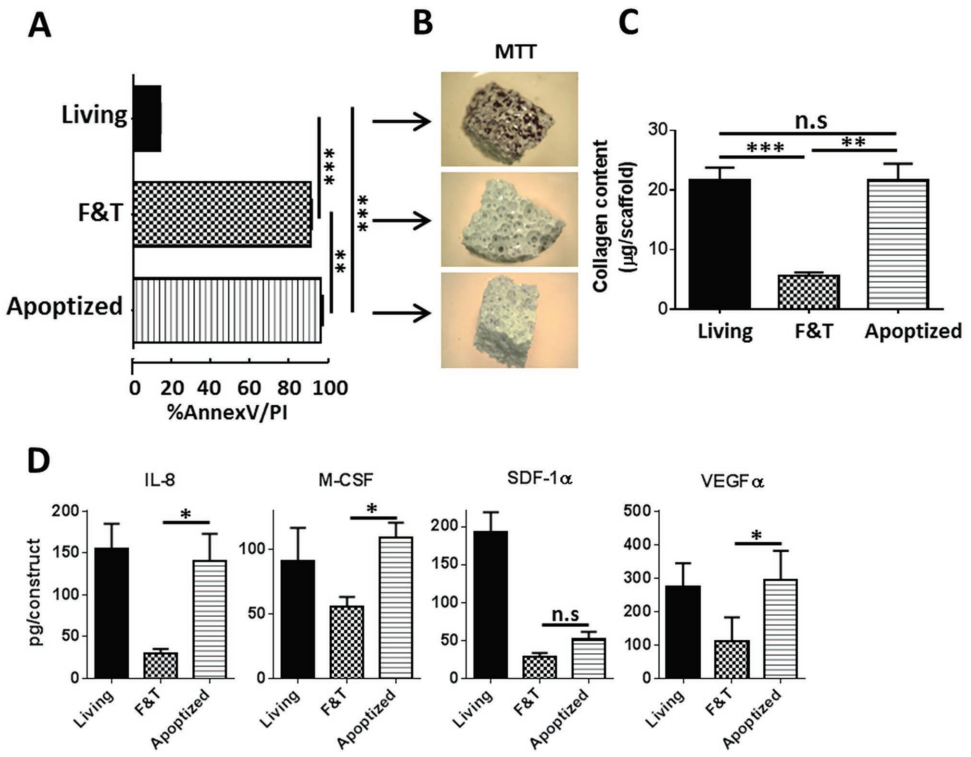

Figure 2. Decellularization of engineered grafts. A) Flow cytometry quantification of cell death by Annexin-V/PI stainings in nondecellularized constructs (Living), decellularized by Freeze & Thaw (F&T), or by apoptosis induction (Apoptized) ($n \geq 3$, $^{**}P < 0.01$, $^{***}P < 0.001$). B) MTT staining of engineered grafts prior to (Living) and after decellularization procedure. C) Total collagens content in constructs before (Living) and postdecellularization treatments by mean of F&T or apoptosis (Apoptized) ($n \geq 4$, $^{**}P < 0.01$, $^{***}P < 0.001$, n.s = not significant). D) Luminex-based quantification of Interleukin-8 (IL-8), macrophage colony-stimulating factor (M-CSF), stromal cell-derived factor 1 alpha (SDF-1α) and vascular endothelial growth factor alpha (VEGF) in corresponding grafts ($n \geq 3$, $^{*}P < 0.05$, n.s = not significant).

After 12 weeks in vivo, μCT analysis of F&T samples indicated the formation of mineralized tissue principally localized at the periphery of the implants, suggesting a mechanism of osteoconduction rather than osteoinduction (**Figure 3**A; Figure S6B, Supporting Information). Conversely, Living and Apoptized grafts promoted mineralized tissue formation up to the inner part of the defect (Figure 3A; Figure S7, Supporting Information), in significantly higher percentages as compared to F&T samples (respectively, 5.2- and 7.8-fold increase, Figure 3B).

The formation of de novo frank bone tissue within implanted grafts was assessed by histological analysis. Remarkably, newly formed bone tissue appeared mature in all groups with no evident qualitative distinction from the host bone matrix (Figure 3C; Figure S6B, Supporting Information). The dark-red Masson's trichrome positivity revealed the presence of elastin in the bone matrix, also strongly stained by Eosin (deep-orange, Figure 3C). Immunohistochemical stainings indicated the presence of mature, Osterix positive osteoblastic cells in the bone matrix, with osteocalcin positivity in the surrounding ECM (Figure 3C). The presence of human cells was only detected in the Living group as revealed by arthrobacter luteus (ALU)-repeats staining (Figure 3C). However, their presence was extremely marginal, suggesting a massive cell death and/or migration outside the defect area. This could be explained by the previously reported unfavorable orthotopic environment for hMSC.[31]

Quantification of de novo bone tissue formation was performed by histomorphometric processing of sectioned samples (Figure 3D), in order to avoid possible μCT biased analysis derived from the presence of ceramic substrate and/or immature calcified tissue. In the Apoptized group, a 5.5-fold increase in the percentage of newly formed bone covering the defect site was found as compared to the F&T (Figure 3D). Interestingly, no statistical difference in the percentage of bone formation was observed between Living and Apoptized groups, suggesting a limited contribution of implanted mesenchymal cells in the bone formation in Living grafts, to be correlated with the low frequency of hMSC detected within Living implants after 12 weeks in vivo.

Overall, we demonstrate the functional superiority of Apoptized grafts in supporting bone regeneration as compared to F&T treated constructs, likely due to the improved preservation of ECM composition.

The generated constructs were then ectopically implanted in nude rats, as a stringent test of osteoinductivity. After 12 weeks, Living and Apoptized samples were more strongly stained for bone sialoprotein and osteocalcin than those decellularized by F&T, indicating the development of a more mature osteoid tissue (Figure S8, Supporting Information). However, since no frank bone tissue was observed in any experimental group, the materials cannot be formally defined as osteoinductive.

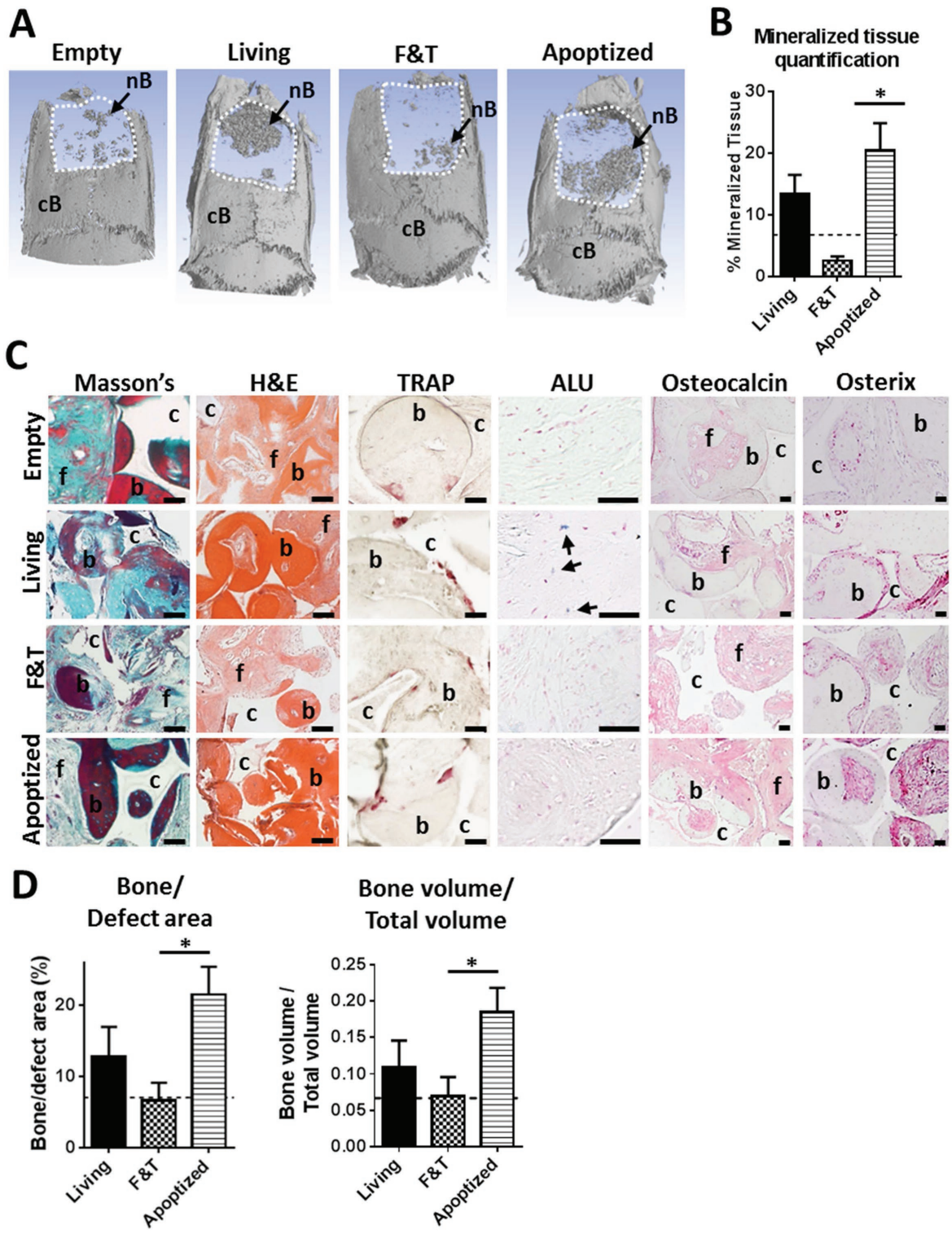

Figure 3. Bone repair capacity of engineered grafts. A) 3D microtome reconstitution of cranial defect 12 weeks postimplantation based on the full *z*-stacks (top view). cB = calvarial bone, nB = new bone. B) Microtome-based quantification of mineralized tissue formation within the cranial defect ($n = 3$, $^*P < 0.05$). C) Histological analysis of the bone tissue by Masson's trichrome, Hematoxylin & Eosin (H&E), tartrate-resistant acid phosphatase (TRAP), ALU, osteocalcin, and osterix stainings of explanted grafts. Arrows indicate positively stained human cells for ALU repeats (scale bars = 50×10^{-6} M). f = fibrous tissue, b = bone, c = ceramic. D) Histomorphometric quantification of newly formed bone tissue within engineered constructs ($n = 3$, $^*P < 0.05$), displayed as bone/defect area based on histological analysis (left) and bone volume/total volume based on microcomputerized tomography analysis (right). Dashed lines represent indicative values of the material without cells/ECM decoration (empty; $n = 1$), consistent with previous literature reports.[45]

2.4. Engineering of VEGF-Enriched ECM-Coated Grafts

The possibility to preserve ECM-associated factors by apoptotic decellularization opens the prospective for a targeted ECM enrichment in specific cues. To exemplify this paradigm, we designed engineered ECM with enhanced content in VEGF, as a potent promoter of vascularization.[32]

To this end, a VEGF-over-expressing hMSC line was generated by retroviral transduction of the original MSOD cells (**Figure 4**A). Successfully transduced cells were purified by

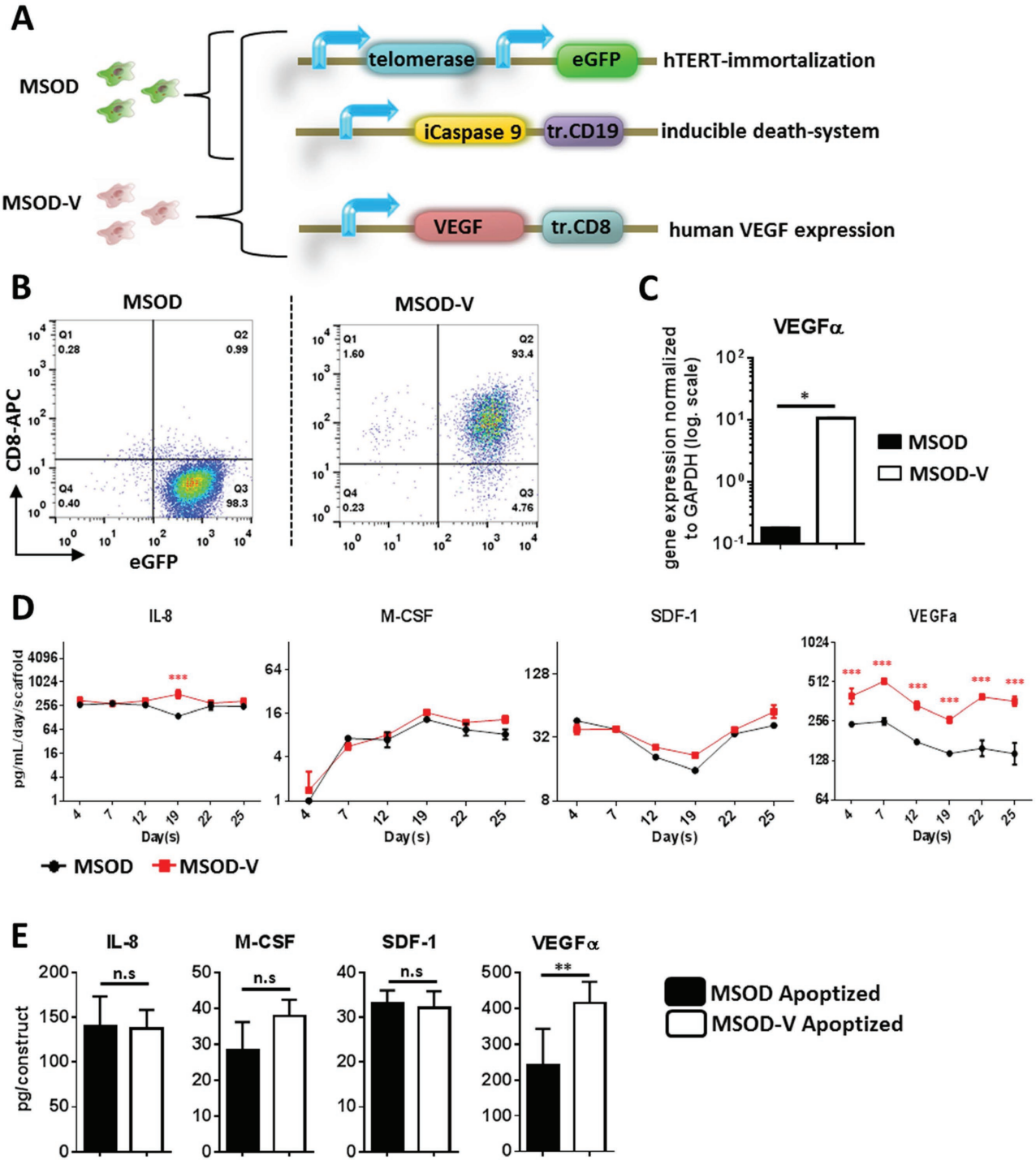

Figure 4. In vitro engineering of ECM-coated scaffold using MSOD and MSOD-V lines. A) Genetic modifications in MSOD and MSOD-V lines (tr: truncated). B) Flow cytometric analysis eGFP and CD8 expression in MSOD and MSOD-V cells. C) Gene expression level of VEGF gene in MSOD and MSOD-V lines ($n = 4$, $^*P < 0.05$). D) Supernatants measurements of 3D bioreactors seeded with MSOD or MSOD-V cells ($n \geq 3$, $^*P < 0.05$). E) Protein quantification of MSOD Apoptized and MSOD-V Apoptized ECM-coated grafts after 3D perfusion culture ($n \geq 3$, $^{**}P < 0.01$, n.s = not significant).

flow cytometry, based on the expression of the truncated CD8 surface marker (>93%, Figure 4B), leading to the isolation of a MSOD population overexpressing VEGF, referred to as the MSOD-V line. MSOD-V cells were shown to significantly overexpress the Vegfa transgene as compared to MSOD (60.2-fold increase, Figure 4C), while retaining apoptotic-induction functionality over a three-week course of 2D osteogenic differentiation (Figure S9A, Supporting Information). MSOD-V cells were also shown to deposit mineralized matrix similarly to the MSOD line upon exposure to osteogenic medium (Figure S9B, Supporting Information).

ECM constructs were engineered as previously described using either the MSOD or the MSOD-V line (Figure S9C, Supporting Information). Over the 3D culture time, secretion profiles of MSOD and MSOD-V for IL-8, M-CSF, SDF-1α, and VEGF proteins were measured from the corresponding perfusion bioreactor systems. Both lines displayed similar patterns of IL-8, M-CSF, and SDF-1α production, whereas VEGF secretion was significantly higher throughout the culture time in bioreactors seeded with MSOD-V than with MSOD (average of 2.0-fold increase; Figure 4D). After 28 d, constructs were decellularized by apoptosis-induction and assessed for the content of representative factors in the ECM. As compared to MSOD, MSOD-V constructs contained similar amounts of IL-8, M-CSF, and SDF-1α, but were significantly enriched in VEGF (1.7-fold, Figure 4E), consistent with the supernatant measurements. We thus validated the possibility to generate ECM specifically enriched in VEGF by engineering of a dedicated cell line, and to maintain it upon apoptosis-driven decellularization.

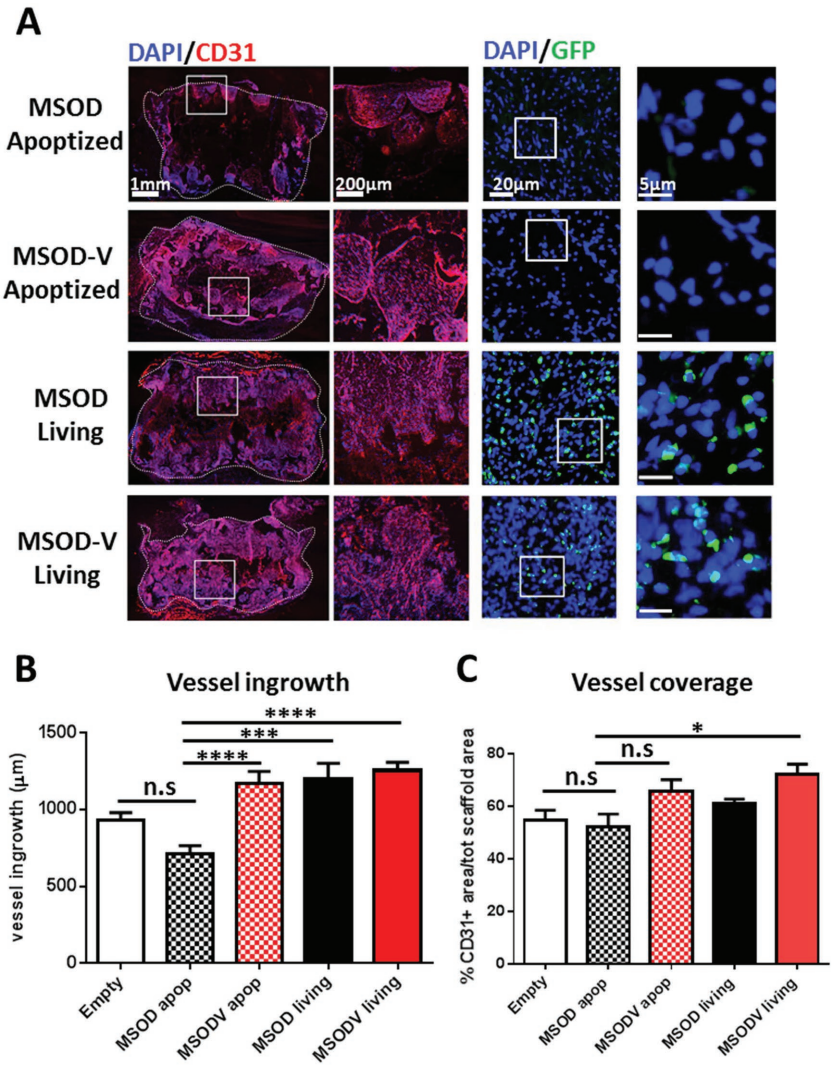

Figure 5. In vivo assessment of angiogenic performance of ECM-coated materials. A) Representative immunofluorescence staining of engineered grafts one week post-in vivo implantation in nude rats. B) Quantification of vessel ingrowth in the corresponding grafts (n = 3, *P < 0.05, ***P < 0.001, ****P < 0.0001, n.s = not significant). C) Quantification of vessel coverage in corresponding explanted samples (*P < 0.05, n.s = not significant).

2.5. Vascularization Efficiency of VEGF-Enriched ECM Constructs

The angiogenic potential of VEGF-enriched engineered ECM was assessed by subcutaneous implantation of Apoptized samples (MSOD and MSOD-V) in the back of nude rats. Constructs were retrieved one week postimplantation and processed to assess vasculature formation. As controls, "naked" ceramic (empty), nondecellularized grafts engineered with the MSOD (MSOD Living) and the MSOD-V (MSOD-V Living) lines were implanted.

Immunofluorescence stainings (CD31 and DAPI, **Figure 5**A) of whole tissue cross-sections revealed different patterns of vasculature. Constructs from the "MSOD Apoptized" group showed formation of vessels principally localized at the periphery and were associated with the presence of a necrotic core characterized by absence of vessels (CD31 staining) and cells (DAPI staining). In contrast, "MSOD-V Apoptized" grafts displayed deeper vessel colonization, approaching the one observed in the MSOD Living constructs. Living MSOD-V grafts reproducibly showed the deepest vessel distribution, with grafts largely vascularized. Importantly, hMSC derived cells were abundantly detected only in Living grafts (green fluorescent protein (GFP) staining, Figure 5A), confirming the efficiency of decellularization.

Quantification of vessel ingrowth, defined as the mean depth penetration of CD31-positive vessels from the edge to the inner part of the scaffolds (Figure S10, Supporting Information), confirmed histological observations. Indeed, a significantly deeper penetration of host vasculature toward the center of the grafts was observed in the "MSOD-V Apoptized" group (1170 ± 79 µm,

Figure 5B) as compared to Apoptized samples without VEGF enrichment (713 ± 54 µm, Figure 5B). Quantification of vessel coverage over the total surface area did not reveal significant differences between the two apoptized groups, despite slightly superior (1.3-fold higher) values in VEGF-enriched samples (Figure 5C). As expected, MSOD-V Living grafts were the most vascularized, with 72.0 ±3.7% of surface invaded by vessels.

Overall, we report that the targeted enrichment of engineered ECM in VEGF resulted in increased angiogenic potential.

3. Discussion

In this study, we report the successful generation of ECM biomaterials, based on the decellularization of pre-engineered tissue within a 3D perfusion culture system, via deliberate activation of apoptosis pathway. The proposed approach resulted in superior preservation of graft integrity, associated with increased performance in the specific context of bone tissue regeneration. The paradigm was extended toward generation of grafts tunable in composition. This was demonstrated through a targeted enrichment in VEGF, ultimately resulting in an enhanced biological functionality. The work exemplifies for the first time the concept of customizable eECM grafts, with the potential to be designed to regulate specific regenerative processes.

The engineered graft materials were generated by proliferation and differentiation of the MSOD line toward the osteoblastic lineage, associated with the deposition of a dense ECM. In this experimental configuration, cell osteogenic differentiation was likely favored by the calcium phosphate composition of the scaffold,[33] in combination with the mechanical conditioning, in the form of flow-induced shear, introduced by the perfusion device.[34] The use of the perfusion-based bioreactor system was pivotal in our model also to (i) facilitate cell seeding into the scaffold pores, (ii) enhance mass transport to support homogenous tissue development, (iii) convect the apoptotic inducer through the deposited ECM, (iv) dynamically remove the cellular debris after construct devitalization and (v) streamline the processes, since scaffolds remained confined within the culture chambers from the cell seeding phase to the decellularization step, with minimal operator handling.

Decellularization by apoptotic induction was shown to efficiently preserve the deposited ECM. In particular, the procedure did not reduce the content of collagens—the most abundant ECM backbones,[35] unlike conventional freeze/thaw treatment. Remarkably, collagens and associated structural proteins have been directly associated with mechanisms of tissue remodeling, longevity and regeneration,[36,37] thus going beyond a merely architectural role, as predominantly reported. Preservation of a collagen-rich ECM was associated with the maintenance of key embedded cytokines and morphogens, including mediators of immune reactions,[28,29] inducers of angiogenesis,[25–27] as well as molecules chemotactic for host progenitors.[29,30] This appeared to be of particular importance to induce de novo bone formation, since the crucial steps driving bone-healing processes include an inflammation phase and the ingrowth of vasculature along with endogenous osteoprogenitors.[38]

The efficiency of ECM preservation upon apoptotic decellularization allowed investigating the possibility of selective enrichment. As a proof-of-principle for the strategy, and considering that rapid vascularization is an essential process in a variety of settings in regenerative medicine,[39] we selected VEGF as potent inducer of angiogenesis. Targeted enrichment of ECM with VEGF by genetic manipulation of the MSOD line resulted in a measurable biological effect, with significant increase of graft vascularization. Although in our model we did not observe evidences of vessel aberrancies, the doses of VEGF in the ECM might need to be carefully controlled, in order to remain in a therapeutic window while avoiding the formation of hemangiomas or a pathologic shift of homeostatic processes (e.g., too high osteoclastic activity in de novo bone formation[40]). In this context, the dose of VEGF could be controlled by the flow cytometry-based isolation of sub populations homogeneously expressing specific levels, as previously shown with primary hMSC.[41]

This study reports the first design of ECM materials through the use of dedicated cell lines. In fact, the generation of cell lines overexpressing defined factors in specific doses is the conceptual basis for the generation of customized eECM. Although the technology was not shown to fully achieve very fine tuning of each factor, the decellularization by apoptosis supports the generation of ECM with distinct, "by design" enrichment. The degree of tunability of the material can be further extended by the degree of ECM maturation and stiffness, which may be regulated through culture time, the use of different scaffolds or pre-conditioning with cytokines priming matrix remodeling.[42] Engineered ECM materials for regenerative medicine could ideally be designed to enhance functions required at early stages after transplantation (e.g., vascularization, host cell recruitment) to target repair effectiveness. This is in line with the concept to induce recapitulation of developmental processes,[5,43] which may not be optimally achieved upon the use of nECM from fully developed tissues.

If cell lines introduce notions of standardization and customization, they also raise safety concerns regarding clinical translation. In fact, despite proven efficiency, the decellularization step does not exclude presence of remaining living cells after treatment. This issue can be addressed through the systematic characterization of the generated cell lines (e.g., tumorigenicity test similarly to those published for the MSOD line[22]), but also by improving the genetic engineering strategy. This includes the possibility to combine the human telomerase and apoptotic cassette under the control of a single promoter, so that silencing of inducible apoptotic function also results in loss of immortalization. In addition, implementation of transgenes by site-specific genome editing using CrispR/Cas9 technology is a relevant alternative for the generation of cell lines with improved safety/control.[44]

4. Conclusions

Our findings consolidate the perspective of bioreactor-based production of eECM as off-the-shelf biomaterials with tunable biological properties based on the presentation of instructive biological signals. The approach represents the first step

toward the generation of customizable eECM for a variety of clinical indications or biological models, which could ultimately compete in modularity and efficiency with current sECM approaches.

5. Experimental Section

Cell Lines: Primary bone-marrow material was obtained after informed signed consent from the patients. The MSOD line was previously generated by modification of primary hMSC.[46] Briefly, cells were immortalized by insertion of the human telomerase gene. Successfully immortalized cells were further modified by insertion of an inducible apoptotic genetic device.[47] A clone was subsequently selected based on the proliferative and differentiation potential, giving rise to the MSOD line.

The MSOD-VEGF line was derived from the previously generated MSOD line transduced with a bicistronic retrovirus expressing human $VEGF_{165}$ (VEGF) linked to a nonfunctional, truncated form of the syngeneic molecule human CD8a, as previously described.[48,49] Successfully transduced cells were purified by flow cytometry sorting based on the expression of the CD8 marker, after staining with Mouse Anti-Human CD8-APC (BD Pharmingen, cat# 561952).

MSOD and MSOD-V lines were cultured in complete medium (CM) consisting of α-minimum essential medium with 10% fetal bovine serum, 1% HEPES (1 M), 1% sodium pyruvate (100×10^{-3} M), and 1% of penicillin-streptomycin-glutamin (100X) solution (all from Gibco). During culture, cells were placed in a humidified 37 °C per 5% CO_2 incubator and medium was changed twice in a week.

Osteogenic Differentiation in 2D: hMSC lines were seeded at 3 000 cells cm^{-2} and differentiated for three weeks in OM. Osteogenic medium consisted of CM supplemented with 10×10^{-9} M dexamethasone, 0.1×10^{-3} ML-ascorbic acid-2-phosphate and 10×10^{-3} M β-glycerophosphate.[50]

Apoptosis-Induction: Induction of apoptosis in MSOD and MSOD-V lines was performed as previously described.[47] Briefly, the B/B homodimerizer (Clontech, cat# 635060) was added at 50×10^{-9} M in culture medium to activate the apoptosis pathway through the dimerization of the modified caspase 9. The percentage of induced death was assessed 12 h later by FACS analysis, after cell harvest and staining with Annexin V-APC (BD Biosciences, cat# 550475) and propidium iodide (PI, BD Biosciences, cat# 51–66211E) in Annexin-V binding buffer (BD Biosciences, cat# 556454).

3D Cell Seeding: The 3D culture was performed using a previously developed perfusion bioreactor system (U-cup, Cellec Biotek AG), allowing controlled flow of a cell suspension or culture medium directly through the scaffold pores.[51] Cells were seeded on hydroxyapatite scaffolds (Engipore, Finceramica-Faenza, Faenza, Italy) in the form of porous cylinders of 4 mm height and 8 mm diameter. Scaffolds were seeded with 0.75×10^6 of cells by overnight perfusion at a superficial velocity of 1 000 µm s^{-1} in proliferation medium (PM), consisting of CM supplemented with 100×10^{-9} M dexamethasone, 0.1×10^{-3} M ascorbic acid-2-phosphate and 5 ng mL^{-1} FGF-2. After 12 h (cell seeding phase), the superficial velocity was reduced to 100 µm s^{-1} for perfusion culture of the cells. The cell homogeneity and viability within constructs was assessed by methyl-tetrazolium staining (MTT, Sigma).

Graft Generation: The protocol for the generation of ECM-coated constructs was adapted from a previous study.[52] Briefly, cells were cultured in the ceramic scaffolds for one week in PM and additional three weeks in OM, within the 3D perfusion bioreactor system. Culture medium was changed twice a week. Cell numbers were assessed after 1, 7, and 28 d to derive cell seeding efficiency and growth.

Graft Decellularization in Bioreactor: Constructs were decellularized using the previously described apoptotic approach or a conventional F&T method.[52] Apoptosis was induced by overnight dynamic convection of the homodimerizer within bioreactors. The F&T technique consisted of three cycles of dry freezing in liquid nitrogen and thawing in a 37 °C water bath for 10 min each. Samples were rinsed in double distilled water after the first thaw in order to hypotonically lyse the cells. Subsequently to F&T or apoptotic treatments, cell debris was removed from the constructs by sterile phosphate-buffered saline (PBS) washing in the perfusion system (100 µm s^{-1} for 30 min at 37 °C).

Gene Expression Analysis: Total RNA was extracted from cells using TRIzol (Invitrogen, Carlsbad, CA), treated with DNAse and retrotranscribed into cDNA, as previously described.[53] Real-time polymerase chain reaction (RT-PCR) was performed with the ABIPrism 77000 Sequence Detection System (Perkin Elmer/Applied Biosystem, Rotkreuz, Switzerland) and expression levels of genes of interest were normalized to glyceraldehyde 3-phosphate dehydrogenase (GAPDH). Primers and probe sets of osteogenic genes (RUNX2, osteocalcin, alkaline phosphatase, osterix, bone sialoprotein type 1, matrix metalloproteinase-13) were designed and used as previously described.[53]

Histological Analysis: After in vitro and/or in vivo cultures, constructs were fixed in 4% (vol/vol) paraformaldehyde and decalcified with 7% (vol/vol) ethylenediaminetetraacetic acid (EDTA) solution (Sigma). For biochemical and immunohistochemical analysis, samples were embedded in paraffin. Sections (5 µm thick) were stained for either Hematoxylin & Eosin (Baker), alizarin red, Masson's trichrome (Sigma, cat# HT15-KT), tartrate-resistant acid phosphatase activity by means of the leukocyte acid phosphatase kit (Sigma, cat# 387A-1KT). Chromogenic in situ hybridization (Zytovision kit) to detect human ALU repeat sequences was performed following the manufacturer's instructions, using nuclear fast red (N3020, Sigma) as nuclear counterstaining. Osterix (Abcam, cat# ab22552), bone sialoprotein type 1 (Abcam ab52128), and osteocalcin (Millipore, cat# AB10911) were stained by use of primary antibodies and the immunobinding was detected with biotinylated secondary antibodies, using the appropriate Vectastain ABC kits. The red signal was developed with the Fast Red kit (Dako Cytomation), and sections were counterstained by hematoxylin. Histological and immunohistochemical sections were analyzed using an Olympus BX-61 microscope.

For immunofluorescence analysis, samples were cryoprotected by overnight incubation in a 20% sucrose solution, followed by embedding in optimal cutting temperature compound (CellPath, UK) and snap frozen in liquid nitrogen. Subsequent cryosections (10 µm thick) were incubated for 1 h in 0.3% Triton X-100 and 2% normal goat or donkey serum (Sigma-Aldrich) in PBS with corresponding primary antibodies. This includes anti-collagen type 1 (Cedarlane CL50151AP), anti-osteocalcin (Biorad 7060-1815), anti-CD31 primary antibody (BD bioscience 555025). Secondary antibodies consisted in Alexafluor 546 and Alexafluor 633 conjugated anti-mouse IgG1 (Life Technologies, Basel, Switzerland). Nuclei were stained using DAPI dye (Invitrogen, Basel, Switzerland) at 1:50 for 1 h. All antibodies were diluted in 0.3% Triton X-100 and 2% normal goat or donkey serum in PBS. Endogenous GFP was detected by samples excitation with a 488 nm laser. Negative controls were performed during each analysis by omitting the primary antibodies. Fluorescence images were acquired using Olympus BX63 microscope (Olympus, Volketswil, Switzerland) and Zeiss LSM 710 confocal microscope (Zeiss).

Osteogenic Marker Analysis: Cells from 2D culture were retrieved by a regular trypsinization step. Cells from 3D generated ECM were extracted from the scaffold pores by sequentially perfusing a solution of 0.3% collagenase (Worthington, USA) for 40 min and 0.05% trypsin/0.53 mm EDTA (GIBCO, Switzerland) for 10 min, both at a superficial velocity of 400 µm s^{-1}. Cells were further permeabilized for 15 min in permeabilization buffer (R&D systems, cat# F005) and stained at 4 °C for 30 min with an antibody against Stro-1 (R&D systems, cat# MAB1038), OC (R&D systems, cat# IC1419P), or ALP (R&D systems, cat# FAB1448A). Cells were washed and stained with PE, PerCP, and APC conjugated secondary antibodies (R&D systems, cat# IC002A) for 30 min and analyzed using a FACSCalibur flow cytometer (BD Biosciences, Germany). Positive expression was defined based on superior fluorescence intensity than the respective controls with omission of primary antibodies.

DNA Quantification: Constructs retrieved from the bioreactor chamber were digested with proteinase K solution (1 mg mL^{-1} proteinase K, 50 mm TRIS, 1 mm EDTA, 1 mm iodoacetamide, and 10 µg mL^{-1} pepstatin-A; Sigma-Aldrich, USA) in double distilled water or potassium phosphate buffer for 16 h at 56 °C as previously described (14). DNA quantification was performed by means of a commercially available fluorescence-based kit, namely CyQUANT Cell Proliferation Assay (Invitrogen, USA). Working solutions were prepared according to the manufacturer's protocols. Analyses were carried out measuring fluorescence with a Spectra Max Gemini XS Microplate Spectrofluorometer (Molecular Devices, USA). Excitation and emission wavelengths were, respectively, 485 and 538 nm. Samples in each plate included a calibration curve.

Collagen and Calcium Quantification: Total calcium was measured using a colorimetric-based assay. Briefly, calcium present in the mineralized ECM was solubilized in 0.5 N hydrochloric acid for 4 h at 4 °C before quantification (Total Calcium Assay, Randox, UK). Total collagen content was determined using the Sircol assay (Biocolor, UK) after samples solubilization in 3% v/v acetic acid (Fluka, Switzerland) and 0.01% w/v pepsin (Sigma-Aldrich, USA) overnight at 4 °C. The calcium/collagen concentration was assessed using a Spectra Max 190 microplate colorimeter (Molecular Devices, USA) following the parameters provided in the respective assay kits.

Luminex-Protein Quantification: Supernatants and/or ECM generated in the 3D bioreactor culture were analyzed for the content of a panel of growth factors (i.e., SDF-1α, VEGF, IL-8, M-CSF), according to the manufacturer's instructions (R&D eBiosciences, Immunoassay Kit). Supernatants were collected twice a week during exchange of culture medium. ECM grafts were collected and entirely lysed at the end of the 3D culture (day 28), prior or subsequently to decellularization treatment. Supernatant values were expressed as amounts produced per day per single construct (pg/mL/day/construct). ECM values correspond to the total content per construct (pg/construct).

SEM: For SEM, cell-seeded constructs were fixed overnight at 4 °C with 4% formaldehyde and washed with PBS. Samples were gradually dehydrated with 30%–50%–70%–90%–100% ethanol, coated with gold and imaged with a Philips XL 30 ESEM microscope.

Microtomography: Microtomography (μCT) was performed at the Biozentrum of the University of Basel (Basel, Switzerland). After fixation in formalin and storage in PBS, microcomputerized tomography data were acquired using a Phoenix nanotom m scanner (General Electric) with 0.5 mm aluminum filtered X-rays (applied voltage, 70 kV; current, 260 µA). Transmission images were acquired during a 360° scan rotation with an incremental rotation step size of 0.25°. Reconstruction was made using a modified Feldkamp algorithm at an isotropic voxel size of 2.5 µm. Threshold-based segmentation and 3D measurement analyses (mineralized tissue density and volume) were performed using the ImageJ software (ImageJ; National Institutes of Health) with the BoneJ[54] and 3D Shape[55] extensions. 3D rendering of the structures was performed using VGStudio MAX 2.2 software (Volume Graphics).

Animal Experiments: Animals were treated in compliance with Swiss Federal guidelines for animal welfare and all procedures were approved by the Veterinary Office of the Canton (Basel, Switzerland), conform to the Directive 2010/63/EU of the European Parliament.

Bone formation efficiency of engineered grafts was assessed by ectopic subcutaneous implantation and orthotopic implantation into generated critically sized cranial defects (8 mm) all in male nude rats (Hsd: RH-rnu/rnu, animal permit 2590). For the surgical procedure, animals were anesthetized by inhalation using a mixture of oxygen (0.6 L min^{-1}) and isoflurane (1.5–3 vol%). Samples were retrieved 12 weeks postimplantation and fixed prior to microtomography and histological analysis.

To assess their angiogenic properties, in vitro engineered grafts were implanted in subcutaneous pockets of male nude rats (Hsd: RH-rnu/rnu, animal permit 2590). At 7 d postimplantation, rats were anesthetized by intraperitoneal injection of a mixture of Ketamine (100 mg kg^{-1}) and Xylazin (10 mg kg^{-1}) and sacrificed by total body vascular perfusion of 1.5% paraformaldehide for graft explantation.

Quantification of Vascularization Efficiency of Engineered Grafts: Vessel ingrowth was defined as the mean depth penetration of CD31-positive vessels from the edge to the inner part of the scaffolds. Briefly, CD31/DAPI images of the entire cross-sections were acquired using a wide-field fluorescence microscope (Olympus BX63). To randomly define the penetration of the blood vessels toward the center of the grafts, each section length was divided in six equal parts (line 1, white ticks; Figure S6, Supporting Information). Vessel ingrowth was measured along the three central perpendicular lines (line 2, green; Figure S6, Supporting Information) as the distance from the edge until a positive signal was detected (line 3, blue; Figure S6, Supporting Information).

Vessel coverage was measured as the ratio between the surface covered by CD31-positive vessels and the total surface of the scaffolds. Statistics were performed based on a minimal of six sections, at about 500 µm distance in depth.

Statistical Analysis: Data are presented as means ± standard error of the mean. For single comparison, differences were evaluated using Mann Whitney U test, with $P < 0.05$ considered to indicate statistical significance (GraphPad Prism 5). Standard One-way ANOVA was used for multiple comparisons test.

Supporting Information

Supporting Information is available from the Wiley Online Library or from the author.

Acknowledgements

This work was supported by the European Community's Seventh Framework Program (MultiTERM, grant agreement number 238551) and the AO Foundation (Grant No. S-15-25B). The authors declare they have no competing financial interests.

Received: October 20, 2016
Published online: January 11, 2017

[1] J. K. Mouw, G. Ou, V. M. Weaver, *Nat. Rev. Mol. Cell Biol.* **2014**, *15*, 771.
[2] S. F. Badylak, D. O. Freytes, T. W. Gilbert, *Acta Biomater.* **2009**, *5*, 1.
[3] P. E. Bourgine, C. Scotti, S. Pigeot, A. Todorov, L. Tchang, I. Martin, *Proc. Natl. Acad. Sci. USA* **2014**, *111*, 17426.
[4] D. F. Williams, *Tissue Eng., Part A* **2014**, *20*, 1129.
[5] A. Papadimitropoulos, C. Scotti, P. Bourgine, A. Scherberich, I. Martin, *Bone* **2015**, *70*, 66.
[6] J. J. Song, H. C. Ott, *Trends Mol. Med.* **2011**, *17*, 424.
[7] W. P. Daley, S. B. Peters, M. Larsen, *J. Cell Sci.* **2008**, *121*, 255.
[8] M. A. Serban, G. D. Prestwich, *Methods* **2008**, *45*, 93.
[9] G. D. Prestwich, *J. Cell. Biochem.* **2007**, *101*, 1370.
[10] M. A. Serban, Y. Liu, G. D. Prestwich, *Acta Biomater.* **2008**, *4*, 67.
[11] P. M. Crapo, T. W. Gilbert, S. F. Badylak, *Biomaterials* **2011**, *32*, 3233.
[12] T. W. Gilbert, T. L. Sellaro, S. F. Badylak, *Biomaterials* **2006**, *27*, 3675.
[13] M. P. Lutolf, F. E. Weber, H. G. Schmoekel, J. C. Schense, T. Kohler, R. Muller, J. A. Hubbell, *Nat. Biotechnol.* **2003**, *21*, 513.
[14] M. M. Martino, P. S. Briquez, E. Güç, F. Tortelli, W. W. Kilarski, S. Metzger, J. J. Rice, G. A. Kuhn, R. Müller, M. A. Swartz, J. A. Hubbell, *Science* **2014**, *343*, 885.
[15] M. P. Lutolf, J. L. Lauer-Fields, H. G. Schmoekel, A. T. Metters, F. E. Weber, G. B. Fields, J. A. Hubbell, *Proc. Natl. Acad. Sci. USA* **2003**, *100*, 5413.
[16] K. A. Mosiewicz, L. Kolb, A. J. van der Vlies, M. M. Martino, P. S. Lienemann, J. A. Hubbell, M. Ehrbar, M. P. Lutolf, *Nat. Mater.* **2013**, *12*, 1072.

[17] K. Y. Lee, M. C. Peters, K. W. Anderson, D. J. Mooney, *Nature* **2000**, *408*, 998.
[18] V. Sacchi, R. Mittermayr, J. Hartinger, M. M. Martino, K. M. Lorentz, S. Wolbank, A. Hofmann, R. A. Largo, J. S. Marschall, E. Groppa, R. Gianni-Barrera, M. Ehrbar, J. A. Hubbell, H. Redl, A. Banfi, *Proc. Natl. Acad. Sci. USA* **2014**, *111*, 6952.
[19] N. Datta, Q. P. Pham, U. Sharma, V. I. Sikavitsas, J. A. Jansen, A. G. Mikos, *Proc. Natl. Acad. Sci. USA* **2006**, *103*, 2488.
[20] Q. P. Pham, F. K. Kasper, A. S. Mistry, U. Sharma, A. W. Yasko, J. A. Jansen, A. G. Mikos, *J. Biomed. Mater. Res., Part A* **2009**, *88*, 295.
[21] N. Sadr, B. E. Pippenger, A. Scherberich, D. Wendt, S. Mantero, I. Martin, A. Papadimitropoulos, *Biomaterials* **2012**, *33*, 5085.
[22] P. Bourgine, C. Le Magnen, S. Pigeot, J. Geurts, A. Scherberich, I. Martin, *Stem Cell Res.* **2014**, *12*, 584.
[23] K. C. Straathof, M. A. Pulè, P. Yotnda, G. Dotti, E. F. Vanin, M. K. Brenner, H. E. Heslop, D. M. Spencer, C. M. Rooney, *Blood* **2005**, *105*, 4247.
[24] A. Page-McCaw, A. J. Ewald, Z. Werb, *Nat. Rev. Mol. Cell Biol.* **2007**, *8*, 221.
[25] P. Carmeliet, *Nature* **2005**, *438*, 932.
[26] B. Wolff, A. R. Burns, J. Middleton, A. Rot, *J. Exp. Med.* **1998**, *188*, 1757.
[27] H. Zheng, G. Fu, T. Dai, H. Huang, *J. Cardiovasc. Pharmacol.* **2007**, *50*, 274.
[28] A. D. Luster, *N. Engl. J. Med.* **1998**, *338*, 436.
[29] E. R. Stanley, K. L. Berg, D. B. Einstein, P. S. Lee, Y. G. Yeung, *Stem Cells* **1994**, *12*, 15.
[30] T. Takano, Y.-J. Li, A. Kukita, T. Yamaza, Y. Ayukawa, K. Moriyama, N. Uehara, H. Nomiyama, K. Koyano, T. Kukita, *Lab. Investig.* **2014**, *94*, 286.
[31] B. E. Pippenger, M. Ventura, K. Pelttari, S. Feliciano, C. Jaquiery, A. Scherberich, X. F. Walboomers, A. Barbero, I. Martin, *J. Cell. Mol. Med.* **2015**, *19*, 1390.
[32] N. Ferrara, H.-P. Gerber, J. LeCouter, *Nat. Med.* **2003**, *9*, 669.
[33] P. Müller, U. Bulnheim, A. Diener, F. Lüthen, M. Teller, E. D. Klinkenberg, H. G. Neumann, B. Nebe, A. Liebold, G. Steinhoff, J. Rychly, *J. Cell. Mol. Med.* **2008**, *12*, 281.
[34] S. Kido, R. Kuriwaka-Kido, T. Imamura, Y. Ito, D. Inoue, T. Matsumoto, *Bone* **2009**, *45*, 1125.
[35] C. Frantz, K. M. Stewart, V. M. Weaver, *J. Cell Sci.* **2010**, *123*, 4195.
[36] C. Y. Ewald, J. N. Landis, J. Porter Abate, C. T. Murphy, T. K. Blackwell, *Nature* **2015**, *519*, 97.
[37] L. Lukjanenko, M. J. Jung, N. Hegde, C. Perruisseau-Carrier, E. Migliavacca, M. Rozo, S. Karaz, G. Jacot, M. Schmidt, L. Li, S. Metairon, F. Raymond, U. Lee, F. Sizzano, D. H. Wilson, N. A. Dumont, A. Palini, R. Fässler, P. Steiner, P. Descombes, M. A. Rudnicki, C.-M. Fan, J. von Maltzahn, J. N. Feige, C. F. Bentzinger, *Nat. Med.* **2016**, *22*, 897.
[38] G. Kumar, B. Narayan, in *Classic Papers in Orthopedics*, Springer, New York city - USA, **2014**, pp. 531–533.
[39] M. W. Laschke, Y. Harder, M. Amon, I. Martin, J. Farhadi, A. Ring, N. Torio-Padron, R. Schramm, M. Rücker, D. Junker, J. M. Häufel, C. Carvalho, M. Heberer, G. Germann, B. Vollmar, M. D. Menger, *Tissue Eng., Part A* **2006**, *12*, 2093.
[40] U. Helmrich, N. Di Maggio, S. Güven, E. Groppa, L. Melly, R. D. Largo, M. Heberer, I. Martin, A. Scherberich, A. Banfi, *Biomaterials* **2013**, *34*, 5025.
[41] U. Helmrich, A. Marsano, L. Melly, T. Wolff, L. Christ, M. Heberer, A. Scherberich, I. Martin, A. Banfi, *Tissue Eng., Part C. Methods* **2012**, *18*, 283.
[42] M. Mumme, C. Scotti, A. Papadimitropoulos, A. Todorov, W. Hoffmann, C. Bocelli-Tyndall, M. Jakob, D. Wendt, I. Martin, A. Barbero, *Eur. Cells Mater.* **2012**, *24*, 224.
[43] P. Lenas, M. Moos, F. P. Luyten, *Tissue Eng., Part B. Rev.* **2009**, *15*, 381.
[44] K. M. Esvelt, P. Mali, J. L. Braff, M. Moosburner, S. J. Yaung, G. M. Church, *Nat. Methods* **2013**, *10*, 1116.
[45] V. S. Komlev, M. Mastrogiacomo, R. C. Pereira, F. Peyrin, F. Rustichelli, R. Cancedda, *Eur. Cells Mater.* **2010**, *19*, 136.
[46] P. Bourgine, C. Le Magnen, S. Pigeot, J. Geurts, A. Scherberich, I. Martin, *Stem Cell Res.* **2014**, *12*, 584.
[47] C. A. Ramos, Z. Asgari, E. Liu, E. Yvon, H. E. Heslop, C. M. Rooney, M. K. Brenner, G. Dotti, *Stem Cells* **2010**, *28*, 1107.
[48] U. Helmrich, A. Marsano, L. Melly, T. Wolff, L. Christ, M. Heberer, A. Scherberich, I. Martin, A. Banfi, *Tissue Eng., Part C* **2012**, *18*, 283.
[49] H. Misteli, T. Wolff, P. Füglistaler, R. Gianni-Barrera, L. Gürke, M. Heberer, A. Banfi, *Stem Cells* **2010**, *28*, 611.
[50] C. Maniatopoulos, C. Maniatopoulos, J. Sodek, J. Sodek, A. H. Melcher, A. H. Melcher, *Cell Tissue Res.* **1988**, *254*, 317.
[51] D. Wendt, A. Marsano, M. Jakob, M. Heberer, I. Martin, *Biotechnol. Bioeng.* **2003**, *84*, 205.
[52] N. Sadr, B. E. Pippenger, A. Scherberich, D. Wendt, S. Mantero, I. Martin, A. Papadimitropoulos, *Biomaterials* **2012**, *33*, 5085.
[53] O. Frank, M. Heim, M. Jakob, A. Barbero, D. Schafer, I. Bendik, W. Dick, M. Heberer, I. Martin, *J. Cell. Biochem.* **2002**, *85*, 737.
[54] G. J. Meijer, J. D. De Bruijn, R. Koole, C. A. Van Blitterswijk, *PLoS Med.* **2007**, *4*, 0260.
[55] D. G. Phinney, G. Kopen, W. Righter, S. Webster, N. Tremain, D. J. Prockop, *J. Cell. Biochem.* **1999**, *75*, 424.

ADVANCED FUNCTIONAL MATERIALS

Supporting Information

for *Adv. Funct. Mater.*, DOI: 10.1002/adfm.201605486

Engineered Extracellular Matrices as Biomaterials of Tunable Composition and Function

*Paul Emile Bourgine, Emanuele Gaudiello, Benjamin Pippenger, Claude Jaquiery, Thibaut Klein, Sebastien Pigeot, Atanas Todorov Jr, Sandra Feliciano, Andrea Banfi, and Ivan Martin**

Supporting Information

Engineered extracellular matrices as biomaterials of tunable composition and function

Paul Emile Bourgine, Emanuele Gaudiello, Benjamin Pippenger, Claude Jaquiery, Thibaut Klein, Sebastien Pigeot, Atanas Todorov Jr, Sandra Feliciano, Andrea Banfi, Ivan Martin*

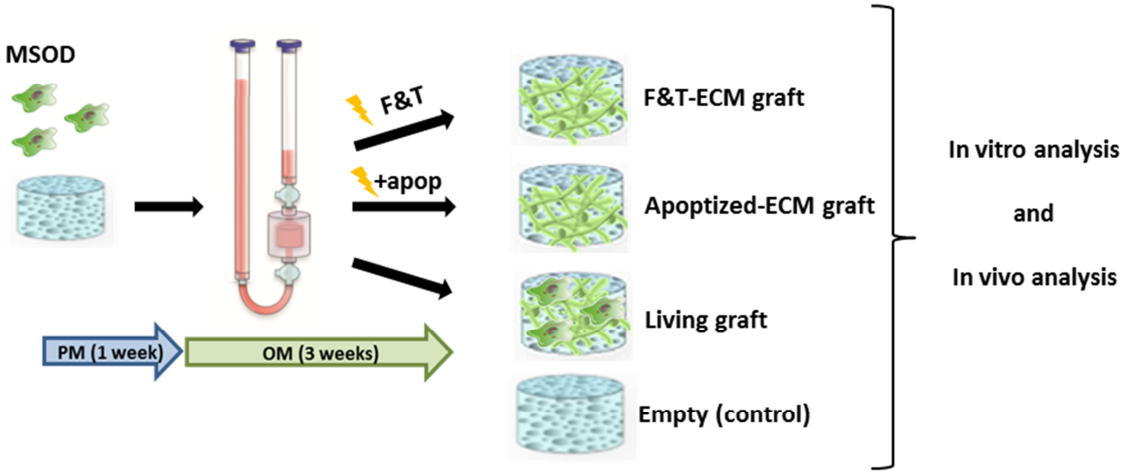

Figure S1. Experimental design for the generation of bone grafts in perfusion bioreactor. Following four weeks of culture, constructs are decellularized (F&T, Apoptized) or not (Living). The resulting grafts are analysed in vitro or implanted in vivo subcutaneously or into critical-sized cranial defect in nude rats (PM = proliferative medium, OM = osteogenic medium).

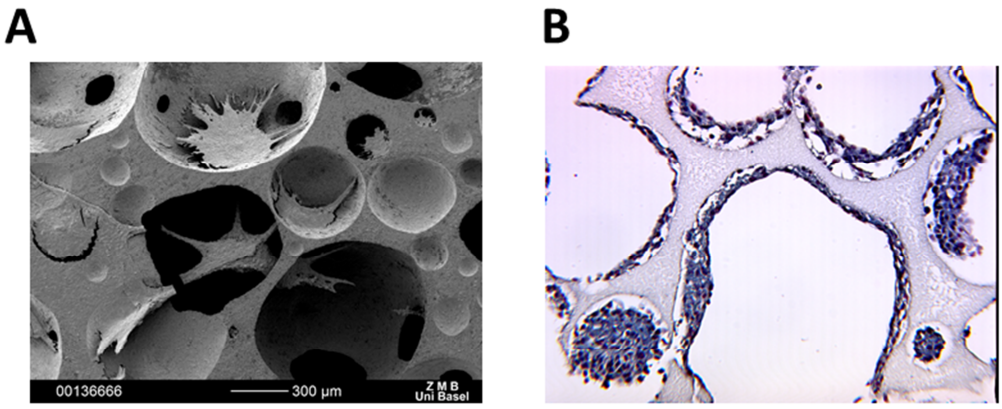

Figure S2. (A) Scanning electron microscopy image of the generated living graft prior to decellularization. Cells and ECM form visible structures interconnected through the pores of

the material. (B) Histological analysis by Masson's trichrome of the deposited ECM prior to decellularization treatment.

A

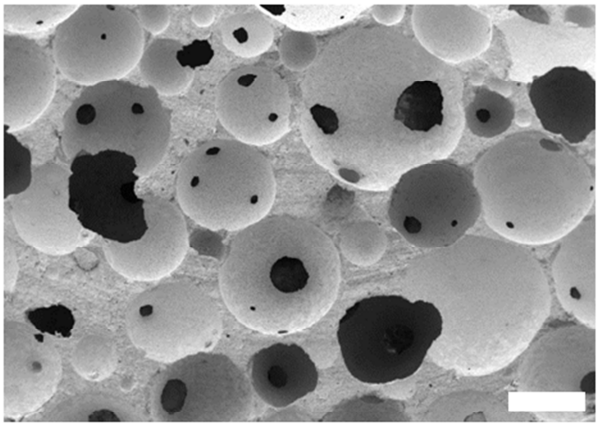

B

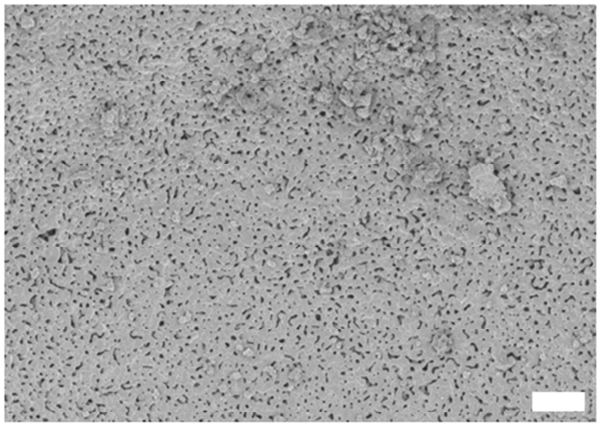

C

Composition	Hydroxyapapatite ($Ca_5(PO_4)_3(OH)$)
Ca/P ratio	1.66
Fabrication process	Powder sintering
Purity	>95%
Pore size distribution	100-200µm (32%) 200-500µm (42%)
Porosity	80 (+/- 3) %
Interconnectivity	>97%
Granulosity	0.25-2.5um
Compressive strength	8.26 Mpa (+/- 0.17)
Flexural strength	1.5 Mpa (+/- 1.08)
Young modulus	1.79 E

Figure S3. (A) Electron microscopy of ceramic scaffold without cell seeding. (left scale bar = 300µm, right scale bar = 10µm). A uniform distribution of the macro-structure with apparent interconnectivity and porosity can be observed. (B) High resolution of electron microscopy ceramic material without cells. The micro-structure reveals the intergranular porosity with

grain size comprised between 0.25-2.5µm. (C) Physical and chemical properties of ceramic scaffold. Data were obtained from previous studies by scanning electron microscopy, X-ray diffraction and inductively coupled plasma analysis.

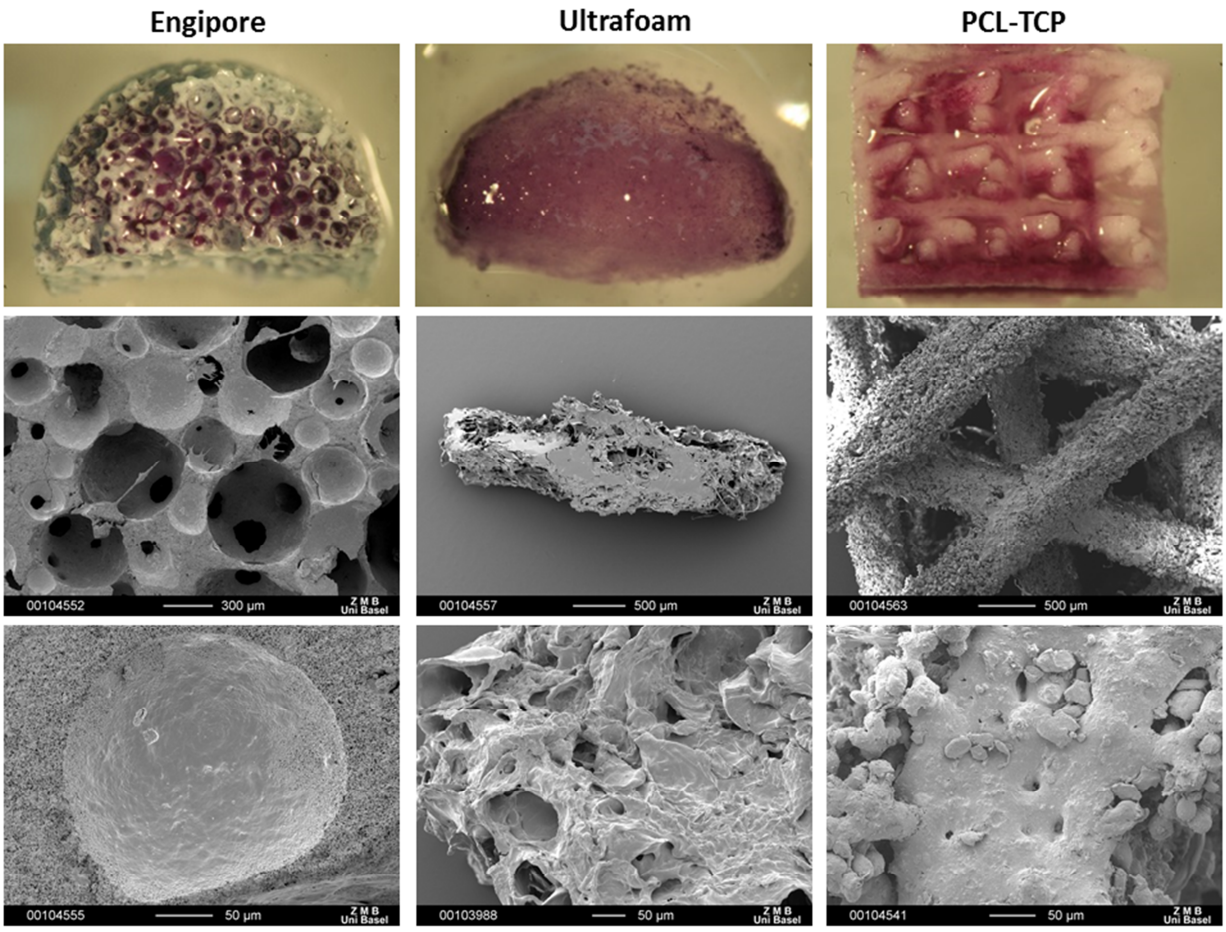

Figure S4. MTT stainings (top) and scanning electron microscopy pictures (central and bottom) of ceramic (Engipore®), collagen (Ultrafoam®) and polycaprolactone-tri calcium phosphate (PCL-TCP) scaffolds, seeded and cultured with MSOD cells for 5 days. All material supported cell viability and ECM deposition.

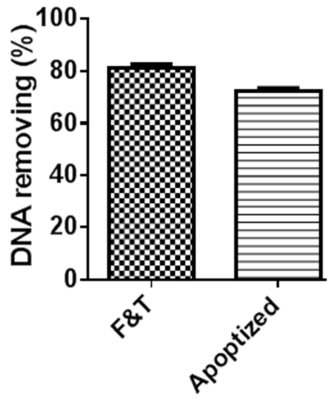

Figure S5. Decellularization efficiency of the F&T and Apoptized methods after four weeks of 3D perfusion culture (n=3). DNA content was measured prior to and after decellularization treatment to express percentage of DNA removed by the decellularization procedure.

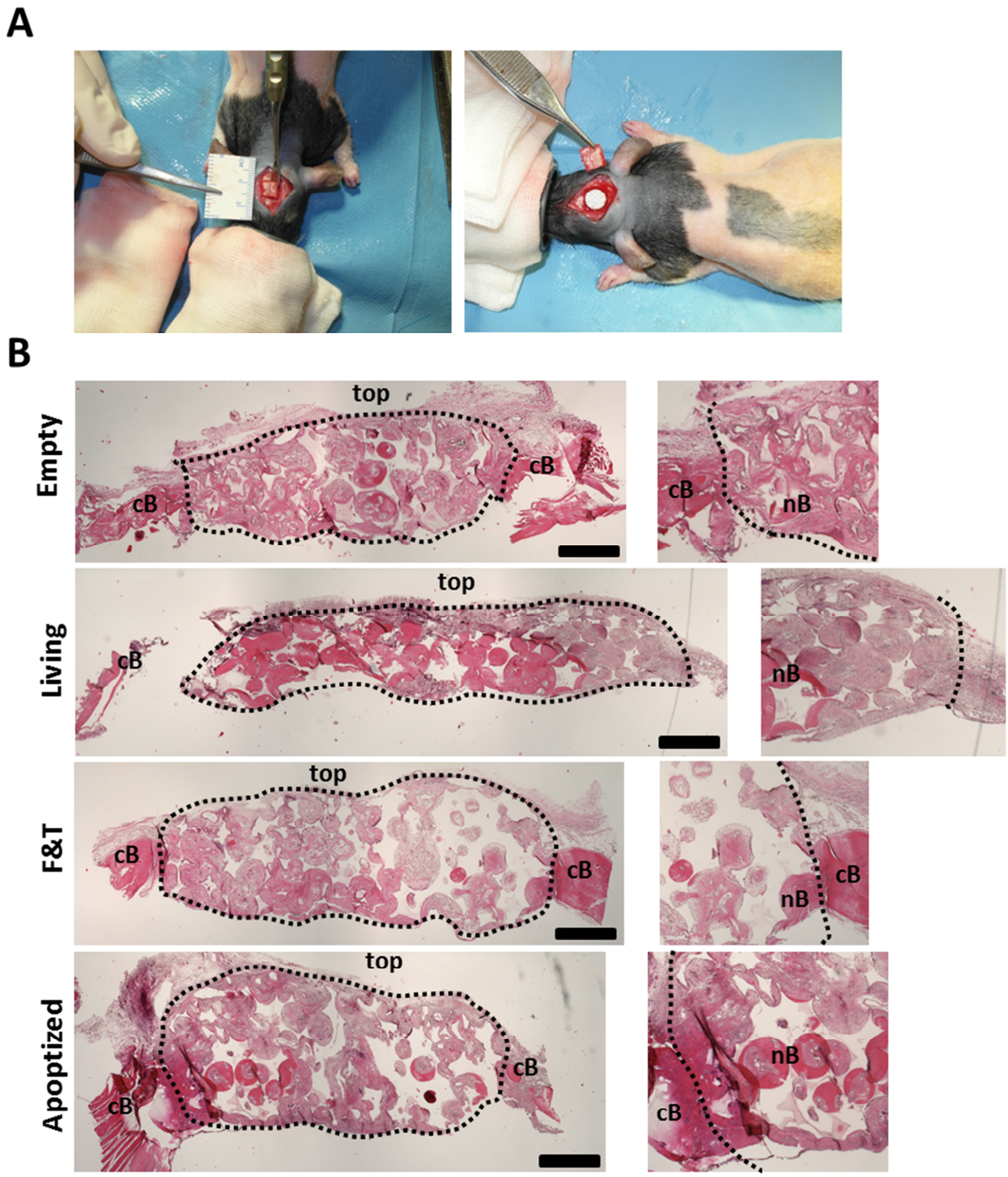

Figure S6. (A) Generation of the critical-sized cranial defect. The defect consisted in a 8mm x 8mm area in which the cranial surface of the animal was removed. (B) Representative Hematoxylin & Eosin stainings of implanted grafts 12 weeks post-in vivo implantation into cranial defect of nude rats. Deep pink staining is indicative of frank bone tissue. Dashed lines delimit graft areas. Low magnification and high magnification images are presented on left and right respectively. Scale bar = 1mm. cB = calvarial bone, nB = new Bone.

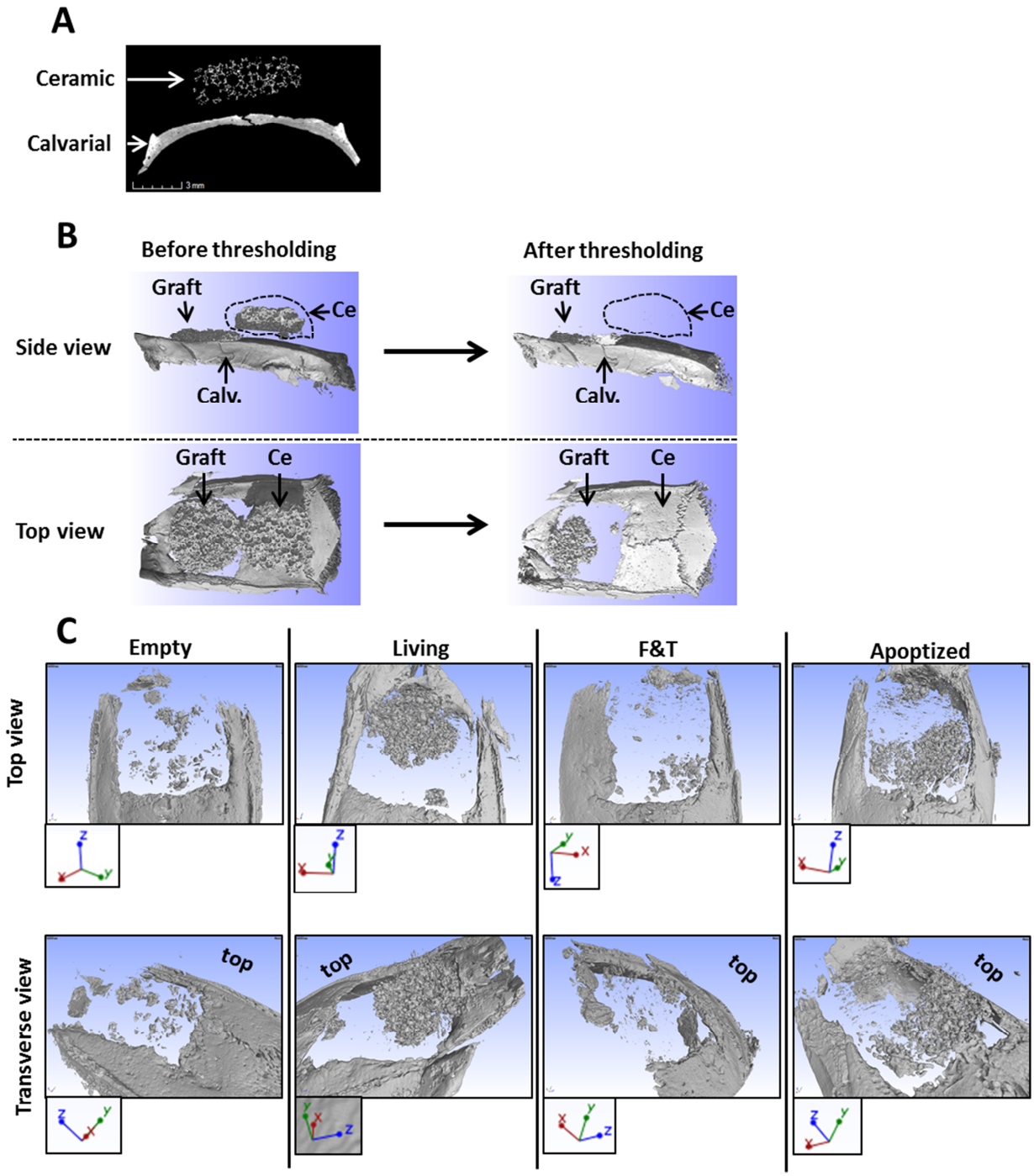

Figure S7. Microtomography analysis of cranial defects. (A) MicroCT analysis allows for the detection of both ceramic scaffolds and rat calvarial bone (side view). (B) Thresholding of MicroCT scanning for bone quantification. During scanning of the rat calvarial defect containing the graft, a "naked" ceramic scaffold is also scanned as internal control to distinguish grey value corresponding to the scaffold or to mature bone. During analysis, the

threshold is set up in order to remove the ceramic traces, thus considering only frank bone formation. (C) Top and transverse views of rat cranial defect 12 weeks post implantation.

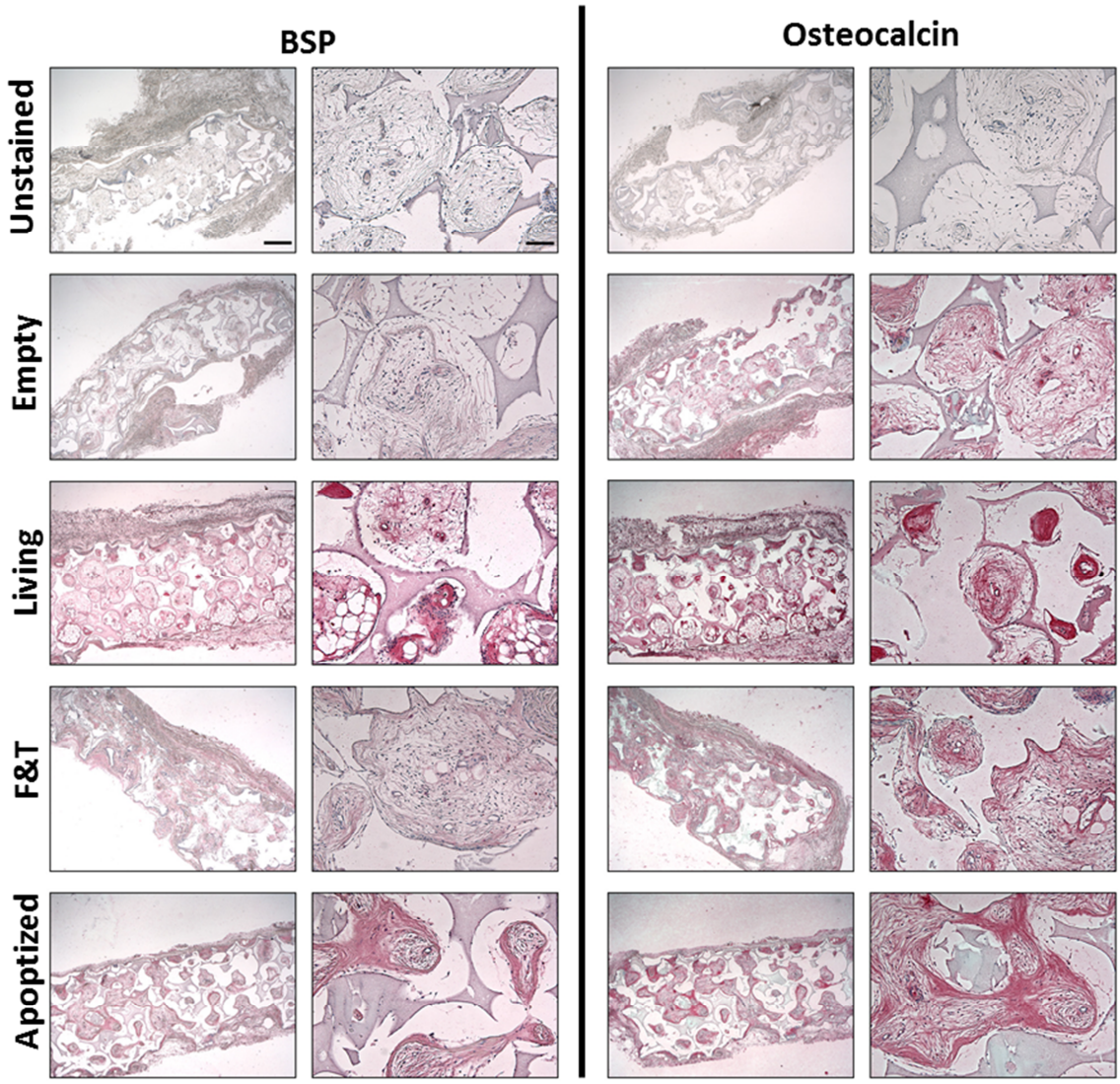

Figure S8. Bone sialoprotein (BSP) and Osteocalcin stainings from retrieved grafts 12 weeks post-subcutaneous implantation. The pink colour is indicative of positivity. A stronger coloration is observed in Living and Apoptized samples. For each group, low magnification (scale bar = 500µm) and high magnification images (scale bar = 100µm) are displayed on the left and right respectively.

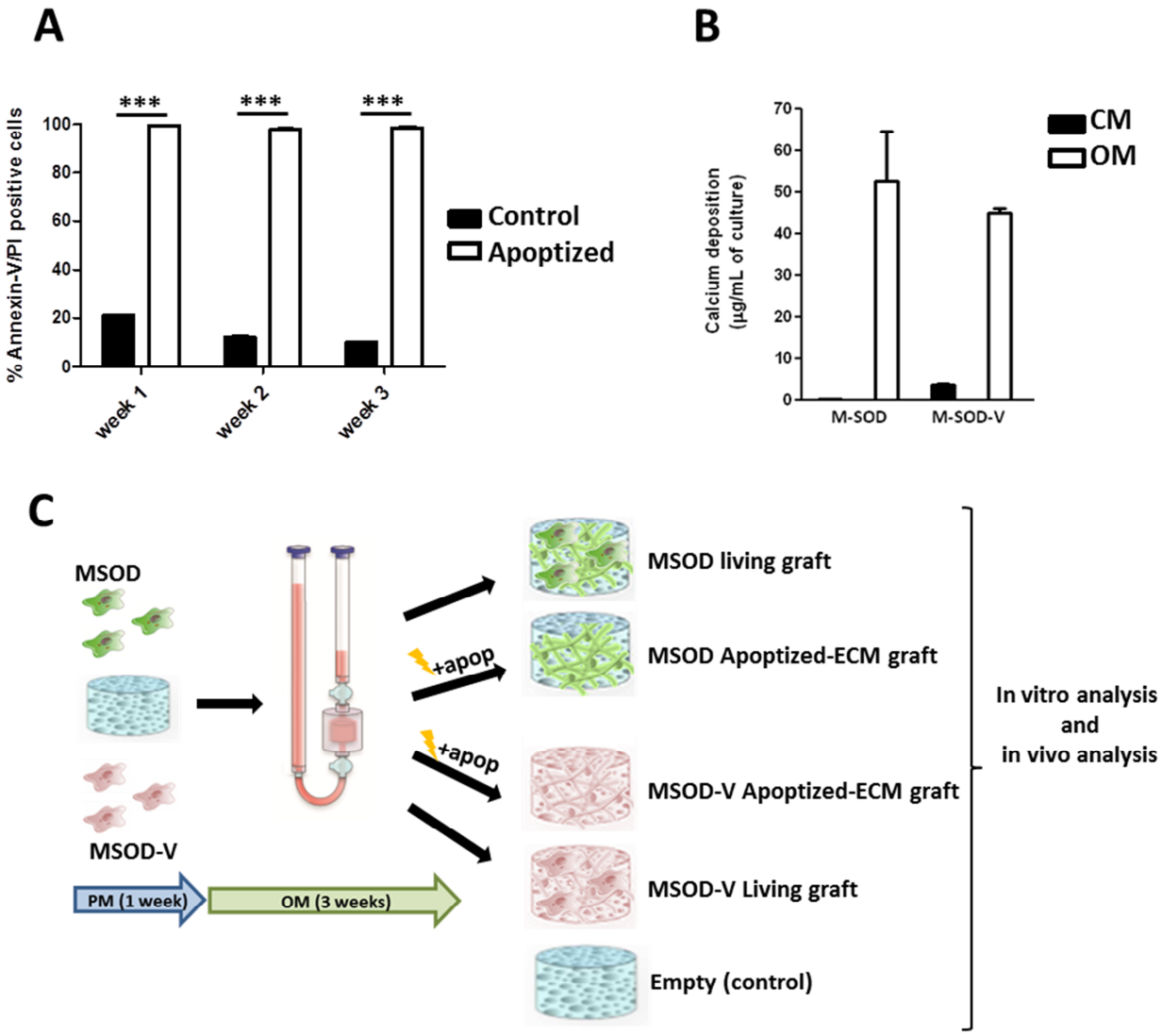

Figure S9. (A) Cell-death assessment of the MSOD-V line in the three weeks course of 2D osteogenic differentiation, following exposure (white, Apoptized) or not (black, control) to the apoptotic inducer. The MSOD-V was successfully induced toward apoptosis (n=3, ***P<0.001). (B) Total calcium deposition of MSOD and MSOD-V lines after three weeks of osteogenic differentiation in 2D. The MSOD and MSOD-V lines displayed similar mineralization potential (CM = complete medium, OM = osteogenic medium). (C) Experimental design for the generation of MSOD or MSOD-V derived grafts. In vivo analysis consisted in subcutaneous implantation in Nude rat for a 1 week period for vascularization assessment.

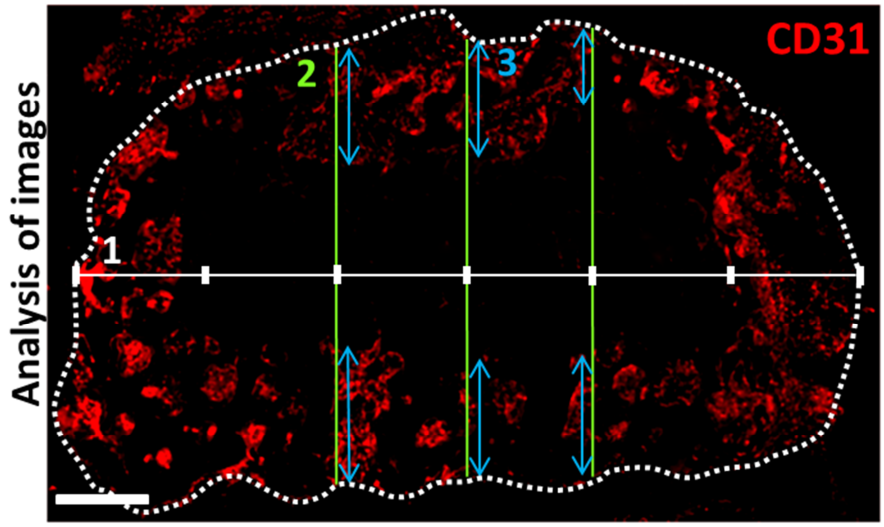

Figure S10. Methodology of vascularization quantification. Vessel ingrowth was defined as the mean depth penetration of CD31-positive vessels from the edge to the inner part of the scaffolds. To randomly define the penetration of the blood vessels towards the centre of the grafts, each section length was divided in 6 equal parts (line 1, white ticks). Vessel ingrowth was measured along the three central perpendicular lines (line 2, green) as the distance from the edge until a positive signal was detected (line 3, blue). Vessel coverage was measured as the ratio between the surface covered by CD31-positive vessels and the total surface of the scaffolds. Statistics were performed based on a minimal of 6 sections, at about 500 µm distance in depth. Scale bar = 1mm.

Chapter 4. Engineering of BMP2-enriched mesenchymal tissues

Project Report: *3D in vitro engineering of decellularized osteoinductive grafts using a custom-designed hMSC line*

3D in vitro engineering of decellularized osteoinductive grafts using a custom-designed hMSC line.

Investigators: Thibaut Klein[1], Fabiana Gullotta[1], Julien Guerrero[1], Claude Jaquiery[1], Sébastien Pigeot[1], Paul Emile Bourgine[1, 2] and Ivan Martin[1]

[1]*Tissue Engineering, Department of Biomedicine, University Hospital Basel, University of Basel, 4031 Basel, Switzerland.*

[2]*Laboratory for Cell, Tissue and Organ engineering, Wallenberg Center for Molecular Medicine, University of Lund, 223 50 Lund, Sweden.*

1. Description of project

Infection, trauma or tumors can generate critical bone defects with a compromised regeneration, thus necessitating the development of suitable strategies to promote the repair. Conventional tissue engineering approaches propose the use of a three-dimensional (3D) scaffold, in which seeded patient-derived osteoprogenitor cells can grow, differentiate and secrete an extracellular matrix (ECM) that coats the scaffold. The resulting bone graft can then be implanted in the patient in an autologous approach. However, a more attractive paradigm consists in the removal of the cellular fraction (decellularization) from the graft prior to its implantation to reduce immuno-matching requirements. This strategy relies on the capacity of osteoinductive signals (e.g. Bone morphogenetic proteins – BMPs) embedded in the ECM to instruct endogenous osteoprogenitor cells toward bone repair. The success of this approach requires a standard cell source capable of secreting an osteo-inductive ECM, but also the development of a suitable decellularization protocol leading to both: efficient cell removal from the graft and preservation of ECM osteoinductive properties. To this aim, we developed a death-inducible human Mesenchymal Stromal Cell (hMSC) line capable to secrete the ECM and undergo apoptosis after induction (MSOD line). Using this unlimited and well-characterized cellular tool, we successfully generated an acellular ECM graft within a perfusion bioreactor. However, the graft contained only traces of BMP2, the main osteoinductive signal. Thus, the enrichment of the deposited ECM enriched in BMP2 through cellular overexpression may lead to an increased bone formation capacity of the graft. The aim of this project is to engineer a death-inducible hMSC line capable to overexpress BMP2, leading to its deposition

within the secreted ECM to achieve the generation of a BMP2-enriched acellular ECM. The resulting acellular bone graft is expected to exhibit increased osteoinductive properties capable to instruct bone regeneration in both ectopic and orthotopic sites.

1. Objectives / Milestones

Hypothesis 1: A human mesenchymal cell line (Mesenchymal Sword of Damocles - MSOD) previously established can be further modified to overexpress BMP2 (MSOD-B).

Aim 1: Develop the MSOD-B line selecting an optimal clone based on BMP2 secretion, proliferation and differentiation capacity as well as the possibility to induce cells toward apoptosis.

Hypothesis 2: Cell-free but cell-laid BMP2 enriched ECM grafts can be generated in vitro.

Aim 2: Generate and characterize cell-free BMP2 enriched grafts in 3D-perfusion bioreactors.

Hypothesis 3: BMP2 enriched grafts can lead to a higher quantity of bone deposition after ectopic and/or orthotopic implantation.

Aim 3: Evaluation of the bone formation capacity of BMP2-enriched graft in comparison with non-enriched grafts and uncoated material in nude mice (ectopic implantation model) and in nude rats (orthotopic critical-sized cranial defect model).

2. Material and methods

    a. Cell lines culture and expansion

The MSOD line was previously generated by modification of primary hMSCs [1]. Briefly, cells were immortalized by insertion of the human telomerase gene. Successfully immortalized cells were further modified by insertion of an inducible apoptotic genetic device [2]. A clone was subsequently selected based on its proliferative and differentiation potential, giving rise to the MSOD line. The MSOD line overexpressing BMP2 (hereinafter referred to as MSOD-B) was derived from the previously generated MSOD, as described below. MSOD and MSOD-B lines were cultured in Proliferating Medium (PM) consisting Complete Medium (CM, α-minimum essential medium with 10% fetal bovine serum, 1% HEPES 1M, 1% sodium pyruvate 0.1M, and 1% of penicillin-streptomycin-glutamin 100X solution (all from Gibco) and supplemented with 5ng/mL of FGF-2. During 2D and 3D culture, cells were placed in a humidified 37 °C per 5% CO_2 incubator and medium was changed twice in a week.

b. MSOD-B line generation

BMP2-ΔNGF lentivirus generation: The new lentivirus (LV) BMP2/ΔNGFR was generated from the bidirectional self-inactivating backbone vector pCCLsin.cPPT.ΔLNGFR.minCMV.hPGK.eGFP.Wpre [3]. Briefly, BMP2 cDNA, taken from Ensambl, was flanked by AgeI e SalI restriction sites. The artificial sequence was cloned in a plasmid by GeneART® (Thermofisher Scientific). Then, the BMP2 plasmid was digested with SalI and AgeI (New England Biolabs, NEB) and the resulting fragment was ligated into the digested backbone vector. *LV BMP2-ΔNGF production: B*MP2-ΔNGFR vector was packaged in 293T cells by an integrase-competent third generation construct and pseudotyped by the VSV. FuGENE 6 was used as transfection reagent. Cell culture medium was changed 16h post-transfection. Viral supernatant was harvested after 48h, passed through a 0.45µm filter and concentrated by ultracentrifugation at 70000g for 2h. The concentrated virus was resuspended in sterile phosphate buffered saline (PBS) and stored at -80°C until use. Viral titer was determined by transduction of 293T cells. Transduced cells were analyzed 72h later by flow cytometry to detect ΔNGFR as described below. Viral titers were typically in the range of $3x10^9$ UI/mL. *Lentiviral transduction:* MSOD were plated at 6000 cells/cm^2 in 150-mm dishes the day preceding the transduction. Various Multiplicity of Infection (MOI) have been tested resulted in successful infections with minimal risk of cell viability impairment [1]. Cells were transduced by incubation with BMP2-ΔNGFR vector at a MOI=5 overnight, followed by fresh medium replacement. Cells stably expressing hTERT-eGFP, inducible caspase 9 (iC9)-ΔCD19 and BMP2-ΔNGFR were purified using a FACS-Vantage SE cell sorter (Becton Dickinson, Basel, Switzerland). Successively, sorted cells were plated at 1000 cells/cm^2 in 150-mm dishes and a clone (MSOD-BMP2) showing good proliferation, osteogenic differentiation and apoptosis-induction responsiveness was selected.

c. 2D Doubling time

MSOD and MSOD-B lines were seeded at 3000 cells/cm^2 and cultured in PM. At time point 24, 48, 72 and 96h after seeding, cells were retrieved by a regular trypsinization step and counted by trypan blue staining. The doubling time was calculating accordingly to an adapted protocol *(Citation Mather, J.P., and P.E. Roberts, 1998. Introduction to Cell and Tissue Culture: Theory and Technique. Plenum Press. New York and London.).*

d. MTT quantitative metabolic activity assessment

MSOD and MSOD-B lines were seeded at 3000 cells/cm^2 and cultured in PM in 96-well plates. At confluence, culture wells were rinsed with PBS and 150 µL of fresh PM supplemented with 0.05mg/mL of Tetrazolium Bromide (MTT, Sigma-Aldrich, and cat # M5655) was placed/well. The plate was incubated for 4 hours at 37°C, 5% CO2. After incubation, 150 µL of cell culture grade DMSO was added per well and the plate was placed on an orbital shaker for 40 minutes in the dark. Supernatant has ultimately been placed in a new plate and absorbance read at 575nm (Spectramax 190).

e. 2D apoptosis-induction

Induction of apoptosis in MSOD and MSOD-B lines was performed as previously described [2].Briefly, the Cell Death inducer (CDi; B/B homodimerizer; Clontech cat# 635060) was added at 50nM in culture medium to activate the apoptosis pathway through the dimerization of the modified caspase 9. The percentage of induced cell-death was assessed 12h later by FACS analysis, after cell harvest and staining with Annexin-V-APC (BD Biosciences, cat#550475) and Propidium Iodide (PI, BD Biosciences, cat# 51-66211E) in Annexin-V binding buffer (BD Biosciences, cat# 556454).

f. Flow cytometry

The immunophenotypic analysis of hMSCs, MSOD and MSOD-B lines was performed using LSR II FORTESSA SORP (BD Biosciences) cell analyzer. Cells were harvested by regular trypsinization step and labelled at 4°C for 20 min with following fluorochrome-conjugated antibodies diluted in PBS 2% FBS 0.5mM EDTA: human anti-CD271 (for ΔNGFR detection, BD BIOSCIENCES cat#562123), human anti-CD19 (BioLegend, cat#119520), human anti-CD34 (BioLegend cat# 343512), human anti-CD45 (BD BIOSCIENCES cat#560973), human anti-CD29 (BioLegend, cat#303014), human anti-CD44 (BD BIOSCIENCES cat# 559942), human anti-CD73 (BD BIOSCIENCES cat# 561014), human anti-CD90 (BD BIOSCIENCES cat# 559869), human anti-CD146 (BioLegend, cat#342003). Positive expression was defined based on superior fluorescence intensity than the respective unstained and controls stained with isotype controls.

g. Osteogenic, adipogenic and chondrogenic differentiation in 2D

MSOD and MSOD-B lines were seeded at 3000 cells/cm^2 and differentiated for 3 weeks towards osteogenic, adipogenic and chondrogenic lineages using following medium. Osteogenic medium (OM) consists CM supplemented with 10nM dexamethasone, 0.1mM ascorbic acid-2-phosphate and 10mM β-glycerophosphate. Adipogenic medium consists in CM supplemented with 10-^{6}M Dexamethasone, 10ug/ml methyl-isobuthylxantine, 0.1mM Indomethacin and 10ug/ml Insulin ACTRAPID HM. Chondrogenic medium consists in serum-free CM supplemented with 10ng/ml TGFβ3, 10-^{6}M Dexamethasone 0.1mM ascorbic acid-2-phosphate. Medium was changed twice per week in each condition.

h. BMP2 quantification

Supernatants from the 2D and 3D culture were analyzed for their BMP2 content by ELISA, according to the manufacturer's instructions (hBMP2 DuoSet, BioTechne, cat#DY355-05). In 2D culture, the supernatants were collected after 24h and 48h of culture. In 3D-perfusion bioreactor culture, an aliquot of retrieved supernatant was saved at each medium change and stored at -80°C prior analysis. For determination of BMP2 content in the living and decellularized generated ECM-coated scaffold, the whole construct was mechanically disrupted and mixed with recommended buffer prior to analysis.

i. Calcium quantification

Total calcium was measured using a colorimetric-based assay. Briefly, calcium present in the mineralized extracellular matrix after 3 weeks of culture in PM or OM was solubilized in 0.5 N hydrochloric acid for 4h at 4°C before quantification (Total Calcium Assay, Randox, UK) following the manufacturer's instructions.

j. Gene expression analysis

Total RNA was extracted from cells using TRIzol (Invitrogen, Carlsbad, CA), treated with DNAse and retrotranscribed into cDNA, as previously described[4].Real-time polymerase chain reaction (RT-PCR) was performed with the ABIPrism 77000 Sequence Detection System (Perkin Elmer/Applied Biosystem) and expression levels of genes of interest were normalized

to glyceraldehyde 3-phosphate dehydrogenase (GAPDH). Primers and probe sets of osteogenic genes (RUNX2, alkaline phosphatase; ALP, bone sialoprotein type 1; BSP, and Osteocalcin, Assay-on-Demand™; all from thermofischer, Switzerland) were designed and used as previously described [4].

k. 3D Graft Generation

The 3D culture was performed using a previously developed perfusion bioreactor system (U-cup, Cellec Biotek AG), allowing controlled flow of a cell suspension or culture medium directly through the scaffold pores [5].Cells were seeded on hydroxyapatite scaffolds (Engipore®, Finceramica-Faenza, Italy) in the form of porous cylinders of 4mm height and 8mm diameter. Scaffolds were seeded with $0.75*10^6$cells by overnight perfusion at a superficial velocity of 2.8ml/min in PM. After 12h (cell seeding phase), the superficial velocity was reduced to 280µl/min for perfusion culture of the cells. The protocol for the generation of ECM-coated constructs was adapted from a previous study [6].

l. Graft decellularization in bioreactor

Constructs were decellularized as described for 2D cultures. Apoptosis was induced by overnight dynamic convection of the homodimerizer within bioreactors. Subsequently, cell debris were removed from the constructs by sterile PBS washing in the perfusion system (280µl/min for 30 min at 37°C).

m. Histological analysis

After in vivo implantation and explantation, constructs were fixed in 4% paraformaldehyde and decalcified with 7% ethylenediaminetetraacetic acid (EDTA) solution. For endogenous fluorescence analysis, samples were embedded in optimal cutting temperature compound (CellPath, UK), and snap frozen in liquid nitrogen. Subsequent cryosections (10 µm thick) were counterstained with DAPI (Invitrogen) for 15 min. MSOD and MSOD-B were revealed by endogenous GFP expression. For biochemical analysis, samples were embedded in paraffin. Sections (5 µm thick) were stained for hematoxylin & eosin (Baker), Masson's trichrome

(Sigma, cat# HT15-KT). Both bright field and fluorescence images were acquired using Nikon Ti2 microscopes.

n. Microtomography

Microtomography (μCT) was performed at the DBE of the University of Basel (Basel, Switzerland). After fixation in formalin and storage in PBS, microcomputerized tomography data were acquired using a Phoenix nanotom m scanner (General Electric) with 0.5 mm aluminum filtered X-rays (applied voltage, 70 kV; current, 260 μA). Transmission images were acquired during a 360° scan rotation with an incremental rotation step size of 0.25°. Reconstruction was made using a modified Feldkamp algorithm at an isotropic voxel size of 2.5 μm. Threshold-based segmentation and 3D measurement analyses (mineralized tissue density and volume) were performed using the ImageJ software (ImageJ; National Institutes of Health) with the BoneJ29 and 3D Shape30 extensions. 3D rendering of the structures was performed using VGStudio MAX 2.2 software (Volume Graphics).

o. DNA quantification

Constructs retrieved from the bioreactor chamber were digested with proteinase K solution (1 mg/ml proteinase K, 50 mm TRIS, 1 mm EDTA, 1 mm iodoacetamide, and 10 μg/ml pepstatin-A; Sigma–Aldrich, USA) in double distilled water or potassium phosphate buffer for 16 h at 56 °C as previously described [7]. DNA quantification was performed by means of a commercially available fluorescence based kit, namely CyQUANT® Cell Proliferation Assay (Invitrogen, USA). Working solutions were prepared according to the manufacturer's protocols. Analyses were carried out measuring fluorescence with a Spectra Max Gemini XS Microplate Spectrofluorometer (Molecular Devices, USA). Excitation and emission wavelengths were respectively 485 nm and 538 nm. Samples in each plate included a calibration curve.

p. Prostaglandin E2 (PGE2) quantification

Supernatants from the 3D perfusion bioreactor culture were analyzed for their Prostaglandin E2 content by ELISA, according to the manufacturer's instructions (PGE2 Parameter Assay, BioTechne, cat#KGE004B). 300µL of supernatant were collected per Bioreactor every hour for 6 hours and avec 12 hours (Overnight) upon apoptosis induction and store at -80°C prior analysis. For determination of PGE2 content in the living and decellularized generated ECM-coated scaffold, the whole construct was mechanically disrupted and mixed with recommended buffer prior to analysis.

q. Animal experiments

Animals were treated in compliance with Swiss Federal guidelines for animal welfare and all procedures were approved by the Veterinary Office of the Canton (Basel, Switzerland), conform to the Directive 2010/63/EU of the European Parliament. MSOD-B-derived osteoinductivity was assessed in vivo by its capacity to form osteoids upon ectopic implantation. Briefly, $1x10^6$ MSOD or MSOD-BMP2 cells were mixed with hydroxyapatite granules (mechanically discrupted ENGIPore scaffolds) and embedded in 60µL of fibrin gel. After 1h at 37°C, resulting constructs were subcutaneously implanted in nude mice. For the surgical procedure, animals were anesthetized by inhalation using a mixture of oxygen (0.6L min^{-1}) and isoflurane (1.5–3vol%). Samples were retrieved 12 weeks post implantation and fixed in formalin 4% and stabilized in Histogel (HG-4000-012, Thermofischer, Switzerland) prior to micro tomography and histological analysis.

3. Results

a) Novel MSOD-B line generation and cellular characterization

Since lentiviral infection is associated with a random integration of the transgene within the genome of the cells, it results in the generation of a highly heterogeneous cell MSOD-B population. The obtained MSOD-BMP2 population has thus been expanded and sorted for GFP (reporter of hTERT immortalization), CD19 (marker of iCas9 system) and Δ-NGFR (marker of BMP2 transgene) positivity by cytofluorimetry. For clonal cell line establishment, 1152 (12x96-wells plates) candidates were screened in the weeks following single-cell sorting for survival, proliferation and BMP2 secretion. The results presented hereafter are generated

from the best candidate based on the previous criteria (**Fig. 1A**). To better characterize the proliferative capacity of the selected MSOD overexpressing BMP2 clone, we established a growth curve to determine the doubling time (**Fig. 1B**). One doubling of the population occurred every 22,1±0,3 hours for MSOD and 19,9±1,2 hours for MSOD-B. Since the new MSOD-B line is constantly stimulated by a strong morphogenic protein, we assessed its metabolic activity by Tetrazolium (MTT) assay. MSOD-B showed a 33.7% higher metabolic activity in comparison to MSOD line (**Fig. 1C**). The inducible Caspase 9 (iC9) functionality was also assessed since the transduction and the chromatin remodeling (occurring during cell differentiation) can potentially hamper its expression and functionality. After 3 weeks of osteogenic induction, an overnight exposure to Cell Death inducer (CDi) resulted in an efficient death induction both in MSOD-B and in MSOD lines (99.55 ± 0.3% vs 99.18 ± 0.2%, respectively, **Fig. 1D**). MSOD-B lines phenotype was further characterized by cytofluorimetry, using the original primary hMSCs donor and MSOD line as control (**Fig. 1E**). MSOD-B line displayed a profile comparable to primary hMSCs and MSOD line: high expression of typical hMSCs markers (>99% positivity for CD29, CD44, CD90 and CD146), while being negative for hematopoietic markers (CD34 and CD45). Nevertheless, although all markers remained stable in their level of expression, we noticed decreased expression of CD73 in MSOD-B. This decrease could be related to chondrogenic or osteogenic commitment, independently of the culture medium used [8]–[10]. Finally, we compared the trilineage differentiation capacity of MSOD-B line versus MSOD line after 3 weeks of 2D culture in adipogenic, osteoblastic or chondrogenic medium (**Fig. 1F**). We could observe commitment in MSOD-B line among tested lineages, with presence of lipids droplets after Oil Red-O staining, mineralized matrix deposition after Alizarin Red staining and presence of glycosaminoglycanin after Safranin-O staining. Overall, these results indicate that we could transduce the MSOD line while preserving its commitment/differentiation features.

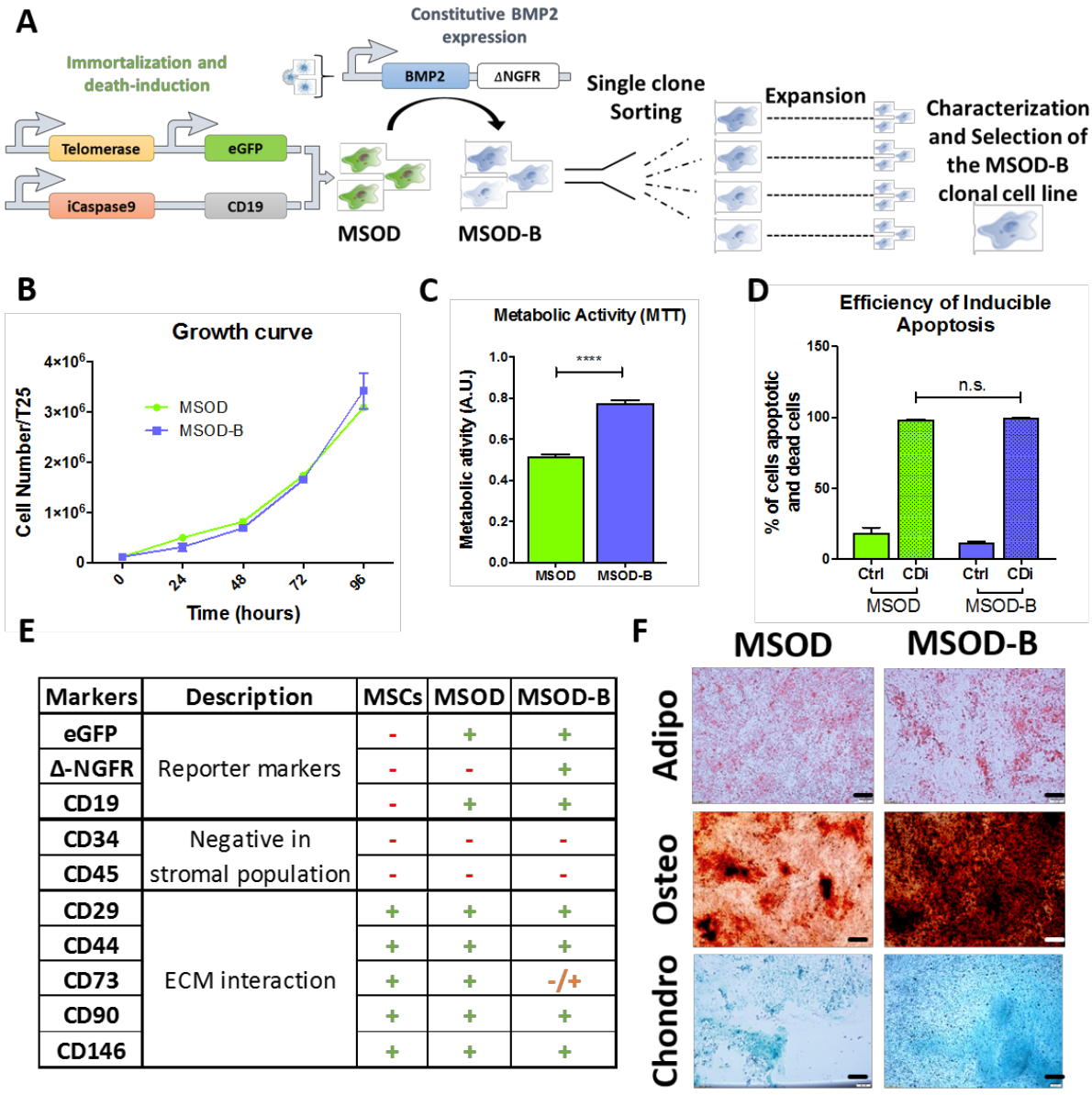

Markers	Description	MSCs	MSOD	MSOD-B
eGFP	Reporter markers	-	+	+
Δ-NGFR		-	-	+
CD19		-	+	+
CD34	Negative in stromal population	-	-	-
CD45		-	-	-
CD29	ECM interaction	+	+	+
CD44		+	+	+
CD73		+	+	-/+
CD90		+	+	+
CD146		+	+	+

Figure 1 : MSOD-B Cell Line generation and characteristcs. (A) Pre-existing immortalized and death inducible MSOD cells were transduced using BMP2/ΔNGFR Lentivirus prior to single cell sorting, expansion and selection of a potent clone. (B) MSOD versus MSOD-B growth curve anabling for population doubling time determination of the selected clone (22,1±0,3 hours and 19,9±1,2 hours respectively). (C) Metabolic activity of MSOD and MSOD-B lines detemined by quantitative MTT Assay (*n=4*). (D) Cytofluorimetric quantification of cell death by Annexin-V/PI stainings in culture without (Ctrl) or with adjunction of Cell Death inducer (Cdi) in the culture medium (*n≥4*). (E) Cytofluorimetric analysis of the primary cells (MSCs), MSOD and MSOD-B lines, +: positivity>90%, -: Negativity<1%, ±: 73%. (F) Representative Oil-Red-O, Alizarin red and Safranine-O stainings of M-SOD and MSOD-B cells after 3 weeks of 2D culture in Adipogenic medium (Adipo), Osteogenic medium (Osteo) and Chondrogenic medium (Chondro) respectively. Scale bar = 200µm; ****p<0,001

b) MSOD-B line possesses intrinsic osteogenic capacity

In order to assess the functionality of the MSOD-B line toward osteoblastic differentiation in 2D culture, we first evaluated the production of BMP2 proteins. MSOD and MSOD-B lines were cultured in proliferative medium and their supernatants were analyzed by ELISA (**Fig. 2A**).

Increasing levels of BMP2 were measured at different time points, indicating an active and sustained secretion (1324 ± 411 pg/mL after 48h of culture). In contrast, MSOD did not produce BMP2 during proliferation. To quantitatively assess the increase in mineralized matrix deposition we measured the calcium deposited (**Fig. 2B**) by both cell lines after osteogenic differentiation in 2D culture. MSOD-B showed 24.5% more calcium in its deposited ECM than original MSOD line. The osteogenic commitment capacity was also confirmed by the up-regulation of both early (Runx2 and ALP) and late (BSP and Osteocalcin) osteogenic genes, as compared to undifferentiated cells (**Fig. 2C**). Intriguingly, Osteocalcin gene was expressed at a lower level after osteogenic differentiation in 2D culture (fold increase<1) in both MSOD and MSOD-B (gene expression normalized to undifferentiated cells). We then studied the in vivo MSOD-B direct osteogenic potential by embedding MSOD-B cells in fibrin gels together with ceramic granules (crushed ENGIPore Scaffolds). MSOD cells were used as control. These basic constructs were subcutaneously implanted in nude mice and explanted after 12 weeks. MSOD-B based osteoids showed a dense collagen matrix and frank bone formation, as demonstrated by H&E and Masson's trichrome staining (**Fig. 2D**). To the contrary, MSOD generated only fibrotic and elastic tissues. Notably, GFP positive MSOD-B cells surrounded by lacunae were detected in the bone suggesting that these cells differentiated in mature osteocytes and give rise to osteogenesis. Overall, these results demonstrated that MSOD-B line is osteogenic *per se* and leads to bone formation upon in vivo implantation.

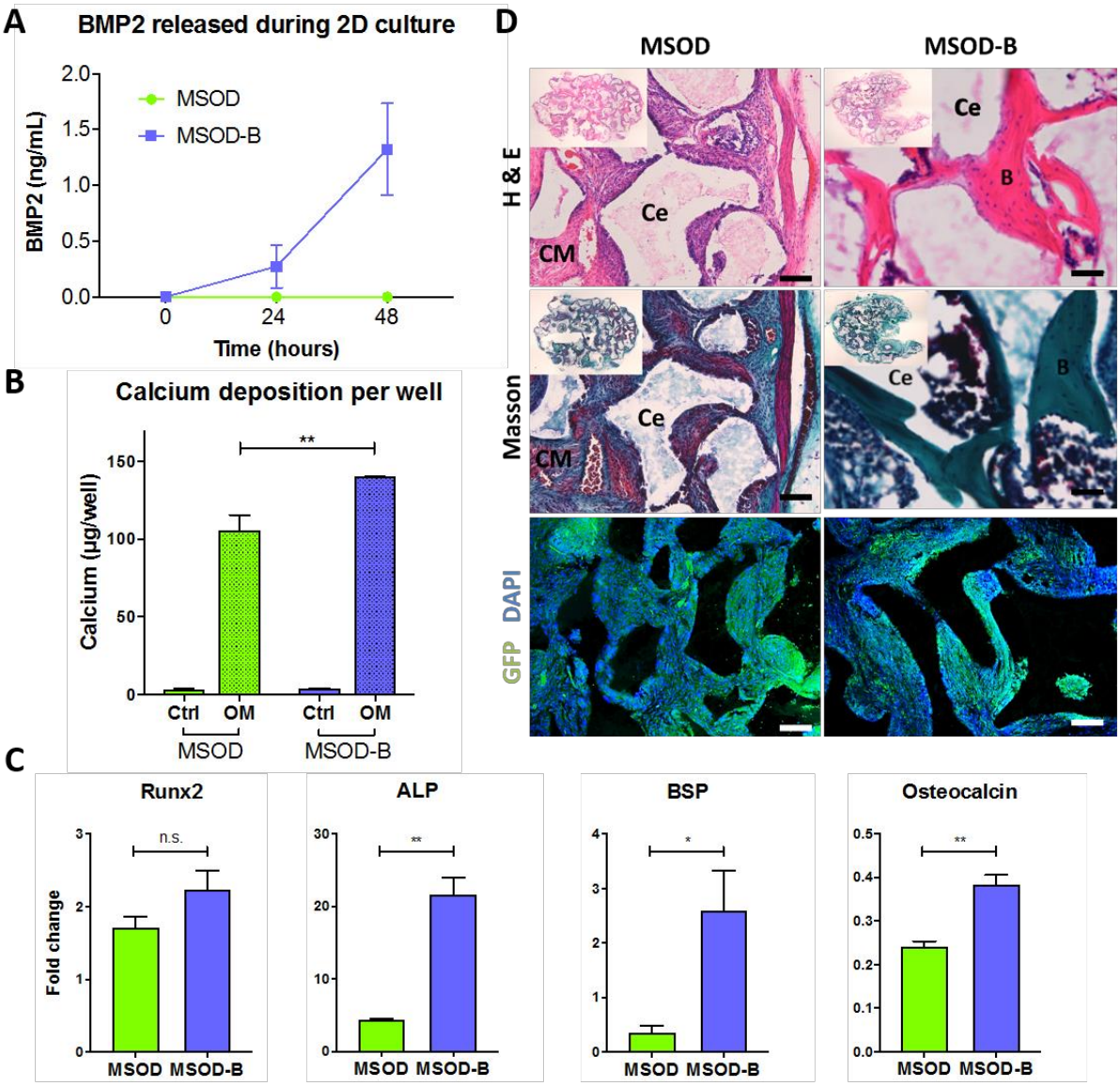

Figure 2: MSOD-B Cell Line functionality. (A) ELISA quantification of BMP2 released in the supernatant by MSOD and MSOD-B lines. Total calcium depositied after 3 weeks of 2D culture in Proliferation Medium (Ctrl) or Osteogenic medium (OM); *n=4.* (C) Fold changes in gene expression levels of key osteoblastic genes in MSOD and MSOD-B (*n=4)*. (D) In vivo osteogenic evaluation of MSOD and MSOD-B embedded in fibrin gel with hydroxyapatite granule and ectopically implanted in nude mice for 12 weeks. H&E: Hematoxilin Eosin; Masson: Masson's Trichrome and GFP/Dapi stainings are shown. Scale bar = 100µm. *p<0,5; **p<0,1;

c) Engineering of BMP2 enriched ECM coated scaffolds

ECM coated scaffolds were then generated according to a previously established two-phase protocol (**Fig. 3A**). To follow and quantify BMP2 release during 3D culture, we assessed the supernatant by ELISA twice a week, at each medium change (**Fig. 3B**). We could detect an increase in BMP2 secretion until Day 14, followed by a plateau until the end of bioreactor culture. This measurement indicated a continuous and stable secretion of the protein of interest. No BMP2 could be detected in the supernatant from MSOD-based tissues. At the end

of the 3D culture phase, we mechanically disrupted living and decellularized grafts to determine the quantity of BMP2 entrapped in the scaffold (**Fig. 3C**). Like in 2D cultures and 3D bioreactor supernatant analyses, no BMP2 was detected in MSOD based grafts. We could observe similar quantities between living and devitalized MSOD-B based scaffold (8.72±2.6 and 9.22±6.4ng/scaffold, respectively), suggesting that BMP2 is tightly embedded within the deposited ECM and stable upon devitalization and debris removal procedures. These findings demonstrate the capacity of MSOD-B line to release BMP2 and generate a ECM-decorated ceramic substrate in a dynamic 3D culture system.

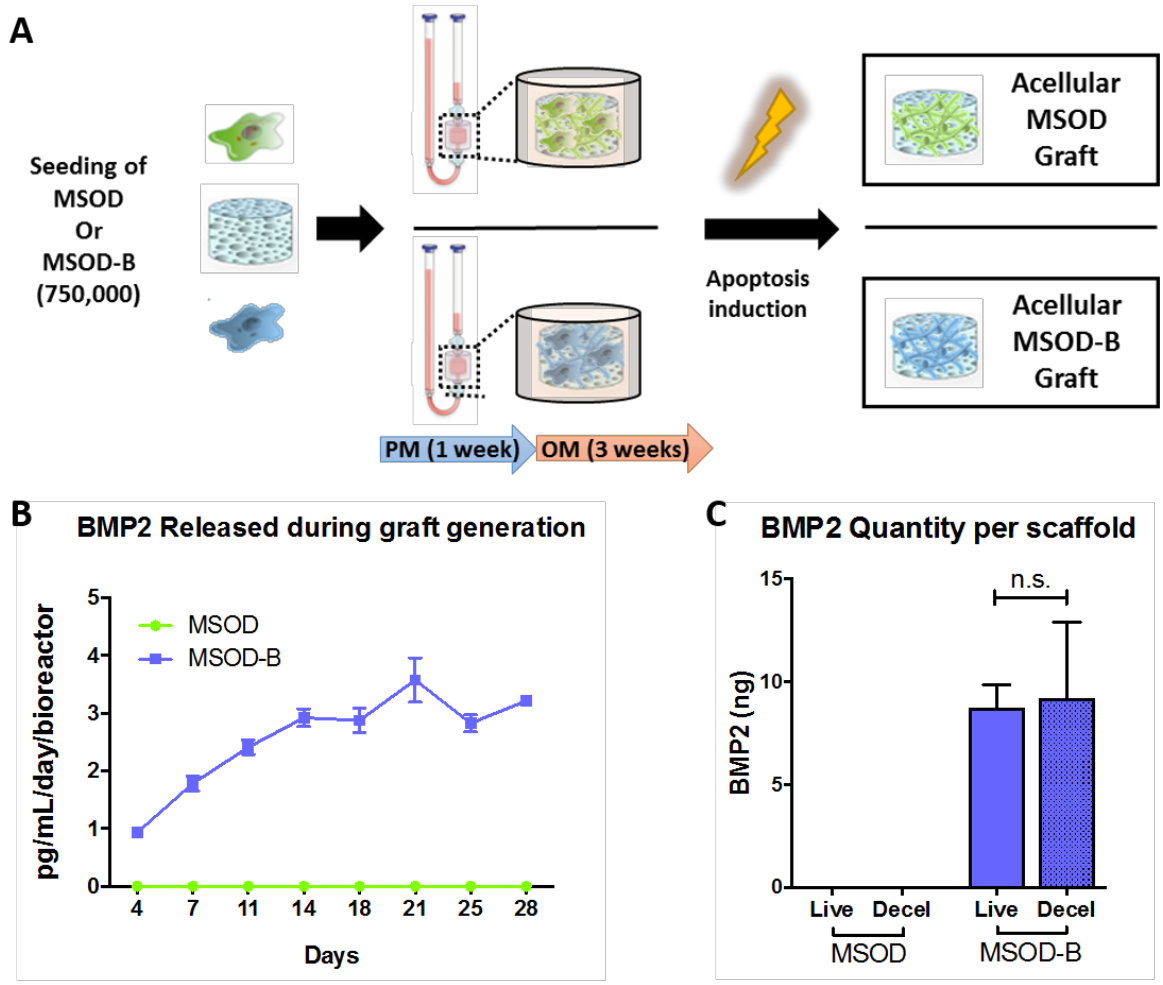

Figure 3: In vitro engineering of ECM-decorated scaffolds in 3D-perfusion bioreactors using MSOD and MSOD-B lines. (A) Schematic representation of the ECM decorated scaffolds engineering. PM, Proliferation Medium; OM, Osteogenic Medium. (B) ELISA quantification of BMP2 released in the supernatant by MSOD and MSOD-B lines during 3D-perfusion bioreactor culture (n=3). (C) ELISA quantification of BMP2 entrapped in the ECM decorating MSOD and MSOD-B grafts before (Live) and after (Decel) Cell Death induction (n=4).

d) MSOD-B devitalized ECM coated scaffold display osteogenic potential.

Finally, we studied the osteogenic potential of generated ECM decorated scaffolds, by in vivo ectopic implantation (subcutaneous pockets) for 12 weeks in nude mice (**Fig. 4A**). MSOD-B

decellularized grafts gave rise to bone marrow (BM)-like structures and bone. The presence of mineralized bone tissue was also confirmed by microtomography. MSOD-B based decellularized graft showed higher bone than the other conditions (**Fig. 4B**). Interestingly, grafts containing living MSOD-B revealed comparable histologic structures to MSOD based grafts (both living and decellularized). Efficiency of the death inducible device ensured that no living cells were implanted. Nevertheless, an important quantity of DNA could be detected in the grafts before implantation (**Fig. 4C**). We estimate that only two third of cells were retrieved from the grafts. As a high number of apoptotic bodies were also implanted, we studied if those could play a role in the generation of bone by MSOD-B based devitalized grafts. Prostaglandin E2 (PGE2) has shown to be involved in tissue regeneration trough the Phoenix-Rising pathway [11]. Briefly, PGE2 is secreted in the local microenvironment by apoptotic bodies after caspase9 and triggers some enzymatic cascades. We thus monitored PGE2 concentration in the bioreactor supernatant every hour upon death induction until the end of the devitalization process. In this assessment, we could not find any significant differences among conditions (data not shown). Nevertheless, when we measured the global quantity of PGE2 released in both supernatant and entrapped in the scaffold, we observed a significantly higher quantity in MSOD-B devitalized graft compared to other conditions (**Fig. 4D**). Taken together, those results suggest that the osteogenic properties of devitalized MSOD-B grafts could impact PGE2 signaling in vivo.

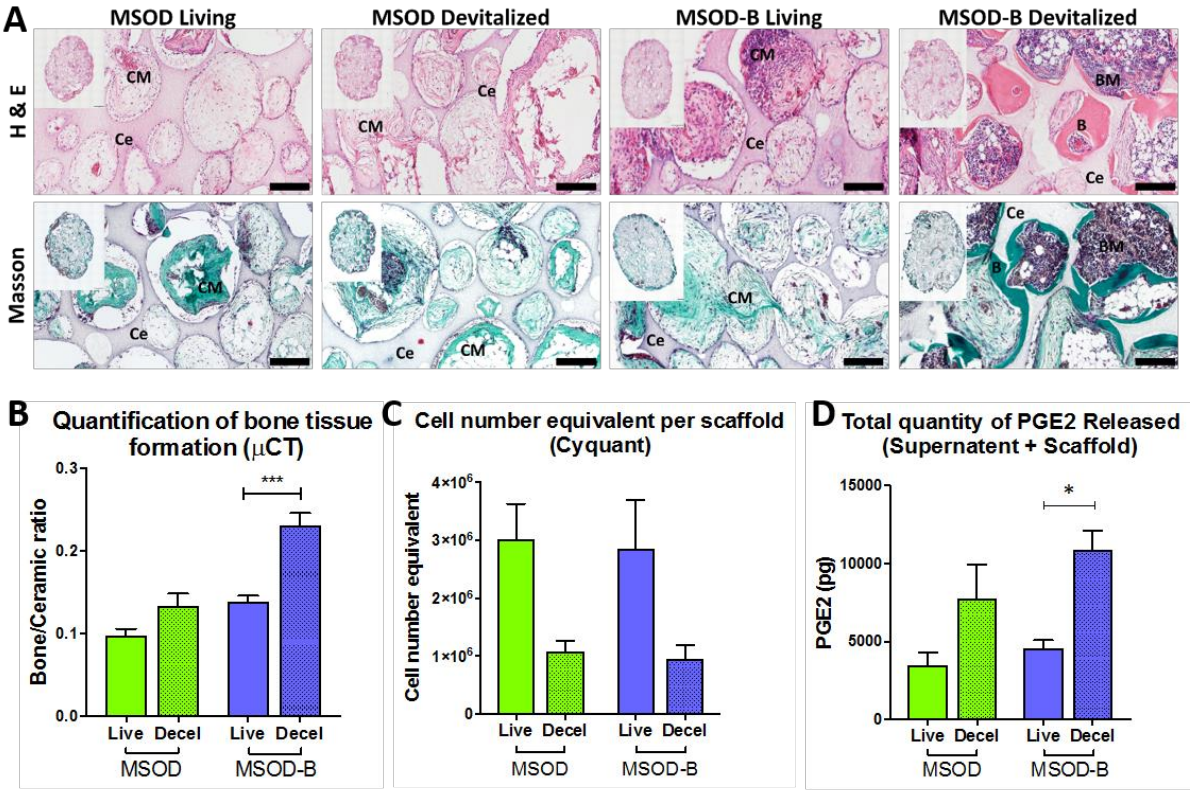

Figure 4: Osteoinductivity of decellularized ECM decorated scaffolds and proposed pathway involved. (A) In vivo osteogenic evaluation of MSOD and MSOD-B ECM decorated scaffolds ectopically implanted in nude mice for 12 weeks. H&E: Hematoxilin Eosin; Masson: Masson's Trichrome ; CM: Collagen Matrix; Ce: Ceramic scaffold; B, Bone; BM, Bone Marrow. (B) Histomorphometric quantification of newly formed bone tissue within ECM decorated scaffolds (n = 3 based on microcomputerized tomography analysis. (C) Quantification of the equivalent of cells per scaffold quantified by Cyquant DNA mesurement. (D) ELISA quantification of Prostaglandin E2 (PGE2) released overnight in the supernatant and entrapped in the scaffolds by MSOD and MSOD-B lines without (Live) or upon Cell Death induction (Decel) in 3D-perfusion bioreactors (n=3). scale bar: 200 µm *p<0,5; ***p<0,01

4. Discussion, conclusions and perspectives

In this study, we report the design of an innovative cellular tool to engineer osteoinductive grafts for bone regeneration. Critical bone defects together with stringent clinical scenarios require the development of novel bone repair strategies. Recently, tissue engineering has proposed attractive approaches based on ECM-decorated cell-free scaffolds [6], [7]. However, the quality of the engineered ECM is typically affected by the interdonor variability [12], [13]. Thus, the use of an hMSC line could suppress the need of primary material, standardize and increase efficiency of osteoinductive grafts by tuning its properties. We previously developed an immortalized hMSC cell line, MSOD [1], engineered with an inducible apoptosis system. Unfortunately, MSOD displayed solely an immature bone formation capacity in vivo [14]. To obtain mature bone, we engineered a novel hMSC starting from the MSOD line capable to constitutively express BMP2, key factor during bone morphogenesis and repair by promoting

MSC recruitment, differentiation, and calcified matrix deposition [15][16]. We describe here that MSOD-B line secretes a high quantities of BMP2 and efficiently differentiates towards the osteoblastic lineage, both in vitro and in vivo, while maintaining its capacity to undergo apoptosis upon exposure to a clinically approved Cell Death inducer [2], [14].

We observed that this new cell line displays a higher metabolic rate than MSOD, likely resulting from continuous BMP2 stimulation. Since cell immortalization could lead to a gradual loss of the undifferentiated status of MSCs, all experiments were performed with MSOD-B at the same passage, ensuring also an equivalent time of BMP2 exposure. In order to better control in space and time the secretion of key factors by cellular tools, we envision the use of inducible promoters [17]. This type of mechanisms would allow the controlled spatiotemporal secretion of several morphogenetic factors by pooling distinct engineered lines re-enacting the embryonic developmental path or regenerative sequence leading to harmonious and stable in vitro tissue engineering.

Since the half-life of rhBMP2 is about 6.7 min due to enzymatic degradation and rapid rate of clearance, to increase its effectiveness in non-union fractures, rhBMPs are combined with biocompatible carriers such as absorbable collagen sponges [18]. To date, commercial collagen sponges loaded with BMP2 (InFUSE, Medtronic) are used for critical-sized long-bone defects repair [19]. Nevertheless, those products exhibit a sub-optimal delivery system characterized by a high initial burst and poor long-term release. This kinetics is associated with development of antibodies against BMP2, ectopic bone formation in fracture treatment and critical soft tissue swelling [20]. In contrast, ECM-decorated scaffolds enriched in BMP2 ensure a long-term morphogen release. Indeed, during ECM deposition, cells also produce other growth factors that are entrapped in the secreted matrix and released in vivo upon matrix remodeling. BMP2 protein distribution and embedding in the ECM should be further explored to increase our understanding in the optimal fashion to present this molecule. This might also help to explain the positive effect in bone formation we observed with a BMP2 dose x times lower than previously described [21].

Physical and enzymatic decellularization procedures affect ECM composition and cause ultrastructure disruption [22]. To avoid these detrimental effects, MSOD-B line expresses an inducible death system that permits complete cell death within 24 hours. This system has already been used to devitalize ECM-decorated scaffolds with better preservation of the

matrix structure and composition, compared to other existing devitalization methods [7]. Nevertheless, we could measure a high quantity of DNA per scaffold after death induction. Exogenous DNA triggers immune reaction and apoptotic vesicles have been shown to modulate tissue regeneration through (PGE2) signalling [11]. Indeed, our data show that PGE2 secretion is increased upon apoptosis induction. This point could also rise concerns in view of any human clinical application for which the presence of cells or free DNA are not acceptable parameters [23]–[25].

Previous studies reported that the BMP2 overexpression in primary MSCs leads to bone formation and critical-sized defects repair. On the other hand, it was demonstrated that immortalized hMSCs were able to differentiate in immature osteoid tissue in vivo [26]–[28]. Interestingly, we firstly showed that the implantation of living hMSC cell line overexpressing BMP2 resulted in mature bone formation highlighting its osteogenic potential. However, we observed non-homogeneous bone distribution throughout the scaffold (higher quantity in the margins of the explant), which could be the next feature to optimise for complete critical size defect regeneration.

Additionally to the elements described in this report, the capacity of MSOD-B to undergo chondrogenesis and to remodel into endochondral bone has also been assessed, driven by the strong presence of glycosaminoglycan after 2D differenciation (**Fig. 1C**). Briefly, cartilaginous templates based on collagen sponge statically seeded with MSOD-B (ref for protocol) were devitalized by apoptosis induction prior to subcutaneous implantation in nude mice (6 weeks). The devitalized tissues were remodelled generating small bone organoids. Microtomography analysis displayed perichondral and trabecular bone structures as well as bone marrow in a very consistent fashion still under investigation. Taken together, those data suggest that MSOD-B could be the first cell line reported to achieve both endochondral and intramembranous ossification.

5. References

[1] P. Bourgine, C. Le Magnen, S. Pigeot, J. Geurts, A. Scherberich, and I. Martin, "Combination of immortalization and inducible death strategies to generate a human mesenchymal stromal cell line with controlled survival," *Stem Cell Res.*, vol. 12, no. 2, pp. 584–598, 2014.

[2] C. A. Ramos *et al.*, "An inducible caspase 9 suicide gene to improve the safety of mesenchymal stromal cell therapies.," *Stem Cells*, vol. 28, no. 6, pp. 1107–1115, 2010.

[3] M. Amendola, M. A. Venneri, A. Biffi, E. Vigna, and L. Naldini, "Coordinate dual-gene transgenesis by lentiviral vectors carrying synthetic bidirectional promoters," *Nat. Biotechnol.*, vol. 23, no. 1, pp. 108–116, 2005.

[4] O. Frank *et al.*, "Real-time quantitative RT-PCR analysis of human bone marrow stromal cells during osteogenic differentiation in vitro," *J. Cell. Biochem.*, vol. 85, no. 4, pp. 737–746, 2002.

[5] D. Wendt, A. Marsano, M. Jakob, M. Heberer, and I. Martin, "Oscillating perfusion of cell suspensions through three-dimensional scaffolds enhances cell seeding efficiency and uniformity," *Biotechnol. Bioeng.*, vol. 84, no. 2, pp. 205–214, Oct. 2003.

[6] N. Sadr *et al.*, "Enhancing the biological performance of synthetic polymeric materials by decoration with engineered, decellularized extracellular matrix," *Biomaterials*, vol. 33, no. 20, pp. 5085–5093, Jul. 2012.

[7] P. E. Bourgine *et al.*, "Engineered Extracellular Matrices as Biomaterials of Tunable Composition and Function," *Adv. Funct. Mater.*, vol. 27, no. 7, 2017.

[8] G. N. Duda and J. Wolff, "(No Title)," vol. 22, pp. 26–42, 2011.

[9] B. Delorme *et al.*, "Specific plasma membrane protein phenotype of culture-amplified and native human bone marrow mesenchymal stem cells," *Blood*, vol. 111, no. 5, pp. 2631–2635, Mar. 2008.

[10] L. Song, N. E. Webb, Y. Song, and R. S. Tuan, "Identification and Functional Analysis of Candidate Genes Regulating Mesenchymal Stem Cell Self-Renewal and Multipotency," *Stem Cells*, vol. 24, no. 7, pp. 1707–1718, Jul. 2006.

[11] F. Li *et al.*, "Apoptotic cells activate the 'phoenix rising' pathway to promote wound healing and tissue regeneration," *Sci. Signal.*, vol. 3, no. 110, Feb. 2010.

[12] R. Siddappa, R. Licht, C. van Blitterswijk, and J. de Boer, “Donor variation and loss of multipotency during in vitro expansion of human mesenchymal stem cells for bone tissue engineering,” *J. Orthop. Res.*, vol. 25, no. 8, pp. 1029–1041, Aug. 2007.

[13] A. R. Amini, C. T. Laurencin, and S. P. Nukavarapu, “Bone tissue engineering: Recent advances and challenges,” *Crit. Rev. Biomed. Eng.*, vol. 40, no. 5, pp. 363–408, 2012.

[14] K. C. Straathof *et al.*, “An inducible caspase 9 safety switch for T-cell therapy,” *Blood*, vol. 105, no. 11, pp. 4247–4254, Jun. 2005.

[15] N. Kamiya and Y. Mishina, “New insights on the roles of BMP signaling in bone-A review of recent mouse genetic studies,” *BioFactors*, vol. 37, no. 2. pp. 75–82, Mar-2011.

[16] V. Rosen, “BMP2 signaling in bone development and repair,” *Cytokine and Growth Factor Reviews*, vol. 20, no. 5–6. pp. 475–480, Oct-2009.

[17] Kallunki, Barisic, Jäättelä, and Liu, “How to Choose the Right Inducible Gene Expression System for Mammalian Studies?,” *Cells*, vol. 8, no. 8, p. 796, 2019.

[18] J. W. Hustedt and D. J. Blizzard, “The controversy surrounding bone morphogenetic proteins in the spine: A review of current research,” in *Getting to Good: Research Integrity in the Biomedical Sciences*, Springer International Publishing, 2018, pp. 9–22.

[19] J. K. Burkus, S. E. Heim, M. F. Gornet, and T. A. Zdeblick, “Is INFUSE Bone Graft superior to autograft bone? An integrated analysis of clinical trials using the LT-CAGE Lumbar Tapered Fusion device,” *J. Spinal Disord. Tech.*, vol. 16, no. 2, pp. 113–122, 2003.

[20] D. G. Schultz, “Public Health Notifications (Medical Devices) - FDA Public Health Notification: Life-threatening Complications Associated with Recombinant Human Bone Morphogenetic Protein in Cervical Spine Fusion,” *Fda*, 2008.

[21] S. Herberg *et al.*, “Low-dose bone morphogenetic protein-2/stromal cell-derived factor-1β cotherapy induces bone regeneration in critical-size rat calvarial defects,” *Tissue Eng. - Part A*, vol. 20, no. 9–10, pp. 1444–1453, May 2014.

[22] P. M. Crapo, T. W. Gilbert, and S. F. Badylak, “An overview of tissue and whole organ decellularization processes,” *Biomaterials*, vol. 32, no. 12. pp. 3233–3243, Apr-2011.

[23] P. Matzinger, “An innate sense of danger,” *Semin. Immunol.*, vol. 10, no. 5, pp. 399–415, 1998.

[24] P. Matzinger, “Tolerance, Danger, and the Extended Family,” *Annu. Rev. Immunol.*, vol. 12, no. 1, pp. 991–1045, Apr. 1994.

[25] E. Medicines Agency, “Guideline on quality, non-clinical and clinical aspects of 4 medicinal products containing genetically modified cells - Revision 1,” 2008.

[26] S. Sharma *et al.*, “Adenoviral Mediated Expression of BMP2 by Bone Marrow Stromal Cells Cultured in 3D Copolymer Scaffolds Enhances Bone Formation,” *PLoS One*, vol. 11, no. 1, p. e0147507, 2016.

[27] M. Pensak *et al.*, “The role of transduced bone marrow cells overexpressing BMP-2 in healing critical-sized defects in a mouse femur,” *Gene Ther.*, vol. 22, no. 6, pp. 467–475, Jun. 2015.

[28] J. L. Dragoo *et al.*, “Bone induction byBMP-2 transduced stem cells derived from human fat,” *J. Orthop. Res.*, vol. 21, no. 4, pp. 622–629, Jul. 2003.

Chapter 5. Engineering of mesenchymal tissues supporting healthy hematopoiesis

Article: *In vitro biomimetic engineering of a human hematopoietic niche with functional properties*

In vitro biomimetic engineering of a human hematopoietic niche with functional properties

Paul E. Bourgine[a,1], Thibaut Klein[b,1], Anna M. Paczulla[c], Takafumi Shimizu[d], Leo Kunz[a], Konstantinos D. Kokkaliaris[a], Daniel L. Coutu[a], Claudia Lengerke[c], Radek Skoda[d], Timm Schroeder[a,2], and Ivan Martin[b,2]

[a]Department of Biosystems Science and Engineering, Eidgenössische Technische Hochschule Zürich, 4058 Basel, Switzerland; [b]Tissue Engineering, Department of Biomedicine, University Hospital Basel, University of Basel, 4031 Basel, Switzerland; [c]Stem Cells and Hematopoiesis, Department of Biomedicine, University Hospital Basel, University of Basel, 4031 Basel, Switzerland; and [d]Experimental Hematology, Department of Biomedicine, University Hospital Basel, University of Basel, 4031 Basel, Switzerland

Edited by Helen M. Blau, Stanford University, Stanford, CA, and approved May 4, 2018 (received for review March 30, 2018)

In adults, human hematopoietic stem and progenitor cells (HSPCs) reside in the bone marrow (BM) microenvironment. Our understanding of human hematopoiesis and the associated niche biology remains limited, due to human material accessibility and limits of existing in vitro culture models. The establishment of an in vitro BM system would offer an experimentally accessible and tunable platform to study human hematopoiesis. Here, we develop a 3D engineered human BM analog by recapitulating some of the hematopoietic niche elements. This includes a bone-like scaffold, functionalized by human stromal and osteoblastic cells and by the extracellular matrix they deposited during perfusion culture in bioreactors. The resulting tissue exhibited compositional and structural features of human BM while supporting the maintenance of HSPCs. This was associated with a compartmentalization of phenotypes in the bioreactor system, where committed blood cells are released into the liquid phase and HSPCs preferentially reside within the engineered BM tissue, establishing physical interactions with the stromal compartment. Finally, we demonstrate the possibility to perturb HSPCs' behavior within our 3D niches by molecular customization or injury simulation. The developed system enables the design of advanced, tunable in vitro BM proxies for the study of human hematopoiesis.

hematopoiesis | bone marrow niche | 3D culture | tissue engineering | hematopoietic stem cell

The bone marrow (BM) microenvironment is responsible for the maintenance of hematopoietic stem cell (HSC) activity, enabling the lifelong production of mature blood cells (1, 2). The regulation of HSC self-renewal and differentiation is achieved by complex cellular (3), molecular (4, 5), structural (6), and physical (7, 8) cues defining the HSC niche (2, 9). The components of the human HSC niche, and how these elements interact to modulate stem cell fate, remain poorly understood.

The field is hampered by the limited possibilities to access and harness information from human specimens. Chimeric animal models (10) most closely recapitulate in vivo human physiology, but, in this setting, the niche has remained inaccessible to experimental manipulation and optical observation (11, 12). In addition, the interspecies-chimerism in both hematopoietic cells and their environment makes interpretation of experimental results difficult. The development of in vitro substitutes is a promising alternative with superior tunability and throughput (13, 14). Previous studies have described the combination of different stromal and hematopoietic progenitors using a variety of culture substrates (9–11), resulting in the phenotypic preservation of specific blood phenotypes. However, the recapitulation of the structural organization of BM, including essential cell–cell and cell–matrix interactions (15–19), and the associated functional preservation of HSCs (20) are still elusive.

The need for advanced culture systems of higher biological complexity has gained increasing recognition (21) to study the fundamental biology of stem cells. Similarly to the "organogenesis in a dish" proposed for complex organs [e.g., lung (22), breast (23), kidney (24), and liver (25)], the in vitro engineering of human BM environments (21, 26–28) capable to sustain HSCs (28, 29) would enable their study in xeno-free settings.

Here, we report an in vitro system supporting the development and maintenance of a human BM analog. Our approach consists in the use of porous hydroxyapatite scaffolds with structural and compositional features of bone (30), functionalized by human mesenchymal stromal cells (hMSCs) and the extracellular matrix (ECM) deposited during their progressive maturation into the osteoblastic lineage. The hMSC culture is performed under direct perfusion flow (31), offering efficient nutrient supply/waste removal, while mimicking interstitial flow and associated shear stress. The blood compartment was introduced into the resulting 3D stromal tissue by perfusion of human purified cord blood (CB)-derived $CD34^+$ cells. This engineered organoid partially recapitulates structural and functional features of the human BM in defined and tunable settings.

Results

Three-Dimensional Microenvironments Can Be Engineered Within the Perfusion Bioreactor System. The generation of the 3D microenvironments was performed by differentiation of primary

Significance

The development of an in vitro human bone marrow (BM) tissue appears essential to compile information on human hematopoiesis. Conventional systems fail at both capturing the complexity of the bone marrow niche while allowing the maintenance of functional hematopoietic stem cells (HSCs). Here, we report the development of a human 3D (BM) analogue in a perfusion-based bioreactor system, partially recapitulating structural, compositional, and organizational features of the native human osteoblastic niche environment. The engineered tissue supports the maintenance of some hematopoietic stem and progenitor cell (HSPC) properties. This provides an advanced technological platform of broad fundamental and translational relevance, including the study of human HSPC biology and interactions with their niche, the manipulation of functional human HSPCs, or the identification of factors influencing human hematopoiesis.

Author contributions: P.E.B., T.S., and I.M. designed research; P.E.B., T.K., A.M.P., and T.S. performed research; L.K., K.D.K., and D.L.C. contributed new reagents/analytic tools; P.E.B., K.D.K., C.L., R.S., T.S., and I.M. analyzed data; and P.E.B., T.S., and I.M. wrote the paper.

The authors declare no conflict of interest.

This article is a PNAS Direct Submission.

[1]P.E.B. and T.K. contributed equally to this work.

[2]To whom correspondence may be addressed. Email: timm.schroeder@bsse.ethz.ch or ivan.martin@usb.ch.

This article contains supporting information online at www.pnas.org/lookup/suppl/doi:10.1073/pnas.1805440115/-/DCSupplemental.

BM-derived hMSCs on ceramic materials within a perfusion bioreactor. Cells were first labeled with a VENUS transgene (>93%) (*SI Appendix*, Fig. S1*A*) to facilitate subsequent analysis. To achieve the engineering of an osteoblastic-like stroma, we adopted a protocol previously used for the generation of bone grafts (32) (Fig. 1*A*). hMSCs were first cultured 1 wk in proliferative medium (PM) to increase cell number and ensure scaffold colonization, followed by 3 wk of osteogenic medium (OM) supplementation, to promote cell differentiation while stimulating extracellular matrix (ECM) production (33). The resulting tissue was defined as "engineered niche" (eN) (Fig. 1*A*) while naked ceramic (Ce) (Fig. 1*A*), not containing hMSCs but loaded with $CD34^+$ cells, was used as internal 3D culture control. The blood compartment was subsequently introduced by injecting CB-derived human $CD34^+$ cells from single donors into the device tubing. The in vitro coculture was sustained for 1 wk in serum-free medium supplemented with a low concentration of hematopoietic cytokines [10 ng/mL thrombopoietin (TPO), stem cell factor (SCF), and Fms-related tyrosine kinase 3 ligand (Flt3-L)]. Upon retrieval from the bioreactor chamber, the Ce was devoid of apparent ECM structures (Ce, *SI Appendix*, Fig. S1*B*) while the eN exhibited features of an engineered tissue with thick gel-like structures homogenously covering the starting material (eN, Fig. 1*B*). Scanning electron microscopy confirmed the deposition of an ECM which embeds cells, presumably of both stromal (fibroblastic shape, Fig. 1*B*) and blood origins (round shape, Fig. 1*B*), including dividing cells (Fig. 1*B*).

Engineered 3D Microenvironments Allow the Maintenance of Hematopoietic Stem and Progenitor Cells with Functional Properties. To characterize their cellular composition, the 3D microenvironments were digested for cell retrieval (>92% retrieval efficiency, with an overall cell death below 1.5%) (*SI Appendix*, Fig. S1 *B* and *C*) and subsequent quantitative phenotypic analysis (*SI Appendix*, Fig. S1 *D* and *E*).

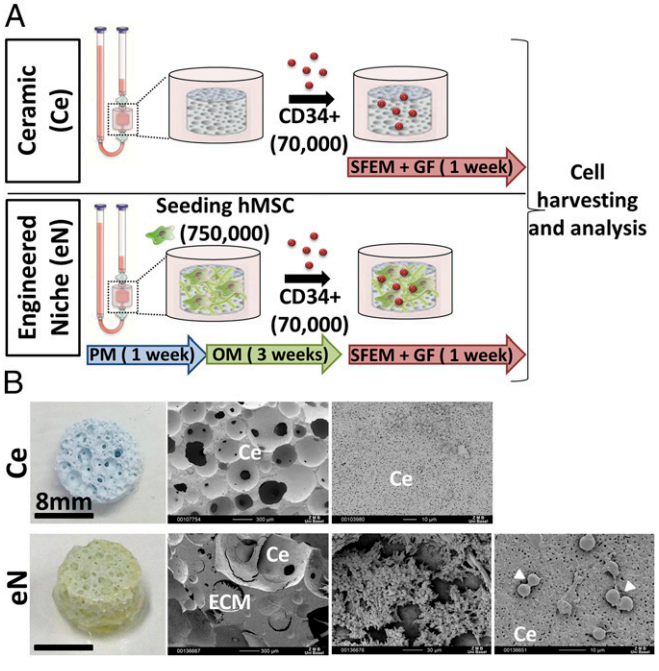

Fig. 1. Three-dimensional microenvironments can be engineered within the perfusion bioreactor system. (*A*) Experimental design for the generation of 3D niches in a perfusion bioreactor. OM, osteogenic medium; PM, proliferative medium; SFEM+GF, serum-free medium plus growth factors stem cell factor, thrombopoietin, and Flt3-ligand. (*B*) The engineered niche (eN, *Left*) exhibits thick gel-like structures homogenously covering the starting material (Ce). Scanning electron microscopy images of eN (*Right*) confirmed the deposition of an ECM which embeds cells, presumably of both stromal and blood origins. Arrowheads indicate the presence of dividing cells.

The eN was composed of over 4.7×10^6 blood cells (*SI Appendix*, Fig. S1*F*) per bioreactor system [61-fold increase (f.i.) over the initial 70,000 $CD34^+$ cells] (*SI Appendix*, Fig. S1*G*). In contrast, in the absence of engineered stroma, blood cell expansion was limited to a 7.8 f.i. (*SI Appendix*, Fig. S1 *F* and *G*). With a ratio of HSPCs over committed cells ($CD34^-/CD38^+$) lower than the Ce (38 vs. 204) (*SI Appendix*, Fig. S1*H*), the eN was shown to sustain the proliferation of differentiated populations. The eN also promoted the maintenance of phenotypic hematopoietic stem and progenitor populations (HSPCs) (Fig. 2*A*), yielding systematically higher total numbers of HSPCs (46.2 f.i. vs. 6.4 for Ce), including HSCs (13.8 f.i. vs. 1.6), multipotent progenitors (MPPs) (8.5 f.i. vs. 2.3), and multipotent lymphoid progenitors (MLPs) (161 f.i. vs. 20) (*SI Appendix*, Fig. S2*A*).

The capacity of hMSCs to support the proliferation of $CD34^+$ cells was further confirmed in a 2D setup (*SI Appendix*, Fig. S2*B*). Using undifferentiated hMSCs as feeder layer (2D hMSCs) compared with a hMSC-free control (2D), we observed a significant increase of phenotypic HSPCs (100 f.i. vs. 15), HSCs (29 f.i. vs. 4), MPPs (43 f.i. vs. 16), and MLPs (279 f.i. vs. 21) (*SI Appendix*, Fig. S2*B*), in line with results derived from well-established Dexter cultures (34, 35). The capacity of the generated stroma to preserve the functionality of cultured blood cells was assessed both by in vitro and in vivo assays. The corresponding donor cells before in vitro culture ("uncultured") were used as functional positive control. In vitro colony-forming unit assays demonstrated the maintenance of stem or progenitor cell capacities (with multilineage and proliferation potential) of cultured $CD34^+$ cells, indicated by the generation of myeloid colonies with the same morphology as their uncultured counterparts (*SI Appendix*, Fig. S2*C*). Colony numbers were increased for cells retrieved from 3D cultures for colony-forming unit-granulocyte and macrophage (GM) (42.8 f.i vs. 4.8 for Ce), burst-forming unit-erythroid (BFU-E) (113 f.i vs. 18), and Colony-forming unit-Granulocyte (GEmM) (36.5 f.i vs. 4.8) colonies (Fig. 2*B*).

Stem and progenitor potential of cultured cells was further tested by intrafemoral transplantation of equal numbers of $CD34^+$ cells from Ce or eN in irradiated NSG mice. The human blood compartment was successfully reconstituted in all groups [>1% human CD45 positive cells (hCD45) in peripheral blood] (Fig. 2*C*). Chimerism was detectable as early as week 6 and persisted over 28 wk posttransplantation, indicating the long-term repopulation capacity of transplanted cells. As anticipated, the highest chimerism was obtained by transplantation of uncultured $CD34^+$ serving as positive control ($27.9 \pm 3.1\%$) (Fig. 2*C*). $CD34^+$ cells derived from Ce and eN exhibited similar reconstitution levels, with an average of $2.7 \pm 0.8\%$ and $6.4 \pm 1\%$ of hCD45 respectively, detected in the peripheral blood (Fig. 2*C*). The chimerism was also assessed in the BM and the spleen of animals with human cells robustly engrafted in all conditions, with a trend for higher hCD45 frequency detected in the eN than in the Ce group, both in BM ($6.4\% \pm 0.5$ vs. $5.2\% \pm 2.5$, Fig. 2*D*) and the spleen ($12.6\% \pm 4.4$ vs. $5.6\% \pm 2.8$, Fig. 2*D*). Functionality of $CD34^+$ cells was further assessed by multilineage reconstitution capacity. At week 18 posttransplantation, cells from all conditions successfully reconstituted the myeloid and lymphoid lineages (*SI Appendix*, Fig. S2*D*).

These data demonstrate that, compared with the Ce counterparts, the eN yields hematopoietic cells with similar reconstitution potential, but in higher numbers. This suggests that the generated tissue provides cues capable to enhance the maintenance/expansion of CFU-HSPCs with in vivo engraftment and multilineages reconstitution potential.

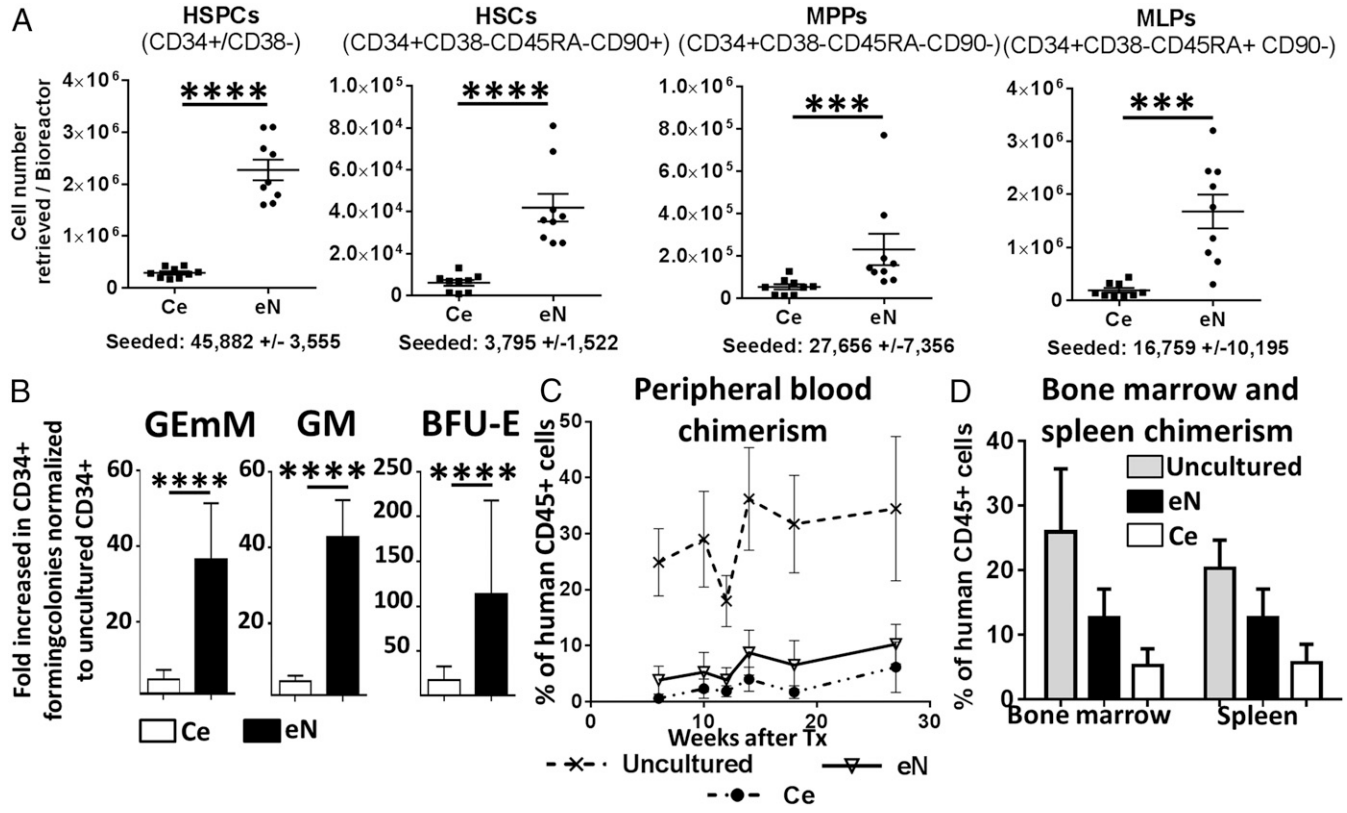

Fig. 2. Engineered 3D microenvironments allow the maintenance of HSPCs with functional properties. (*A*) The engineered niche (eN) supports the expansion of phenotypic hematopoietic stem and progenitor cells (HSPCs), hematopoietic stem cells (HSCs), multipotent progenitors (MPPs), and multipotent lymphoid progenitors (MLPs), as assessed by quantitative flow cytometry analysis post-3D culture. $n \geq 8$ biological replicates. Ce, ceramic only. ***$P < 0.001$, ****$P < 0.0001$. (*B*) Improved maintenance of colony-forming potential of eN versus Ce cultured CD34$^+$ cells. BFU-E, burst-forming unit-erythroid; GEmM, colony-forming unit-granulocyte, erythroid, macrophage, megakaryocyte; GM, colony-forming unit-granulocyte and macrophage. $n \geq 9$ biological replicates. (*C*) The long-term repopulation capacity of eN and Ce cultured CD34$^+$ cells. Reconstitution of the human blood compartment (percentage of human CD45$^+$ cells in mononuclear cells) in NSG mice is shown by flow cytometry analysis of peripheral blood. Uncultured CD34$^+$ cells served as positive control. $n \geq 4$ biological replicates. Human CD34$^+$ cells cultured on eN and Ce also robustly engrafted in the bone marrow and spleen (*D*) of transplanted mice, as assessed by flow cytometry 28 wk posttransplantation. $n \geq 4$ biological replicates.

Molecular Characterization of the Engineered Niche Reveals the Establishment of an Osteoblastic-Like 3D Environment. To identify factors associated with robust hematopoiesis development, the eN was further characterized. First, we monitored the secretion of key cytokines throughout culture times. Inflammatory factors [interleukin 6 (IL-6), interleukin 8 (IL-8), macrophage colony-stimulating factor (MCSF) (Fig. 3*A*), and monocyte chemoattractant protein-1 (MCP-1)] showed the highest differences and were found at high concentrations in eN. In particular, IL-6 and IL-8 production increased substantially upon HSPC addition (eN, Fig. 3*A*). Flt3-L, TPO, and SCF proteins were found at concentrations similar to those supplemented in the coculture medium (*SI Appendix*, Fig. S3*A*), suggesting that hMSCs secrete low levels of those HSPC supportive factors. Vascular endothelial growth factor α (VEGFα) and angiopoietin 1 (Ang-1) were also detected at significant levels (eN, *SI Appendix*, Fig. S3*A*) although Ang-1 decreased over time to remain stable after HSPC loading.

To obtain a more comprehensive understanding of the cellular compartments associated with factor secretion, we isolated both blood progenitors (CD34$^+$) and mesenchymal populations before (defined as hMSC day 28) (*SI Appendix*, Fig. S3*B*) and after CD34$^+$ coculture (defined as eN-hMSC day 35, *SI Appendix*, Fig. S3*B*). This confirmed the strong expression of inflammatory cytokines (IL-6, MCSF) by hMSCs during coculture with HSPCs, with levels markedly higher than those in blood progenitor cells (Fig. 3*B*). IL-8 and MCP-1 were expressed by both blood and mesenchymal cells (Fig. 3*B*). Interestingly, following coculture with CD34$^+$ cells, hMSCs substantially increased their IL-6 and IL-8 expression (Fig. 3*B*).

To assess the role of IL-6 and IL-8 in the system, we investigated the effect of their addition in the Ce condition (*SI Appendix*, Fig. S4*A*). IL-6 and IL-8 at doses corresponding to those measured in the eN led to a significant increase in the number of HSPCs, committed progenitors (CD34$^+$/CD38$^+$), Granulocyte-monocytes progenitors (GMPs), and MLPs (*SI Appendix*, Fig. S4*B*). However, no effect was measured on HSCs and MPPs (*SI Appendix*, Fig. S4*B*). This suggests that these inflammatory cytokines mediate the proliferation of committed populations in the eN whereas the observed stem cell compartment expansion is driven by other hMSC factors.

Before CD34$^+$ loading, hMSCs in the engineered tissue predominantly consisted of not only osteoblastic-like cells, but also of a pool expressing progenitor markers (*SI Appendix*, Fig. S5). We further analyzed the transcription profile of eN-hMSCs as niche cells at the end of the culture (eN-hMSC day 35) and compared it to postexpanded hMSCs (hMSC Day 0) and hMSCs in the eN before CD34$^+$ loading (hMSC day 28). This confirmed the osteoblastic profile of hMSC (day 35) at the end of the 3D culture, evidenced by the up-regulation of alkaline phosphatase (ALP) and bone sialoprotein (BSP) (17 and 869 f.i., respectively) (Fig. 3*C*). Interestingly, a marked increase in Nestin expression (117 f.i.) was acquired by hMSCs after coculture with blood cells (Fig. 3*C*), as well as a decrease in hypoxia-inducible factor 1-alpha (HIF1α, 8.9-fold) expression.

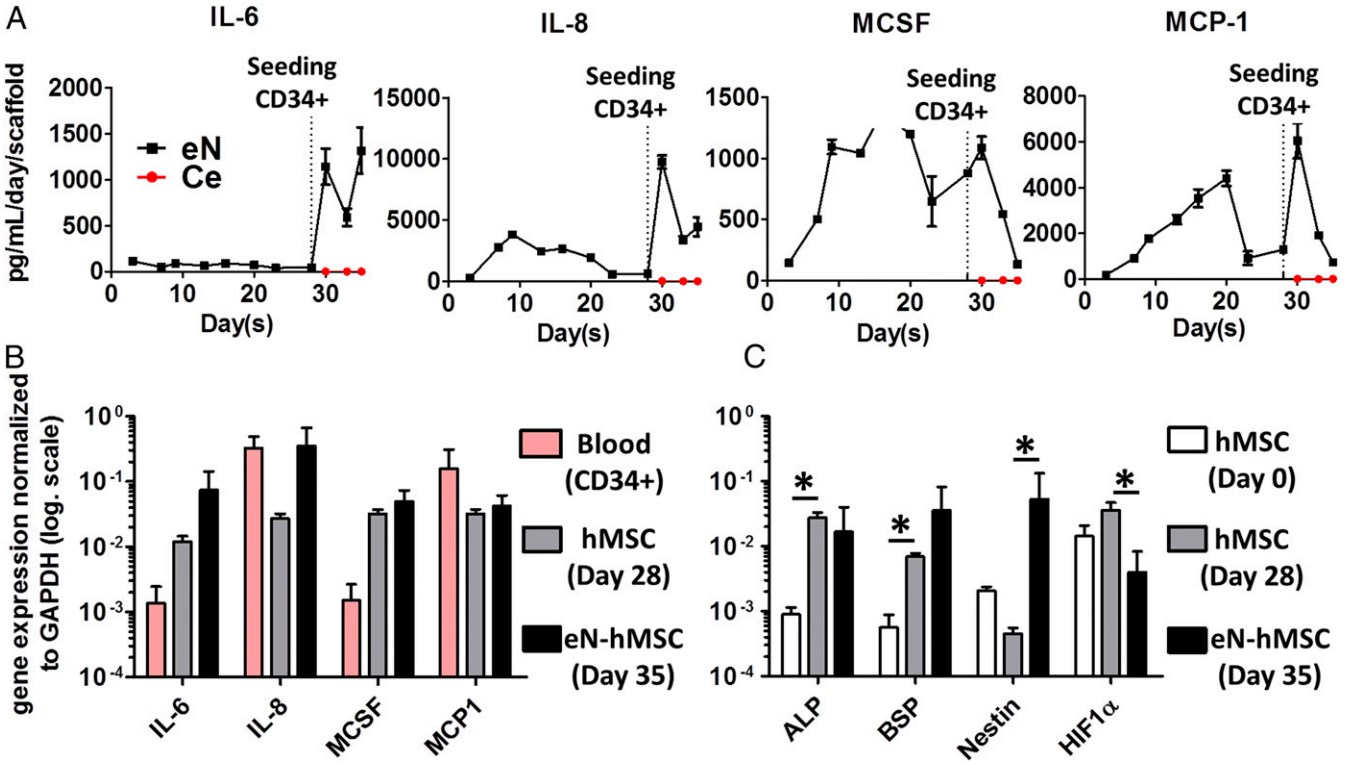

Fig. 3. Molecular characterization of the engineered niche reveals the establishment of an osteoblastic-like 3D environment. (*A*) The engineered niche (eN) condition presents a higher concentration in inflammatory cytokines than the ceramic condition (Ce), based on Luminex analysis of 3D culture supernatants. IL-6, interleukin 6; IL-8, interleukin 8; MCP-1, monocyte chemotactic protein 1; MCSF, macrophage colony-stimulating factor. $n \geq 3$ biological replicates. Addition of $CD34^+$ cells to the niches only induces cytokine secretion in eN conditions. (*B*) hMSCs are principally responsible for the high levels of inflammatory cytokines detected in the eN. This was assessed by gene expression analysis of blood progenitor cells ($CD34^+$), and hMSCs before (day 28) and after coculture with blood cells (day 35). $n \geq 3$ biological replicates. (*C*) hMSCs acquire an osteoblastic-like niche genetic profile in culture. Gene expression analysis of hMSCs retrieved from the eN (eN hMSC). hMSCs (hMSC day 0) indicate the basic gene expression levels before their 3D culture. ALP, alkalyne phosphatase; BSP, bone sialoprotein; HIF1α, hypoxia-inducible factor 1α. $n \geq 3$ biological replicates.

Thus, by combining protein and gene expression analyses, we describe an osteoblastic (36, 37) and niche-associated (1) molecular signature of hMSCs, associated with proinflammatory features, which is acquired following the coculture with the blood compartment. This suggests the establishment of an osteoblastic-like niche environment, mutually interacting with hematopoietic cells and capable of regulating HSPC activities, including proliferation and functional regulation.

The Engineered Niche Shares Structural and Compositional Features with Native Human BM. The role of hMSCs in the establishment of a supportive environment for the hematopoietic compartment was further investigated by studying the organization and composition of the eN. Immunofluorescence analysis of thick construct sections revealed a homogeneous network formed by hMSCs within the scaffold (VENUS signal, Fig. 4*A*). This observed mesenchymal fraction consisted in 1.3×10^6 hMSC-derived cells (Fig. 4*B*), as assessed by flow cytometry. The generated tissue resulting from the osteoblastic differentiation of hMSCs consisted in a dense human stroma filling the material pores and embedding mesenchymal cells (Fig. 4*C*). The composition of the deposited ECM included collagen type 1, collagen type 4, and fibronectin (Fig. 4*C*), reported as the main structural proteins of BM (38). Indeed, these were also abundantly found in healthy donor-derived BM specimens (human niche, Fig. 4*D*). The similarities between the human tissue and our engineered niche were not restricted to structural proteins. In human biopsies, osteocalcin staining revealed the presence of osteoblasts lining the bone surface (Fig. 4*D*). Remarkably, in the eN, a comparable pattern was observed by detection of osteocalcin in cells at the interface between the ceramic material and the cellular/ECM stroma (Fig. 4*C*).

Altogether, these results evidence the successful formation of a complex tissue under perfusion culture, associated with the development and support of human hematopoiesis (Fig. 2). The engineered environment was shown to share structural and compositional features typical of native human BM, suggesting the partial reconstitution of an osteoblastic-like niche environment.

The Bioreactor-Engineered Niche Displays a Functional Compartmentalization. The developed culture system comprises two distinct phases: a liquid-fraction consisting in the supernatant (SN) *SI Appendix*, Fig. S6) and the stromal/ECM tissue confined within the scaffold chamber (ECM, *SI Appendix*, Fig. S6). This led us to further hypothesize that the two environments could differently impact the distribution of blood cell phenotypes. We thus separately analyzed HSPCs derived from these two phases by flow cytometry (*SI Appendix*, Fig. S6).

Despite the convection induced by perfusion flow, a specific cellular allocation was observed as 80% of the retrieved HSPC ($CD34^+/CD38^-$) populations resided in the ECM (Fig. 5*A*, *Left*). Conversely, more committed populations ($CD34^-/CD38^+$) exhibited a balanced distribution with 54% in ECM and 46% in SN (Fig. 5*A*, *Right*). A distinct pattern could be identified by further assessing the preferential localization of stem and progenitor populations, according to their progressive commitment (Fig. 5*B*). Remarkably, HSCs were found almost exclusively in the stroma (98%) (Fig. 5*B*) together with a vast majority of MPPs

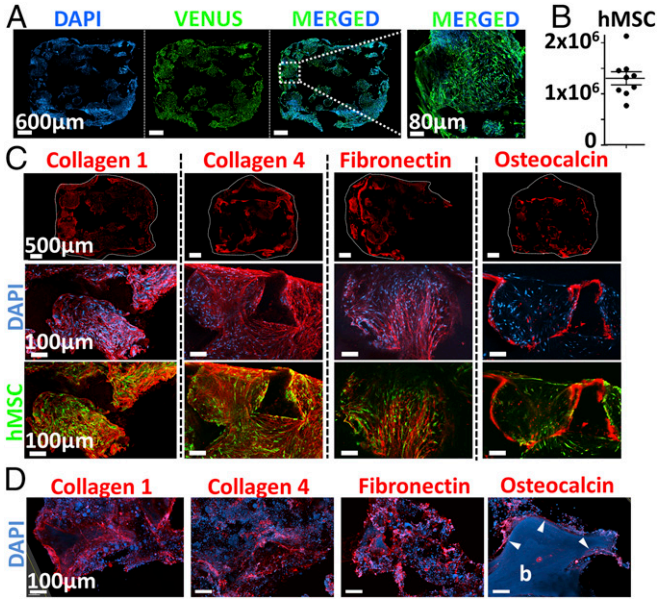

Fig. 4. The engineered niche shares structural and compositional features with native human BM. (*A*) hMSCs form a homogeneous cellular network distributed within the scaffolding material (confocal microscopy, representative images shown). (*B*) eN consists of 1.3 × 106 hMSC-derived cells at the end of the 3D culture (flow cytometry quantification). $n = 9$ biological replicates. Compositional and structural similarities of extracellular matrix in engineered niche (*C*) and human bone marrow samples (*D*), assessed by confocal microscopy. b, bone tissue (autofluorescence in the blue channel). Arrowheads indicate the presence of osteocalcin in osteoblasts lining at the bone surface.

(76% in ECM) (Fig. 5*B*). This applied to a lower extent to common myeloid progenitors (CMPs) and megakaryocyte-erythroid progenitors (MEPs) (67% in ECM) while GMPs were more abundant in the SN (61%) (Fig. 5*B*). The localization was also shown to impact on the in vitro functionality of cells since $CD34^+$ cells retrieved from ECM exhibited an increased capacity to form myeloid colonies compared with their SN counterpart (Fig. 5*C*). This includes the superior formation of GEmM, GM, and BFU colonies (2.6, 3.7, and 3.1 f.i., respectively).

The presence of human blood cells in the niche was confirmed by immunofluorescence, with human $CD34^+$ cells abundantly detected within the ECM of the engineered tissue (Fig. 5*D*). Cells were predominantly located at the periphery of the scaffolds (Edge, Fig. 5*D*) but also largely infiltrated the tissue as shown by presence in the inner pores (Inner, Fig. 5*D*) and in the more central area (Central, Fig. 5*D*). Importantly, the mesenchymal and hematopoietic fractions in the engineered stroma were found within an organized ECM (Fig. 5*E*, *Left*) and closely interacted, as shown by explicit physical contacts (Fig. 5*E*, *Right*).

Altogether, this demonstrates the existence of a functional compartmentalization in the 3D perfusion system. The eN displays a hierarchical chemoattractant property on HSPC populations while commitment is progressively associated with a release into the liquid phase. The preferential stem cell confinement in the stroma, together with evidences of hMSC–$CD34^+$ interactions, suggests an essential hMSC-triggered regulation of HSPC activities, resulting in a superior preservation of stem cell functionality.

BM Niches with Customized Molecular Signatures Can Be Genetically Engineered. We next aimed at a proof of principle for the use of our system for the generation of customized hematopoietic niches with tailored molecular signature.

To this end, primary hMSCs were efficiently transduced using a VENUS-SDF1α lentivirus (>95%) (*SI Appendix*, Fig. S7 *A* and *B*), resulting in SDF1α overexpression (*SI Appendix*, Fig. S7*C*). SDF1α-engineered niches (eN-SDF1α) were subsequently produced, following the previously described protocol, and compared with eN without SDF1α enrichment. Throughout the culture period, substantial levels of SDF1α protein were continuously produced by the eN-SDF1α (>2,000 pg/mL/day/bioreactor) (Fig. 6*A*) compared with the eN (<300 pg/mL/day/bioreactor) (Fig. 6*A*).

When retrieved from the bioreactor chambers, the different engineered tissues were macroscopically identical (Fig. 6*B*). Immunofluorescence analysis revealed the presence of hMSCs in both niches, but eN-SDF1α displayed an increased presence of SDF1α protein, confirming the secretion pattern previously observed and validating the molecular customization of the niche. The protein was particularly abundant intracellularly within hMSCs directly lining on the ceramic surface (eN-SDF1α, Fig. 6*B* and *SI Appendix*, Fig. S7*D*).

Flow cytometry quantitative phenotypic analysis was performed to assess the effect of the SDF1α enrichment in the system. The

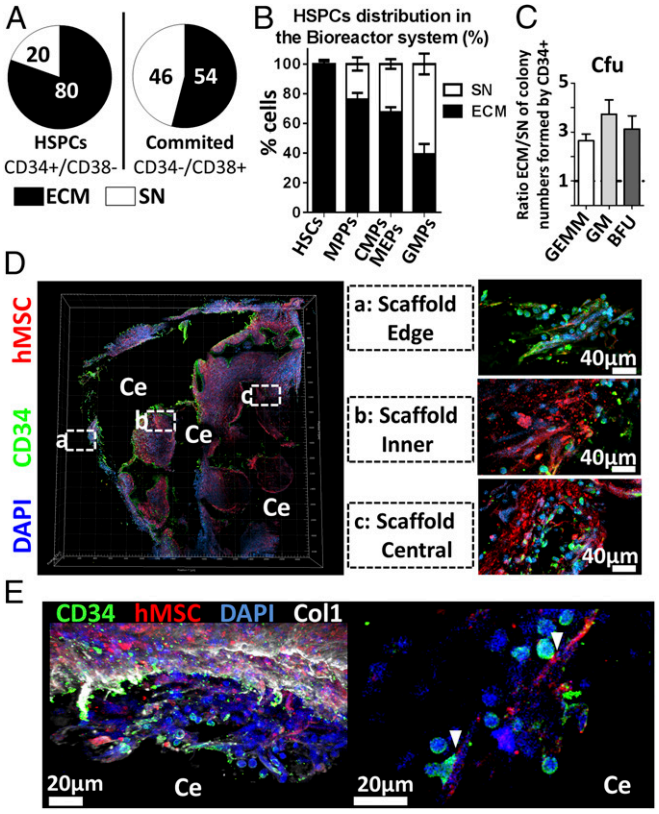

Fig. 5. The bioreactor-engineered niche displays a functional compartmentalization. (*A*) In the bioreactor system, the majority of HSPCs localized in the tissue (ECM) while committed cells are more equally distributed between the ECM and the supernatant (SN). $n \geq 8$ biological repeats. (*B*) HSC, MPP, and CMP/MEP populations preferentially localize in the stroma (ECM), not in the liquid phase. $n \geq 8$ biological repeats. (*C*) Superior myeloid colony formation potential of $CD34^+$ cells retrieved from the ECM. BFU, burst-forming unit-erythroid; GEmM, colony-forming unit-granulocyte, erythroid, macrophage, megakaryocyte; GM, colony-forming unit-granulocyte and macrophage. $n \geq 12$ biological replicates. (*D*) Confocal microscopy analysis of the eN demonstrates the presence of $CD34^+$ cells at different depths throughout the tissue (*Right*, magnification). The $CD34^+$ and hMSC fractions were found within an organized extracellular matrix (*E*, *Left*) in which they established physical interactions (*E*, *Right*). Ce, ceramic; Col1, collagen type 1.

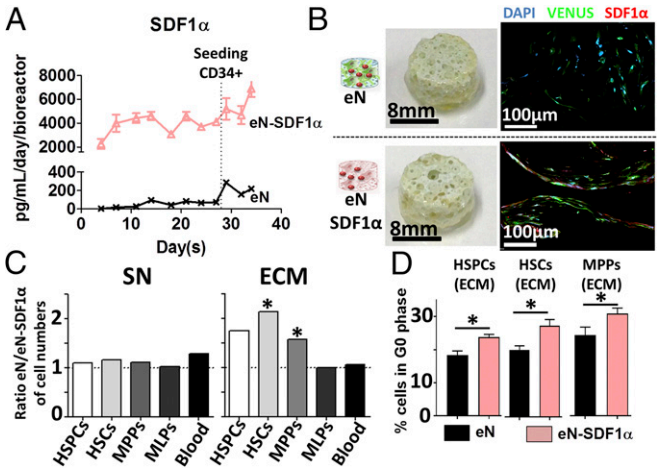

Fig. 6. Bone marrow niches with customized molecular signature can be genetically engineered. (*A*) The SDF1α-engineered niche (eN-SDF1α, red triangles) secretes superior levels of SDF1α than the control engineered niche (eN, black crosses) throughout the 3D culture period. $n \geq 3$ biological replicates. (*B*) The eN and eN-SDF1α appeared macroscopically identical (*Left*), but confocal microscopy images revealed the increased presence of the SDF1α protein in the eN-SDF1α tissue. (*C*) Comparing the ratio of absolute number of hematopoietic populations from the eN and eN-SDF1α revealed an identical supernatant content (SN, *Left*) while the stroma of eN-SDF1α (ECM, *Right*) contained a reduced number of HSPCs, HSCs, and MPPs. $n \geq 8$. (*D*) The SDF1α customization significantly increased the percentage of quiescent HSPCs, HSCs, and MPPs in the ECM of eN-SDF1α, as assessed by cell cycle analysis of corresponding populations. $n = 5$. HSCs, hematopoietic stem cells; HSPCs, hematopoietic stem and progenitor cells; MLPs, multilymphoid progenitors; MPPs, multipotent progenitors. $^*P < 0.05$.

total number of blood cells pooled from both compartments (ECM and SN) was similar in the eN and eN-SDF1α groups (*SI Appendix*, Fig. S8*A*). However, a marked reduction in the number of HSPCs was observed in the eN-SDF1α, reflected by a significant fold increase in HSCs (1.9 f.i.) and MPPs (1.4 f.i.) in the eN systems compared with the eN-SDF1α. Importantly, the SDF1α effect appeared to be restricted to these populations since the MLPs and general blood contents were identical in both niches (*SI Appendix*, Fig. S8*A*). Interestingly, observed differences were correlated with the system compartmentalization. Indeed, the SN cellular content of both eN and eN-SDF1α was identical in composition (SN, Fig. 6*C*). Instead, the ECM compartment of the eN showed a higher number of HSPCs, including superior content in HSCs and MPPs (2.1. and 1.6 f.i., respectively) while, again, the MLPs and global blood numbers were not affected.

We investigated the cell cycle status of HSPC, HSC, and MPP populations retrieved from our 3D conditions. This revealed a quiescence-inducing effect of SDF1α in eN-SDF1α, with a significant increase of HSPCs, MPPs, and HSCs in G0 phase (Fig. 6*D* and *SI Appendix*, Fig. S8 *B* and *C*). In particular, in cells retrieved from the ECM, we measured an increase of 29.6%, 36.1%, and 26.9% in the number of quiescent HSPCs, HSCs, and MPPs, respectively (Fig. 6*D*). Thus, the observed lower proportions of HSCs and MPPs in the ECM of eN-SDF1α niches were due to the quiescence induction by SDF1α overexpression.

These findings exemplify the possibility to use the described model to engineer customized BM niches, capable to specifically impact on HSC and MPP distribution and behavior in the system.

Perturbation of HSC Behavior by Simulation of Injury in Engineered Niche. We further assessed whether the blood cell distribution can be perturbed by simulating a niche injury (*SI Appendix*, Fig. S9*A*). Before $CD34^+$ loading, the eN were exposed to bleomycin (eN-Bleo), as potent drug inducing DNA damage (39). The drug altered hMSC metabolism (30% reduction of activity) (*SI Appendix*, Fig. S9*B*) but not their viability in the system (*SI Appendix*, Fig. S9*C*).

While both niches displayed similar HSPC content, the total number of HSCs was significantly higher in the eN-Bleo (*SI Appendix*, Fig. S9 *D* and *E*). The observed increase resulted from a higher HSC content in the ECM of eN-Bleo (Fig. 7*A*) while blood composition was identical in the SN of both eN and eN-Bleo (*SI Appendix*, Fig. S7*A*). Cells isolated from respective ECM niches showed a substantial decrease in the percentage of quiescent HSCs in eN-Bleo (8% vs. 20% in eN) (Fig. 7*B*). Interestingly, this was restricted to HSCs, and the cell cycle of HSPC and MPP populations was not affected.

These data indicate that the exposure to bleomycin impairs the capacity of hMSCs to maintain HSCs in a quiescent status, resulting in their increased proliferation. We thus validate the possibility to exploit our system for the study of human hematopoiesis in particular scenarios, like after injury.

Discussion

We report the successful in vitro engineering of BM-like tissues in a perfusion bioreactor system. The generated niches displayed high biological complexity, capturing structural, compositional, and organizational features of a native human osteoblastic environment, resulting in the support of HSPC functions. Moreover, using a proof-of-principle molecular customization of the 3D niche and through the design of specific injury scenarios, the system was validated as a BM engineering platform with tunable properties.

Tissue engineering offers new opportunities for stem cell research, enabling us to address fundamental biological questions that cannot be otherwise investigated using traditional culture plates. However, its application to the generation of viable BM environments in vitro has remained challenging, due to modeling constraints associated with the tissue complexity. This includes a precisely defined spatial organization, cellular diversity, and combined proliferation and maintenance of functionality of the blood compartment. Since existing models (14, 15) do not recapitulate all these features without bypassing the use of animals (40), we alternatively proposed the design of an "organ-like" tissue to support the development and maintenance of hematopoiesis.

Our system offers key advantages over existing approaches. First, unlike synthetic materials (41–43), the cell-deposited ECM more closely replicates native microenvironments. Despite substantial advances in the field, artificial matrices cannot recapitulate the distribution and diversity of signals existing in

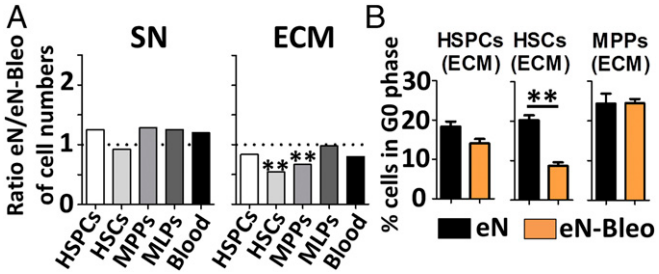

Fig. 7. Perturbation of HSC behavior by simulation of injury in engineered niche. (*A*) Engineered niches exposed to bleomycin (eN-Bleo) displayed a higher number of HSCs and MPPs in the ECM. In contrast, bleomycin injury did not affect the blood composition of the SN. $n \geq 3$. (*B*) Injured niches (eN-Bleo) displayed an impaired capacity to maintain HSCs in a quiescent status, as assessed by cell cycle analysis. $n \geq 3$. HSCs, hematopoietic stem cells; HSPCs, hematopoietic stem and progenitor cells; MLPs, multilymphoid progenitors; MPPs, multipotent progenitors. $^{**}P < 0.01$.

natural ECM nor offers their suitable and physiological presentation (44–46). Moreover, through hMSC genetic modifications and their tailored profile of secreted factors, we introduced the notion of modularity previously achieved by synthetic matrices (41–43). The biological delivery of defined cytokines by cells is a continuous process, as opposed to exogenous supplementation to culture medium, potentially associated with the issue of stability over time. This strategy is highly relevant when extended to putative niche factors, toward the identification of key cellular subsets/molecules that influence stem cell behavior (47). In this regard, the presence of a compartmentalization in our system can be exploited to address specific questions. These span from the possibility to study the chemoattractant effects of factors of interest to the investigation of mechanisms driving the release of stem cells outside of their niche, and the associated functional differences.

Despite being biologically inspired, our approach does not fully reflect the complexity of its in vivo counterpart (9). Important lacking components are, for instance, vascular and neuronal networks known to be regulators of HSC activity (48–50). This warrants the investigation of their integration into the system, though requiring the establishment of culture conditions sustaining the viability of multiple cell types (51). Nevertheless, the described model has reached a next step in complexity, illustrated by the observed self-organization of the mesenchymal and blood compartments that suggests the development of a BM proxy with organoid features.

As opposed to microfluidic approaches, we targeted the design of macroscale niches to combine reasonable throughput and multiple readouts. While microfluidic platforms consist in miniaturized systems with a high level of parallelization, the limited volume and cell numbers restrain multiplex analyses. Instead, the dimension of our system was compatible with several simultaneous assessments, including gene expression, flow cytometry, imaging, and necessary in vivo determination of stem and progenitor cell functionality.

We observed in our system an important increase in phenotypic HSC number. This was achieved in stringent xeno-free conditions, including low concentration of hematopoietic cytokines, and was validated with the use of single CB donors and multiple hMSC primary materials. However, HSC functionalities still need to be rigorously assessed by secondary transplantation and limiting-dilution assays before claiming a functional expansion of HSCs. Toward this objective, development and optimization of 3D parameters could be adopted to challenge gold-standard suspension cultures (52), currently requiring high levels of cytokine (53, 54) and agonist supplementation (52). Some of the parameters which may be tuned in the 3D-engineered culture platform include the types of niche cells, their specific stage of differentiation, the scaffolding material (e.g., structure/composition), or the physical factors driven by the perfusion system (e.g., shear stress, oxygen/hypoxia levels). All these act in concert with synergistic and competing effects and can be harnessed to modulate stem cell fate (55).

Finally, our system could be adapted to recapitulate pathological settings (56). The use of hMSCs and/or HSPCs harvested from patients suffering from blood disorders (e.g., leukemia) can offer the opportunity to model the disease in vitro, in an entirely human and ideally personalized setting. This could represent a powerful tool with a wide range of applications, from the identification of factors deregulating niche or blood functions to the screening of drugs to predict a patient-specific response to defined treatments.

Methods

Cord blood (CB) cells and human bone marrow aspirates were collected from healthy donors at the University Hospital Basel and the Universitäts-Kinderspital beider Basel (Ref.78/07), after obtaining informed consent. The study was approved by the ethics board of the canton Basel, Switzerland.

Osteoblastic niches were generated using hMSCs, following a preestablished protocol (32). Briefly, hydroxyapatite scaffolds were seeded directly in a perfusion bioreactor with 0.75×10^6 of hMSCs by overnight perfusion at a superficial velocity of 2,800 μL/s. After 24 h (cell-seeding phase), the superficial velocity was reduced to 280 μL/s for the perfusion culture of hMSCs. Cells were then cultured for 1 wk in proliferative medium (PM), followed by 3 wk of osteogenic medium (OM). Human $CD34^+$ hematopoietic stem and progenitor cells (HSPCs) isolated from cord blood samples were seeded after 4 wk of hMSCs, by overnight perfusion at a superficial velocity of 2,800 μL/s with 7×10^5 HSPCs resuspended in serum-free expansion medium, supplemented with the following cytokines: SCF (10 ng/mL; cat. no. 130-093-991), FLT3-ligand (10 ng/mL; cat. no. 130-093-854); TPO (10 ng/mL; cat. no. 130-094-011), all from Miltenyi Biotec. After 24 h (cell-seeding phase), the superficial velocity was reduced to 280 μL/s for perfusion culture during 1 wk. Cells were then collected from the bioreactor system by collagenase and trypsinization treatments for subsequent analysis. A more detailed description of the methods can be found in *SI Appendix*.

ACKNOWLEDGMENTS. This work was supported by the Swiss National Science Foundation (Systems-X program, 2014/266) (to R.S., T.S., and I.M.), as well as by the Freenovation program (Novartis AG) (to P.E.B.).

1. Méndez-Ferrer S, et al. (2010) Mesenchymal and haematopoietic stem cells form a unique bone marrow niche. *Nature* 466:829–834.
2. Morrison SJ, Scadden DT (2014) The bone marrow niche for haematopoietic stem cells. *Nature* 505:327–334.
3. Kfoury Y, Scadden DT (2015) Mesenchymal cell contributions to the stem cell niche. *Cell Stem Cell* 16:239–253.
4. Rieger MA, Hoppe PS, Smejkal BM, Eitelhuber AC, Schroeder T (2009) Hematopoietic cytokines can instruct lineage choice. *Science* 325:217–218.
5. Zhang CC, Lodish HF (2008) Cytokines regulating hematopoietic stem cell function. *Curr Opin Hematol* 15:307–311.
6. Guilak F, et al. (2009) Control of stem cell fate by physical interactions with the extracellular matrix. *Cell Stem Cell* 5:17–26.
7. Keung AJ, Healy KE, Kumar S, Schaffer DV (2010) Biophysics and dynamics of natural and engineered stem cell microenvironments. *Wiley Interdiscip Rev Syst Biol Med* 2:49–64.
8. Engler AJ, Sen S, Sweeney HL, Discher DE (2006) Matrix elasticity directs stem cell lineage specification. *Cell* 126:677–689.
9. Baryawno N, Severe N, Scadden DT (2017) Hematopoiesis: Reconciling historic controversies about the niche. *Cell Stem Cell* 20:590–592.
10. Rongvaux A, et al. (2014) Development and function of human innate immune cells in a humanized mouse model. *Nat Biotechnol* 32:364–372.
11. Shanks N, Greek R, Greek J (2009) Are animal models predictive for humans? *Philos Ethics Humanit Med* 4:2.
12. Doulatov S, Notta F, Laurenti E, Dick JE (2012) Hematopoiesis: A human perspective. *Cell Stem Cell* 10:120–136.
13. Raic A, Rödling L, Kalbacher H, Lee-Thedieck C (2014) Biomimetic macroporous PEG hydrogels as 3D scaffolds for the multiplication of human hematopoietic stem and progenitor cells. *Biomaterials* 35:929–940.
14. Ferreira MS, et al. (2012) Cord blood-hematopoietic stem cell expansion in 3D fibrin scaffolds with stromal support. *Biomaterials* 33:6987–6997, and erratum (2012) 33:9165.
15. Prewitz MC, et al. (2013) Tightly anchored tissue-mimetic matrices as instructive stem cell microenvironments. *Nat Methods* 10:788–794.
16. Leisten I, et al. (2012) 3D co-culture of hematopoietic stem and progenitor cells and mesenchymal stem cells in collagen scaffolds as a model of the hematopoietic niche. *Biomaterials* 33:1736–1747.
17. Jing D, et al. (2010) Hematopoietic stem cells in co-culture with mesenchymal stromal cells–Modeling the niche compartments in vitro. *Haematologica* 95:542–550.
18. Lee J, Cuddihy MJ, Kotov NA (2008) Three-dimensional cell culture matrices: State of the art. *Tissue Eng Part B Rev* 14:61–86.
19. Burdick JA, Vunjak-Novakovic G (2009) Engineered microenvironments for controlled stem cell differentiation. *Tissue Eng Part A* 15:205–219.
20. Vazin T, Schaffer DV (2010) Engineering strategies to emulate the stem cell niche. *Trends Biotechnol* 28:117–124.
21. Vunjak-Novakovic G, Scadden DT (2011) Biomimetic platforms for human stem cell research. *Cell Stem Cell* 8:252–261.
22. Wilkinson DC, et al. (2017) Development of a three-dimensional bioengineering technology to generate lung tissue for personalized disease modeling. *Stem Cells Transl Med* 6:622–633.
23. Eliopoulos N, Francois M, Boivin M-N, Martineau D, Galipeau J (2008) Neo-organoid of marrow mesenchymal stromal cells secreting interleukin-12 for breast cancer therapy. *Cancer Res* 68:4810–4818.
24. Takasato M, et al. (2015) Kidney organoids from human iPS cells contain multiple lineages and model human nephrogenesis. *Nature* 526:564–568.
25. Schmidt H, et al. (2015) Vascularized and functional human liver from an iPSC-derived organ bud transplant. *Nature* 516:435–438.

26. Di Maggio N, et al. (2011) Toward modeling the bone marrow niche using scaffold-based 3D culture systems. *Biomaterials* 32:321–329.
27. Dellatore SM, Garcia AS, Miller WM (2008) Mimicking stem cell niches to increase stem cell expansion. *Curr Opin Biotechnol* 19:534–540.
28. Peerani R, Zandstra PW (2010) Enabling stem cell therapies through synthetic stem cell-niche engineering. *J Clin Invest* 120:60–70.
29. Flores-Guzmán P, Fernández-Sánchez V, Mayani H (2013) Concise review: Ex vivo expansion of cord blood-derived hematopoietic stem and progenitor cells: Basic principles, experimental approaches, and impact in regenerative medicine. *Stem Cells Transl Med* 2:830–838.
30. Porter JR, Ruckh TT, Popat KC (2009) Bone tissue engineering: A review in bone biomimetics and drug delivery strategies. *Biotechnol Prog* 25:1539–1560.
31. Wendt D, Marsano A, Jakob M, Heberer M, Martin I (2003) Oscillating perfusion of cell suspensions through three-dimensional scaffolds enhances cell seeding efficiency and uniformity. *Biotechnol Bioeng* 84:205–214.
32. Sadr N, et al. (2012) Enhancing the biological performance of synthetic polymeric materials by decoration with engineered, decellularized extracellular matrix. *Biomaterials* 33:5085–5093.
33. Bourgine PE, et al. (2017) Engineered extracellular matrices as biomaterials of tunable composition and function. *Adv Funct Mater* 27:1605486.
34. Mayani H, et al. (1998) Kinetics of hematopoiesis in Dexter-type long-term cultures established from human umbilical cord blood cells. *Stem Cells* 16:127–135.
35. Gutiérrez-Rodríguez M, Reyes-Maldonado E, Mayani H (2000) Characterization of the adherent cells developed in Dexter-type long-term cultures from human umbilical cord blood. *Stem Cells* 18:46–52.
36. Pittenger MF (1999) Multilineage potential of adult human mesenchymal stem cells. *Science* 284:143–147.
37. Frank O, et al. (2002) Real-time quantitative RT-PCR analysis of human bone marrow stromal cells during osteogenic differentiation in vitro. *J Cell Biochem* 85:737–746.
38. Gattazzo F, Urciuolo A, Bonaldo P (2014) Extracellular matrix: A dynamic microenvironment for stem cell niche. *Biochim Biophys Acta* 1840:2506–2519.
39. Nicolay NH, et al. (2016) Mesenchymal stem cells are sensitive to bleomycin treatment. *Sci Rep* 6:26645.
40. Torisawa YS, et al. (2014) Bone marrow-on-a-chip replicates hematopoietic niche physiology in vitro. *Nat Methods* 11:663–669.
41. Gobaa S, et al. (2011) Artificial niche microarrays for probing single stem cell fate in high throughput. *Nat Methods* 8:949–955.
42. Gjorevski N, Ranga A, Lutolf MP (2014) Bioengineering approaches to guide stem cell-based organogenesis. *Development* 141:1794–1804.
43. Perl A, Reinhoudt DN, Huskens J (2009) Microcontact printing: Limitations and achievements. *Adv Mater* 21:2257–2268.
44. Discher DE, Mooney DJ, Zandstra PW (2009) Growth factors, matrices, and forces combine and control stem cells. *Science* 324:1673–1677.
45. Wilgus TA (2012) Growth factor-extracellular matrix interactions regulate wound repair. *Adv Wound Care (New Rochelle)* 1:249–254.
46. Frantz C, Stewart KM, Weaver VM (2010) The extracellular matrix at a glance. *J Cell Sci* 123:4195–4200.
47. Kokkaliaris KD, et al. (2016) Identification of factors promoting ex vivo maintenance of mouse hematopoietic stem cells by long-term single-cell quantification. *Blood* 128: 1181–1192.
48. Katayama Y, et al. (2006) Signals from the sympathetic nervous system regulate hematopoietic stem cell egress from bone marrow. *Cell* 124:407–421.
49. Nakamura Y, et al. (2010) Isolation and characterization of endosteal niche cell populations that regulate hematopoietic stem cells. *Blood* 116:1422–1432.
50. Itkin T, et al. (2016) Distinct bone marrow blood vessels differentially regulate haematopoiesis. *Nature* 532:323–328.
51. Bourgine PE, Martin I, Schroeder T (2018) Engineering human bone marrow proxies. *Cell Stem Cell* 22:298–301.
52. Boitano AEA, et al. (2010) Aryl hydrocarbon receptor antagonists promote the expansion of human hematopoietic stem cells. *Science* 329:1345–1348.
53. Ueda T, et al. (2000) Expansion of human NOD/SCID-repopulating cells by stem cell factor, Flk2/Flt3 ligand, thrombopoietin, IL-6, and soluble IL-6 receptor. *J Clin Invest* 105:1013–1021.
54. Tsuji K, Ueda T, Ebihara Y (2003) Cytokine-mediated expansion of human NOD-SCID-repopulating cells. *Methods Mol Biol* 215:387–395.
55. Lane SW, Williams DA, Watt FM (2014) Modulating the stem cell niche for tissue regeneration. *Nat Biotechnol* 32:795–803.
56. Sánchez-Aguilera A, Méndez-Ferrer S (2017) The hematopoietic stem-cell niche in health and leukemia. *Cell Mol Life Sci* 74:579–590.

Supplementary Materials

Hematopoietic Stem and Progenitor Cells extraction and purification

Cord blood (CB) samples were collected from placenta of full-term healthy caesarean section. The CB was drained from the umbilical vein into a single-use bag containing anticoagulants (MSC1206DU - Cord blood collection bag – MacoPharma, France) and mononuclear Cells (MNC) were isolated within the 24 hours after collection by density gradient centrifuge separation on Ficoll (Histopaque®: cat# 1077, SIGMA-ALDRICH: cat# 1077-1) after a 1:1 dilution in PBS. HSPCs were then isolated from MNCs based on their positive CD34 expression using the magnetic EasySep CD34+ positive selection Kit (Stemcell Technologies, Grenoble, France), following manufacturer's protocol and ultimately stored in liquid nitrogen.

Lentiviral transduction

HMSCs were lentivirally transduced using VENUS or VENUS-SDF1α virus particles, at a Multiplicity of Infection (MOI) of 20. Four days post-transduction, cells were collected and analysed by flow cytometry to assess their VENUS expression. Cell populations with purity inferior to 90% were further purified by flow cytometry sorting prior to their experimental use in 3D.

HMSC culture

Marrow aspirates (20 ml volumes) were harvested from healthy donors ($n \geq 3$) using a bone marrow biopsy needle inserted through the cortical bone and immediately transferred into plastic tubes containing 15,000 IU heparin. After diluting the marrow aspirates with phosphate buffered saline (PBS) at a ratio of 1:4, nucleated cells were isolated using a density gradient solution (Histopaque, Sigma Chemical, Buchs, CH). Complete medium consisting in α-minimum essential Medium (αMEM) with 10% fetal bovine serum, 1% HEPES (1 M), 1% sodium pyruvate (100 mM) and 1% of Penicillin–Streptomycin– Glutamine (100X) solution (all from Gibco). Nucleated cells were plated at a density of 3.106 cells/cm2 in complete medium supplemented with 5 ng/ml of fibroblast growth factor-2 (FGF-2, R&D Systems) and cultured in a humidified 37 °C/5% CO2 incubator. Medium was changed twice

in a week. HMSC were selected on the basis of adhesion and proliferation on the plastic substrate one week after seeding.

Generation of osteoblastic niches

Osteoblastic niches were generated using hMSC, following a pre-established protocol(32). Briefly, hydroxyapatite scaffolds (Engipore®, Finceramica-Faenza, Faenza, Italy) of 4 mm height and 8 mm diameter were seeded directly in perfusion bioreactor with $0.75x10^6$ of Venus hMSC or Venus-SDF1α hMSC by overnight perfusion at a superficial velocity of 2800 µL/s. After 24 hours (cell seeding phase), the superficial velocity was reduced to 280 µL/s for the perfusion culture of hMSC. Cells were then cultured for one week in proliferative medium (PM), consisting in CM supplemented with 100 nM dexamethasone (SIGMA: cat# D4902), 0.1 mM ascorbic acid-2-phosphate (SIGMA-ALDRICH: cat# A92902) and 5 ng/ml FGF-2, followed by 3 weeks of Osteogenic Medium (OM) consisting in CM supplemented with 100 nM dexamethasone, 10 mM β-glycerophosphate, and 0.1 mM ascorbic acid-2-phosphate**.** Culture medium was changed twice a week.

HSPC Seeding

Human CD34+ Hematopoietic Stem and Progenitor Cells (HSPCs) isolated from cord blood samples were seeded after 4 weeks of hMSC culture. Initial experiments comparing Ceramic (Ce) and engineered niche (eN) conditions were performed with different single donors (n=3). Comparison between eN and eN enriched in SDF1α were performed with batch of pooled donors ($n \geq 4$). In both case, scaffolds were seeded by overnight perfusion at a superficial velocity of 2800µL/s with $7x10^5$ HSPCs resuspended in Serum Free Expansion Medium (SFEM, Stemcell Technologies: StemSpan™), supplemented with of the following cytokines: SCF (10ng/mL; cat#130-093-991), FLT3-ligand (10ng/mL; cat#130-093-854); TPO (10 ng/mL; cat#130-094-011), all from Miltenyi Biotec. After 24 h (cell seeding phase), the superficial velocity was reduced to 280µL/s for perfusion culture during one week. Culture medium was changed twice a week, during which the retrieved medium was harvested and spun down (300g, 10min) to collect cells in suspension. The pelleted cells were resuspended in fresh medium and injected back in the corresponding bioreactor.

Cell harvesting from 3D systems

Floating and loosely attached cells (Supernatant fraction, SN) were collected from the medium contained in the bioreactors tubes and chamber, combined with the fraction retrieved from the scaffold after one wash with 6mL of PBS under perfusion.

Cells present on the scaffolding material (ECM) were collected by collagenase (0.3%, Thermofischer 17101015) and trypsinization treatments (0.05% Trypsin-EDTA, Gibco 25300-054). For collagenase treatment: 6 ml of collagenase/bioreactor, under perfusion at a superficial velocity of 2800µL/s for 5 min, 37°C followed by 2 washes with 6 mL of PBS. For trypsin treatment: 6mL of Trypsin/bioreactor, under perfusion at a superficial velocity of 2800µL/s for 5 min, 37C 2x wash ~6 mL of PBS. Harvested cells were spun down (300g, 10min) and resuspended in IMDM (Sigma: cat# I3390-500ML)

Flow cytometry

The purity of purified CB CD34+ cells was determined with BD Accuri™ C6 Cytometer - BD Biosciences by labelling cells using a human antiCD34 antibody (BD BIOSCIENCES: cat# 555824).

The quantitative phenotype of hematopoietic cells retrieved from bioreactors has been determined using the LSR II FORTESSA SORP (BD Biosciences) cell analyser. Blood cells harvested from the Ce, eN or eN-SDF1α were labelled using following surface antibodies: human anti-CD34 (BioLegend cat# 343512 or BD BIOSCIENCES cat# 563756), human anti-CD38 (BD BIOSCIENCES cat# 555460), human anti-CD45RA (BD BIOSCIENCES cat# 563429), human anti-CD90 (BD BIOSCIENCES cat# 559869).

Human hematopoietic *in vivo* engraftment was determined with either the LSR II FORTESSA SORP or CytoFLEX (BD Biosciences) cell analysers by labelling cells with the following antibodies: human anti-CD45 (BD BIOSCIENCES, cat# 560973), mouse anti-CD45 (BioLegend: cat# 103126), human anti-CD3 (BD BIOSCIENCES: cat# 340663), human anti-CD33 (BD BIOSCIENCES: cat# 555450), human anti-CD19 (BD BIOSCIENCES: cat# 555412). Cells viability was assessed using Propidium Iodide (BioLegend: cat# 79997).

For cell cycle analysis, harvested cells were first labelled using the surface markers described above. After fixation with 1% paraformaldehyde for 10 minutes on ice, cells were permeabilized according to the manufacturers protocol (eBioscience Permeabilization Buffer Invitrogen cat#00-8333-56) and intracellularly labelled using human antiKI67 (BD BIOSCIENCES cat#563756) and Hoechst (BD BIOSCIENCES cat# 561908).

Flow cytometry analysis of Venus hMSC was performed using the following surface antibodies: human anti-CD105 (BD BIOSCIENCES cat# 560839), human anti-CD146 (BioLegend cat# 342003), human anti-CD73 (BD BIOSCIENCES cat# 561014), human anti-CD49e (BD BIOSCIENCES cat# 555617), human anti-CD166 (BioLegend cat# 343903) and human anti-CD31 (BD BIOSCIENCES cat# 340297). For Intracellular protein analysis, cells were first fixed with 1% paraformaldehyde for 10 minutes on ice and permeabilized according to the manufacturer's protocol (eBioscience Permeabilization Buffer Invitrogen cat# 00-8333-56). Cells were subsequently labelled using the following antibodies: Osteocalcin (R&D Systems cat# IC1419P), Alkaline Phosphatase (R&D Systems cat# AFB1448A), STRO-1 (BioLegend cat# 340104).

Colony Forming Unit Assay

The colony forming unit assay was performed according to the provided R&D Systems's protocol. Briefly, 500 cells were collected before and 1200 cells after expansion under the different conditions, washed with PBS, resuspended in 240 mL Cell Suspension Media and mixed with 2.4 mL Human Methylcellulose Complete Media (all from R&D Systems). The mixture was plated in duplicates (2 times 1.1 mL) in 35mm petri dishes and incubated for 14 days. The colonies were identified by light microscopy and characterized after Cytospin and Haematostaining (Hematek 2000; Stain Pack Modified Wright Stain – Bayer Healthcare) according to the "Atlas of human haematopoietic colonies from cord blood" (Stemcell Technologies). The numbers of counted colonies were normalized to express the fold increase in the number of cultured CD34+/CD38- cells capable to give rise to the GM, BFU or GEmM colonies in comparison with the uncultured condition. The percentage of colonies formed was applied to the total number of CD34+/CD38- (able to give rise to each colonies types) retrieved cells, determining the absolute number of functional cells : ((Number of colony Type)*100/Total number of colonies)*(Number of CD34+/CD38- Cells)/100. This number was ultimately divided by the one obtained in the uncultured condition for each colony type, resulting in a fold increase.

Proteins expression levels- Luminex

The protein levels in the culture supernatant was measured according to manufacturer's instructions using a Luminex screening assay (R&D), based on the following analytes:

Angiopoietin-1, IL-6: Interleukin 6, IL-8: Interleukin 8, MCP-1: monocyte chemotactic protein 1, SCF: Stem Cell Factor, TPO: Thrombopoietin, Flt3-L: Fms-related tyrosine kinase 3 ligand, MMP-13: Matrix metallopeptidase 13 (Collagenase 3), G-CSF: Granulocyte colony-stimulating factor, BMP-4: Bone morphogenetic protein 4, MMP-9: Matrix metallopeptidase 9 (Gelatinase B), SDF1α: (Stromal-Derived Factor-1), VEGF: Vascular endothelial growth factor, M-CSF: macrophage colony-stimulating factor, BMP-2: Bone morphogenetic protein 2. Briefly, ECM-coated graft were lysed and minced in provided lysis buffer. 100uL was loaded on the designed place and latterly analysed using a Bio-Plex® 200 Systems.

Gene expression analysis

Total RNA was extracted from cells using TRIzol (Invitrogen, Carlsbad, CA), treated with DNAse and retrotranscribed into cDNA, as previously described(1). Real-time RT-PCR was performed with the ABIPrism 77000 Sequence Detection System (Perkin Elmer/Applied Biosystem, Rotkreuz, Switzerland) and expression levels of genes of interest were normalized to GAPDH. Primers and probe sets of investigated genes (Alkalyne Phosphatase = ALP, Bone Sialoprotein = BSP, interleukin-8 = IL-8, interleukin-6 = IL-6, Monocyte chemoattractant protein 1 = MCP-1, Stromal derived factor 1α = SDF1α, Nestin, Hypoxia-inducible factor 1α = HIF1α, neuron-glial antigen 2 = NG2, von Willebrand factor = vWF, Fatty Acid Binding Protein 4 = FABP4, Peroxisome Proliferator-Activated Receptor gamma = PPARγ) were purchased as assays on demands (ThermoFischer scientific).

Confocal immunofluorescence staining

Immunofluorescence protocol was adapted from a previously published study(2). Briefly, prior to sectioning, samples were fixed in 4% formalin, decalcified in 10% EDTA solution and subsequently embedded in 4% low-melting agarose (Sigma). Sections of 150-250µm thickness were obtained using a Leica VT1200S vibratome with Endurium® low-profile ceramic injector blades (Cadence Inc.).

Sections were blocked and permeabilized with TBS (final concentration 0.1M Tris, 0.15M NaCl, pH: 7.5) containing 0.05% Tween-20, 20% DMSO (both from Sigma) and 10% donkey serum (Jackson ImmunoResearch). This buffer was also used to dilute all primary antibodies, secondary detection reagents and blocking reagents. After blocking/permeabilization, endogenous avidins and biotins were block using the kit from Vector Labs, each step one

hour followed by 30 minute washes. Sections were then sequentially stained with primary, secondary antibodies, each overnight with 5x1h washes in between using TBS containing 0.05% Tween-20. A list of primary and secondary antibodies is provided (**SI Appendix Figure S10**).

Optical clearing and mounting of sections

Sections were optically cleared with graded series of 2,2'-thiodiethanol (TDE, Sigma) diluted in TBS until 100% TDE was reached. The final mounting solution consisted of 100% TDE with 0.1M N-propyl gallate (pH: 8.5, Sigma). The refractive index of this solution was measured using a handheld refractometer (Atago) and adjusted to 1.518 with TDE or TBS. Sections were mounted using custom-made silicone spacers (Grace Biolabs) on custom-made size 00, D263M borosilicate coverglass (RI: 1.518, Menzel-Gläser). Alternatively, sections were mounted directly in Prolong Gold Antifade (Thermo) or dehydrated with methanol and mounted in BABB33. In both cases, sections were mounted on size 1.5 coverslips. For Prolong Gold Antifade, images were acquired with glycerol immersion.

Confocal microscopy

Confocal microscopy was performed on a Leica TCS SP5 equipped with three photomultiplier tubes, two HyD detectors, five lasers (405nm blue diode, argon [458, 476, 488, 496 and 514nm], and three helium neon [543, 594 and 633nm]) using type F immersion liquid (RI: 1.518) and a 20X multiple immersion lens (NA 0.75, FWD 0.680mm). All scans were acquired at 20-25oC, 400Hz, in the bidirectional mode, with z-spacing of 2.49mm (the optical slice thickness of the optics used was 2.69mm). Images were acquired either with a 2.2x optical zoom at 512x512 resolution or with a 1.1x zoom at 1024x1024 resolution.

Scanning electron microscopy

For SEM, cell-seeded constructs were fixed overnight at 4°C with 4% formaldehyde and washed with PBS. Samples were gradually dehydrated with 30-50-70-90-100% ethanol, coated with gold and imaged with a Philips XL 30 ESEM microscope.

Mice and xenotransplantation procedure

All mice were maintained at the University Hospital Basel animal facility according to the guidelines of the Swiss Federal Veterinary Office, and all the experiments were approved by the Veterinäramt of Kanton Basel, Basel, Switzerland (permit 2697). NOD.Cg-Prkdcscid IL2rgtmWjl/Sz (also termed NOD/SCID/IL2Rγnull, NSG) mice were purchased from Jackson Laboratory (Bar Harbor, ME, USA) and maintained under pathogen-free conditions according Swiss federal and state regulations. 6 weeks old female animals were sublethally irradiated (225 cGy) 24 hours prior to receiving an intrafemoral injection of 30,000 CD34+ cells resuspended in 25 µl PBS. From week 4 onwards, PB mononuclear cells were analysed regularly by flow cytometry to monitor engraftment using either the LSR II FORTESSA SORP or CytoFLEX (BD Biosciences) cell analysers. Cells were labelled using following antibodies: human anti-CD45-APC (BD BIOSCIENCES: cat# 560973), mouse anti-CD45-PB (BioLegend: cat# 103126), human anti-CD3-PerCP (BD BIOSCIENCES: cat# 340663), human anti-CD33-PE (BD BIOSCIENCES: cat# 555450), human anti-CD19-FITC (BD BIOSCIENCES: cat# 555412). In accordance with the animal protocol, animals were euthanized if signs of wasting were observed.

Dexter-inspired 2D culture

2D culture was performed by seeding $1{,}5x10^4$ Venus hMSC per well in 12-wells plates. Cells were seeded and cultured in Complete Medium supplemented with 5 ng/ml of fibroblast growth factor-2 (FGF-2, R&D Systems) and cultured in a humidified 37 °C/5% CO2 incubator. Medium was changed twice in a week. After one week, hMSC reached confluency and $1{,}65x10^4$ Human CD34+ from pooled cord blood samples were seeded in each well. This number was determined in order to correspond to the inital hMSC/CD34+ ratio in the eN condition. Cells were co-cultured in Serum Free Expansion Medium (SFEM, Stemcell Technologies: StemSpan™), supplemented with of the following cytokines: SCF (10ng/mL; cat#130-093-991), FLT3-ligand (10ng/mL; cat#130-093-854); TPO (10 ng/mL; cat#130-094-011), all from Miltenyi Biotec. Culture medium was changed twice a week, during which the retrieved medium was harvested and spun down (300g, 10min) to collect cells in suspension. The pelleted cells were resuspended in fresh medium and placed back in the corresponding well. After one week of co-culture, cells were collected by trypsinization (0.05% Trypsin-EDTA, Gibco 25300-054), spun down (300g, 10min) and resuspended in IMDM (Sigma: cat# I3390-500ML).

Assessment of Interleukin supplementation in 3D

Experiments comparing Ceramic (Ce) and Ceramic with IL-6 and IL-8 supplementation (Ce + IL6/IL8) conditions were performed with CD34+ cells isolated from pooled cord blood samples. Scaffolds were seeded by overnight perfusion at a superficial velocity of 2800µL/s with $7x10^4$ HSPCs resuspended in Serum Free Expansion Medium (SFEM, Stemcell Technologies: StemSpan™), supplemented with of the following cytokines: SCF (10ng/mL; cat#130-093-991), FLT3-ligand (10ng/mL; cat#130-093-854); TPO (10 ng/mL; cat#130-094-011), all from Miltenyi Biotec, IL-6 (22.28 µg/mL) and IL-8 (128.34 µg/mL) from R&D Biosystems. After 24 h (cell seeding phase), the superficial velocity was reduced to 280µL/s for perfusion culture during one week. Culture medium was changed twice a week, during which the retrieved medium was harvested and spun down (300g, 10min) to collect cells in suspension. The pelleted cells were resuspended in fresh medium and injected back in the corresponding bioreactor.

Niche impairment using Bleomycin treatment

The impact of Bleomycin treatment on Venus hMSCs was first determined in 12-wells plates, based on a pre-existing study(3). Cells were seeded at a density of $3x10^4$ cells per well and cultured in Complete Medium supplemented with 5 ng/ml of fibroblast growth factor-2 (FGF-2, R&D Systems). Medium was changed twice in a week. After one week cells were exposed to bleomycin at a concentration of 1800 ng/ml for 4 hours. At the end of the treatment the wells were rinsed twice with Complete Medium. The metabolism of Venus hMSC was assessed 48 hours later by MTT staining (Yellow Tetrazolium salt, SIGMA cat#: M5655). Briefly, cells were incubated with 500 µl of Complete Medium supplemented with MTT (50 µg/ml) and incubated for 4 hours in a humidified 37 °C/5% CO2 incubator. 200 µl of DMSO (Dimethylsulfoxyde, SIGMA cat#: D2650) was added to each emptied well and the plate was placed on an orbital shaker for 40 minutes in the dark. The absorbance of the supernatant was ultimately measured at 575nm using a Synergy™ H1 BioTek microplate reader.

Engineered osteoblastic niches were exposed to Bleomycin (Bleomycin 15000I.U. Baxter AG Switzerland) at Day 28, prior to CD34+ seeding. Bleomycin was purchased from the central pharmacy of University Hospital Basel. The drug was reconstituted in 0.9% NaCl injectable solution (Bichsel cat#100 0 090) and further diluted in Osteogenic Medium at 1800 ng/mL

prior to carrying out the experiment. The engineered tissue was exposed to Bleomycin during 4 hours under perfusion at a superficial velocity of 280µL/s then rinsed twice with SFEM (Stemcell Technologies: StemSpan™) prior to CD34+ loading.

Statistics

Data are presented as means ± standard error of the mean and were analysed using the GraphPad Prism software. Unless indicated, single comparison was performed using the non-parametric Mann Whitney t-test assuming a non-gaussian distribution of the values. Multiple comparisons were performed using the one way ANOVA assuming a non-gaussian distribution of the values. Statistical significant differences were defined as: * =$p < 0.05$, ** = $p < 0.01$, *** = p <0 .001, **** = p <0 .0001.

References

1. Frank O, et al. (2002) Real-time quantitative RT-PCR analysis of human bone marrow stromal cells during osteogenic differentiation in vitro. *J Cell Biochem* 85(4):737–746.

2. Coutu DL, Kokkaliaris KD, Kunz L, Schroeder T (2017) Multicolor quantitative confocal imaging cytometry. *Nat Methods*. doi:10.1038/nmeth.4503.

3. Nicolay NH, et al. (2016) Mesenchymal stem cells are sensitive to bleomycin treatment. *Sci Rep* 6. doi:10.1038/srep26645.

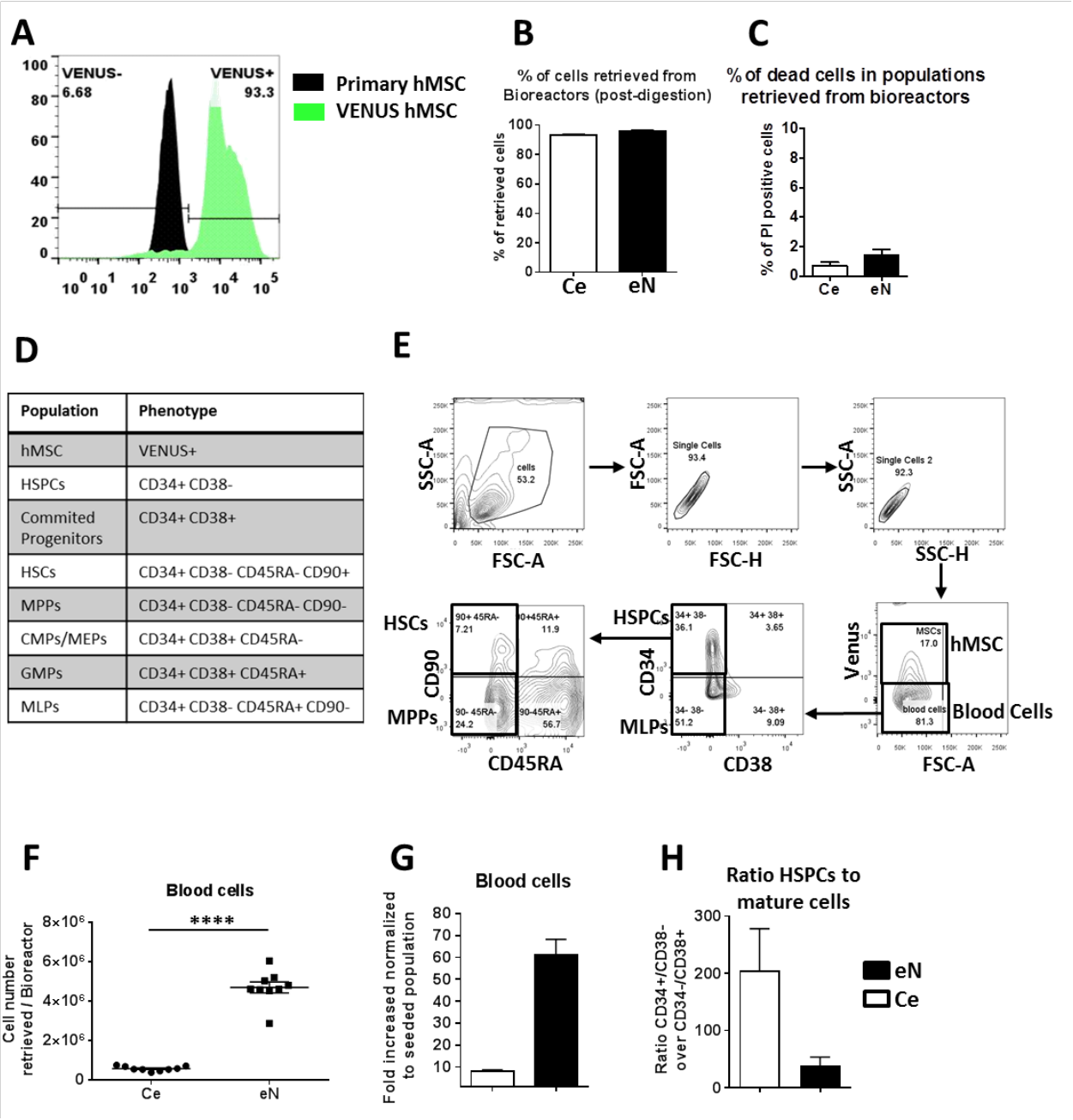

Population	Phenotype
hMSC	VENUS+
HSPCs	CD34+ CD38-
Commited Progenitors	CD34+ CD38+
HSCs	CD34+ CD38- CD45RA- CD90+
MPPs	CD34+ CD38- CD45RA- CD90-
CMPs/MEPs	CD34+ CD38+ CD45RA-
GMPs	CD34+ CD38+ CD45RA+
MLPs	CD34+ CD38- CD45RA+ CD90-

Figure S1. (A) Primary hMSC are successfully labelled with the VENUS transgene (>90%, VENUS hMSC) by lentivirus transduction, as assessed by flow cytometry. (B) Percentage of cells retrieved from 3D conditions determined by number of cells left on digested scaffolds (DNA quantification). (C) Percentage of cell death in the retrieved populations from the Ce and eN bioreactors measured by flow cytometry after propidium iodide (PI) staining. n≥3. (D) Phenotypes of hMSC and human blood populations. (E) Gating strategy for the flow cytometry analysis of cells retrieved from 3D culture. (F) Absolute number of blood cells at the end of the 3D culture. n=9 biological replicates. (G) Fold increase of blood cells at the end of the 3D culture. n=9 biological replicates. (H) Ratio HSPCs (CD34+CD38-) over mature

cells (CD34-/CD38+) in corresponding conditions. ****p<0.0001.

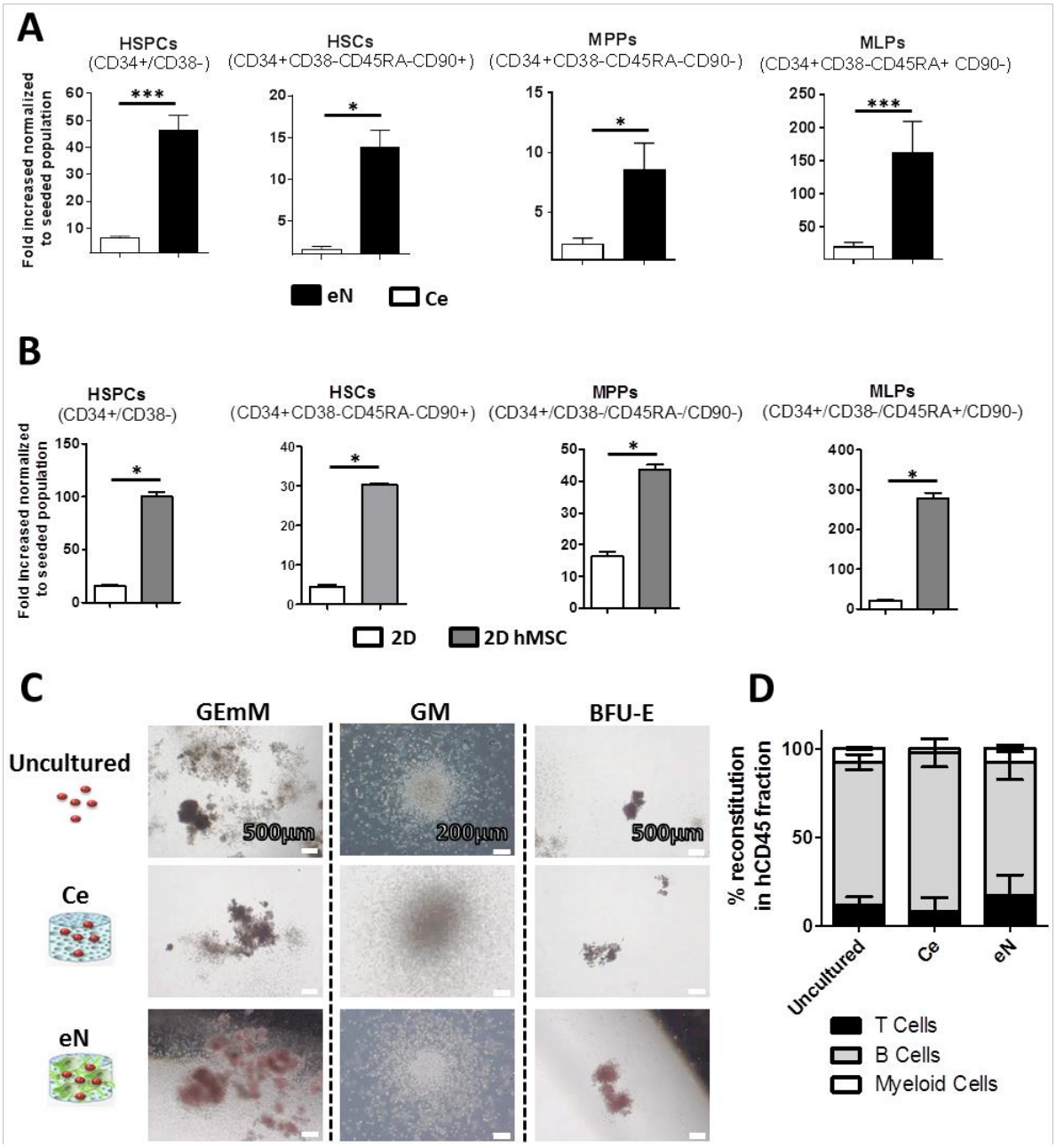

Figure S2. (A) Fold increase in the number of HSPCs, HSCs, MPPs and MLPs retrieved from eN and Ce conditions, normalized to the seeded populations. n=8 biological replicates. (B) Fold increase in the number of HSPCs, HSCs, MPPs and MLPs retrieved from 2D Dexter-inspired conditions. 2D: culture of CD34+ cells for 1 week without hMSC as feeder layer. 2D hMSC: culture of CD34+ cells for 1 week with hMSC as confluent feeder layer. Data were normalized to the seeded populations. n≥4. (C) Representative morphology (Inverted microscope, bright field) of colonies formed by HSPCs before (uncultured) and after 3D

culture on ceramic (Ce) or engineered niche (eN). GM: Colony-forming unit-granulocyte and macrophage, BFU-E: Burst-forming unit-erythroid, GEmM: Colony-forming unit-Granulocyte, Erythroid, macrophage, Megakaryocyte). *p<0.05 ***p<0.001. (D) Assessment of multi-lineage reconstitution capacity of uncultured and cultured CD34+ cells (Ce and eN) in NSG animals, 18 weeks post-transplantation. n≥3. *p<0.05.

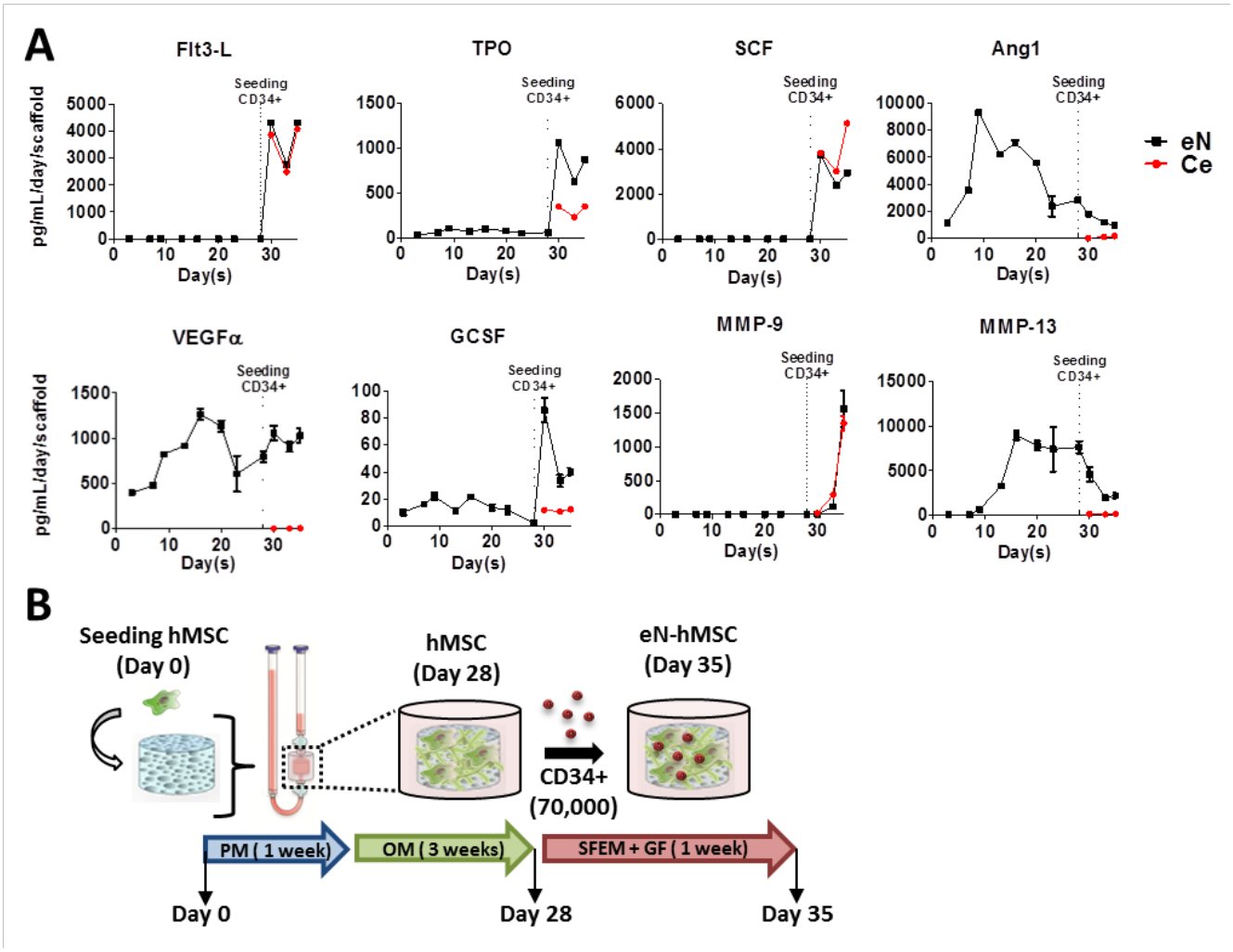

Figure S3. (A) Luminex-based analysis of secreted proteins during 3D cultures. Flt3-L: Fms-related tyrosine kinase 3 ligand, TPO: thrombopoietin, SCF: stem cell factor, Ang-1: angiopoietin 1, VEGFα: vascular endothelial growth factor α, GCSF: granulocyte colony-stimulating factor, MMP-9: matrix metalloproteinase 9, MMP-13: matrix metalloproteinase 13. n≥3. (B) Nomenclature given to the different hMSC populations according to the culture time; Post-expanded hMSC initially seeded on the material: hMSC (Day 0), hMSC after proliferation and osteogenic differentiation: hMSC (Day 28), hMSC at the end of the 3D co-culture with CD34+ cells: eN-hMSC (Day 35).

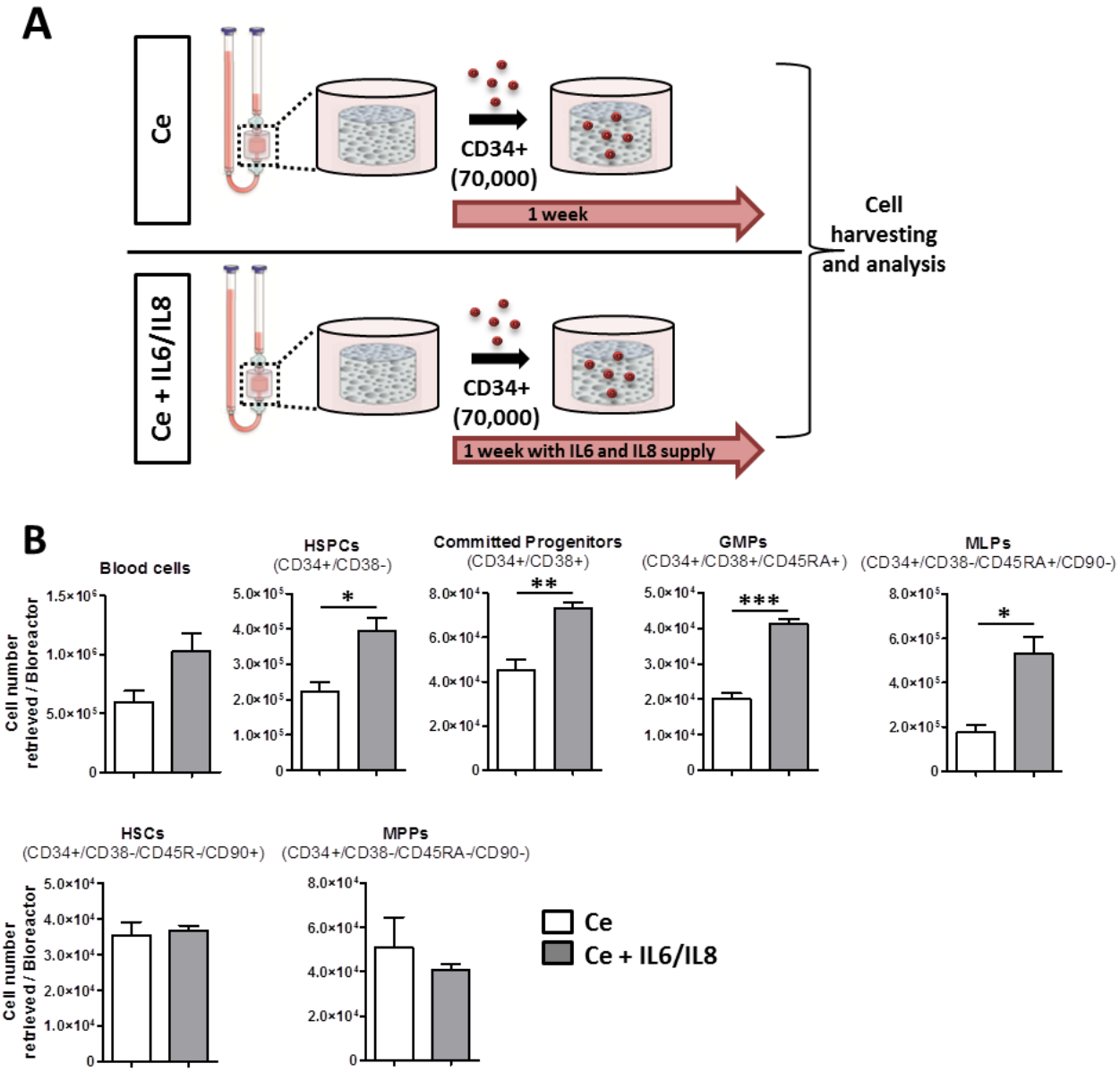

Figure S4. (A) Experimental plan for the quantitative assessment of blood populations in ceramic conditions with or without interleukin 6 (IL-6) and interleukin 8 (IL-8) supply. The concentrations of IL-6 (22.28 µg/mL) and IL-8 (128.34 µg/mL) correspond to the average values measured in the eN conditions during the co-culture period with CD34+ cells. (B) The combined addition of IL-6 and IL-8 led to an increased number of phenotypic Hematopoietic Stem and Progenitor Cells (HSPCs), Committed Progenitors, Granulocyte Macrophage Progenitors (GMPs) and Multipotent Lymphoid Progenitors (MLPs). No effects on the number of Hematopoietic Stem Cells (HSCs) and Multipotent Progenitors (MPPs) were observed. Data were collected by quantitative flow cytometry analysis one week post-

seeding of the CD34+ fraction. n=3 biological replicates. Ce: ceramic only. Ce + IL6/IL8: ceramic supply with interleukin 6 and interleukin 8. *p<0.05, **p<0.01, ***p<0.001.

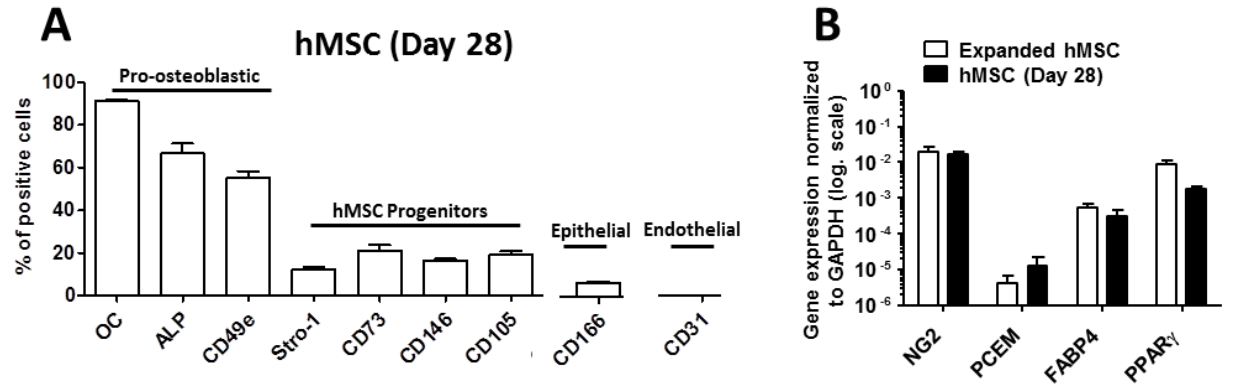

Figure S5. (A) Phenotypic analysis of the hMSC (Day 28) composing the engineered tissue. n=4. (B) Gene expression analysis of hMSC (Day 28) composing the engineered tissue prior to CD34+ loading. n≥4.

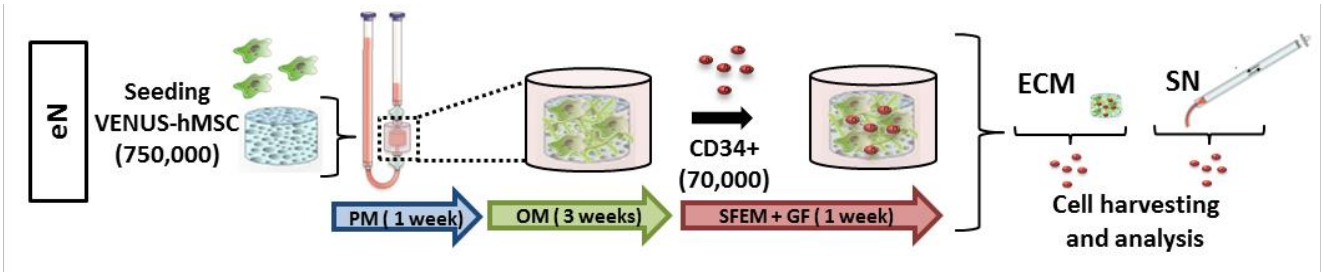

Figure S6. Experimental design for the generation of niches in 3D perfusion bioreactor, with distinct analysis of cells retrieved either from the liquid phase (supernatant, SN) or from the digested tissue (ECM)**.** PM: proliferative medium. OM: osteogenic medium. SFEM+GF: serum free medium supplemented with hematopoietic growth factors. For both conditions, cells were collected 1 week post co-culture for quantitative assessment of population's distribution. PM: proliferative medium. OM: osteogenic medium. SFEM+GF: serum free medium supplemented with hematopoietic growth factors.

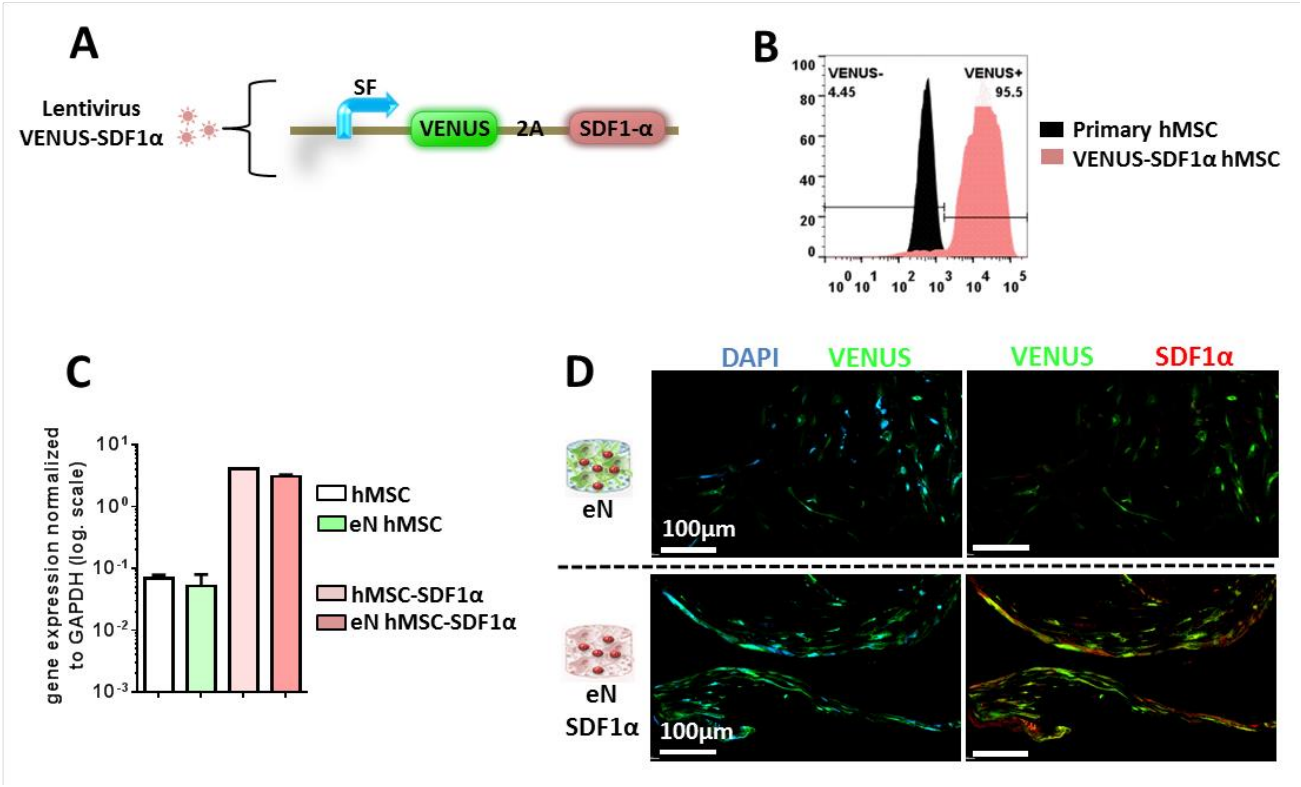

Figure S7. (A) Lentivector map of the SDF1α construct. The overexpression is driven by the Steroidogenic Factor-1 (SF) consitutive promoter, while a 2A sequence between VENUS and SDF1α ensure the stochiometric expression of both sequences. (B) Transduction efficiency of Primary Human Mesenchymal Cells using the SDF1α lentiviruse measured by flow-cytometry analysis of VENUS expression in cells. (C) Gene expression analysis of SDF1α in hMSC and hMSC-SDF1α transduced populations, prior to and after 3D culture (eN). (D) Confocal microscopy of the eN and eN-SDF1α images revealing the presence of the VENUS positive hMSC (green) and the SDF1α protein (red).

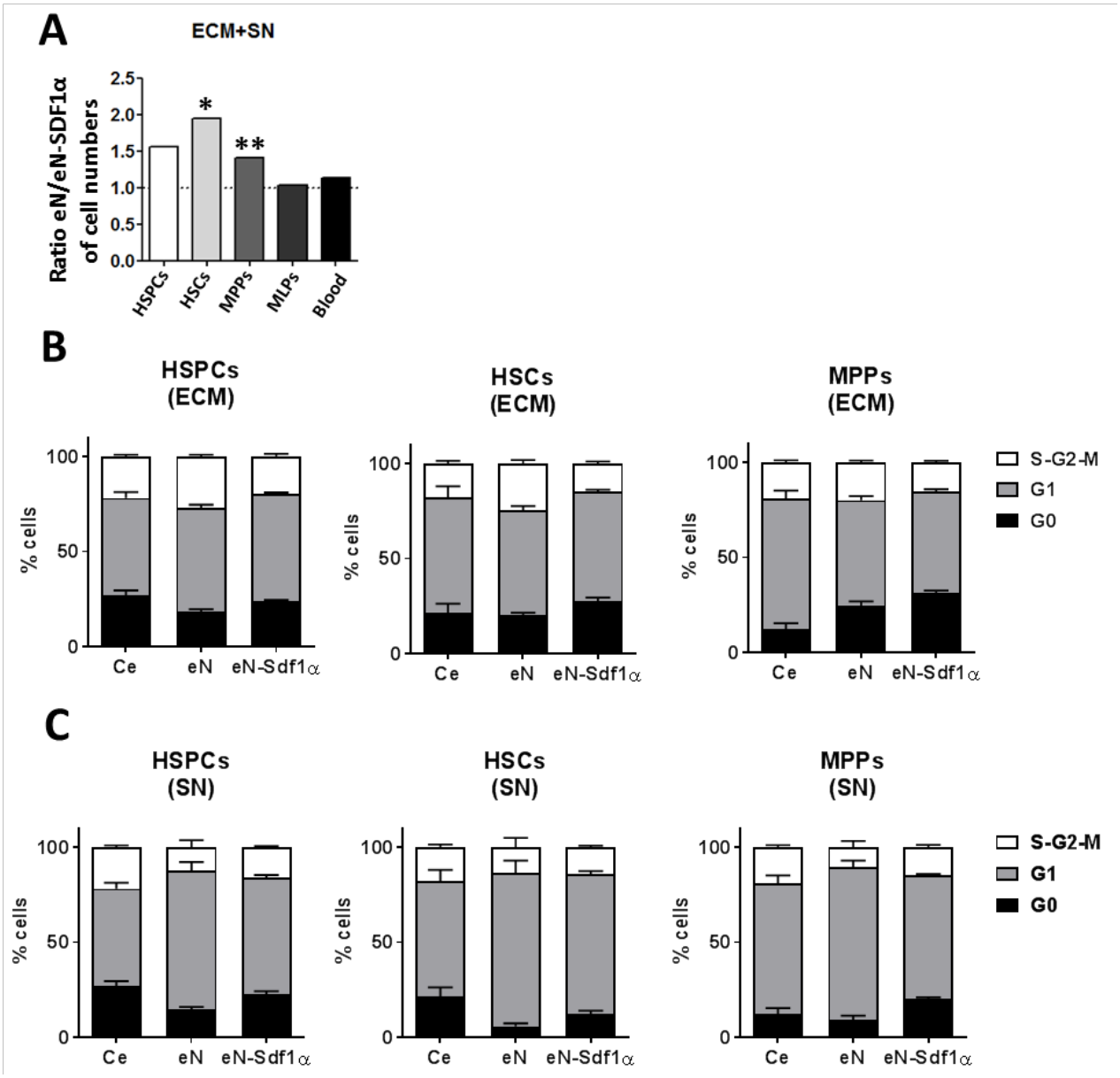

Figure S8. (A) The eN-SDF1α displayed a lower total number (ECM and SN combined) of HSPCs, HSCs and MPPs than the eN. n≥8. (B) Cell cycle analysis of populations retrieved from the ECM of Ce, eN and en-SDF1α conditions. n≥3. (C) Cell cycle analysis of populations retrieved from the ECM of Ce, eN and en-SDF1α conditions. n≥3. HSPCs: Hematopoietic Stem and Progenitor Cells, HSCs: Hematopoietic Stem Cells, MPPs: Multipotent Progenitors. MLPs: Multilymphoid progenitors. *p<0.05, **p<0.01.

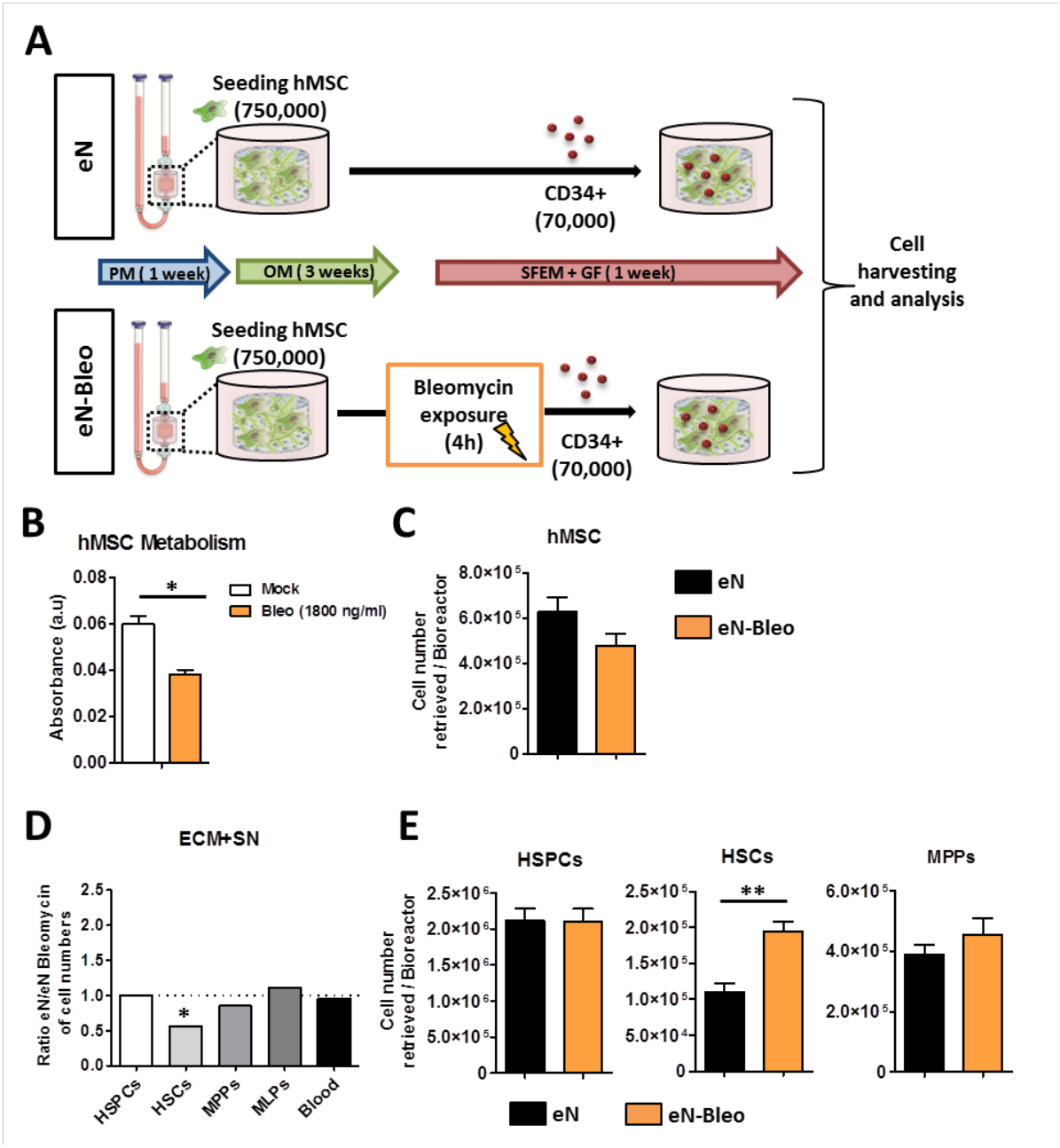

Figure S9. (A) Experimental design for the generation of niches in 3D perfusion bioreactor, with (eN-Bleo) or without (eN) injury by Bleomycin exposure. In the eN-Bleo, the engineered tissue was exposed 4h to 1800 ng/mL prior to CD34+ loading. For both conditions, cells were collected 1 week post co-culture for quantitative assessment of population's distribution. (B) Assessment of Bleomycin impact on hMSC metabolism. The exposure to bleomycin led to a 30% reduction of hMSC metabolism. n=3. Data were measured 48h after the 4h exposure to bleomycin. n=4. (C) Quantitative assessment of the number of hMSC in respective conditions and the end of the 3D culture (Day 35). The 4h exposure to bleomycin did not significantly impact hMSC viability. n≥3. (D) The ratio eN/eN-Bleo of cells retrieved

from the bioreactors (ECM and SN combined) indicates that eN-Bleo displayed a higher number of HSCs. (E) Total quantification of retrieved blood cells confirmed the specific increased number of HSCs in the eN-Bleo. PM: proliferative medium. OM: osteogenic medium. SFEM+GF: serum free medium supplemented with hematopoietic growth factors. n≥3. HSPCs: Hematopoietic Stem and Progenitor Cells, HSCs: Hematopoietic Stem Cells, MPPs: Multipotent Progenitors. MLPs: Multilymphoid progenitors. Bleo: Bleomycin. *p<0.05., **p<0.01.

A

Primary antibody	Company	product number
Collagen type 1	Cedarlane	CL50151AP
Collagen type 4	Abcam	ab19808
Osteocalcin	AbD Serotec	7060-1815
Fibronectin	Abcam	ab-23750-100
SDF1α	eBiosciences	14-7992-81
CD34	Novus Biologicals	NBP2-38322
CD90	R&D systems	AF2067
GFP	Aves	GFP-1020

B

Secondary antibody	Company	product number
Anti-rat Alexa Fluor 488	Thermofischer	A-21208
Anti-rabbit Alexa Fluor 555	Thermofischer	A-31572
Anti-mouse Alexa Fluor 555	Thermofischer	A-31570
Anti-rat CF633	Biotium	20137
Anti-goat Alexa fluor 594	Thermofischer	A-11058
Anti-rabbit CF633	Biotium	20125

Figure S10. (A) List of primary antibodies used for confocal immunofluorescence. (B) List of secondary antibodies used for confocal immunofluorescence.

Chapter 6. Engineering of mesenchymal tissues supporting malignant hematopoiesis

Project Report: *In vitro engineering of a human bone marrow proxy to model myeloproliferative neoplasms.*

In vitro engineering of a human bone marrow proxy to model myeloproliferative neoplasms.

Investigators: Thibaut Klein[1], Morgane Hilpert[2], Andrés García-García[1], Radek Skoda[2], Paul E. Bourgine[1, 3] and Ivan Martin[1]

[1]*Tissue Engineering, Department of Biomedicine, University Hospital Basel, University of Basel, 4031 Basel, Switzerland.*

[2]*Experimental Hematology, Department of Biomedicine, University Hospital Basel, University of Basel, 4031 Basel, Switzerland.*

[3]*Laboratory for Cell, Tissue and Organ engineering, Wallenberg Center for Molecular Medicine, University of Lund, 223 50 Lund, Sweden.*

1. Description of project

Lack of *in vitro* culture systems sustaining human primary myeloid malignancies severely impairs development, test and personalized selection of drugs. Existing protocols do not allow *in vitro* maintenance of myeloproliferative neoplasms (MPN) clinical samples, and the surrogate JAK2-mutated cell lines do not reflect diseases features (e.g., proliferation and response to drugs). Similarly to their healthy counterpart, MPN stem cells reside and are regulated in the bone marrow (BM), providing unique structural/physical/cellular/molecular cues defining the hematopoietic niche. Conventional 2D models do not mimic this complex BM microenvironment associated with MPN functional maintenance. Here we thus aim at *in vitro* engineering 3D BM niches thanks to the use of bone-like scaffolds, functionalized by human Mesenchymal Stromal Cells (hMSC) and their extracellular matrix deposited during perfusion culture. The resulting organoids will then be used as supportive BM niches substrate for MPN cells. The system will be validated towards the capacity to (i) maintain MPN cell phenotypes/function and (ii) test their response to drugs. Validation of this target will open new perspectives to investigate MPN therapeutic strategies. The same paradigm will also warrant extension to the modelling of other hematopoietic malignancies.

2. Objectives / Milestones

Hypothesis 1: A 3D engineered BM niche previously established for healthy HSPCs can maintain human MPN cells *in vitro*

Aim 1: Demonstrate the capacity of our 3D approach in maintaining MPN phenotypes and function.

Hypothesis 2: The 3D engineered BM niche loaded with patient-derived MPN cells can be used as a drug-testing platform

Aim 2: Validate the possibility to use the developed 3D model to assess the effect of drugs on MPN.

3. Material and methods

a. 3D perfusion culture

Two different systems have been used in this study to generate 3D BM niches.

Engineered niches based on culture of human bone marrow mesenchymal stromal cells (hBM-MSCs) in ENGIpore ceramic scaffolds (eN-E) were generated as previously described in Bourgine PE *et al.* 2018. Briefly, hydroxyapatite scaffolds (ENGIpore, Fin-Ceramica Feanza S.p.A. cat# SP-ENGI-PROD-01) were directly seeded in perfusion bioreactors (CELLEC, Switzerland) together with $0.75*10^6$ hMSCs by overnight perfusion at a superficial velocity of 2,800 µL/s. After 24 h (cell-seeding phase), the superficial velocity was reduced to 280 µL/s for the perfusion culture of hMSCs. Cells were then cultured for 1 week in proliferative medium (PM). This medium is composed by complete medium (CM; α- MEM with 10% fetal bovine serum, 1% HEPES (1M), 1% sodium pyruvate ($100*10^{-3}$M), and 1% of penicillin-streptomycin-glutamine (100X); supplemented with dexamethasone ($10*10^{-9}$M), ascorbic acid-2-phosphate ($0.1*10^{-3}$M) and fibroblast growth factor 2 (5 ng/mL). Then, cells were cultured by 3 weeks in osteogenic medium (OM). This is CM supplemented with dexamethasone ($10*10^{-9}$M), ascorbic acid-2-phosphate ($0.1*10^{-3}$M) and β-glycerolphosphate ($10*10^{-3}$ M) (See Fig. 1A).

Alternatively, standardized engineered niches based on culture of MSOD mesenchymal stromal cell line in collagen sponges scaffolds (eN-CM) niches were generated as follows. 10^6 MSOD cells (Bourgine PE *et al.* 2017) were directly seeded on collagen sponge scaffolds (ULTRAFoam, Avitene cat# 1050050) in perfusion bioreactors (CELLEC, Switzerland). Perfusion flow rate was maintained at 2,800 µL/s for cell seeding phase, and reduced to 280 µL/s for culture phase. Cells were then cultured directly for 3 weeks of osteogenic medium (OM) (See Fig. 4A).

Bioreactors containing engineered niches were maintained in humidified 37 °C per 5% CO_2 incubators. For both systems, human $CD34^+$ hematopoietic stem and progenitor cells (HSPCs) isolated from cord blood, buffy coat or phlebotomies from MPN patients were seeded on our 3D engineered niches by overnight perfusion at a superficial velocity of 2,800 µL/s in serum-free expansion medium (SFEM), supplemented with the following growth factors (GF): SCF (10 ng/mL; cat. no. 130-093-991), FLT3-ligand (10 ng/mL; cat. no. 130-093-854); TPO (10 ng/mL; cat. no. 130-094-011), all from Miltenyi Biotec. After 24 h (cell-seeding phase), the superficial velocity was reduced to 280 µL/s for perfusion culture during 1 week. Cells were then retrieved from the bioreactors by collagenase digestion and trypsinization for subsequent analysis.

b. HSPC extraction and purification

Cord blood (CB) samples were collected from human placenta of full-term healthy caesarean section. The CB was drained from the umbilical vein into a single-use bag containing anticoagulants (MSC1206DU - Cord blood collection bag – MacoPharma, France) and mononuclear Cells (MNC) were isolated within the 24 hours after collection. Buffy Coat (BC) were obtained from the University Hospital Basel (Blutspendezentrum) from healthy volunteer donors. MPN cells were obtained from patients undergoing phlebotomy at the University Hospital Basel as part of their treatment.

In all cases, blood mononuclear cell fraction was separated by density gradient centrifuge separation on Ficoll (Histopaque®: cat# 1077, SIGMA-ALDRICH or Lymphoprep™: cat# 07851, Stemcell Technologies, Grenoble, France) in SepMate™-50 tubes (cat# 85460 Stemcell Technologies, Grenoble, France) after a 1:1 dilution in PBS. HSPCs were then isolated based on CD34 expression using the magnetic EasySep $CD34^+$ positive selection Kit (Stemcell Technologies, Grenoble, France) following manufacturer's protocol and ultimately stored in liquid nitrogen.

c. Flow cytometry

The purity of purified CB, BC and MPN $CD34^+$ cells was determined with BD Accuri™ C6 Cytometer (BD Biosciences) by labelling cells with human anti-CD34 antibody (BD BIOSCIENCES: cat# 555824).

The immunophenotypic analysis of HSPCs retrieved from bioreactors was performed using LSR II FORTESSA SORP (BD Biosciences) cell analyzer. Harvested blood cells were labelled using

following antibodies diluted in PBS 2% FBS 0.5M EDTA: human anti-CD34 (BioLegend cat# 343512 or BD BIOSCIENCES cat# 563756), human anti-CD38 (BD BIOSCIENCES cat# 555460), human anti-CD45RA (BD BIOSCIENCES cat# 563429), human anti-CD90 (BD BIOSCIENCES cat# 559869), human anti-CD14 (BioLegend cat# 301840), human anti-CD66b (BioLegend cat# 305106), human anti-CD71 (BioLegend cat# 334110), human anti-CD3 (BioLegend cat# 100236) and human anti-CD19 (BioLegend cat# 302216).

d. Colony Forming Unit in culture (CFU-C) Assays

CFU-C assays were performed according to Stemcell Technologies's protocol. Briefly, 500 HSPCs pre- culture and 1200 HSPCs post-culture were washed with PBS, resuspended in 240 µL IMDM (Gibco, cat# 12440-053) and mixed with 2.4 mL MethoCult (Stemcell Technologies, cat# 04034). The mixture was plated in duplicates (1.1 mL) in 35mm petri dishes and incubated for 14 days at 37ºC and 5% CO_2. The colonies were identified by light microscopy and characterized according to the "Atlas of human haematopoietic colonies from cord blood" (Stemcell Technologies).

e. Histological Analysis:

eN-CM samples were fixed adding 4% paraformaldehyde (vol/vol) directly inside the bioreactor prior to unmounting and embedding the generated tissue in paraffin. Sections (5 µm thick) were stained with Hematoxylin & Eosin (Baker) or processed for immunostaining. Briefly, antigen retrieval was performed using citrate buffer pH 6 (10mM Sodium Citrate, 0.05% Tween 20) in a pressure cooker at 100 °C during 1 h. Slides were rinsed and blocked with PBS containing 10% goat serum for 30 min to reduce nonspecific bindings. Then, samples were incubated for 1 h at room temperature with mouse anti human alkaline phosphatase (ALP) (Abcam ab54778). Sections were washed 3 times with PBS and incubated with A546 goat anti-mouse antibody (Thermofischer, A11030). Nuclei were counterstained with DAPI (Invitrogen) for 15 min. hMSC were revealed by endogenous GFP expression. Negative controls for each analysis were run by omitting the incubation with primary antibodies. Both bright field and fluorescence images were acquired using Nikon Ti2 microscopes.

f. Allele burden measurement:

The allele-specific PCR for JAK2 genotyping was carried out using 20 ng genomic DNA, 45 nM forward primer JAK2-F, and 22.5 nM each of the allele-specific reverse primers JAK2-R-T and JAK2-R-G (table below) in a buffer containing 50 mM KCl, 10 mM Tris pH 8.0, and 1.5 mM MgCl2. Thirty PCR cycles with denaturing at 94°C for 30 seconds, annealing at 61°C for 30 seconds, and extension at 72°C for 30 seconds were applied. The PCR products were analyzed using the 3100 Genetic Analyzer (Applied Biosystems, Carlsbad, CA). The percentage of chromosomes carrying the G>T transversion representing the $JAK2^{V617F}$ allele (%T) were calculated using the formula: %T = (height of T-peak) / (height of T-peak + G-peak) * 100.

Assay	Primer	5' dye	Sequence	Annealing
JAK2 PCR	JAK2-F	-	gtttcttAGTGCATCTTTATTATGGCAGA	61 °C
(genomic DNA)	JAK2-R-G	6FAM	TTACTCTCGTCTCCACAGAC	
	JAK2-R-T	6FAM	aaaTTACTCTCGTCTCCACAGAA	

4. Results

a. Survival and maintenance of MPN cells in 3D engineered BM niches

We initially hypothesized that 3D engineered BM niches, previously shown to maintain healthy HSPCs (Bourgine *et al.* 2018), could also support malignant HSPCs such as MPN progenitor cells. For this purpose, osteoblastic-like engineered niches were generated using ENGIpore scaffolds (from here referred as eN-E) following our validated protocol. hBM-MSCs, which were lentivirally transfected to overexpress Venus protein (yellow fluorescent protein, YFP), were seeded in eN-E and cultured for 4 weeks to engineer 3D BM niches. Then, $CD34^{+}$ HSPCs isolated from phlebotomies of MPN patients were loaded into the system and co-cultured for 1 week. HSPCs isolated from peripheral blood (buffy coat, BC) of healthy donors and cord blood (CB)-derived HSPCs were used as controls. After one week of co-culture under perfusion, eN-E were disrupted by enzymatic digestion and cells harvested for quantitative phenotypic and functional assessment (**Fig. 1A**). Taking advantage of Venus fluorescent protein expression to identify hBM-MSCs, we firstly analysed the percentage of stromal and hematopoietic cells in our system. Independently of HSPC source, generated eN-E were mainly composed of blood cells (CB: 78.43 % ± 4.37, BC: 55.40 % ± 15.26 and MPN: 60.23 % ±3.03; **Fig. 1B**). As expected based on their higher proliferative capacity (Sotnezova *et al.* 2016), CB-HSPCs exhibited higher hematopoietic expansion than peripheral blood HSPCs (BC and MPN), confirming different HSPC potential according to the cell source. Then, we evaluated the

expansion of both total blood cells (negative for Venus fluorescence) and immunophenotypically defined HSPCs ($CD34^+CD38^-$) normalized to cells seeded and cultured in eN-E. Our results reveal that, similar to CB-HSPCs although at lower extent, both healthy BC and MPN cell numbers increased in eN-E in comparison to empty ENGIPore ceramic (Ce). Intriguingly, total blood cells fold increase for MPN cells trended to be higher than for BC cells (BC: 7,21 ± 1.32 vs MPN: 23.48 ± 4.08), while HSPC fold increase was slightly reduced (BC: 8.53 ± 1.58 vs. MPN: 4.45 ± 0.62) (**Fig. 1C-D**). This might suggest that MPN-HSPCs could differentiate into more mature cells in eN-E. Overall, these results indicate that both healthy (BC) and malignant (MPN) peripheral blood-derived HSPCs exhibit are able to survive and can be maintained in eN-E.

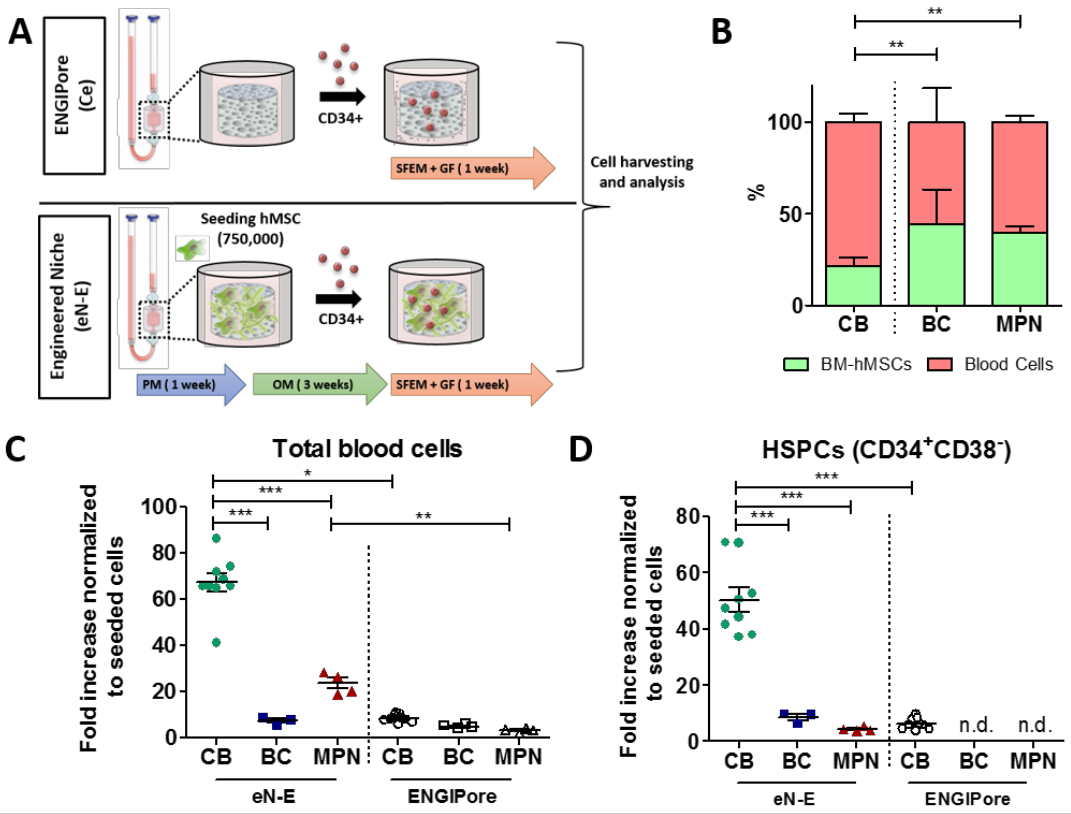

Figure 1. Osteoblastic-like eN-E does not only maintain but also expands both phenotypic BC-derived HSPCs and primary MPN HSPCs, albeit at lower extent than CB-derived HSPCs. (A) Experimental design for the generation of 3D niches in a perfusion bioreactor system based on ENGIPore Ceramic scaffold and hBM-MSCs. OM, osteogenic medium; PM, proliferative medium; SFEM+GF, serum-free medium plus growth factors: Stem Cell Factor, Thrombopoietin, and Flt3-ligand. (B) Percentage of stromal (BM-hMSCs) and blood cells retrieved from the bioreactor at the end of the culture. (C-D) Fold increase in the numbers of total blood cells (C) and HSPCs (D) at the end of the culture period in eN-E. n ≥ 3 biological replicates. 1 dot = 1 bioreactor.

** $p < 0.001$; *** $p < 0.0001$

hMSC, human Mesenchymal Stromal Cells (2 donors); CB, cord blood ($70*10^4$ $CD34^+$ cells seeded/bioreactor, 3 donors); BC, buffy coat ($62*10^4$ $CD34^+$ cells seeded/bioreactor, 8 pooled donors); MPN, myeloproliferative neoplasm primary cells ($30*10^4$ $CD34^+$ cells seeded/bioreactor, 1 donor).

In order to further explore MPN-HSPC maintenance, proliferation and differentiation in eN-E, we analysed committed HSPC subsets by quantitative flow cytometry. According to the trends observed for total blood cells and primitive HSPCs (**Fig. 1C-D**), we observed a dramatic expansion of MPN committed progenitors (40-fold increase; **Fig. 2A**), common-myeloid progenitors/megakaryocytic-erythroid progenitors (CMPs/MEPs) (35-fold increase; **Fig. 2B**) and granulocyte-macrophage progenitors (GMPs) (225-fold increase; **Fig. 2C**). We next measured the *in vitro* functionality of HSPCs cultured in eN-E with colony-forming unit in culture (CFU-C) assays. In agreement with HSPC fold increase data, CB cells had the highest colony forming capacity, while peripheral blood derived-BC and MPN cells showed a similar potential. But more interestingly, BC and MPN progenitors only gave rise to burst-forming unit erythroid (BFU-E) and colony-forming unit granulocyte and macrophage (GM) colonies; whereas CB progenitors also formed less-committed granulocyte, erythroid, macrophage and megakaryocyte (GEmM) colonies (**Fig. 2D**). Moreover, we assessed the maintenance of MPN mutant HSPCs after culture in eN-E through $JAK2^{V617F}$ allele burden measurement (percentage of cells carrying the $JAK2^{V617F}$ mutation). Findings revealed that $JAK2^{V617F}$ allele burden was not only maintained in HSPCs after culture in eN-E, but it was particularly high in sorted primitive HSPCs ($CD34^{+}CD38^{-}$ cells) (**Fig. 2E**). Furthermore MPN-HSPCs differentiated in eN-E, leading to a very pronounced myeloid skewing, while preserving $JAK2^{V617F}$ mutation.

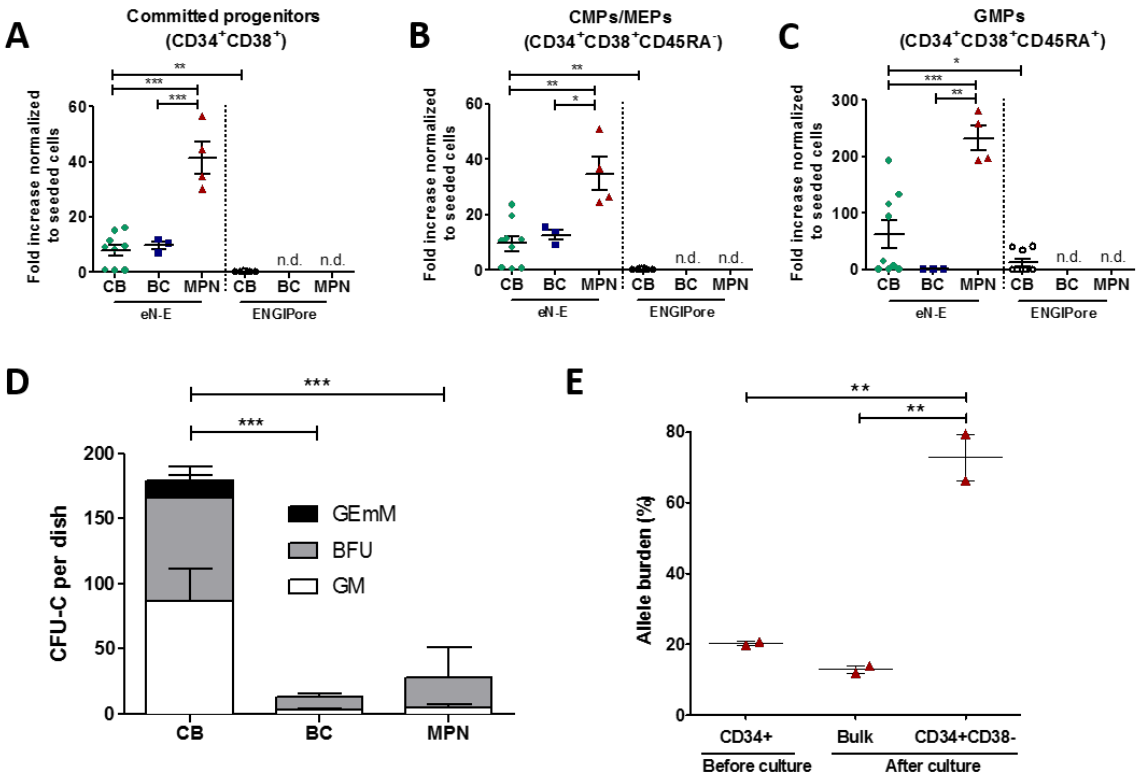

Figure 2. Osteoblastic-like eN-E promotes the myeloid skewing of MPN progenitor cells while increasing JAK2^{V617F} allele burden. (A-C) Fold increase in the numbers of committed progenitors (A), CMPs/MEPs (B) and GMPs (C) assessed by quantitative FACS analysis at the end of the culture period. CMPs/MEPs, common-myeloid progenitors/megakaryocytic-erythroid progenitors; GMPs, granulocyte-macrophage progenitor. n ≥ 3 biological replicates. 1 dot = 1 bioreactor. (D) Colony-forming unit capacity of HSPCs retrieved after culture in eN-E. GEmM, colony forming unit granulocyte, erythroid, macrophage and megakaryocyte; BFU-E, burst-forming unit erythroid; GM, colony-forming unit granulocyte and macrophage. n ≥ 6 biological replicates. (E) Allele burden measurement as the percentage of specified cells carrying the JAK2^{V617F} mutation post-culture.
* P < 0.05; ** p < 0.001; *** p < 0.0001
hMSC, human Mesenchymal Stromal Cells (2 donors); CB, cord blood (70*10^4 CD34$^+$ cells seeded/bioreactor, 3 donors); BC, buffy coat (62*10^4 CD34$^+$ cells seeded/bioreactor, 8 pooled donors); MPN, myeloproliferative neoplasm primary cells (30*10^4 CD34$^+$ cells seeded/bioreactor, 1 donor).

Since eN-E seemed to promote myeloid differentiation in MPN-HSPCs, we wanted to test mature hematopoietic cell lineages generated in this system after culture. Unfortunately, we did not manage to get robust data yet due to scarcity of MPN material available. However, our preliminary results showed that all different subsets of mature hematopoietic cells (monocytes, neutrophils, erythroid cells, B and T cells) could be detected in eN-E at the end of the culture period (**Fig. 3A-E**). Therefore, we have now proven that our eN-E is not only able to harbor highly proliferative CB-derived HSPCs (as previously reported), but also healthy (BC-derived) and malignant (MPN) HSPCs isolated from peripheral blood. Nevertheless, the eN-E system has several limitations. Since eN-E is generated using primary hBM-MSCs, the functionality of the system is highly influenced by donor cell variability. In addition, the hard hydroxyapatite of ENGIPore scaffolds hinders good histological analysis. In order to overcome

these constraints, we followed the same principles of eN-E to develop standardized 3D engineered BM niches (from here referred as eN-CM) based on the use of a mesenchymal cell line (MSOD; (Bourgine PE *et al.* 2017)) and collagen sponge scaffolds (ULTRAFoam). In contrast to eN-E, HSPCs were directly cultured for 3 weeks in OM in eN-CM (**Fig. 4A**).

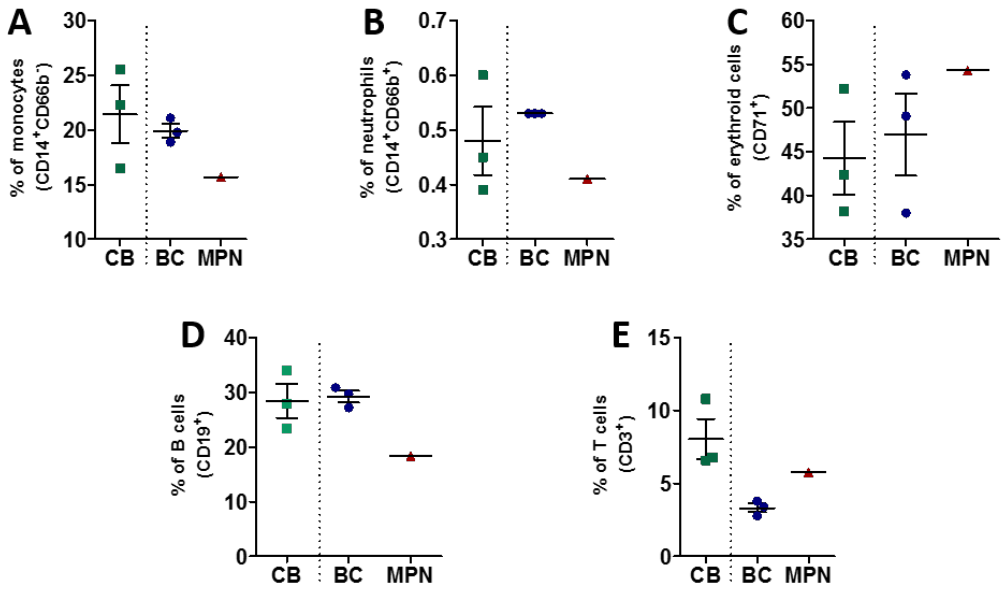

Figure 3. Mature blood cell lineages are detected after HSPC culture in eN-E. Percentage of (A) monocytes ($CD14^+CD66b^-$), (B) neutrophils ($CD14^+CD66b^+$), (C) erythroid cells ($CD71^+$), (D) B cells ($CD19^+$) and (E) T cells ($CD3^+$), assessed by FACS in eN-E at the end of the culture period. n = 3 biological replicates for CB and BC, n=1 for MPN.
CB, cord blood ($70*10^4$ $CD34^+$ cells seeded/bioreactor); BC, buffy coat ($62*10^4$ $CD34^+$ cells seeded/bioreactor); MPN, myeloproliferative neoplasm primary cells ($30*10^4$ $CD34^+$ cells seeded/bioreactor).

In sharp contrast to eN-E, the vast majority of cells harvested from eN-CM were stromal MSOD cells, which might reflect a higher proliferation rate of MSOD cells in comparison to hBM-MSCs. Yet, we detected that the percentage of blood cells was higher in eN-CM seeded with MPN-HSPCs (similar to CB-HSPCs) than in those seeded with BC-HSPCs (**Fig. 4B**). As previously shown for eN-E, eN-CM promoted BC and MPN cell numbers increase in comparison to empty ULTRAFoam scaffolds (**Fig. 4C**). Intriguingly, when we focused in primitive HSPCs, we detected that BC HSPC fold increase was similar in eN-CM and empty ULTRAFoam scaffolds, while MPN HSPC fold increase was 2-fold higher in eN-CM (compared to empty scaffold) (**Fig. 4D**). ULTRAFoam collagen sponge consistency let us to obtain histological sections from eN-CM without decalcification (required for eN-E). Hematoxylin-Eosin staining was used to reveal general structures in eN-CM (**Fig. 4E**). Then, we performed immunofluorescence stainings to focus in more specific aspects. Immunostaining against alkaline phosphatase (ALP; osteoblastic marker) showed co-expression (yellow) of MSOD cells (GFP; green) and ALP (red)

(**Fig. 4F-H**). These results validate eN-CM as osteoblastic-like BM niches, which are able to maintain and expand immunophenotypically-defined healthy BC-HSPCs and malignant MPN-HSPCs.

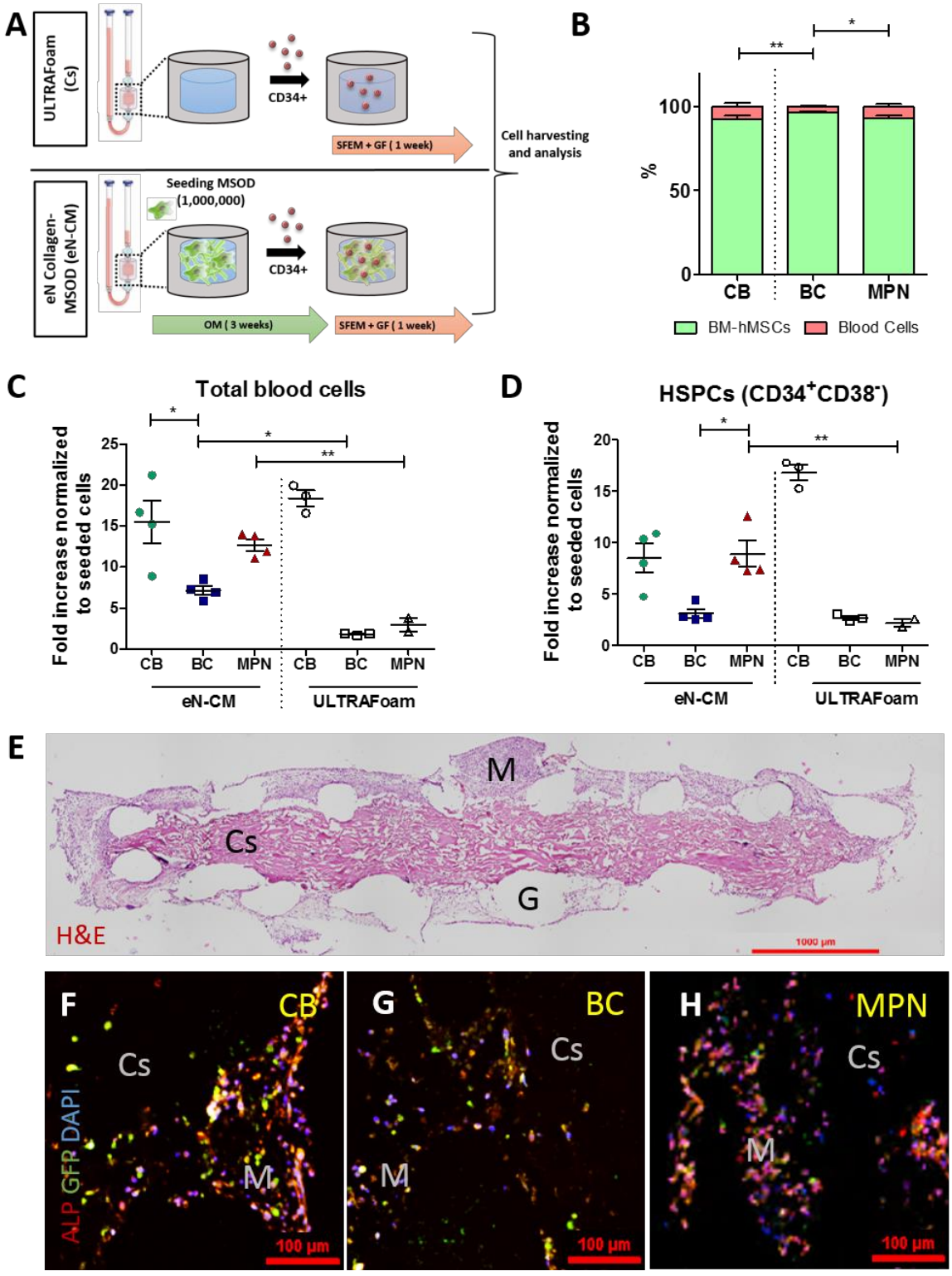

Figure 4. Standardized eN-CM allows similar expansion of phenotypic CB-derived HSPCs and MPN HSPCs, but reduced in comparison to eN-E. (A) Experimental design for the generation of 3D niches in a perfusion bioreactor based on ULTRAFoam collagen scaffold and MSOD cells. OM, osteogenic medium; PM, proliferative medium; SFEM+GF, serum-free medium plus growth factors: Stem Cell Factor, Thrombopoietin, and Flt3-ligand. (B) Percentage of stromal (BM-hMSCs) and blood cells retrieved from the bioreactor at the end of the culture. (C-D) Fold increase in the numbers of total blood cells (C) and HSPCs (D) at the end of the culture period in eN-CM. (E) Representative hematoxylin-eosin (H&E) staining showing a transversal section in frontal plane of a eN-CM at the end of the culture. Scale bar: 1000µm. M: MSOD cells; Cs: ULTRAFoam Collagen sponge G: Grid mecanically stabilizing the Cs in the bioreactor. (F-H) Immunofluorescence staining for alkaline phosphatase (ALP; red) in sections of eN-CMs hosting CB (F), BC (G) and MPN (H) blood cells. MSOD cells are revealed by GFP fluorescence. Nuclei are labelled with DAPI. Scale bar : 100µm.
n ≥ 3 biological replicates. 1 dot = 1 Bioreactor. * P < 0.05; ** p < 0.001.
CB, cord blood; BC, buffy coat, MPN, myeloproliferative neoplasm primary cells ($62*10^4$ $CD34^+$ cells seeded/bioreactor for each conditions).

Mimicking eN-E, we also observed an important expansion of committed progenitors (10-fold increase; **Fig. 5A**), common-myeloid progenitors/megakaryocytic-erythroid progenitors (CMPs/MEPs) (10-fold increase; **Fig. 5B**) and granulocyte-macrophage progenitors (GMPs) (20-fold increase; **Fig. 5C**). CFU-C experiments with HSPCs harvested from eN-CM confirmed that, similarly to eN-E, GEmM colonies were only generated from CB-HSPCs, whereas BC- and MPN-HSPCs only form erythroid BFU-E and granulocyte/macrophage GM colonies (**Fig. 5D**). Finally, $JAK2^{V617F}$ allele burden assessment revealed that $JAK2^{V617F}$ mutation was similarly represented in MPN-HSPCs before and after culture in eN-CM (**Fig. 5E**).

Thus, we have used two different models of 3D engineered BM niches to reveal that, similar to CB-HSPCs, healthy BC-HSPCs and malignant MPN-HSPCs isolated from peripheral blood could be maintained in 3D engineered BM niches. However, in contrast to BC-HSPCs, MPN-HSPCs tend to differentiate and exhibit a pronounced myeloid skewing.

b. Test the possibility of using 3D engineered BM niches loaded with patient-derived MPN cells as a drug testing platform

Once we demonstrated that our *in vitro* 3D engineered BM niches can maintain patient-derived MPN-HSPCs, we hypothesized that we could use our system as drug testing platform. Since drug testing platforms require high reliability and reproducibility, we engineered standardized 3D BM niches using a mesenchymal cell line (eN-CM) and validated their capacity to host MPN-HSPCs (**Fig. 4 and 5**). The standardized eN-CM could circumvent donor-to-donor variability inherent to the use of primary hBM-MSCs to engineer 3D BM niches. Although

functional, eN-CM system exhibits a limited capacity to maintain MPN-HSPCs in comparison to eN-E. Therefore, this system requires further optimization prior to its application as a drug-testing system. This, together with the limited availability of MPN patient material, have prevented the full achievement of this goal at the expected period.

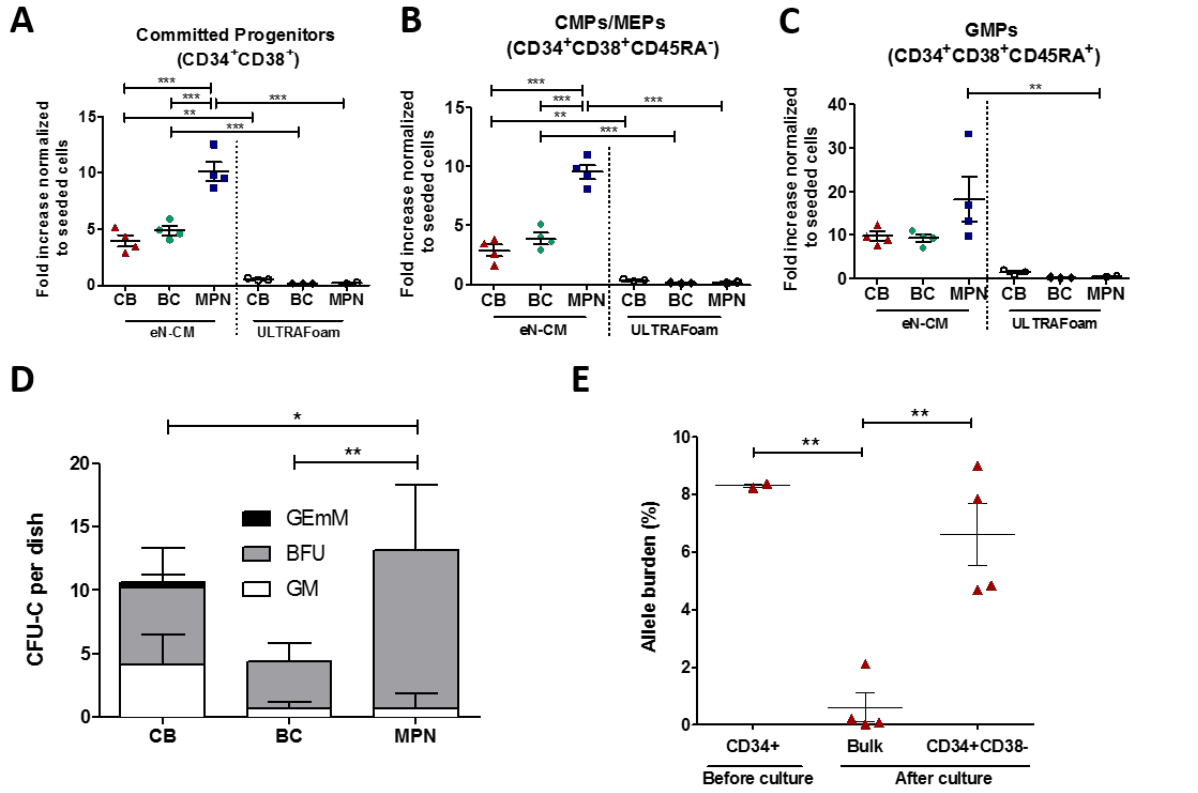

Figure 5. Standardized eN-CM supports the expansion of MPN megakaryocytic-erythroid progenitors resembling MPN pathogenesis. (A-C) Fold increase in the numbers of committed progenitors (A), CMPs/MEPs (B) and GMPs (C) assessed by quantitative FACS analysis at the end of the culture period. CMPs/MEPs, common-myeloid progenitors/megakaryocytic-erythroid progenitors; GMPs, granulocyte-macrophage progenitor. n = 4 biological replicates. 1 dot = 1 bioreactor. (D) Colony-forming unit capacity of HSPCs retrieved after the culture in eN-CM. GEmM, colony-forming unit granulocyte, erythroid, macrophage and megakaryocyte; BFU-E, burst-forming unit erythroid; GM, colony-forming unit granulocyte and macrophage. n = 8 biological replicates. (E) Allele burden measurement as the percentage of cells carrying the $JAK2^{V617F}$ mutation post-culture.
* $P < 0.05$; ** $p < 0.001$.
CB, cord blood; BC, buffy coat, MPN, myeloproliferative neoplasm primary cells ($62*10^4$ $CD34^+$ cells seeded/bioreactor for each conditions).

5. Discussion, conclusions and perspectives

Classic 2D and 3D cultures have been reported to be inefficient in maintaining human HSPCs *ex vivo* (Ferreira *et al.* 2012; Prewitz *et al.* 2013), since they fail to recapitulate the complexity of signaling networks governing native BM niches (Morrison and Scadden 2014). We recently reported the *in vitro* engineering of BM niches in a perfusion bioreactor system, which were capable to maintain and expand human CB-derived HSPCs (Bourgine *et al.* 2018). This

encouraged us to use our system to model hematological diseases *in vitro* and explore its potential application as drug-testing platform. In this work, we followed similar principles to develop two different models of 3D engineered BM niches that can maintain not only CB-HSPCs, but also mutant JAK2^{V617F} HSPCs isolated from phlebotomies of MPN patients and healthy counterparts isolated from buffy coats.

In first instance, we demonstrated that BM niches engineered with hBM-MSCs and hydroxyapatite scaffolds (eN-E) were able to sustain and expand immunophenotypically-defined BC-HSPCs and MPN-HSPCs. Moreover, MPN-HSPCs exhibited a marked skewing toward erythroid/myeloid differentiation while preserving JAK2^{V617F} mutation, which are some of the key traits revealed in MPN patients (Jamieson *et al.* 2006). In order to generate a customizable and standardized system which could be used as drug-testing platform, we also developed engineered BM niches using a mesenchymal cell line (MSOD; (Bourgine PE *et al.* 2017)) and collagen sponges. We adapted this system by increasing the amount of cells seeded in the bioreactor and modulating the culture period for niche engineering. However, its capacity to maintain and expand both healthy (BC) and malignant (MPN) HSPCs isolated from peripheral blood remains limited. In this regard, we noticed that, in sharp contrast to eN-E, most cells harvested from eN-CM were non-hematopoietic cells. This might result from a higher proliferative capacity of MSOD cell line in comparison to hBM-MSCs. Therefore, envisioned strategies to optimize eN-CM should consider a reduction in the amount of mesenchymal cells seeded to reach a better balance between stromal and hematopoietic cells. Furthermore, the mechanisms underlying the positive impact of 3D engineered BM niches on HSPCs are completely unknown. In this regard, the analysis of stromal cells secretome and extracellular matrix deposited in these engineered BM niches might provide important insights.

In summary, here we have applied tissue engineering to develop a customizable and standardized 3D *in vitro* culture system capable to maintain healthy and malignant JAK2^{V617F} HSPCs in a BM niche-like environment. Although, this system still requires further investigation to increase its efficiency, it might be exploited to explore other hematological diseases (e.g. leukemia) or as a platform for drug testing (e.g. JAK1/2 inhibitor Ruxolitinib) in personalized settings.

6. Other research

In this report, we have presented and discussed the results generated for the funded project. However, we have also performed other experiments in the context of this project that were not included in the results chapter because either they failed or they are still ongoing. In this sense, we attempted to evaluate the *in vivo* functionality of peripheral blood-derived HSPCs cultured in eN-E. Briefly, immunodeficient NOD.Cg-Prkdcscid IL2rgtmWjl/Sz (also termed NOD/SCID/IL2Rγnull) 6-weeks old female mice were sublethally irradiated (225 cGy) and transplanted (intravenously) with 260000 post-culture cells (mix of both MSOD stromal and hematopoietic cells) resuspended in 25µl PBS. We measured human peripheral blood mononuclear cells at week 4, 8 and 12 by flow cytometry to assess the engraftment of human HSPCs cultured in eN-E. Unfortunately, we could not detect human blood chimerism (>1% human hematopoietic cells in mouse peripheral blood) at any of the tested time points. Following the established protocols (Animal permit 2697, Veterinäramt of Kanton Basel), mice were euthanized 12 weeks after transplantation. This result might be explained by the insufficient number of primitive hematopoietic stem cells inside the HSPC pool isolated from peripheral blood and later *in vitro* expanded in eN-E. Therefore, the transplantation of sorted HSCs could be a potential solution for future experiments.

On the other hand, we are currently assessing Dexter-inspired 2D cultures as controls to better evaluate the potential of our 3D engineered BM niches. To this end, hBM-MSCs or MSOD cells are allowed to reach confluence in 12-well plates and then cultured with 7000 human $CD34^+$ HSPCs isolated from BC or MPN phlebotomies. Cells are co-cultured in SFEM complemented with growth factors as previously described. After one week of co-culture, cells are retrieved from the bioreactor and quantified by flow cytometry. These analysis will allow us to directly compare 2D and 3D cultures in our established settings.

Finally, we also had to perform multiple experiments in order to optimize techniques and protocols (e.g. $CD34^+$ cells isolation from peripheral blood, FACS antibodies cocktails, etc). These experiments were not detailed here but they were essential for the success of this project.

7. References

Bourgine, P. E., Gaudiello, E., Pippenger, B., Jaquiery, C., Klein, T., Pigeot, S., & Martin, I. (2017). Engineered extracellular matrices as biomaterials of tunable composition and function. Advanced Functional Materials, 27(7), 1605486.

P Bourgine, T Klein, A M Paczulla, T Shimizu, L Kunza, K D Kokkaliaris, D L Coutu, C Lengerke, R Skoda, T Schroeder, and I Martin, 2018. Proceedings of the National Academy of Sciences 115 (25) E5688-E5695

Sotnezova, E. V., Andreeva, E. R., Grigoriev, A. I., & Buravkova, L. B. (2016). Ex vivo expansion of hematopoietic stem and progenitor cells from umbilical cord blood. Acta Naturae (англоязычная версия), 8(3 (30)).

Ferreira, M. S. V., Jahnen-Dechent, W., Labude, N., Bovi, M., Hieronymus, T., Zenke, M., ... & Neurs, S. (2012). Cord blood-hematopoietic stem cell expansion in 3D fibrin scaffolds with stromal support. Biomaterials, 33(29), 6987-6997.

Prewitz, M. C., Seib, F. P., Von Bonin, M., Friedrichs, J., Stißel, A., Niehage, C., ... & Bornhäuser, M. (2013). Tightly anchored tissue-mimetic matrices as instructive stem cell microenvironments. Nature methods, 10(8), 788.

Morrison, S. J., & Scadden, D. T. (2014). The bone marrow niche for haematopoietic stem cells. Nature, 505(7483), 327.

Jamieson, C. H., Gotlib, J., Durocher, J. A., Chao, M. P., Mariappan, M. R., Lay, M., ... & Weissman, I. L. (2006). The JAK2 V617F mutation occurs in hematopoietic stem cells in polycythemia vera and predisposes toward erythroid differentiation. Proceedings of the National Academy of Sciences, 103(16), 6224-6229.

Chapter 7. Discussion and perspectives

The aim of this thesis was to explore the potential of hMSCs cultured within 3D perfusion-based bioreactors to engineer functional bone organs in vitro. This approach has given rise to innovative models for fundamental biology, but also for regenerative medicine. On the one hand, our results showed that cell-free ECM coated material enriched with potent morphogens (e.g. VEGFa and BMP2) exhibits osteoinductive features and remodel into bone upon in vivo implantation (Chapters 1 and 2). On the other hand, we have engineered BM microenvironments or niches that can sustain human hematopoiesis in both health and disease (Chapters 3 and 4).

The first two chapters of this thesis represent a step forward in the generation of cell-laid but cell free material as off-the-shelf products for bone tissue regeneration. This relies on the advantage of devitalizing ECM using a death-inducible mesenchymal cell line (MSOD) instead of more aggressive traditional methods (e.g., freeze & thaw), which results in a better conservation of ECM components. Furthermore, the genetic modification of MSOD as ECM-depositing cellular tool enables the overexpression of key factors for angiogenesis and bone regeneration (e.g., VEGFa and BMP2) that remain entrapped within the matrix during graft generation.

VEGFa-enriched grafts showed a clear increase in vascularization and enhanced bone repair capacity upon in vivo implantation. These advantages over the unmodified MSOD line validate the possibility of customization and gain of function for specific regenerative features of the resulting implantable material. In case of MSOD-B based grafts, results were more variable. Even if we could observe more bone formation with BMP2-enriched devitalized grafts after in vivo implantation, this was not distributed homogeneously throughout the construct. Full tissue mineralization should be the next milestone to achieve with this model since this is the most important feature of osteogenic grafts. Indeed, when considering large defects compromising mechanical stability of the skeleton, perfect graft integration, maturation, homogeneity and stability are mandatory. For this purpose, a better understanding of both composition and kinetic of grafts generation and remodeling upon implantation is still required.

The half-life of those growth factors entrapped in the ECM is an important aspect to take into consideration. VEGFa and BMP2 stability in this context has to be assessed to validate the

possibility of long-term, storable and off-the-shelf graft with high and preserved regenerative potential. At cellular level, we have engineered grafts using a single cell type but this could be implemented to generate more elaborated grafts combining different customized cell lines secreting growth factors through activation of distinct inducible promoters. This possibility would allow the spatiotemporal secretion of several morphogenetic factors for synergic instructive signals. Aside of growth factors, and since grafts will trigger an immune response upon in vivo implantation, customized cell lines might be used to enrich ECM-coated materials in key factors to instruct a favourable immune response for endogenous tissue regeneration [1].

Finally, in perspective of an efficient transition from bench to bedside, our approach should be adapted to use material validated for clinical applications as early as possible in the research process. In this sense, our cellular tools should be engineered in a more GMP compliant way. The use of lentiviral vectors for genetic modification result in permanent insertion of the sequence of interest in an uncontrolled fashion (e.g., multiple insertions or side mutations). This can potentially disrupt the expression of key genes for cell metabolism or trigger the expression of oncogenes. Thus, we propose the use of CRISPR-Cas methods and target gene insertion in Safe Harbors sequences [2] and to strictly control genome integration of vectors followed by a strict tumorogenecity test [3].

Our results suggest that the synergy of entrapped growth factors and secreted PGE2 promote bone formation and tissue integration. Interestingly, PGE2 has been described to be secreted in vesicles by apoptotic bodies [4], like those present in the ECM after devitalization (Chapter 2). Therefore, the role of those extracellular vesicles (EVs) needs to be further explored in this context. As EVs also contain nucleic acids and proteins promoting tissue regeneration [5] they could enhance efficiency of ECM decorated grafts for cell-free based therapeutic strategies.

Current clinical attempts to repair the bone organ are not limited to the sole use of mineral materials. Indeed 5-10% of fractures are resulting in non-union but 94% of them can be avoided by the use of concentrated bone marrow aspirate (cBMA) combined with allograft [6]. Even if the role of hematopoietic stem cell fraction in cBMA still needs to be further investigated, better bone grafts should include a functional BM, capable to sustain hematopoiesis.

To target this question, we took advantage of a previously established model developed for 3D bone generation in vitro and based on primary cells to generate a BM niche (Ref Arnaud primary MSCs in BR). After adding CD34+ hematopoietic stem and progenitors cells (HSPCs), the resulting osteoblastic engineered niche (eN) resembles the BM organ, recapitulating some of the main components of the in vivo hematopoietic microenvironment. Furthermore, eN maintains and expands HSPCs in xeno-free conditions with limited supply of cytokines/agonists while preserving their functionality both in vitro and in vivo.

Despite the relevance of this model, to better resemble the native hematopoietic niche, a higher level of complexity should be reached. So far, in vitro systems are mainly under constraint of cell culture parameters (e.g., culture media and cytokines required to fulfil different cell requirements). We envision that niche complexity could be increased introducing other well-known players of the hematopoietic stem cell niche to increase the cell diversity (e.g. nerve cells, endothelial cells, etc).

For a better evaluation of the possibilities offered by this innovative tool, a more complete characterization of the system is needed. Some physical cues inside of the bioreactors' chamber still remain uncertain (medium fluidics movements and speed, shear stress…). Those parameters could influence stromal and hematopoietic homeostasis but also HSPCs distribution in the niche.

Once we established the healthy eN as a bone marrow proxy, we took the opportunity to use it to model malignant hematopoiesis in vitro by using malignant HSPCs from patients with myeloproliferative neoplasms (MPN). Myeloid skewing of the niche and expansion of mutated MPN hematopoietic progenitors are some of the traits revealed by this niche in vitro.

This niche might set the basis for the development of personalized and custom-designed drug testing platforms. As therapeutic agent screening requires minimal system variability, we studied the possibility to standardize the eN, by using the MSOD cell line. MSOD based eN also sustained hematopoiesis (in health and disease) although to a lower extent than primary MSCs based eN. MSOD based eN can be considered as the first step toward standardization, but it still needs to be improved. Our results showed an uncontrolled proliferation of the resulting stromal tissue, which could lead to the collapse of the niche in the long-term. To circumvent excessive stromal cell proliferation, MSOD based eN could be treated with anti-mitotic drugs [7] or irradiated [8]. Importantly, engineered tissues' stability over time is under assessment

and eN has been shown to maintain cord blood HSPCs for 3 weeks in vitro. Extending the time of co-culture opens new possibilities to study complex functions like HSC engraftment in the niche in vitro, but also key parameters in blood diseases initiation and maintenance.

Taken together, the results generated in my thesis are paving the way to the development and engineering of devitalized grafts with instructive properties, but also the generation of innovative in vitro culture systems recapitulating some aspects of the structure and function of a bone organ. Importantly, this technology might be beneficial for humans (clinical grafts), but also for experimental animals, since it can be used as a tool to study human biology, reducing costs and number of animals required in science. (3Rs principles; W. M. S. Russell and R. L. Burch, 1959).

1.7 References

[1] A. García-García and I. Martin, "Extracellular Matrices to Modulate the Innate Immune Response and Enhance Bone Healing," Front. Immunol., vol. 10, no. September, pp. 1–8, 2019.

[2] F. Oceguera-Yanez et al., "Engineering the AAVS1 locus for consistent and scalable transgene expression in human iPSCs and their differentiated derivatives," Methods, vol. 101, pp. 43–55, 2016.

[3] P. Bourgine, C. Le Magnen, S. Pigeot, J. Geurts, A. Scherberich, and I. Martin, "Combination of immortalization and inducible death strategies to generate a human mesenchymal stromal cell line with controlled survival," Stem Cell Res., vol. 12, no. 2, pp. 584–598, 2014.

[4] F. Li et al., "Apoptotic Cells Activate the Phoenix Rising Pathway," Sci. Signal., vol. 3, no. 110, p. ra13, 2010.

[5] Q. ling Yuan, Y. gang Zhang, and Q. Chen, "Mesenchymal Stem Cell (MSC)-Derived Extracellular Vesicles: Potential Therapeutics as MSC Trophic Mediators in Regenerative Medicine," Anat. Rec., no. June 2018, 2019.

[6] A. L. Gianakos, L. Sun, J. N. Patel, D. M. Adams, and F. A. Liporace, "Clinical application of concentrated bone marrow aspirate in orthopaedics: A systematic review," World J. Orthop., vol. 8, no. 6, pp. 491–506, 2017.

[7] L. Ponchio, L. Duma, B. Oliviero, N. Gibelli, P. Pedrazzoli, and G. R. Della Cuna, "Mitomycin C as an alternative to irradiation to inhibit the feeder layer growth in long-term culture assays," Cytotherapy, vol. 2, no. 4, pp. 281–286, 2000.

[8] S. Llames, E. García-Pérez, Á. Meana, F. Larcher, and M. Del Río, "Feeder Layer Cell Actions and Applications," Tissue Eng. - Part B Rev., vol. 21, no. 4, pp. 345–353, 2015.

Russell, W.M.S. and Burch, R.L., (1959). The Principles of Humane Experimental Technique, Methuen, London. ISBN 0900767782.

Curiculum Vitae

europass

Thibaut Klein

Date of birth: 22/03/1985 | **Nationality:** French | **Gender** Male | (+33) 677935078 |

klein.thibaut@gmail.com | https://www.linkedin.com/in/thibaut-klein-13243a79/ |

82 rue de Mulhouse, 68300, Saint-Louis, France

WORK EXPERIENCE

01/02/2020 – CURRENT – Basel, Switzerland
POST DOCTORAL SCIENTIST – UNIVERSITY OF BASEL HOSPITAL, DEPARTMENT OF BIOMEDICINE

Innovation and expertise in tissue enginneering of bone and cartillaginous tissues as evidenced by the ongoing translation towards clinical trial of a cell line developped during my PhD.
High technical dexterity and organisation skills applied to classic and 3D cell or tissue culture in the particular context of clean room and Good Manufacturing Practice (GMP) compliant production of investigational medicinal products for clinical trials.
Development of a problem solving attitude, critical thinking and good communication skills.
Management and maintenance of 3D printers and laser cutting device for the Department of Biomedicine.

Department of Biomedicine - Tissue Engineering | Professional, scientific and technical activities |

ivan.martin@unibas.ch | https://biomedizin.unibas.ch/en/research/research-groups/martin-lab/ |

Hebelstrasse 20, 4031, Basel, Switzerland

01/11/2014 – 31/03/2020 – Basel, Switzerland
PHD STUDENT – UNIVERSITY OF BASEL HOSPITAL, DEPARTMENT OF BIOMEDICINE

Planning and completing scientific projects concluded by two original publications and the thesis entitled "Engineering of 3D mesenchymal tissues for bone regeneration and hematopoiesis modeling." Excellent teamwork and collaboration skills demonstrated by managing 5 research projects, resulting in the development of international collaborations involving both academic and industrial partners.
Public presentations and communication of results during international congresses.

Department of Biomedicine - Tissue Engineering | Professional, scientific and technical activities |

https://biomedizin.unibas.ch/en/research/research-groups/martin-lab/ |

Hebelstrasse 20, ivan.martin@unibas.ch, 4031, Basel, Switzerland

01/11/2010 – 01/10/2013 – Strasbourg, France
PRESIDENT – AFGES - ASSOCIATION FÉDÉRATIVE GÉNÉRALE DES ETUDIANTS DE STRASBOURG

Strategic planning and daily management of the association and its restaurant's staff management.
Students and student associations representation in national institutions and local Prefecture, Rector, Local Government and University of Strasbourg.
Regular media relation (television, print, radio) and social media.
Expertise gained in project management, conflict resolution, negociation and communication.
15000 members, 32 federated associations, 300 volunteers, 1M€ turnover, 40 employees.

Administrative and support service activities | https://www.afges.org/ |

1, Place de l'Université, 67000, Strasbourg, France

EDUCATION AND TRAINING

20/10/2020 – 21/10/2020 – Rischerstraße 8, Heidelberg, Germany
GOOD MANUFACTURING PRACTICES (GMP) FOR BEGINNERS – European Compliance Academy - Concept Heidelberg

GMP History and Trends
Hygiene / Personnel Hygiene
Training / Personnel
Documentation
Premises / Production
General & Specific Aspects of a QA system
Risk Management
Qualification / Calibration / Maintenance
Validation
Audits and self-inspection
Packaging / Storage / Transportation
Falsified Products

Field(s) of study

- Engineering, manufacturing and construction : *Manufacturing and processing not further defined* | *Manufacturing and processing not elsewhere classified*

https://www.concept-heidelberg.com/

01/11/2014 – 31/01/2020 – Klingelbergstrasse 50, Basel, Switzerland
PHILOSOPHIÆ DOCTOR - CELL BIOLOGY – Philosophisch - Naturwissenschaftliche Fakultät

Field(s) of study

- Natural sciences, mathematics and statistics : *Biology*

EQF level 8 | https://philnat.unibas.ch/de/forschung/promotionphd/

01/09/2010 – 30/06/2014 – 28 rue Goethe, Strasbourg, France
MASTER IN SCIENCE, TECHNOLOGIES, HEALTH, MENTION LIFE SCIENCE, SPECIALITY INTEGRATED MOLECULAR AND CELLULAR BIOLOGY, OPTION DEVELOPMENT AND STEM CELLS – Université de Strasbourg - Faculté des Sciences de la Vie

Field(s) of study

- Natural sciences, mathematics and statistics : *Biology* | *Biochemistry*

EQF level 7 |

https://sciencesvie.unistra.fr/formation/master/genetique-moleculaire-du-developpement-et-des-cellules-souches

2010 – 2011 – 4 rue Blaise Pascal, Strasbourg, France
UNIVERSITY DEGREE IN STUDENT COMMITMENT – Université de Strasbourg

Field(s) of study

- Education : *Inter-disciplinary programmes and qualifications involving education*
- Generic programmes and qualifications : *Personal skills and development*
- Business, administration and law : *Business, administration and law not elsewhere classified*

EQF level 6 | https://svu.unistra.fr/vie-des-campus/vie-universitaire/diplome-universitaire-dengagement-etudiant

01/09/2009 – 30/06/2010 – 28 rue Goethe, Strasbourg, France
BACHELOR IN CELL BIOLOGY AND PHYSIOLOGY – Université de Strasbourg - Faculté des Sciences de la Vie

Field(s) of study

- Natural sciences, mathematics and statistics : *Biology* | *Biochemistry* | *Biological and related sciences not further defined*

EQF level 6 | https://sciencesvie.unistra.fr/formation/licence/biologie-cellulaire-et-physiologie-des-organismes

01/09/2007 – 30/06/2009 – 5 Rue Edmond Labbé, Strasbourg, France
ADVANCED TECHNICIAN'S CERTIFICATE IN BIOTECHNOLOGY (FRENCH HDN EQUIVALENT) – LEGTP Jean Rostand

Field(s) of study

- Natural sciences, mathematics and statistics : *Biology* | *Biological and related sciences not further defined* | *Biochemistry*

EQF level 5 | https://www.lycee-jean-rostand.fr/

01/09/2003 – 30/06/2007 – 28 rue Goethe, Strasbourg, France
UNIVERSITY DEGREE LEVEL IN LIFE SCIENCE AND GEOLOGY – Université de Strasbourg - Faculté des Sciences de la Vie

Field(s) of study

- Natural sciences, mathematics and statistics : *Biology* | *Environmental sciences*

https://sciencesvie.unistra.fr/

2003 – 9a, Boulevard Hanauer, Haguenau, France
BACCALAURÉAT - SPECIALITY PHYSICS AND CHEMISTRY (A LEVEL EQUIVALENT) – Institution Sainte Philomène

Field(s) of study

- Generic programmes and qualifications
- Natural sciences, mathematics and statistics : *Biology* | *Natural sciences, mathematics and statistics not further defined*

EQF level 4 | http://www.sainte-philo.com/

LANGUAGE SKILLS

Mother tongue(s): FRENCH

Other language(s):

	UNDERSTANDING		SPEAKING		WRITING
	Listening	Reading	Spoken production	Spoken interaction	
ENGLISH	C2	C2	C1	C1	C1
GERMAN	B2	B2	B1	B1	A2

Levels: A1 and A2: Basic user; B1 and B2: Independent user; C1 and C2: Proficient user

DIGITAL SKILLS

Communication

Presenting | Zoom | Excellent writing and verbal communication skills | Presentation and negotiation skills | Cross cultural skills | Written and Verbal skills

Office Suite

Microsoft Excel | Microsoft PowerPoint | Microsoft Word | Google Docs | Google Drive

Data analysis and scientific research

Research and analytical skills | Internet user | Detail-Oriented | curious | Critical thinking

Project management

Reliability | Highly adaptable | Project management | resilient | innovative | Creativity | Good at being proactive and efficient in high stress situations | Efficient multi-tasking | Quick Learner and adaptable to new exposures and experiences | Problem-solving | Strategic Planning

Leadership and Teamwork

Conflict resolution | integrity | Motivator | Responsibility | Excellent organizational planning and solving problems in short time | leadership | positive thinking | Team-work oriented | Decision-making | Friendly | Good listener and communicator

Social Media

WhatsApp | Skype | LinkedIn | Facebook | Gmail

PUBLICATIONS

Analysis of the subcapital two-part humerus fracture by fluoroscopy – objective criteria for classification and decision making Archives of Orthopaedic and Trauma Surgery

Accepted and under publication process in Archives of Orthopaedic and Trauma Surgery under reference AOTS-D-20-01674R2.

PhD Thesis - Engineering of 3D mesenchymal tissues for bone regeneration and hematopoiesis modeling

2020
The bone organ has two main functions in the adult. a) It provides mechanical support and protects organs, while b) the bone marrow hosts hematopoiesis, a process ensuring lifelong production and renewal of the blood tissue. Therefore, the general aim of my thesis is to engineer mesenchymal tissues able to support bone healing and bone marrow functions. Their recapitulation *in vitro* by using primary hMSCs (or mesenchymal cell lines) could: (i) help fulfilling a clinical need in bone regenerative medicine by providing engineered off-the-shelf coated extracellular matrix (ECM) with tunable compositions, and (ii) provide an animal-free model to study bone biology and hematology in health and disease. These aims are addressed through a combination of hMSCs and 3D perfusion bioreactor systems.

In vitro biomimetic engineering of a human hematopoietic niche with functional properties

https://doi.org/10.1073/pnas.1805440115 – 2018
In adults, human hematopoietic stem and progenitor cells (HSPCs) reside in the bone marrow (BM) microenvironment. Our understanding of human hematopoiesis and the associated niche biology remains limited, due to human material accessibility and limits of existing in vitro culture models. The establishment of an in vitro BM system would offer an experimentally accessible and tunable platform to study human hematopoiesis. Here, we develop a 3D engineered human BM analog by recapitulating some of the hematopoietic niche elements. This includes a bone-like scaffold, functionalized by human stromal and osteoblastic cells and by the extracellular matrix they deposited during perfusion culture in bioreactors. The resulting tissue exhibited compositional and structural features of human BM while supporting the maintenance of HSPCs. This was associated with a compartmentalization of phenotypes in the bioreactor system, where committed blood cells are released into the liquid phase and HSPCs preferentially reside within the engineered BM tissue, establishing physical interactions with the stromal compartment. Finally, we demonstrate the possibility to perturb HSPCs' behavior within our 3D niches by molecular customization or injury simulation. The developed system enables the design of advanced, tunable in vitro BM proxies for the study of human hematopoiesis.

Engineered Extracellular Matrices as Biomaterials of Tunable Composition and Function

https://onlinelibrary.wiley.com/doi/full/10.1002/adfm.201605486 – 2017
Engineered and decellularized extracellular matrices (ECM) are receiving increasing interest in regenerative medicine as materials capable to induce cell growth/differentiation and tissue repair by physiological presentation of embedded cues. However, ECM production/decellularization processes and control over their composition remain primary challenges. This study reports engineering of ECM materials with customized properties, based on genetic manipulation of immortalized and death-inducible human mesenchymal stromal cells (hMSC), cultured within 3D porous scaffolds under perfusion flow. The strategy allows for robust ECM deposition and subsequent decellularization by deliberate cell-apoptosis induction. As compared to standard production and freeze/thaw treatment, this grants superior preservation of ECM, leading to enhanced bone formation upon implantation in calvarial defects. Tunability of ECM composition and function is exemplified by modification of the cell line to overexpress vascular endothelial growth factor alpha (VEGF), which results in selective ECM enrichment and superior vasculature recruitment in an ectopic implantation model. hMSC lines culture under perfusion-flow is pivotal to achieve uniform scaffold decoration with ECM and to streamline the different engineering/decellularization phases in a single environmental chamber. The findings outline the paradigm of combining suitable cell lines and bioreactor systems for generating ECM-based off-theshelf materials, with custom set of signals designed to activate endogenous regenerative processes.

Selective proapoptotic activity of polyphenols from red wine on teratocarcinoma cell, a model of cancer stem-like cell

https://link.springer.com/article/10.1007%2Fs10637-009-9352-3 – 2011
Cancer stem cells are expected to be responsible for tumor initiation and metastasis. These cells are therefore potential targets for innovative anticancer therapies. However, the absence of bona fide cancer stem cell lines is a real problem for the development of such approaches. Since teratocarcinoma cells are totipotent stem cells with a high degree of malignancy, we used them as a model of cancer stem cells in order to evaluate the anticancer chemopreventive activity of red wine polyphenols (RWPs) and to determine the underlying cellular and molecular mechanisms. We therefore investigated the effects of RWPs on the embryonal carcinoma (EC) cell line P19 which was grown in the same culture conditions as the most appropriate normal cell line counterpart, the pluripotent embryonic fibroblast cell line NIH/3T3. The present study indicates that RWPs selectively inhibited the proliferation of P19 EC cells and induced G1 cell cycle arrest in a dose-dependent manner. Moreover, RWPs treatment specifically triggered apoptosis of P19 EC cells in association with a dramatic upregulation of the tumor suppressor gene p53 and caspase-3 activation. Our findings suggest that the chemopreventive activity of RWPs on tumor initiation and development is related to a growth inhibition and a p53-dependent induction of apoptosis in teratocarcinoma cells. In addition, this study also shows that the EC cell line is a convenient source for studying the responses of cancer stem cells to new potential anticancer agents.

MANAGEMENT AND LEADERSHIP SKILLS

President - AFGES

- Team building and co-ordination (Board direction, bureau meeting, administration conciles; from 5 to 150 participants)
- Starting, follow up and completion of several projects
- Delegation of specific tasks
- Strategic decision making (annual and pluriannual policies)
- Human resources related question management in crisis context

Project Management Fundamentals

• Understand what a project is,
• Know what project management is about,
• Implement key concepts of project management in a research environment,
• Formulate a project goal,
• Analyse the stakeholder setting and devise ways of how to handle stakeholders,
• Plan their project, define milestones and set realistic deadlines, and
• Acquire skills to deal with the high degrees of uncertainty in research.
https://www.leadtotrust.com/

COMMUNICATION AND INTERPERSONAL SKILLS

Conflict Management and Better Communication

- Background to conflict situations and the effects of conflicts
- The stages and phases of conflict and Methods for conflict resolution
- Managing confluct - practical strategies
- Transactional Analysis
- Benefits of conflict
- Communication techniques and action plan
- Reflection and discussion

Improve Negotiation Skills

- Recognize the characteristics and consequences of various styles of interactions, whether conflictual or not
- Understand how to build relationships based on interest and opportunity, rather than on conflict or persuasion
- Acquire the objectivity and competence necessary to prepare and lead negotiations for building sustainable partnerships
- Know how to prepare in an efficient and detailed way: what they want, how to quantify their aim, how to break it down into negotiable units
- Learn how to use effective questioning techniques, and verbal / non-verbal communication
- Increase their negotiation capacities (hands-on practice) in a “risk-free” environment, thus enabling them to be more efficient.

SOCIAL AND POLITICAL ACTIVITIES

01/12/2010 – 01/12/2012
Board Member of the University of Strasbourg

Strasbourg
Development and approval of strategic goals and objectives, and establishment of policies related to programs and services.
Negociation and approval of the annual budget of the University.

01/12/2009 – 01/12/2013
Student Dean of the Life Science Faculty of Strasbourg

Strasbourg
Student representation among the Faculty Board and first interlocutor to the Dean regarding student related questions.
Participation to the implementations of pedagogic offer, rules of procedure and methods of control.
Verification and approval of the budget.

CREATIVE WORKS

CURRENT
3D printing and modelling

Design and modification of basic models. Building, maintenance and regular usage of 3D printers (Fused Deposition Modeling -FDM and resin Stereolithography -SLA). Prints are then used for professional application (laboratory related prototypes, bioreactors...) or personnal application (tool-building, models for metal work in lost-wax casting technique, decoration...).

CURRENT
Experimental archeology and metallurgy

Experimentation and reconstitution based on archeologic findings and scientific publications of ancient tools, weapons, jewellery and sculptures. Mastery of nonferrous (copper, bronze, silver) melting and casting. Collaborations with museum and archeologic parcs for demonstration of Bronze Age and Iron Age metal working reenactment. In this activity I have recreated my own tools according to historical findings. I also built my own complete propane forge/ melting oven and vacuum assisted casting device.

CURRENT
Craftsman furniture upholsterer and decorator

Born into a family of craftsmen, my grand father, master craftsman, taught me the rudiments of the profession of woodworking, upholstering and sewing that I still practice on a weekly basis.

DRIVING LICENCE

Driving Licence: B1

Driving Licence: B